Hurricane Risk 1

Jennifer M. Collins
Kevin Walsh *Editors*

Hurricane Risk

RMS
Aegean Conferences
USF UNIVERSITY OF SOUTH FLORIDA
Springer

Hurricane Risk

Volume 1

Series Editor
Jennifer Collins, School of Geosciences, NES 107, University of South Florida, Tampa, FL, USA

More information about this series at http://www.springer.com/series/16154

Jennifer M. Collins • Kevin Walsh
Editors

Hurricane Risk

Springer

Editors
Jennifer M. Collins
School of Geosciences
University of South Florida
Tampa, FL, USA

Kevin Walsh
School of Earth Sciences
The University of Melbourne
Parkville, VIC, Australia

ISSN 2662-3064 ISSN 2662-3072 (electronic)
Hurricane Risk
ISBN 978-3-030-02401-7 ISBN 978-3-030-02402-4 (eBook)
https://doi.org/10.1007/978-3-030-02402-4

Library of Congress Control Number: 2018965215

This Springer imprint is published by the registered company Springer Nature Switzerland AG
The registered company address is: Gewerbestrasse 11, 6330 Cham, Switzerland

Preface

This book comprises both extended versions of papers presented at the 6th International Summit on Hurricanes and Climate Change: from Hazard to Impact, held in Heraklion in June 2017, as well as some additional contributions. Talks presented at this conference ranged from numerical simulation of tropical cyclones through tropical cyclone hazard estimation to damage estimates and their implications for commercial risk. This series of conferences has evolved over time to include a substantial component on climate risk, and this shift in emphasis is reflected in the content of this new volume. This book provides a source reference for both risk managers and climate scientists for topics on the interface between tropical cyclones, climate, and risk.

These topics are of particular interest to the insurance industry, and Chap. 1 provides an overview of the tropical cyclone risk issues that are of concern to the industry, with a particular emphasis on the importance to industry of appropriate time horizons for prediction and risk management. A review of the development and processes of the reinsurance industry is also given, to provide useful background for the technical and scientific work required to address industry-specific concerns. Better estimates of tropical cyclone hazard are of course a key concern to industry and policy makers, and Chap. 2 details new methods for assessing the damage potential of tropical cyclones, a key input for estimates of tropical cyclone impacts. Another measure for assessing the intensity of tropical cyclones that is relevant to their total potential impact during a season, namely, their integrated kinetic energy, is discussed in Chap. 3 along with the climatology and year-to-year variations of this parameter. The links between tropical cyclone energy and wind hazards are investigated in Chap. 4, as a visualization tool for hazard impact assessment.

Accurate risk assessment of current tropical cyclone hazard involves an intimate understanding of the specific risks in a particular location, and Chap. 5 gives a detailed description of the current vulnerabilities in the Tampa Bay region, a location that seems particularly at risk due to a combination of substantial hurricane hazard, its geography and its vulnerable infrastructure. Studies of the year-to-year variations in tropical cyclone occurrence and the reasons for this variation are important for

understanding what leads to high-impact years, and Chap. 6 details the relationship between the climate conditions during the tropical cyclone season in 2015 and the observed tropical storm and hurricane occurrence in that year. There is a growing body of work on the relationship between variations in climatically important atmospheric conditions and tropical cyclone occurrence, and Chap. 7 investigates the possibility of the influence of dust particles on tropical cyclone incidence in the Australian region, since this continent is a considerable source of dust. While the influence of Saharan dust on Atlantic tropical cyclones appears to be noticeable and is a topic of active research, the effect in the Australian region appears to be much less.

While there have been advances in our understanding of the links between climate and tropical cyclones, we still do not have a general theory of the relationship between climate and tropical cyclones that would enable us to predict the number of tropical cyclones from the current climate, even to within an order of magnitude. Chapter 8 discusses some of the main issues in establishing such a theory, with particular relevance to the possible implications for tropical cyclone risk assessment. Any such well-established theoretical relationship would have implications for future predictions of tropical cyclones in a warmer world, and Chap. 9 provides new estimates of the potential tropical cyclone damage and loss of life due to future climate change. This chapter emphasizes the crucial role of adaptation to future changes in hazards in minimizing the increase in tropical cyclone risk. A possible outcome in a warmer world is the poleward movement of typical regions of tropical cyclone occurrence, a scenario that has received some support from recent research. Chapter 10 outlines some of the challenges for the built environment of this potential risk, with a consideration of possible adaptation options. In addition to possible effects of climate change on the land-based built environment, ocean infrastructure is potentially vulnerable to future changes in hurricane climate. Chapter 11 quantifies some of these future hazards for offshore infrastructure, with a focus on integrating projections of future wave hazards with engineering design. Finally, a tool that is increasingly being used for estimating the effects of climate change on tropical cyclones is the climate model, as constantly improving computing resources enable horizontal resolutions for these models to be increased to the point where their simulations of tropical cyclones are becoming more realistic. Chapter 12 outlines a method whereby very fine resolution simulations of tropical cyclones can be designed to test the hypothesized impact of climate change, including the possible effect on hurricanes of the global and regional warming that has already occurred to date.

Tampa, FL, USA — Jennifer Collins
Parkville, VIC, Australia — Kevin Walsh

Acknowledgments

The authors would like to thank the expert reviewers for their time and careful review of the chapters. In addition, the authors are grateful to Lauren Carter for the editorial assistance she provided. We would like to acknowledge Rick Murnane who co-organized the 6th International Summit on Hurricanes and Climate Change: From Hazard to Impact with Jennifer M. Collins. We also thank Dimitrios Lambris and Aegean Conferences for their logistic support of the summit. We appreciate our sponsors Risk Management Solutions (RMS), Aegean Conferences, and the University of South Florida (USF). Finally, the authors deeply appreciate the productive collaboration with the professionals at Springer, particularly Margaret Deignan and the copy editing team.

Contents

Contributors

Laura A. Bakkensen University of Arizona School of Government and Public Policy, Tucson, AZ, USA

Rupsa Bhowmick Department of Geography and Anthropology, Louisiana State University, Baton Rouge, LA, USA

Cindy L. Bruyère National Center for Atmospheric Research, Boulder, CO, USA

Environmental Sciences and Management, North-West University, Potchefstroom, South Africa

Jennifer M. Collins School of Geosciences, University of South Florida, Tampa, FL, USA

James M. Done National Center for Atmospheric Research, Boulder, CO, USA

Willis Research Network, London, UK

Rowan Douglas Willis Towers Watson, London, UK

Stephen G. Evans Natural Disaster Systems, Department of Earth and Environmental Sciences, University of Waterloo, Waterloo, ON, Canada

Ming Ge National Center for Atmospheric Research, Boulder, CO, USA

Greg J. Holland National Center for Atmospheric Research, Boulder, CO, USA

Willis Research Network, London, UK

Michael E. Kozar Risk Management Solutions (RMS), Tallahassee, FL, USA

Richard J. Krupar III Berkshire Hathaway Specialty Insurance, San Ramon, CA, USA

Robert O. Mendelsohn Yale University School of Forestry and Environmental Studies, New Haven, CT, USA

Vasubandhu Misra Center for Ocean-Atmospheric Prediction Studies, Florida State University, Tallahassee, FL, USA

Department of Earth, Ocean and Atmospheric Science, Florida State University, Tallahassee, FL, USA

Florida Climate Institute, Florida State University, Tallahassee, FL, USA

Christina Patricola Lawrence Berkeley National Laboratory, Berkeley, CA, USA

Charles H. Paxton Channelside Weather LLC, Tampa, FL, USA

Tom Philp Science and Natural Perils, AXA XL, London, UK

David R. Roache School of Geosciences, University of South Florida, Tampa, FL, USA

Christina Robertson Model Development, RMS, London, UK

Tom Sabbatelli Model Development, RMS, London, UK

Geoffrey R. Saville Willis Towers Watson, London, UK

Daniel J. Smith Cyclone Testing Station, James Cook University, Townsville, QLD, Australia

Jill C. Trepanier Department of Geography and Anthropology, Louisiana State University, Baton Rouge, LA, USA

Kevin Walsh School of Earth Sciences, The University of Melbourne, Parkville, VIC, Australia

Michael F. Wehner Lawrence Berkeley National Laboratory, Berkeley, CA, USA

Paul Wilson Model Development, RMS, London, UK

Colin Zarzycki National Center for Atmospheric Research, Boulder, CO, USA

Yi-Jie Zhu Natural Disaster Systems, Department of Earth and Environmental Sciences, University of Waterloo, Waterloo, ON, Canada

School of Geosciences, University of South Florida, Tampa, FL, USA

The original version of this book was revised: ISSN numbers for both print and electronic versions corrected. The correction to this chapter is available at https://doi.org/10.1007/978-3-030-02402-4_13

Chapter 1
Issues of Importance to the (Re)insurance Industry: A Timescale Perspective

Tom Philp, Tom Sabbatelli, Christina Robertson, and Paul Wilson

Abstract Of any single weather or climate peril, tropical cyclones constitute the largest annual average loss to the global insurance and reinsurance industry, and in any given year are often the drivers of the largest catastrophic losses to the entire industry. These losses come in the form of payments covering insurance claims, initiated through damage caused by a tropical cyclone's physical effects. They are thus looked upon within the industry as hugely important perils for study and analysis. This chapter provides an introduction to traditional methods for pricing risk, with an emphasis on hurricanes, and how the catastrophe modeling industry has arisen out of limitations with those traditional methods specifically when looking at extreme, relatively rarely occurring perils that have the potential to cause catastrophic loss.

Keywords Insurance · Catastrophe · Modeling · Hurricane

Of any single weather or climate peril, tropical cyclones constitute the largest annual average loss to the global insurance and reinsurance (henceforth "re/insurance") industry, and in any given year are often the drivers of the largest catastrophic losses to the entire industry. Initial estimates of the insured loss caused by Hurricanes Harvey, Irma, and Maria in 2017 total approximately US$92 billion. Another trio of hurricanes – Katrina, Rita, and Wilma – struck the U.S. in 2005, causing losses (trended to 2017 dollars) in excess of US$110 billion (Swiss Re 2018).

These losses come in the form of payments covering insurance claims, initiated through damage caused by a tropical cyclone's physical effects. They are thus looked upon within the re/insurance industry as hugely important perils for study

T. Philp
Science and Natural Perils, AXA XL, London, UK

T. Sabbatelli (✉) · C. Robertson · P. Wilson
Model Development, RMS, London, UK
e-mail: Tom.Sabbatelli@rms.com

J. M. Collins, K. Walsh (eds.), *Hurricane Risk*, Hurricane Risk 1,
https://doi.org/10.1007/978-3-030-02402-4_1

and analysis. Although tropical cyclones in all basins are of large concern, those that form in the Atlantic basin usually come in for the highest scrutiny due to the large concentration of insured assets that exist in that basin – particularly along the high population density sections of the U.S. coastline. This chapter will therefore focus on Atlantic hurricanes as its fundamental basis, but the concepts introduced here are easily transferrable to any other basin that experiences tropical cyclones.

In order to give the unacquainted reader a general overview of the industry, a very brief historical background of re/insurance is first provided, before some important operational practices and market dynamics are introduced. The chapter then goes on to provide an introduction to traditional methods for pricing risk, and how the catastrophe modeling industry has arisen out of limitations with those traditional methods specifically when looking at extreme, relatively rarely occurring perils that have the potential to cause catastrophic loss. From this point, the chapter will focus on one of the key debates that is taking place within the industry at present: how to best build a view of Atlantic hurricane frequency risk. This section will constitute the main body of the chapter. It will then provide a discussion on new innovations within re/insurance with regard to alternative risk transfer mechanisms, before concluding with a brief review of ways in which climate change impacts are being explicitly incorporated into industry risk assessments at present.

1.1 An Introduction to the Re/insurance Industry

Insurance, as a concept, can be described as the quantification and securitization (usually via monetization) of a risk, and the subsequent transfer (ceding) of that risk from one party to another, in order that the (re)insured is indemnified from any loss resulting from that risk. It is known to have existed in one form or another since around 2250 B.C., with the Babylonians using it to indemnify traders from losses in cases where they were found to be non-negligent (Trennery 1926). In its more modern form of insurance-specific contracts, the earliest existing (or, at least, surviving) documents provided indemnity to traders susceptible to maritime risk in and around Genoa shortly before 1300 A.D. (Briys and Joos de ter Beerst 2006).

Reinsurance, the concept of an insurer itself ceding the already taken-on risk to another party, was first documented shortly afterward, again in a contract emanating from Genoa in 1340, in which the risk during the most hazardous part of a voyage was ceded to another insurer (Holland 2009). The principles developed in Genoa spread across the Mediterranean and Europe, finding root during the 1600s in Edward Lloyd's coffee house in the City of London, later growing into the Lloyd's of London insurance market. With global marine exploration becoming competitive at this time, the ideas quickly spread throughout the world, leading to the global re/insurance industry.

Today, re/insurance covers all types of risk, from specific natural perils such as hurricanes, to general life insurance and even war and terrorism risk. Policies are sold to individuals, businesses, and governments alike, with insurance products being created for any insurable interest that can be quantified and compensated should deleterious events occur. The transfer of risk from one party to another generally has to involve a "consideration" – effectively, something of value passing from any potential policyholder to a re/insurer – in order for the insurance contract to become active. This consideration usually takes the form of an insurance "premium".

On a simplistic level, it is intuitive to think that the frequency and magnitude of any risk can be directly translated into a fair insurance premium. This type of analysis leads to what is known as a "pure risk" premium, or our best evaluation of the price for the pure risk at a given location. This is, unsurprisingly, known within the industry as insurance pricing, and will be introduced in further detail in the next section.

Before delving into pricing methods, however, it is important to understand that, in reality, premiums are susceptible to market dynamics and business strategies, which can influence the final price – both negatively and positively – that the customer sees. These influences will be introduced below as they have extremely important impacts for the re/insurance industry.

1.1.1 Insurance Cycles

One of the most important of the market dynamics to understand is the concept of insurance cycles. These cycles, although often complex and with influences originating from many sources, can be generally said to exist because of the flow of capital into and out of the re/insurance industry. This capital flow results in changes in supply and demand for insurance products (or vice versa), which drives alternating "hard" and "soft" market conditions. The cycles between the two states are often cited as the top challenge the re/insurance market faces (Lloyd's 2008), mostly due to the potential need to quickly vary business strategy without disrupting client relationships; methods to deal explicitly with minimizing the effects of these cycles have become prevalent within the risk pricing and capital reserving communities in the past 10 years or so following recommendations made by the General Insurance Reserving Issues Taskforce to the Institute of Actuaries (Jones et al. 2006).

Figure 1.1 provides a schematic to describe the cycle and the points of the hard and soft market. In this example, we can see that shortly after a catastrophe, market conditions "harden". This is driven by a flow of capital out of the industry due to claims paid by re/insurers at the point of catastrophe, and of related shareholder losses/lack of return causing a withdrawal of investment. This leads to a less competitive underwriting environment, and thus premium rates increase. However,

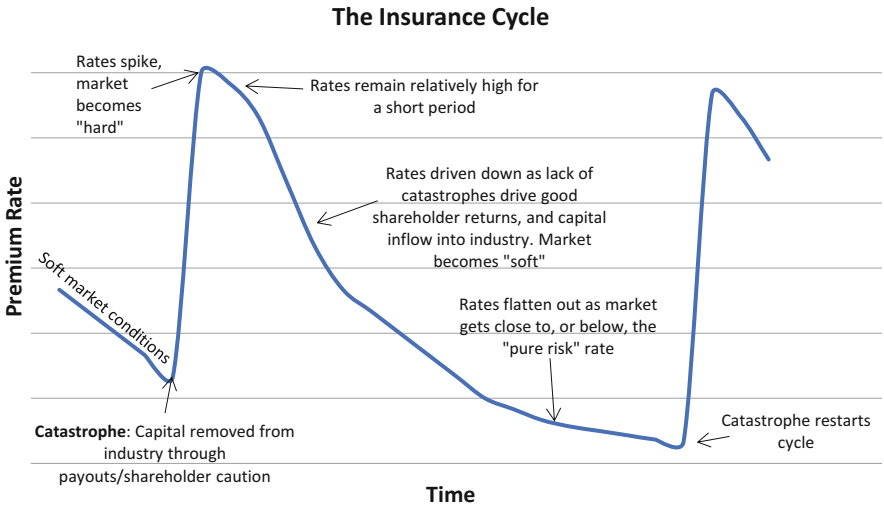

Fig. 1.1 Schematic of the insurance cycle through time

as time goes on without large, industry-impacting catastrophes, returns on investments from shareholders tend to be good, and thus capital begins to flow back into the industry. This leads to more competition, and a general driving down of insurance premiums. It is worth noting that, although the occurrence of catastrophes may cause a shift to hard market conditions, this is not always the case; on a related note, the shift to hard market conditions can also be driven by capital-impacting events other than a catastrophe. Finally, there is an argument to be made that because of recent alternative capital pathways to the market (see later section), the re/insurance market may be shifting away from these cycles. However, in the present, it is necessary to at least acknowledge their historical existence.

1.1.2 Expense Loading

The work done to quantify, price, and then underwrite a risk obviously requires skilled practitioners, processes, and systems, as do claims when they are made. These contribute to what is known as "expense loading" of the pure risk premium. Due to the high level of competition in financial markets, these are usually driven down to as an affordable level as possible and, at present, there are also attempts to minimize these costs through innovative alternative risk transfer solutions, such as insurance-linked securities – these alternative solutions are introduced in more detail later in the chapter.

Background competition and innovation are not the only mechanism through which loading costs of expenses are driven down. Re/insurance brokers, often tasked

with the placing a risk for a customer, effectively act as well-informed intermediaries to assess the needs of a customer, and to find them the most appropriate coverage terms and most competitive rates.

1.1.3 Regulation and Market Control

Alongside brokers being a key part of many re/insurance policy chains, regulation has increasingly become an important part of re/insurance practice. Regulation of the insurance industry takes place through multiple regional, national, and international bodies, and exists in order to protect policyholders in two key ways.

The first is through rate regulation which, although not universal, aims to help to protect customers against excessive premiums. Here, the regulator is tasked with independently producing a view on any manner of a risk, and defining appropriate bounds for the pricing of that risk. If re/insurers flaunt those guidelines, they may face financial penalties, or may even be unable to gain access to the market over which the regulator has licensing authority, though these types of penalties are typically only seen for some insurance products (e.g. property and casualty insurance for individuals).

The second way regulation aims to protect policyholders is through solvency capital requirements. Here, regulators require re/insurers to prove, as far as is deemed possible, that they will be able to remain resilient to losses and to pay out insured claims up to a probability that is considered reasonable by the regulator. The meaning of the word "reasonable" can differ between regulators, but the recent EU's Solvency II insurance requirement is that insurers be able to pay out with a 99.5% probability – or, effectively, that in any given year there is only a 1 in 200 chance that the insurer will become insolvent and unable to pay claims. These guidelines are expected to find equivalence in U.S. law in the near future.

A key issue for re/insurers on the regulation front arises from the fact that not all regulators hold the same opinion on best-practice for pricing risk. This can leave re/insurers in difficult situations if a local regulator in one jurisdiction advocates a contradictory method for pricing the risk than a different regulator in another jurisdiction. With specific regard to North Atlantic hurricane risk, this has been a topic of debate within the industry for a number of years. As an example, the Florida Commission on Hurricane Loss Projection Methodology (FCHLPM) has historically approved catastrophe models with a view of Atlantic hurricane frequency risk different from the stance adopted by Lloyd's of London over the past few years. Although Lloyd's isn't strictly an independent regulator, its requirement that syndicates operating within it follow its guidelines effectively means that it has the same effect on re/insurance entities as a regulator.

As this issue on differing views of frequency risk is the focus of the main body of this chapter, these issues will be delved into in more detail later. However, before doing that, let us conclude this section with two more key factors that play a role in re/insurance decision-making.

1.1.4 Ratings Agencies

Although independent of regulators, ratings agencies have a similar effect on re/insurers: in assessing an insurer's ability to remain resilient and profitable, and assigning ratings to those companies based on those assessments, ratings agencies effectively add a second layer of regulation. This again adds more complication to the overall picture, as these assessments are not standardized between ratings agencies, and one ratings agency may have different requirements and techniques for assigning ratings.

However, as re/insurance companies are ultimately accountable to their shareholders, they must operate in a manner that is thought to generally positively impact share prices. As higher ratings from ratings agencies tends to attract capital from market investors, it clearly makes intuitive sense that most re/insurers must align with these independent assessments enough that their ratings will be seen positively.

With these governing market dynamics and practices introduced, it is important to understand how these issues come together from a business planning strategy, and how they impact the decisions that re/insurers make as to how best to operate within the market.

1.1.5 Business Planning: Finding Appropriate Stability

The ultimate purpose of re/insurance is to remove the volatility of loss that could otherwise have long-lasting negative impacts on economic and broader societal development. This implicitly suggests a desire on the part of any potential insured parties to remove the risk of volatility from their business or assets, which in turn suggests that a reasonably stable premium would be anticipated and desired by potential clients. Finding such a stable premium for any risk is indeed something that is often looked upon as a sign of proficiency in the market.

In reality, however, the market dynamics and practices described above make finding and setting a stable premium very difficult. However, the concept of a "pure risk" premium (as mentioned in Fig. 1.1) free from these influences does allow one, at least theoretically, to find a reasonable baseline to work from; this pure risk premium can be loosely thought of as a best estimate of the "current" risk.

With this concept of current risk in mind, it is worth introducing two time-horizon aspects of risk management that are of importance to a re/insurance company building a view of risk; namely, to what timescale would re/insurers ideally:

(i) Price risk?
(ii) Plan broader business operations?

Regarding (i) – although re/insurers typically underwrite policies on an annual basis, it may appear evident, given the description above, that an annually changing

view of the risk is not ideal for traditional re/insurance pricing because of the premium (and also the consequent operational) volatility that such a method would introduce. This issue may be more or less important for some re/insurers than others, dependent on business structure and strategy, and also likely varies depending on whether the risk is a direct insurance cover placed with an insurer, or a reinsurance cover placed with a reinsurer. For an insurer, clients not well-accustomed to risk modeling may look on premium stability as desirable for their business and cost planning; yet reinsurers, with clients who themselves are already re/insurers and thus are likely to have direct expertise in risk modeling, may be much less concerned by year-to-year premium volatility and may even seek it.

However, on the assumption that minimizing premium volatility on current risk is an important issue from at least a general insurance perspective, there is a need to define a multi-annual time window that can smooth year-to-year variability in the risk. The question therefore evolves to the following: over what multi-annual time period should insurers (and any similarly concerned reinsurers) look at to price risk? This is a tricky question to answer and, in reality, the time horizon for "current" risk pricing differs between catastrophe models.

For hurricane risk, the minimum length of the multi-year time window is thought to be approximately 5 years, as this is around the time needed to smooth out fairly well known inter-annual effects on Atlantic hurricane activity driven by the El Niño-Southern Oscillation (ENSO) and other short-term climate influences. Defining the maximum length of the window introduces some difficult choices, however, with each carrying benefits and detriments. For example, pricing risk from very long-term historical data (i.e. the entire HURDAT2 record) may not be entirely appropriate given knowledge of a changing climate coupled with potential multi-annual variability, and issues with record certainty as one goes back in time. Yet, in limiting the data to more recent years, we would be shrinking an already small dataset further, while potentially removing useful historical information and extreme event behavior from pricing. Thus, questions arise around whether it should be seen as most appropriate to utilize ideas such as 10–20 year persistence (i.e. beginning to approach levels of multi-decadal variability) or merely just the long-term (i.e. ~100 year) average in order to avoid influence from occasionally uncertain scientific theories.

In reality, there are currently no best-practice answers to the above challenges, and this is a theme which should be encouraged as an area for active research within the scientific community. The catastrophe modeling industry has begun to attempt to answer some of those questions; some of these specific attempts are detailed later in the chapter, including detailing attempts to take forward-looking, multi-year forecasts of the risk.

Before moving forward, however, it is important to introduce the distinction between questions (i) and (ii) above due to the issue of climate change, and how its impact is viewed differently in pricing and business planning.

With regard to question (i): as re/insurance pricing is concerned with the present, climate change research as currently undertaken by the academic community (i.e. projections typically out to 2030, 2050, or even 2100) may not be well-aligned

with that needed by the re/insurance pricing community, which is focused chiefly on the present day, and perhaps only looks forward up to 5 years into the future.

However, with regard to question (ii), from a long-term business planning perspective, re/insurers are very mindful of the potentially changing risk landscape, and how they should be evolving their business accordingly. To borrow the language of climate science policy, the re/insurance industry is asking, "What can or should I be doing now to mitigate the impacts of climate change on my business, if any exist?" and secondly, "What can or should I be doing now and in the future to adapt my business to account for the challenges and possible opportunities these changes may represent?"

Thus, there is definite need for explicit climate change work with a more traditional insurance-pricing timeline view in mind. Regarding the business-planning aspect, a secondary issue here arises when we consider explicitly what time horizons are appropriate. From discussions raised at past industry workshops carried out by the SECTEUR project acting on behalf of the Copernicus Climate Change Project (C3S), it is generally believed that the maximum forward looking timescale for appropriate business planning lies at around 10 years (Caron 2017). Longer than this and views of the risk become too abstract and detached from re/insurance practices and strategies that change on an annual basis. The re/insurance industry has contributed to studies related to climate change impacts, to be described later in this chapter, but to date they have been exploratory in nature.

In conclusion to this section, it can be seen that there are many complexities introduced by market dynamics, operations, and business practices that must be taken into account when building the most appropriate view from which to price risk. Although it is hoped that some of the drivers of pricing variability have been elucidated, it is clear that the already complex task becomes even more complicated for risks originating from a background climate that is inherently non-linear and ever-changing. The next section will briefly introduce the traditional framework that has traditionally been used for pricing risk, before it progresses to describe the reasons for, and evolution of, the growth of the catastrophe modeling industry.

1.2 An Introduction to Actuarial Pricing

An insurance entity can loosely be envisaged as having three main components (although a number of other vital functions also exist):

- An actuarial department, in which risks are given a technical price and appropriate financial reserves are calculated.
- An underwriting department, in which risk selection is made, the final price is quoted, and business is written.
- A claims department, in which claims management takes place should deleterious events occur.

Of paramount significance to the understanding of issues of importance to the re/insurance industry is a comprehensive understanding of the interface between the actuarial departments of re/insurance companies, and the research centers that control and produce scientific hazard data.

Actuarial science has a long and storied history, establishing itself shortly after the first published work on probability theory (Huygens 1657). Edmond Halley's "life tables", in which he devised appropriate premiums for life annuities based upon the historical probability of mortality given a person's age (Halley 1693) have provided the blueprint for actuarial science ever since.

Still today, actuaries use mathematical methods to analyze past claims and relevant risk data to build up a representative view of probabilities of loss from which to calculate appropriate premiums. These methods often rely on building ideas about the distribution of losses and perils in order to accurately capture the likelihood of events happening.

However, within the past 30 or so years, the industry has begun to reassess the appropriateness of some of these methods for risks that have not necessarily occurred before, or that have the potential to cause catastrophic losses given the changing demographics, wealth, and insured assets of societies that have the potential to be impacted. A comprehensive evaluation and pricing of tropical cyclone risk, specifically, out to the probability required by many regulators (e.g. 1 in 200 years), would ideally utilize a record much longer than the length of the historical Atlantic hurricane record (HURDAT2), but traditional pricing methods – typically constrained by purely historical data – are somewhat limited in their ability to overcome these issues.

Ideas for progress on these concerns were originally hinted at in decision and policy papers (e.g. Kunreuther and Miller 1985), but did not fully materialize in a very practical way until the foundation of the catastrophe modeling industry in the late 1980s and early 1990s.

1.3 From Actuarial Pricing Models to Hurricane Catastrophe Models

The first catastrophe modeling firm, AIR Worldwide, was founded in 1987 and introduced the re/insurance industry's first catastrophe model devoted to Atlantic tropical cyclones. RMS, a company first established with a focus on earthquake modeling, soon followed in 1989. In the 30 years that followed, other firms and data providers have strived to enhance industry practices through the use of catastrophe models.

During the infancy of catastrophe models, the re/insurance industry, recovering from the 1989 Loma Prieta earthquake in California, primarily focused its attention on natural hazard risk from earthquakes. That focus quickly shifted in 1992 when Hurricane Andrew became a major catastrophe for the re/insurance industry.

Following a long stretch of quiet Atlantic activity, the industry was overwhelmed from a lack of preparedness for such a severe hurricane loss. In the wake of Andrew's devastation, nine companies became insolvent (Towers Watson 2013), leading to a demand for comprehensive hurricane modeling solutions.

Andrew served as the catastrophe modeling industry's first major opportunity to learn from a real-time hurricane and helped define the present-day hurricane model framework. Discoveries from subsequent hurricanes have inspired expanded functionality. While Andrew and other landfalling hurricanes in the 1990s predominantly caused property damage with high winds, a number of hurricanes making landfall in the 2000s, including Ivan, Katrina, Ike, and Sandy, highlighted the importance of capturing loss associated with storm surge. Destructive storm surges caused by these events revealed difficulties in distinguishing between wind and surge damage in the settlement of insurance claims covering only wind damage. Even further still, Hurricane Harvey in 2017 demonstrated that a hurricane's main source of damage could be rainfall-induced inland flooding, rather than the more traditional sources of wind or storm surge. With each event, catastrophe modeling firms expand their archives of data that serve to calibrate, validate, and expand model functionality.

A considerable amount of external oversight ensures the scientific credibility of commercially available hurricane models, particularly in Florida, a U.S. state subject to high annual hurricane risk where insurance rates often permeate political discourse. As discussed previously, an insurance regulator seeks to protect a policyholder through key considerations. The Florida Office of Insurance Regulation (OIR) in part seeks to achieve this goal by relying heavily on the expertise of the FCHLPM to evaluate hurricane risk. Established in 1995, in response to the industry's adoption of hurricane catastrophe models following Hurricane Andrew, the FCHLPM sets standards to rigorously evaluate model methodologies used to calculate insurance premiums. FCHLPM rigorously reviews model methodologies and revises its standards by which it evaluates hurricane catastrophe models every two years. These revisions lead to a regular cycle of frequent updates that ensure a model's timeliness. For model vendors, FCHLPM standards are not mere suggestions; the Florida OIR requires that insurance companies use a catastrophe model certified by FCHLPM when filing insurance rates. Insurance regulators in other hurricane-prone states also survey catastrophe models for robustness but largely rely on the stringent FCHLPM process as an indicator of a model's capability.

In the years after Hurricane Andrew, the use of hurricane catastrophe models became standard practice for most of the re/insurance industry. The industry would not see such devastating losses again until the active 2004 and 2005 hurricane seasons. RMS calculates that insured losses from the 2004 to 2005 hurricanes, trended to 2017, total more than two times the insured loss incurred during Hurricane Andrew, trended in the same manner. However, only one insured company failed under the weight of these losses (Grace and Klein 2009), demonstrating the powerful impact of models on the re/insurance industry's catastrophe preparedness.

1.4 Contemporary Catastrophe Modeling

A vast majority of catastrophe models – whether built for hurricanes, earthquakes, or other perils – follow the same basic framework and include the same components, as illustrated in Fig. 1.2 below.

Each model contains "stochastic" events (1) – a suite of thousands of simulated, physically realistic events designed to expand upon a limited historical data record. This step effectively attempts to negate the aforementioned issue of a short historical record, as the historical record does not provide enough years to sufficiently calculate return periods required by re/insurers and regulators. An important point to note here is that, although the Atlantic hurricane record is shorter than would be ideal, it is much longer and more robust than any other tropical cyclone record for any other basin worldwide; in actuality, HURDAT2 is likely by far the most comprehensive historical record of any natural climate peril that has potentially catastrophic impacts for the re/insurance industry. Thus, these techniques are applicable, and often deemed necessary, for many other extreme perils.

Thus, modelers use statistical techniques to extrapolate the historical record, generating a set of stochastic storm tracks from genesis to lysis with similar characteristics and parameters to past hurricanes. Stochastic storms realistically fluctuate in strength with changes in sea surface temperature while over water and weaken while over land. The modelers' aim is to represent the full distribution of hurricanes that could realistically occur, including hurricanes of intensity or landfall location that have yet to occur.

In catastrophe modeling, "hazard" (2) refers to the means by which a stochastic event can cause damage to each location in a re/insurance portfolio. Commercially available hurricane models measure hazard in the form of high winds, at a minimum, but some also measure storm surge and rainfall-driven flood depths. Much like stochastic track modeling, hazard modeling creates a realistic wind field for each stochastic event based upon observed relationships of parameters (e.g. maximum wind, radius of maximum wind, shape parameters) that defined historical wind fields. As a stochastic event's wind field crosses over land, models approximate wind speeds experienced at the surface through the consideration of man-made or natural friction. This translation occurs at grid cells that span the entire over-land

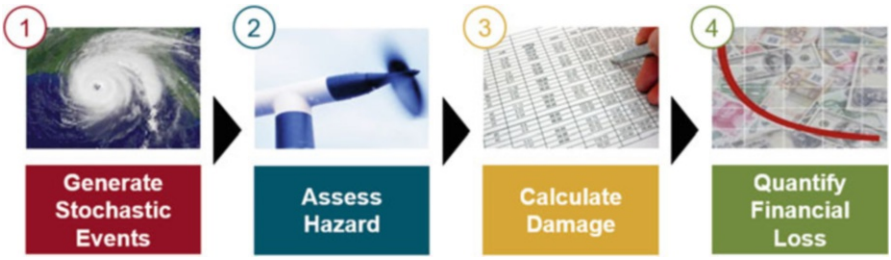

Fig. 1.2 Typical catastrophe model framework. (Image provided by RMS)

domain. Data identifying the local and upstream land use and topography at each cell can inform modelers on the degree to which surface winds should slow down or accelerate, relative to speeds at upper levels. Thus, models can assign surface winds incurred at each property within a re/insurer's portfolio.

Among the commercially available hurricane models, hydrodynamical or statistical modeling evaluates the buildup of storm surge caused by a hurricane's wind stress. Ground elevation and local flood defense data helps define the extent of storm surge inundation as water crosses the shoreline. Model users can further enhance storm surge modeling with property-specific flood mitigation information (e.g. stilts or sea walls).

The susceptibility to property damage caused by a specific hazard is commonly referred to as a structure's "vulnerability" (3), which varies at each property according to its underlying structural components. The most common components that determine a building's vulnerability include:

- Construction type: The material used to construct the building's exterior (e.g. wood, concrete), including possible reinforcement. During hurricanes, concrete and steel buildings tend to perform better than wood and light metal buildings.
- Occupancy type: The building's primary use (e.g. residential, commercial, industrial), used to indicate the predominant type and sensitivity of contents stored within the building.
- Number of stories: The building's height. For example, taller buildings tend to be built to rigid structural standards.
- Year of construction: A building's date of construction typically indicates the standards to which it was built, as catastrophe modelers document historical changes in local and regional building codes over time.
- Floor area: The size of the building's physical footprint. Larger buildings typically tend to be built to better standards than smaller buildings.

Catastrophe models contain relationships, typically stored in "vulnerability curves," that relate wind speeds and storm surge depths to average damage levels, and an uncertainty around that average, for combinations of the aforementioned components.

A number of data sources inform the vulnerability curves embedded within catastrophe models. In some countries and regions, modelers have collected insurance claims that represent billions of dollars in insured losses from past hurricanes. These claims, when used in conjunction with reconstructions of historical hurricane wind and storm surge fields, serve as the "gold standard" in building vulnerability curve relationships. In areas where insurance claims may be unavailable, engineering studies and building codes provide indications of expected amounts of damage.

Although an increasing volume of claims data collected across a number of past hurricanes and varying wind speeds can improve the accuracy of a vulnerability curve, the robustness of damage estimates relies upon the catastrophe model user's understanding of each building. In general, a more complete account of every structure at risk increases the damage estimate accuracy. In some cases, users collect

detailed structural data from engineering reports, including features installed to mitigate hurricane damage (e.g. wind shutters, wind-resistant glass panes).

In a final step, financial algorithms translate damage levels into loss (4) incurred at each property and accumulate this loss for the entirety of a company's insurance portfolio. This final step produces a loss distribution, one for each stochastic event, for every property in an insurance portfolio.

These losses constitute a loss distribution, called an exceedance probability (EP) curve, that defines the probability of annual catastrophe losses exceeding loss thresholds. These distributions can define loss probabilities associated with a single event or multiple events in a given year.

Several risk metrics that insurance and reinsurance companies use in their business processes are drawn directly from EP curves. These metrics include:

- Average annual loss (AAL) – the expected value of the loss distribution or, in other words, the average expected loss per year to an asset over the long term. The AAL is frequently used in pricing algorithms that calculate the policy premium charged by an insurer. Since the AAL represents only an average, the actual annual losses will fluctuate around this value in any given year, including years with no losses whatsoever.
- A return period, which corresponds to a point on the EP curve, relating a financial loss to its probability of exceedance in a single year. Each return period is defined as a number of years that is the reciprocal of each loss probability. For example, a 10-year return period corresponds to a loss with a 10% probability of exceedance in 1 year, a 100-year return period with a 1% probability, and a 1000-year with a 0.1% probability. The larger the return period, the higher the loss. These long return periods typically indicate losses to a company's portfolio caused by the severest of catastrophes.

To construct an exceedance probability curve, a catastrophe model must define the likelihood with which stochastic events and their associated losses are expected to occur over time. Loss metrics highly depend on how often events are expected to occur. For example, a loss distribution's AAL would be expected to increase with an increase in hurricane frequency: more landfalling hurricanes each year would increase annual re/insurance losses. Thus, event frequency plays a critical role in the output of a catastrophe model and the use of this output by the insurance industry in business decisions.

1.5 Building a View of Atlantic Hurricane Frequency Risk

Choosing the most appropriate view of hurricane event frequency, however, perhaps remains one of the most contentious and debatable issues in catastrophe modeling. A limited, uncertain history and a continually changing climate open up a number of possible ways to represent frequency risk.

An examination of historical hurricane observations over the past century or more reveal periods lasting up to a few decades of Atlantic basin hurricane frequency higher and lower than the historical average (Goldenberg et al. 2001). The 2004–2005 seasons remain notable in the insurance industry not only for their catastrophic losses, but also for calling the re/insurance industry's attention to the heightened state of Atlantic hurricane activity in the late 1990s and early 2000s. As mentioned earlier, the industry began adopting catastrophe models in the final years of a prolonged period of below average Atlantic hurricane genesis and landfalls.

Up until 2004–2005, catastrophe modelers offered only one view of event frequency in hurricane models: a long-term, historical average. However, this average ignores potential medium-term and multidecadal trends in hurricane activity that may well be of significant interest to re/insurers due to the previously mentioned desire for an outlook that covers the period approximately 5–10 years ahead. Therefore, there is demand for models to consider this multi-annual variability in hurricane frequency.

Multiple theories within the peer-reviewed literature, sometimes conflicting, attempt to connect climatological influences with fluctuations in the mean frequency state. The literature most commonly ties multidecadal trends in cyclogenesis to influence from sea surface temperatures and the Atlantic Multidecadal Oscillation (Goldenberg et al. 2001; Sutton and Hodson 2005), but research describing their impact on hurricane steering and landfall patterns remains less mature (Wang et al. 2011; Kossin 2017). Hindsight allows for modelers to draw correlations between climate indices and historical frequency fluctuations, yet uncertainty exists in forecasting and anticipating future fluctuations (Klotzbach et al. 2015). Less certain are the potential impacts of longer-term climate change on hurricane frequency and severity (Landsea 2005; Emanuel 2005; Webster et al. 2005; Hoyos et al. 2006; Mann and Emanuel 2006; Knutson et al. 2010).

This section will thus focus on summarizing current approaches and debates ongoing within the insurance and catastrophe modeling industries surrounding this topic, in the hope that it will enable the scientific community to become better aligned in order to have direct impacts to these modes of thinking.

1.5.1 Long-Term View

A long-term view represents the viewpoint that current risk can reasonably be assumed stationary, operating around a mean frequency calculated from a significant period of the historical record. This behavior is defined as the observed average of hurricane landfall position and intensity over the most reliable period of past hurricane data. Modelers will commonly count historical hurricane landfalls and intensity in segments of less than 100 miles that divide a country's coastline. A long-term view of frequency risk is calibrated and validated on the resulting landfall distribution.

A vast majority of models construct this average from HURDAT2 data (Jarvinen et al. 1984; Landsea and Franklin 2013) beginning in 1900, a point at which confidence in hurricane landfall information significantly increases. Thus, a long-term view is built from over 100 years of available storm track and intensity data. Confidence in open-water hurricane data in the North Atlantic basin does not extend back as far and begins with the advent of aircraft and satellite reconnaissance in the 1950s and 1960s.

As the HURDAT2 database typically provides historical hurricane intensity measurements in six-hourly increments, track points rarely coincide with a storm's landfall. At present, HURDAT2 assigns specific landfall intensity measurements to only a subset of historical storms. This opens up a number of potential methods of determining the intensity of a tropical cyclone as it crosses a landfall segment. Common methods include drawing from the six-hourly observation point prior to landfall or an interpolation of the observations before and after landfall. A hurricane catastrophe model must also include the loss contribution of bypassing storms (those that cause damaging onshore winds but do not physically make landfall) to capture the full distribution of possible hurricane losses. A modeler's choice in intensity measurement therefore plays a critical role in understanding the construction of a long-term frequency view.

As mentioned previously, although one of the more robust historical datasets available across any geography and peril, a distribution of hurricane landfall location and intensity constructed from the HURDAT2 record cannot represent a complete view of current or future landfall risk. For example, in the United States, parts of the coastline exist where no past hurricanes have historically made landfall, and counts become sparser with increasing intensity. Calibrating a long-term view of the future solely on the historical record introduces potential overfitting to data; a segment with no recorded landfalls since 1900 remains at risk to a future landfall. Modelers therefore use varying techniques to spatially distribute regional landfall counts in a manner that preserves relative risk by segment but also assigns risk to segments with no historical landfalls. Stochastic events in a hurricane model are tuned to occur with a frequency to meet this final distribution.

As an average over this relatively long period, long-term projections of frequency risk and insured loss should not change significantly (i.e. a few percent) annually on a national or regional basis with the additions of future seasons to the record. Some in the insurance industry appreciate the relative stability provided by a long-term view as the historical record expands with time based on the perceived business benefits it can provide, as mentioned previously in this chapter.

1.5.2 Near-Term View

That being said, there are others that believe that varying their view from this long-term history is more likely to capture the potential activity of the near future. This has

resulted in alternative views of frequency risk being built, often called near-term views.

Seeking to address the re/insurance industry's concern about a period of potentially higher-than-average Atlantic basin activity, catastrophe modelers solicited opinions from the global insurance industry following the destructive 2004–2005 hurricane seasons. Much of the feedback sought to strike the proper balance between scientific insight and premium price stability. Many re/insurance contract renewals occur in January but forecasts of an upcoming season's activity typically lack significant skill at this point. Furthermore, changes in inter-annual climate influences (e.g. ENSO) may lead to substantial changes in hurricane activity year over year (Sabbatelli and Mann 2007). A hurricane model tuned to such changes could produce largely varying losses for the same insurance contracts each year and thus introduce price instability.

In 2006, catastrophe modelers introduced these solutions addressing the heightened hurricane risk to the market. Two prominent approaches emerged:

- One approach follows the long-term average method but limits the historical record to a subset of hurricane seasons featuring above-average sea surface temperatures. While the use of historical data introduces stability, this approach reduces an already statistically limited dataset and may overlook potential trends in future activity not fully evident in this dataset.
- A second approach attempts to independently forecast future medium-term activity, relative to the long-term average, based on the influence of the current climate state. Although this approach is more responsive to present-day and future changes in climate, this responsiveness may introduce changes to risk metrics that are larger and more frequent than a view of risk based on historical data.

This second approach aims to capture the interaction of hurricanes and climate variability in a way that can then be used to quantify hurricane risk for the insurance and reinsurance market.

Much of the discussion in the scientific community regarding hurricane variability in the Atlantic basin focuses on storm counts. For this to be of real value to the re/insurance industry, it must be translated into an estimation of potential loss. The nature of landfalling hurricanes, their locations, and likely intensities needs to be captured and, thus, the impact of climate variability on the spatial distribution of hurricanes is particularly important.

A challenge facing catastrophe modelers when considering a near- to medium-term view of risk is to assess whether any of the proposed drivers of hurricane variability can be incorporated into a catastrophe model, how this can best be achieved, and, most importantly, if it will add value to the resulting assessment of risk.

When considering whether to include a driver or not, the two key points need to be addressed.

1. What is the consensus within the scientific community? There are many different theories to explain the variability in hurricane activity in the Atlantic, with some attracting much more agreement than others.

As an example, RMS has chosen sea surface temperatures (SSTs) as one of the proxies for climate variability when making predictions for hurricane risk in a near-term view. This is in large part due to the depth of the discussion regarding fluctuations in SSTs and their impact on Atlantic hurricane activity. In addition, raised SSTs have been repeatedly linked to both the frequency and severity of events (Webster et al. 2005; Elsner and Jagger 2006; Hoyos et al. 2006; Mann and Emanuel 2006; Elsner et al. 2008; Saunders and Lea 2008). There is also research into mechanisms through which increased SSTs in the Pacific Ocean can inhibit hurricane activity in the Atlantic (Vecchi and Soden 2007; Swanson 2008; Vecchi et al. 2008).

A major factor when evaluating hurricane risk in the near- to medium-term, therefore, is how the SSTs in both the Atlantic and Pacific Oceans are expected to behave over the relevant time-period. By using SSTs as one of the inputs to run the stochastic model described earlier, it is possible to create multiple sets of stochastic events, with each set representing an alternative forecast of the SSTs under different scenarios driven by the various theories. These can then be combined to create an overall view of risk.

2. Is the predictability of the driver sufficient, and with appropriate lead-time, for it to be used in a forecast for the insurance industry?

ENSO provides an interesting example of a pattern of climatic variability whose impact on hurricanes is well known, but nevertheless creates a challenge for catastrophe modelers. ENSO is described as having a positive phase, 'El Niño', which is defined by anomalously warm SSTs in the eastern equatorial Pacific Ocean, and a negative phase, 'La Niña', when the SSTs in the eastern equatorial Pacific Ocean are colder than usual. A review of historical records has shown a link between ENSO and tropical cyclone activity in the Atlantic, with El Niño phases typically corresponding to a decrease in Atlantic hurricane counts, and conversely, La Niña events are related to an increase (Gray 1984; Bove et al. 1998).

It is also possible to seasonally forecast ENSO with at least moderate skill (Barnston et al. 2012), and it is a major factor considered when producing seasonal forecasts of hurricane activity. Skillful forecasts, however, are extremely difficult more than a few months in advance of the hurricane season (Lloyd-Hughes et al. 2004), by which point work on most re/insurance renewals will already be well underway, if not fully completed. It is therefore not possible to explicitly include ENSO when creating a forecast for use within the re/insurance industry. Its link to hurricane activity is widely recognized, however, that catastrophe modelers endeavor to find a way to consider it somehow.

One approach is to consider the timescale of ENSO; as a short timescale phenomenon, it lasts for 1 or 2 years at irregular 2 to 7-year intervals. By producing a view of risk for a 5-year period, a complete cycle of ENSO is likely to occur within

this time, alternating between phases of suppressed and enhanced hurricane activity. Hurricane variability over this period can therefore be captured independently of ENSO, removing the need to forecast it explicitly.

Given fundamental uncertainties that exist in explicit forecast data, however, alternatives to using SST forecasts to drive near-term views of the risk have been investigated. One simplistic approach, using only general knowledge about current (and most likely future) climate has been to subset the historical data to just include hurricane statistics from hurricane seasons that have seen warmer than average SSTs – given that climate change will likely cause warming into the future – and thus to create a stochastic set from these data. This has the upside that it is not beholden to any scientific narrative other than a well-understood climate change narrative, but its downside is that it assumes that sea surface temperature is the sole key driver of variability in hurricane activity. In addition, its simplicity may mean that much information is lost from the cool-SST half of the catalogue.

1.5.3 Alternative View

So far, we have only discussed frequency risk from a traditional re/insurance perspective, which has given rise to the above discussion surrounding the need for a multi-year perspective of the risk. As mentioned earlier in the chapter, however, there is increasing investment by the industry to find more creative and innovative ways to produce risk transfer solutions that may be able to utilize potentially skillful forecasts at numerous lead times. This innovation has primarily been driven by a large amount of available capital in the market looking for better returns on investments in what has been a soft market environment over the past few years.

One such mechanism for alternative risk transfer is via Insurance-Linked Securities (ILS), which are effectively financial instruments to transfer risk into alternative markets – most importantly, into ones that don't require a capital structure that a traditional re/insurer has to take due to regulation. This opens up investment from many alternative sources, with one class of ILS being particularly topical when discussing hurricane risk: the catastrophe (or cat) bond market.

Cat bonds are typically high risk, high reward products that exist in order for re/insurers to shift risk of extreme losses off their books, and are often based on much more simplistic processes than traditional re/insurance and catastrophe modeling. These bonds can be based on simple triggers such as: number of events; number of landfalls; losses exceed a certain figure; or, in reality, any theoretical trigger that can be held to account in practice. In the event that a catastrophe occurs, the bonds pay to the re/insurance company, but if not, investors can expect high rates of return. It is expected that, with the catastrophic events of 2017s Q3 causing around $100 billion of total insured loss, the alternative capital market may be picking up approximately $25 billion of that loss (Artemis 2017), a much larger proportion than has ever been seen in history. This area is therefore ripe for research as to how

best structure these alternative risk covers and how to most appropriately use scientific predictions. The fact that the securities can be structured to be sold and paid within days means the issue of appropriate time horizons discussed above may well disappear in the future, and the question may eventually be reversed – instead of "how can scientific research be best directed to fit to re/insurance timeframes", the question may become "how can ILSs be appropriately structured to best utilize scientific information". Whether ILS, and cat bonds specifically, will remain relatively stable and attractive propositions for investors, however, remains to be seen, and it is therefore strongly encouraged that both questions are investigated by research and industry communities alike.

1.6 Catastrophe Models and Climate Change

As discussed in the previous sections, the definition of "current" hurricane risk can differ in catastrophe models produced by different companies. A changing climate compounds the challenge of representing the "current" risk, given evidence of change that has already occurred and projections of change that is yet to occur.

While long-term and near-term views seek to address current hurricane frequency risk, commercial catastrophe models incorporate present-day effects of climate change where evidence is most certain. For example, most hurricane models calculate storm surge risk based on the most recent sea levels, thus incorporating climate change to date. In contrast, historic average sea levels would fall below present levels; all other things being equal, use of historic levels would underestimate the financial risk of storm surge.

Few, if any, commercial catastrophe models are specifically designed to represent the potential impacts of mid- to end-of-century climate change on Atlantic hurricane risk, which are far more uncertain. Any approach to include the impact of future, long-term climate change would need to consider the consequences of a warmer world beyond simply hurricane frequency and intensity, including changes in sea levels and the spatial distribution of hurricane landfalls, among other effects. Multiple studies, however, have used catastrophe models or similar methods as tools to explore these potential impacts by combining a catastrophe model with projections of the future climate.

Such projects of this nature include:

- The Risky Business project in 2014 looked at the impacts of climate change on the U.S. economy using a version of the RMS North Atlantic Hurricane Models, modified to account for both increased sea levels and hurricane landfalls, to estimate expected damages under Intergovernmental Panel on Climate Change scenarios (Hsiang et al. 2017; Houser et al. 2014; Kopp et al. 2014). The results of this study were later used by the U.S. Congressional Budget Office to understand the implications of increases in hurricane damages for the federal budget (Dinan 2016; Dinan 2017).

- As part of the World Bank's Pacific Catastrophe Risk Assessment and Financing Initiative, an AIR Worldwide tropical cyclone model, modified based on the output from 11 general circulation models provided by Geoscience Australia, was used to assess how changing tropical cyclone risk would impact 15 Pacific islands (Lloyd's 2014).
- The UK Met Office and AIR Worldwide collaborated on an Association of British Insurers report to measure the impact of global temperature increases on the UK insurance industry, specifically as it related to several domestic and international natural perils (Robinson et al. 2017).

These studies address public policy concerns and typically reflect the longer timescales common in climate change studies. However, as discussed previously, these timescales typically exceed the timescales currently evaluated by the re/insurance industry for business planning. Thus, catastrophe modeler involvement in climate change research remains limited to these preliminary studies at present.

1.7 Conclusions

In a perpetual effort to illustrate the "current" hurricane risk facing the insurance industry, commercial catastrophe models will continue to evolve as the effects of a changing climate unfold. Although tropical cyclones already cause the largest annual insured losses of any natural peril, the effects of a warmer world may serve to make these losses more frequent or severe. The calculation of these losses will consider data gathered from future landfalling Atlantic hurricanes, in the same way that hurricanes like Ike, Sandy, and Harvey inform present-day catastrophe models. Each future hurricane serves as an opportunity to add a data point to a statistically limited record. As the debate between long-term and near-term views of frequency risk continues, catastrophe modelers and re/insurers will no doubt pay attention to this expanding record to determine which view best represents the industry's "current" hurricane risk.

References

Artemis (2017) Another large loss year could test ILS permanence. http://www.artemis.bm/blog/2017/11/24/another-large-loss-year-could-test-ils-permanence-kurt-karl-swiss-re/. Accessed 15 Dec 2017

Barnston AG, Tippett MK, L'Heureux ML, Li S, DeWitt DG (2012) Skill of real-time seasonal ENSO model predictions during 2002–11: is our capability increasing? Bull Am Meteorol Soc 93:631–651. https://doi.org/10.1175/BAMS-D-11-00111.2

Bove MC, O'Brien JJ, Eisner JB, Landsea CW, Niu X (1998) Effect of El Niño on U.S. landfalling hurricanes, revisited. Bull Am Meteorol Soc 79:2477–2482. https://doi.org/10.1175/1520-0477(1998)079<2477:EOENOO>2.0.CO;2

Briys E, Joos de ter Beerst D (2006) The Zaccaria deal: contract and options to fund a genoese shipment of alum to bruges in 1298. Paper presented at the XIV International Economic History Congress, Helsinki, August 2006

Caron LP (2017) The copernicus climate change service: perspective from the insurance industry. Consorseguros Digital. http://www.consorsegurosdigital.com/almacen/pdf/the-copernicus-climate-change-service-perspective-from-the-insurance-industry.pdf. Accessed 12 Dec 2017

Dinan T (2016) Potential increases in hurricane damage in the United States: implications for the Federal Budget. https://www.cbo.gov/publication/51518. Accessed 15 Dec 2017

Dinan T (2017) Projected increases in hurricane damage in the United States: the role of climate change and coastal development. Ecol Econ 138:186–198. https://doi.org/10.1016/j.ecolecon.2017.03.034

Elsner JB, Jagger TH (2006) Prediction models for annual U.S. hurricane counts. J Clim 19:2935–2952. https://doi.org/10.1175/JCLI3729.1

Elsner JB, Kossin JP, Jagger TH (2008) The increasing intensity of the strongest tropical cyclones. Nature 455:92–95. https://doi.org/10.1038/nature07234

Emanuel KA (2005) Increasing destructiveness of tropical cyclones over the past 30 years. Nature 436:686–688. https://doi.org/10.1038/nature03906

Goldenberg SB, Landsea CW, Mestas-Nunez AM, Gray WM (2001) The recent Increase in Atlantic hurricane activity: causes and implications. Science 293:474–479. https://doi.org/10.1126/science.1060040

Grace MF, Klein RW (2009) The perfect storm: hurricanes, insurance, and regulation. Risk Manag Ins Rev 12:81–124. https://doi.org/10.1111/j.1540-6296.2009.01155.x

Gray WM (1984) Atlantic seasonal hurricane frequency Part I: El Niño and 30 mb Quasi-Biennial oscillation influences. Mon Wea Rev 112:1649–1668. https://doi.org/10.1175/1520-0493(1984)112<1649:ASHFPI>2.0.CO;2

Halley E (1693) An estimate of the degrees of the mortality of mankind, drawn from curious tables of the births and funerals at the city of Breslaw; with an attempt to ascertain the price of annuities upon lives. Phil Trans R Soc London 17:596–610. https://doi.org/10.1098/rstl.1693.0007

Holland DM (2009) A brief history of reinsurance. Reins News (Sp. ed.) 65: 4–29

Houser T, Kopp R, Hsiang S, Delgado M, Jina A, Larsen K, Mastrandrea M, Mohan S, Muir-Wood R, Rasmussen DJ, Rising J, Wilson P (2014) American climate prospectus: economic risks in the United States. Rhodium Group, New York

Hoyos CD, Agudelo PA, Webster PJ, Curry JA (2006) Deconvolution of the factors contributing to the increase in global hurricane intensity. Science 312:94–97. https://doi.org/10.1126/science.1123560

Hsiang S, Kopp R, Jina A, Rising J, Delgado M, Mohan S, Rasmussen DJ, Muir-Wood R, Wilson P, Oppenheimer M, Larsen K, Houser T (2017) Estimating economic damage from climate change in the United States. Science 356:1362–1369. https://doi.org/10.1126/science.aal4369

Huygens C (1657) De ratiociniis in ludo aleae. In: van Schooten F (ed) Exercitationum mathematicarum. Johannis Elsevirii, Leiden, pp 517–534

Jarvinen BR, Neumann CJ, Davis MAS (1984) A tropical cyclone data tape for the North Atlantic basin, 1886–1983: contents, limitations, and uses. Memo NWS NHC, NOAA 22: 24pp

Jones AR, Copeman PJ, Gibson ER, Line NJS, Lowe JA, Martin P, Matthews PN, Powell DS (2006) A change agenda for reserving. Report of the general insurance reserving issues taskforce (GRIT). Brit Actuar J 12:435–599. https://doi.org/10.1017/S135732170000461X

Klotzbach P, Gray W, Fogarty C (2015) Active Atlantic hurricane era at its end? Nat Geophys 8:737–738. https://doi.org/10.1038/ngeo2529

Knutson TR, McBride JL, Chan J, Emanuel K, Holland G, Landsea C, Held I, Kossin JP, Srivastava AK, Sugi M (2010) Tropical cyclones and climate change. Nat Geophys 3:157–163. https://doi.org/10.1038/ngeo779

Kopp RE, Horton RM, Little CM, Mitrovica JX, Oppenheimer M, Rasmussen DJ, Strauss BH, Tebaldi C (2014) Probabilistic 21st and 22nd century sea-level projections at a global network of tide-gauge sites. Earth Future 2:383–406. https://doi.org/10.1002/2014EF000239

Kossin JP (2017) Hurricane intensification along United States coast suppressed during active hurricane periods. Nature 541:390–393. https://doi.org/10.1038/nature20783

Kunreuther H, Miller L (1985) Interactive computer modeling for policy analysis: the flood hazard problem. Water Resour Res 21:105–113. https://doi.org/10.1029/WR021i002p00105

Landsea CW (2005) Meteorology: hurricanes and global warming. Nature 438:E11–E12. https://doi.org/10.1038/nature04477

Landsea CW, Franklin JL (2013) Atlantic hurricane database uncertainty and presentation of a new database format. Mon Weather Rev 141:3576–3592. https://doi.org/10.1175/MWR-D-12-00254.1

Lloyd's (2008) Annual underwriter survey results 2008. https://www.lloyds.com/~/media/lloyds/reports/annualunderwritersurveyresults2008.pdf. Accessed 12 Dec 2017

Lloyd's (2014) Catastrophe modelling and climate change. https://www.lloyds.com/news-and-insight/risk-insight/library/natural-environment/catastrophe-modelling-and-climate-change. Accessed 15 Dec 2017

Lloyd-Hughes B, Saunders MA, Rockett P (2004) A consolidated CLIPER model for improved August September ENSO prediction skill. Weather Forecast 19:1089–1105

Mann M, Emanuel K (2006) Atlantic hurricane trends linked to climate change. Eos 87:233–241. https://doi.org/10.1029/2006EO24000

Robinson E, Cipullo M, Sousounis P, Kafali C, Latchman S, Higgs S, Maisey P, Mitchell L (2017) UK windstorms and climate change. https://www.abi.org.uk/globalassets/files/publications/public/property/2017/abi_final_report.pdf. Accessed 12 Mar 2018

Sabbatelli TA, Mann ME (2007) The influence of climate state variables on atlantic tropical cyclone occurrence rates. J Geophys Res 112:D17114. https://doi.org/10.1029/2007JD008385

Saunders MA, Lea AS (2008) Large contribution of sea surface warming to recent increase in Atlantic hurricane activity. Nature 451:557–560. https://doi.org/10.1038/nature06422

Sutton RT, Hodson DLR (2005) Atlantic ocean forcing of North American and European summer climate. Science 309:115–118. https://doi.org/10.1126/science.1109496

Swanson KL (2008) Nonlocality of Atlantic tropical cyclone intensities. Geochem Geophys Geosyst 9:Q04V01. https://doi.org/10.1029/2007GC001844

Swiss Re (2018) sigma No 1/2018. http://institute.swissre.com/research/overview/sigma/1_2018.html. Accessed 25 Jun 2018

Towers Watson (2013) Hurricane Katrina: analysis of the impact on the insurance industry. https://biotech.law.lsu.edu/blog/impact-of-hurricane-katrina-on-the-insurance-industry-towers-watson.pdf. Accessed 13 Dec 2017

Trennery CF (1926) The origin and early history of insurance, including the contract of bottomry. P. S. King & Son Ltd., London, pp 5–8

van Schooten F (1657) Exercitationum Mathematicarum. Johannis Elsevirii, Leiden

Vecchi GA, Soden BJ (2007) Increased tropical Atlantic wind shear in model projections of global warming. Geophys Res Lett 34:L08702. https://doi.org/10.1029/2006GL028905

Vecchi GA, Swanson KL, Soden BJ (2008) Whither hurricane activity? Science 322:687–689. https://doi.org/10.1126/science.1164396

Wang C, Liu H, Lee S-K, Atlas R (2011) Impact of the Atlantic warm pool on United States landfalling hurricanes. Geophys Res Lett 38:L19702. https://doi.org/10.1029/2011GL049265

Webster PJ, Holland GJ, Curry JA, Chang HR (2005) Changes in tropical cyclone number and intensity in a warming environment. Science 309:1844–1846. https://doi.org/10.1126/science.1116448

Chapter 2
Global Tropical Cyclone Damage Potential

Greg J. Holland, James M. Done, Rowan Douglas, Geoffrey R. Saville, and Ming Ge

Abstract An approach to assessing the damage potential of tropical cyclones (TCs) is developed using a combination of physical reasoning and results of previous studies. The key TC damage parameters of intensity, size, and translational speed are incorporated into a single index of Cyclone Damage Potential (CDP). The CDP is developed to represent offshore wind, wave, and current damage. Further testing is needed to establish the importance of each TC parameter for onshore wind and coastal surge damage. The CDP is applicable to individual TCs and to seasonal, global, and climatological assessments. Global climatological summaries reveal high damage potential pathways and the dominant contribution of the Northwest Pacific to total global damage potential. Assessing actual impact requires an additional step of combining the CDP with an exposure and vulnerability assessment derived from a range of local factors.

Keywords Tropical cyclones · Impact indices · Potential damage

G. J. Holland (✉) · J. M. Done
National Center for Atmospheric Research, Boulder, CO, USA

Willis Research Network, London, UK
e-mail: gholland@ucar.edu; done@ucar.edu

R. Douglas · G. R. Saville
Willis Towers Watson, London, UK
e-mail: rowan.douglas@willistowerswatson.com; Geoffrey.Saville@willistowerswatson.com

M. Ge
National Center for Atmospheric Research, Boulder, CO, USA
e-mail: mingge@ucar.edu

J. M. Collins, K. Walsh (eds.), *Hurricane Risk*, Hurricane Risk 1,
https://doi.org/10.1007/978-3-030-02402-4_2

2.1 Introduction

There is a growing need for objective and timely information on the damage caused by tropical cyclones (TCs) for both response and planning purposes. This has led to the development of a number of indices that estimate the potential for TCs to cause damage (hereafter damage potential) from available TC data. Such indices include (Table 2.1): the Saffir-Simpson Scale (SSS, Simpson and Riehl 1981); the Power Dissipation Index (PDI, Emanuel 2005); the Kantha (2006) Hurricane Intensity Index (HII), and Hurricane Hazard Index (HHI); the Hurricane Severity Index (HSevI, Hebert and Weinzapfel 2006); the Chicago Mercantile Exchange Hurricane Index, formerly Carvill Hurricane Index (CHI, Smith 2010); and the Integrated Kinetic Energy (IKE, Powell and Reinhold 2007; Kozar and Misra 2014). Basin-wide summaries of seasonal TC activity that can be used as a basis for assessing damage potential include the Hurricane Destruction Potential (HDP, Gray and Landsea 1992), the Accumulated Cyclone Energy (ACE, Bell et al. 2000); and the Revised Accumulated Cyclone Energy (RACE, Yu et al. 2009).

As shown in Table 2.1, all indices use storm intensity in various forms: one uses just the maximum wind speed; six the maximum wind speed squared; and three use wind-speed cubed. Of these, six rely entirely on maximum wind speed, four include size in some form and one includes translation speed. These intensity relationships have been used in wind engineering (Pita et al. 2015), and to assess future changes in TC damage (Pielke 2007; Emanuel 2011; Schmidt et al. 2010).

The goal of this study is to develop an approach for assessing the damage potential of TCs that incorporates intensity, size, and wind duration, and is applicable individually, seasonally, and globally for a range of societal purposes. The resulting index of Cyclone Damage Potential (CDP) is based primarily on physical principles and utilizes only information readily available in the warnings from TC warning centers. It is developed to be applicable to offshore damage from wind, waves, and currents. For onshore direct wind and coastal surge damage, the relative importance of each parameter will differ, and the applicability of the CDP to onshore losses needs to be tested against suitable loss data. The CDP is not necessarily applicable to damage resulting from rainfall or to indirect damage such as business interruption or demand surge (Olsen and Porter 2011).

We emphasize that the CDP does not refer to actual damage in any specific circumstance. It is intended to provide easily understood indications of the relative damage potential for individual storms, or for collections of storms over, for example, basins and seasons. Actual impact assessment and prediction requires an assessment of exposure, E, and vulnerability, V, with a typical relationship being:

$$\text{Damage} = CDP \times E \times V \tag{2.1}$$

Exposure may be defined a number of different ways, such as population or the numbers or value of structures. Vulnerability may also be defined in various ways, such as the location of structures or population relative to the storm track, elevation,

Table 2.1 Existing TC damage indices and their major components

Index	Equation	Cyclone components included			Reference
		Max wind	Size	Translation	
Saffir Simpson Scale	None	✓	✗	✗	Simpson and Riehl (1981)
Power Dissipation Index	$PDI\alpha\sum_{6h} v_m^3$,	✓	✗	✗	Emanuel (2005)
Hurricane Destruction Potential	$HDP = \sum_{6h} v_m^2, v_m > 65kt,$	✓	✗	✗	Gray and Landsea (1992)
Accumulated Cyclone Energy	$ACE = 10^{-4}\sum_{6h} v_m^2.$	✓	✗	✗	Bell et al. (2000)
Hurricane Intensity Index	$HII = \left(\frac{v_m}{v_{m0}}\right)^2,$	✓	✗	✗	Kantha (2006)
Revised Accumulated Cyclone Energy	$RACE = 10^{-4}\sum_{6h} \frac{v_m^2}{r_c^2}\left(0.5 + \frac{r_c^{-0.2} - 1}{0.49}\right),$	✓	Partly	✗	Yu et al. (2009)
Integrated Kinetic Energy	$IKE = \int \frac{1}{2}\rho v^2 dV,$	✓	Partly	✗	Powell and Reinhold (2007)
Hurricane Severity Index	Look-up Table	✓	✓	✗	Hebert and Weinzapfel (2006)
CME Hurricane Index	$CHI = \left(\frac{v_m}{v_{m0}}\right)^3 + \frac{3}{2}\frac{R_h}{R_{h0}}\left(\frac{v_m}{v_{m0}}\right)^2,$	✓	✓	✗	Smith (2010)
Hurricane Hazard Index	$HHI = \left(\frac{R_h}{R_{h0}}\right)^2\left(\frac{v_m}{v_{m0}}\right)^3\left(\frac{v_{t0}}{v_t}\right),$	✓	✓	✓	Kantha (2006)

Here v is the wind speed, v_m is the maximum wind speed at 10 m above the surface, and v_{m0} is a wind scaling factor; r_c is the radial area over which the RACE is calculated and is derived from a relationship with v_m; ρ is air density; V is volume; R_h is the mean radius of hurricane force winds and R_{h0} is a scaling factor; v_t is the translation speed of the storm and v_{t0} is a scaling factor

topography that can act to channel winds into low-level jets (Walker et al. 1988), coastal bathymetry that can enhance or impede storm surge (e.g. Chavas et al. 2013), or structural response to downbursts and other factors creating streaks of enhanced damage (Pita and de Schwarzkopf 2016; Miller et al. 2013). In addition, prior TC experiences of the local population, TC warning time, and pre-landfall weather conditions may also affect local vulnerability. Assessing exposure and vulnerability across these multiple factors is beyond this study. In broad terms, the CDP can be used as a baseline from which to benchmark more detailed impact or damage assessments.

The data used are described in the next section. Details of the CDP development are then described in Sect. 2.3, followed by a demonstration of global historical CDP and the use of CDP in forecasting in Sect. 2.4.

2.2 Data

TC nomenclature varies substantially around the globe. Here, "TC" is used to refer to all named storms with maximum 1-min sustained wind speed >34 kt, and "hurricane" for all named storms with maximum 1-min sustained winds >64 kt. TC data are taken from the IBTrACS archive (Knapp et al. 2010), a compilation and standardization of 6-hourly archives from worldwide TC warning centers. Unfortunately, some World Meteorological Organization (WMO) designated TC warning centers do not archive size, despite this being included in the WMO standard for archives. For the North Atlantic, size is included using the mean radius of hurricane force winds obtained from US National Hurricane Center advisory archives collated by Demuth et al. (2006) and known as the Extended Best Track Dataset. The archive at the Joint Typhoon Warning Center (JTWC, http://www.usno.navy.mil/NOOC/nmfc-ph/RSS/jtwc/best_tracks/) is used for assessing size in the other TC basins.

The CDP components and full index are tested against the Willis Energy Loss Database (WELD, Willis, unpublished data 2009), an archive of losses to the offshore energy industry, including offshore and onshore physical property damage (platforms, rigs, pipelines, storage systems, refineries, loading terminals) and operator costs. Loss data are available for seven historical hurricanes that traversed the main rig area (Andrew 1992; Lili 2002; Ivan 2004; Katrina and Rita 2005; Gustav and Ike 2008) and are adjusted to 2008 values using the Chemical Engineering Plant Cost Index (Arnold and Chiltern 1963; Vatavuk 2002). The tracks of these hurricanes are shown in Fig. 2.1 together with the locations of offshore facilities.

Although the WELD data is limited to only seven storms, it has a key advantage in that the recorded damage occurred in a quasi-uniform distribution of facilities across the Northern Gulf of Mexico with roughly similar vulnerability characteristics. All hurricanes are therefore assumed to impact similar exposure and vulnerability, leaving damage differences attributable to TC parameters.

One source of potential error may arise from new facilities and increased production that has occurred over the period of the cyclone impacts used. From 1992

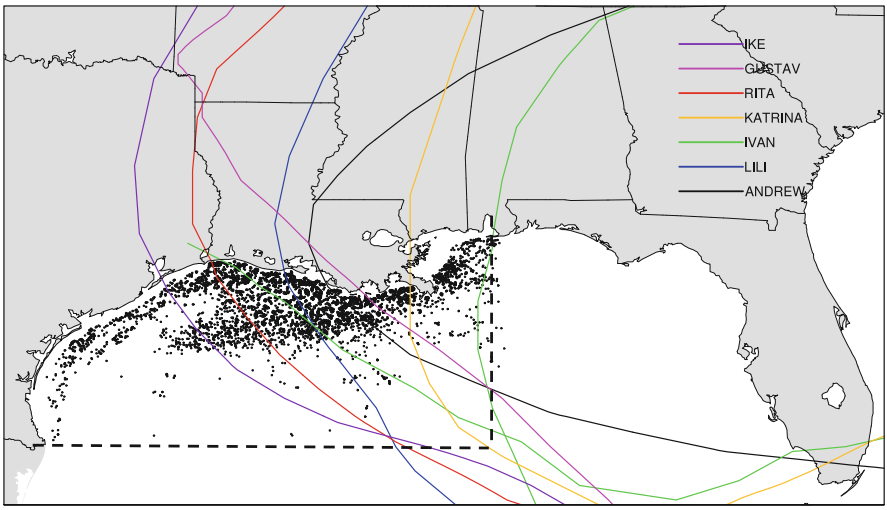

Fig. 2.1 Platform locations in the Gulf of Mexico as of 02/03/15 (black dots) and tracks of seven hurricanes for which offshore loss data are available (colored lines). Note that there are two tracks for Ivan as this hurricane passed through the region twice. Loss and hurricane analyses are done for the area between the dashed lines (26° N, 88° W) and the coast. (Data sources: Bureau of Ocean Energy Management, IBTrACS)

through 2003, oil production in the Gulf increased from approximately 23 million barrels per month to approximately 50 million barrels. After 2005, it declined to about 40 million barrels (U.S. Energy Information Administration, www.eia.gov). However, due to a lack of suitable data, we do not correct for change in exposure. It is likely that some of these changes may have stemmed from change in levels of operations at existing facilities. It is also likely that most of the damage referred to here came from older rigs that had been in place for substantial lengths of time.

2.3 The Cyclone Damage Potential Index

2.3.1 Selection of Parameters

That damage increases with cyclone intensity is well established (Geiger et al. 2016; Murnane and Elsner 2012). Cyclone intensity is emphasized in warnings, and intensity-based indices such as the Saffir-Simpson Scale (Simpson and Riehl 1981) are widely adopted.

It also is intuitively obvious that size can contribute to damage potential since a larger storm extends damaging winds over a larger area, and previous studies confirm this. Zhai and Jiang (2014) found using maximum wind speed and size together captures more variance in normalized TC losses than using maximum wind speed or size alone. Czajkowski and Done (2014) found TC size (in terms of radial

extent of strong winds) to be important in controlling the size of the impacted area, the duration of damaging winds, and the likelihood of wind directional change. Further examination by Done et al. (2018) found duration was only important for weaker TCs (peak wind speeds less than 95 knots). Size, in terms of the radius of closed isobar, also appears to correlate with rainfall extent (Matyas 2010).

Increasing damage with duration can arise from several factors, including increased ocean waves and currents, increased rainfall, fatigue, and flying debris. The longer gusty winds impact a structure, the more likely there will be a failure in a critical component due to fatigue. The potential for further catastrophic failure then increases rapidly with continuing wind duration. Airborne debris is a major cause of damage. The longer the wind blows, the more likely it is that debris will strike a vulnerable building component. The importance of duration and directional change in wind was demonstrated using insured losses (Done et al. 2018). Jain (2010) also found increased insurance losses for storm-strength wind-duration events >10 h compared to those of <10 h. For offshore losses, wind extent and duration (a combination of translation speed and size) drive ocean waves, and ocean currents that are a major influence on offshore damage (e.g., Holland 2012).

For storm surge, TC intensity and TC size correlate with surge height (Grinsted et al. 2012; Lin et al. 2012). TC size also correlates with areal coverage of surge (Rego and Li 2009). The effects of TC forward speed on surge are less clear. While linear theory and numerical simulations show that slower-moving storms dampen the peak surge height (Proudman 1953; Irish et al. 2008), there is evidence that slower moving storms drive larger volumes of water inland (Rego and Li 2009).

Having established the physical basis for incorporating intensity, size, and duration in the damage index, it is instructive to examine their relative importance for reproducing the observed damage from the WELD database (Fig. 2.2). Here, intensity is defined as the maximum 1-min mean wind speed anywhere in the cyclone at 10 m above the surface. We start by exploring linear correlations between damage and individual terms. Intensity variation, alone, has the weakest relationship with these losses ($R^2 = 0.23$, Fig. 2.2a), and similar results are found for the square or the cube of the maximum winds (not shown). Next in importance is the radius of hurricane winds ($R^2 = 0.48$, Fig. 2.2a). The inverse of the translation speed explains the majority of the variance in hurricane damage ($R^2 = 0.71$, Fig. 2.2b). This relative ordering is robust to removal of individual cyclones. However, there is a substantial correlation between size and translational speed ($R^2 = 0.52$ for the data in Fig. 2.2). Previous work has shown that this relationship is at least partly due to translational speed responding to size variations through asymmetrical circulations induced by the TC itself (known as the beta effect, Holland 1983).

We next explore relationships between combinations of terms and damage. Assuming that the inverse of the translation speed is a crude indicator of the duration of impact, then an indication of the importance of duration for both the maximum winds and surrounding damaging winds may be obtained by dividing the intensity and the hurricane extent by the translational speed. Including duration of the maximum winds explains 81% of the WELD damage variance compared to 23%

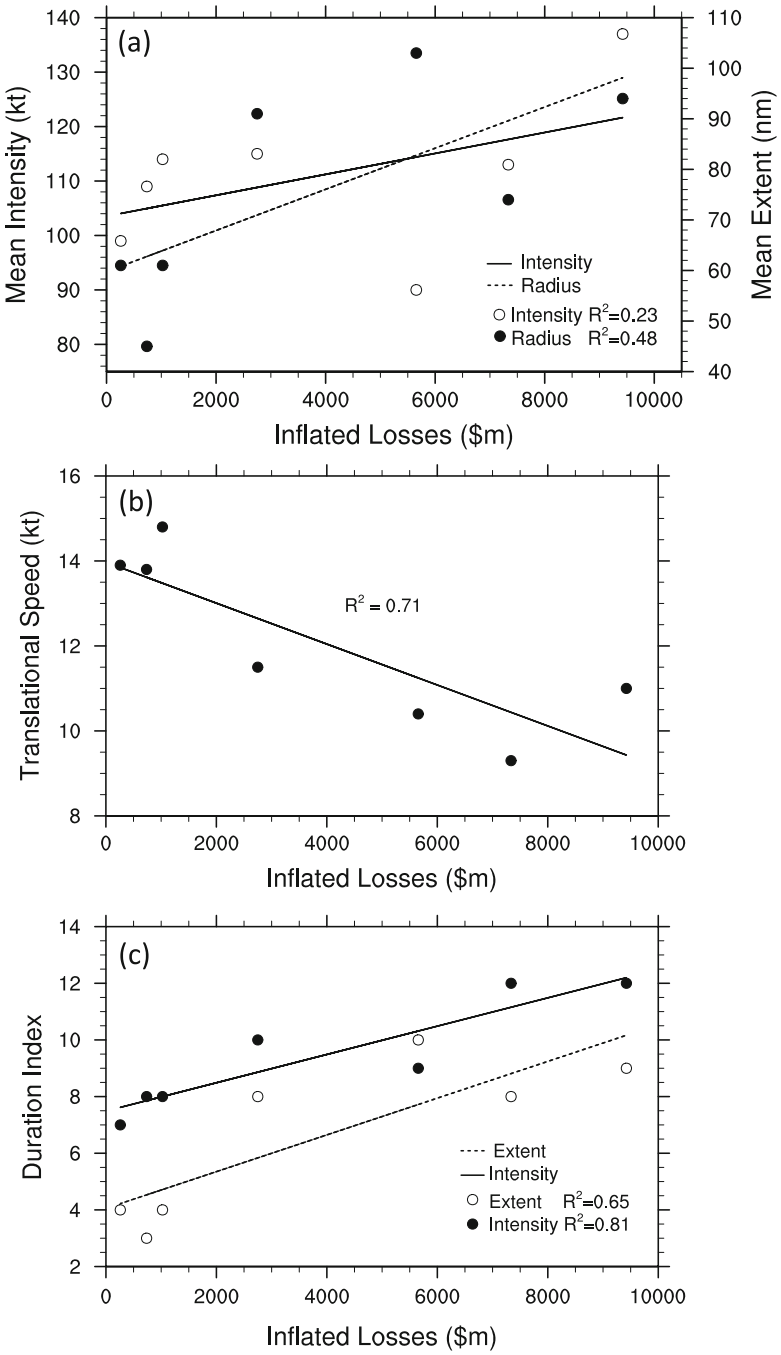

Fig. 2.2 Relationships between TC components and offshore insurance losses in the Gulf of Mexico: (**a**) mean maximum intensity and extent as defined by radius of hurricane winds, (**b**) mean translation speed, and (**c**) duration index for intensity and extent. Means are over all 6-hourly hurricane data points in the region shown in Fig. 2.1. Linear lines of best fit and variance explained are also indicated

for intensity alone (Fig. 2.2c). Adding duration to the extent of hurricane winds increases the linear variance explained from 48% to 65% (Fig. 2.2c).

Offshore losses are primarily driven by the sea state, which is highly sensitive to TC size and translation speed through wind duration and wind fetch effects. We therefore expect the importance of size and translation speed to be less for onshore losses (in those onshore regions away from the coastal surge zone) than for offshore losses. The lack of readily available spatial onshore loss data precludes a thorough analysis here, but as discussed earlier in this section, previous work suggests duration explains additional variance for onshore losses.

2.3.2 The Index

The prior work discussed in the previous section, plus the evidence from the small selection of offshore observations from the WELD data, point towards a damage potential index made up of some combination of the two terms used for Fig. 2.2c:

$$CDP = a\frac{\left(\frac{v_m}{v_{m0}}\right)^{aa}}{v_t^{ci}} + b\frac{\left(\frac{R_h}{R_{h0}}\right)^{bb}}{v_t^{cr}}, \tag{2.2}$$

where v_m is the maximum 1-min wind speed (kt) at 10 m above the surface, R_h is the radius the hurricane force (64 kt) winds, v_t is the translation speed (kt), a, b, aa, bb, ci, cr are constants to be determined, and v_{m0}, R_{h0} are normalization factors. The first term on the right-hand side represents the magnitude and duration of intense winds, and the second term is the extent and duration of hurricane winds. A summation rather than multiplication is based on the following reasoning: it enables different weighting of each term; it reduces the influence that sharp changes in any one term may have on the overall index; it reduces the influence of errors in individual terms; and, it better represents the individual damage mechanisms at work due to wind speed and duration. Sufficient and consistent damage data are not available to enable empirical determination of all of the constants in Eq. 2.1, so these are estimated largely on physical grounds. The sensitivity of the CDP to the final choices is established a posteriori.

Previous damage indices (Table 2.1) have used an exponent of aa = 1, 2, or 3. The static force of wind on an object aligned perpendicular to the wind, such as an individual building, varies with the square of the wind speed, as can readily be seen from Bernoulli's equation (pressure = $\rho v^2/2$). But the work done by the wind in directly damaging a collection of buildings and generating storm surge, currents, and waves varies with the wind speed cubed (Emanuel 2005). Additional dynamic effects such as the gustiness in the wind and vortex shedding also contribute (Davenport 1967), but these are impossible to assess with available warning data. Other collateral effects, for example the disruption to major facilities leading to a rise

in fuel costs, as occurred after Katrina and Rita in 2005, and increases in building costs due to expertise and supply shortages after a major disaster, are best handled as a component of the separate exposure and vulnerability assessment. Hence, following Emanuel (2005), we set aa = 3. The normalization value is taken as $v_{m0} = 65$ kt for consistency, with the choice of radius of hurricane force winds for the wind field extent. Note that nautical units are used to ensure global consistency, as these are the only units used in all cyclone basins.

For parameter ci, Fig. 2.2b indicates a potential quadratic relationship of damage to the inverse of translation speed, but this is largely due to there being several storms of different sizes and intensities at translation speeds of around 10 kt. There is little change in variance explained by setting ci = 1 or 2. Therefore, in the absence of additional information, ci is set to 1. For similar reasons, cr is set to 1. Further work is needed to assess the implications of this choice. To remove problems with the inverse of v_t for slow moving hurricanes, a minimum value of v_t is arbitrarily set at 5 kt.

The azimuthal mean radius of hurricane force winds, R_h, is used to indicate hurricane extent, since this parameter can be readily obtained from available data. There are associated uncertainties in its analysis, its azimuthal variability, and the variety of wind-field shapes that occur. One logical physical basis is to set bb = 2 to represent the areal coverage of the storm. However, the variance explained is not overly sensitive to the value of bb, as shown later. Therefore, to keep the index as simple as possible, bb is set to 1 with a reference value of $R_{h0} = 50$ nm.

This leaves two parameters, a and b. Sensitivity analysis indicates rapidly increasing overall scatter for a > 1 (partially due to the sensitivity arising from setting aa = 3), so a is set to 1. Much less sensitivity is found to the choice of b, provided it is substantially > 1, so b is set to 5. The sensitivity analysis discussed later (Table 2.2) supports these choices.

Finally, CDP is limited to hurricane force systems. This is consistent with all other indices summarized in Table 2.1. The resulting CDP is:

$$CDP = 4\frac{\left[\left(\frac{v_m}{65}\right)^3 + 5\left(\frac{R_h}{50}\right)\right]}{v_t}, \qquad \text{for } v_m > 65, \text{and if } v_t < 5, \text{set } v_t = 5. \tag{2.3}$$

As noted earlier, the HHI (Kantha 2006) also combines intensity, size, and forward speed into a single index. Nevertheless, the summation of terms in the CDP permits different weighting of terms and stability to sharp changes or error in a component term. The coefficient of 4 is introduced to scale the CDP across the approximate range of 0–10, and within this range we recommend rounding to one decimal place. By comparison, operational cyclone categories are based on five intensity levels (e.g. NHC 2017; BOM 2017). This integer intensity scale has been remarkably successful, but the relatively large step between categories means a small actual intensity change can result in a large jump to a new category of quite different TCs. A more continuous scale is recommended here as it enables objective

Table 2.2 CDP sensitivity to changes in each parameter for each hurricane in WELD

Parameter	a = ±0.5	b = ±2.5	aa = 4	aa = 2	bb = 1.5	bb = 0.5	ci,cr = 1.5	ci,cr = 0.5
% change	±50%	±50%	33%	−33%	50%	−50%	50%	−50%
Andrew	3%	−3%	8%	−4%	−8%	5%	−3%	40%
Lili	6%	−6%	9%	−5%	−16%	13%	−2%	26%
Ivan	−2%	2%	−4%	1%	8%	−6%	0%	−8%
Katrina	5%	−5%	26%	−9%	4%	−3%	2%	−20%
Rita	0%	0%	0%	0%	−1%	0%	4%	−44%
Gustav	−2%	2%	−13%	5%	−7%	4%	−2%	28%
Ike	−10%	10%	−25%	12%	21%	−14%	2%	−23%
Variance explained	−2%	−1%	−9%	−6%	−5%	−2%	3%	−8%

The top two lines show the Eq. 2.2 parameter changes and percentages. The next block shows the relative percentage changes in CDP, with the columns for parameters a and b representing ±%. The bottom row indicates the changes to WELD variance explained for all cyclones

Table 2.3 CDP sensitivity to changes in the normalizing values for each hurricane in WELD

Parameter	$R_{h0} = 75$	$R_{h0} = 25$	$v_{mo} = 95$
% change	50%	−50%	46%
Andrew	11%	1%	−5%
Lili	18%	2%	−8%
Ivan	−5%	−1%	2%
Katrina	14%	2%	−6%
Rita	1%	0%	−1%
Gustav	−7%	−1%	3%
Ike	−32%	−4%	14%
Variance explained	−11%	0%	−8%

The top two lines show the Eq. 2.2 parameter changes and percentage changes. The next block shows the relative percentage changes in CDP. The bottom row indicates the changes to variance explained for all cyclones

application to analysis methods or direct industry and societal applications. Our approach is consistent with the Moment magnitude scale used in earthquake assessment.

2.3.3 CDP Assessment

The sensitivity of the CDP (Eq. 2.3) to parameter choice is shown in Table 2.2, where each constant and exponent is varied while keeping the others constant, and the resulting change in variance explained for the WELD data is noted (last row of Table 2.2). In all cases, there is a substantially dampened response of the CDP to relatively large changes in the constants or exponents. The lowest sensitivity is for intensity and the highest for translation speed. Most importantly, there is low sensitivity in total variance explained arising from parameter variation. The sensitivity of CDP to changes in the normalizing values for each hurricane in WELD (Table 2.3) also indicates a dampened response. The CDP is thus relatively robust both to the choice of parameters and to reasonable levels of observational uncertainty. While this analysis indicates robustness, it also indicates that the choice of parameter values is rather arbitrary.

2.4 Example Applications of CDP

The CDP is suitable for use in a variety of contexts, including real-time forecasting, seasonal assessments, and understanding and predicting impacts arising from climate variability and change. Examples of its use are examined using historical events together with seasonal and basin summaries.

Table 2.4 CDP of selected TCs at the available 6-hourly track point prior to landfall together with published damage

Country	Storm name	Year	CDP	Vm (knots)	R64 (nm)	Vt (knots)	Total economic damage (nonadjusted USD bn)
Mexico	Wilma	2005	10.7	120	71	5	5
USA	Katrina	2005	6.6	140	80	11	81
Philippines	Haiyan	2013	5.9	170	41	15	*10*
USA	Ivan	2004	5	110	83	11	14.2
USA	Ike	2008	4.6	95	84	10	19.3
India	Phailin	2013	4.3	125	25	9	0.7
Philippines	Fengshen	2008	4.3	100	38	7	0.3
Honduras	Mitch	1998	4.2	85	30	5	*3.8*
Australia	Tracy	1974	4.1	102	12	5	*0.8*
Australia	Yasi	2011	3.9	135	55	15	*2.5*
USA	Rita	2005	3.5	100	59	11	10
Philippines	Bopha	2012	3.5	140	33	15	0.95
Myanmar	Nargis	2008	3.4	115	30	10	*4*
Bangladesh	Sidr	2007	3.3	130	43	15	*2.3*
Taiwan	Morakot	2009	3.3	80	30	6	3.3
USA	Sandy	2012	3	80	95	15	50
USA	Andrew	1992	2.9	130	29	15	24
USA	Dennis	2005	2.4	120	23	14	2.2
USA	Charley	2004	2.3	125	15	15	13.5
Australia	Larry	2006	2	115	15	14	*1.2*

For TCs with multiple landfalls the landfall at the region of maximum damage is shown. All values are for the year of cyclone landfall and no adjustments are made for inflation, increasing populations and value of infrastructure, or engineering and code changes. Note that Sandy and Mitch are included for comparison only, since Sandy was a hybrid and for Mitch the damage largely resulted from rainfall. Total economic damage data are sourced from http://www.icatdamageestimator.com and, where italicized, the Emergency Events Database (EM-DAT): http://www.emdat.be

2.4.1 Historical Events

A summary of CDP and damage estimates for selected historical TCs just prior to landfall is provided in Table 2.4. While Needham et al. (2015) showed that surge potential is best described using data at 18 h prior to landfall, TC winds often decrease in the 18 h prior to landfall. To capture more accurate landfalling winds while capturing a portion of the potential surge, we use the closest 6-hourly track point to landfall. The CDP column is in descending order, yet the damage values are widely scattered. This, again, emphasizes that while the CDP provides an objective estimate of the relative damage potential of TCs worldwide, the actual damage is very much dependent on exposure and vulnerability at the impact site.

2.4.2 Seasonal Basin Summaries

Scaling up to seasonal and basin summaries provides insight into the spatial variability of damage potential for the major cyclone basins (Fig. 2.3, limited size data precludes a climatological analysis over the North Indian Ocean). CDP data are visualized by binning the 6-hourly track data into equal-area hexagons, following Elsner et al. (2012).

High CDP pathways follow the major belts of recurving storms off the US East Coast, arcing towards southwest Japan, and down the Northwest and Northeast Australian coasts. Other damage pathways track from the Caribbean into the Gulf of Mexico, off the West Coast of Mexico up into Baja California, and east of Madagascar. These summaries thus show a rich spatial texture that is masked by a consideration of TC intensity alone. For example, in the North Atlantic basin, the Yucatan and North Carolina are highlighted as hotspots for cyclones with high damage potential, but this does not show if intensity, alone, is used.

All basins have been able to generate maximum CDP values of 10 (right side of Fig. 2.3), with the Northwest Pacific containing the widest area and most frequent occurrences of maximum damage potential cyclones.

A 26-year time series from 1988 to 2012 of seasonal (August to October) accumulated CDP for the North Atlantic (Fig. 2.4) indicates no real trend for the entire basin but a small (but not statistically significant) increase for land falling storms. There also is a large interannual variability for which TC lifetime and frequency are additional contributors to the three component terms of the CDP. For example, the high frequency years of 1995 and 2005 have the highest seasonal CDP – reflecting a contribution from TC frequency – yet the high frequency period of 2010–2012 is not a period of high CDP – reflecting contributions from other processes.

The El Niño Southern Oscillation (ENSO) appears to modulate seasonal, basin-wide Atlantic CDP, with a correlation that is statistically significant ($p < 0.04$). No significant ENSO relationship is observed for the land falling storms.

2.4.3 Real-Time Forecasting

The final use explored here is real-time forecasting of damage potential. Hurricane Wilma (2005) is a chosen case study because of the large changes in the component terms of CDP along the hurricane track.

Real-time hurricane forecasts issued by TC warning centers are combinations of ensemble dynamical and statistical model output and subjective assessment. Here, we explore an ensemble real-time forecast generated by the Advanced Research Weather Research and Forecasting model (Davis et al. 2008). The ensemble

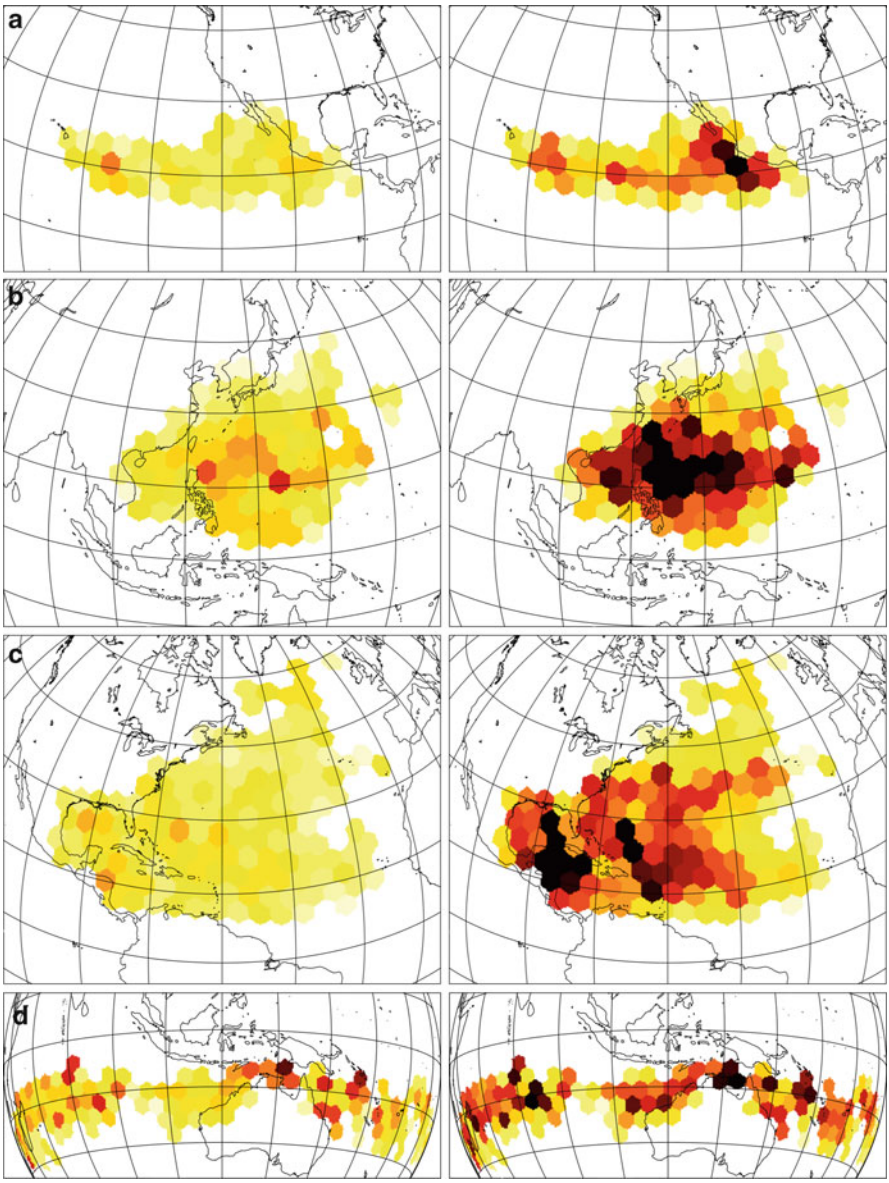

Fig. 2.3 Median (left) and maximum (right) seasonal accumulated CDP for (**a**) the Eastern North Pacific (2001–2013), (**b**) the Western North Pacific (2004–2013), (**c**) the North Atlantic (1988–2013), and (**d**) the Southern Hemisphere (2004–2013)

comprises six real-time forecasts of Hurricane Wilma, initialized every 12 h from 00Z Oct 20 to 12Z Oct 22 2005, with lead times of 72–96 h. An outer 12 km fixed domain, initialized with the Geophysical Fluid Dynamics Laboratory model at 1/6°

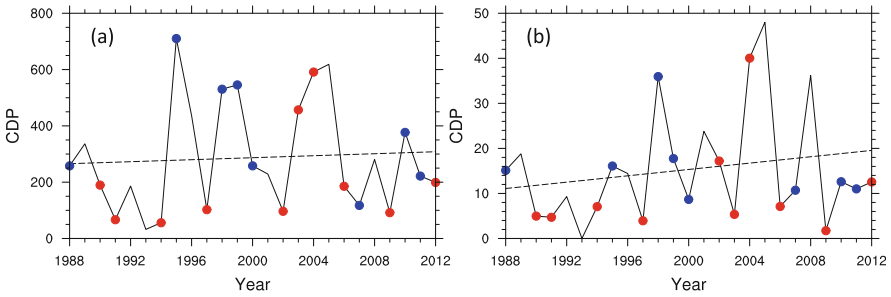

Fig. 2.4 Time series of seasonal accumulated CDP (1988–2012) for (left) the entire North Atlantic basin, and (right) land falling storms at the 6-hourly track points prior to landfall. Years with Oceanic Niño Index (ONI, 3 month running mean SST anomalies in the Niño 3.4 region 5 °N–5 °S, 120°–170 °W) for August-September-October >0.5 K (El Niño) are indicated in red, and ONI <0.5 K (La Niña) are indicated in blue. (ONI data source: NOAA/CPC)

grid spacing, contains a 4 km movable nest centered over the vortex. Further details of the model setup are available in Davis et al. (2008).

The observed hurricane attained peak CDP of 10.7 as a slow moving, intense hurricane in the Caribbean (Fig. 2.5a, b) and maintained peak CDP as it made landfall in Mexico late on Oct 21, resulting in 5bn USD damages (Table 2.4). The hurricane slowed further, tracked North over the Yucatán Peninsula over 24 h with a weakening and reduction in the area of damaging winds, resulting in a CDP of 3 as it emerged into the Gulf of Mexico. Crossing the Gulf, the hurricane re-intensified and increased in size, yet these changes were offset by a forward acceleration, maintaining CDP values around 3 at landfall in South Florida with US damages of $21bn.

All forecasts capture the general hurricane track (Fig. 2.5a), although the earliest forecast missed the landfall in South Florida. All forecasts were initialized with a cyclone of high damage potential but, whereas the observed cyclone maintained peak CDP until Mexico landfall, the forecast CDP fluctuated between 10 and 5 with an overall decreasing trend (Fig. 2.5b). This lower CDP results from a combination of a smaller size and a faster forward translation speed leading to earlier landfall in Mexico (Fig. 2.5d, e). The forecasts performed much better as the hurricane emerged into the Gulf of Mexico, capturing the increase in intensity, size, and forward speed, and the observed CDP at US landfall 3 days in advance.

Application of CDP to ensemble real-time hurricane forecasts offers an alternative presentation of the forecast information that is more closely related to damage potential than consideration of intensity alone. Real-time CDP forecasts issued during the active 2017 North Atlantic hurricane season provided new views of potential damage, and were compared to the CDP of historical hurricanes to better communicate potential damage. Moreover, CDP may be inherently more predictable than maximum wind speeds alone due to the dampening effect of the less volatile size and forward speed components (as suggested by the small range of forecast CDP values compared to intensity prior to US landfall for the case of Hurricane Wilma).

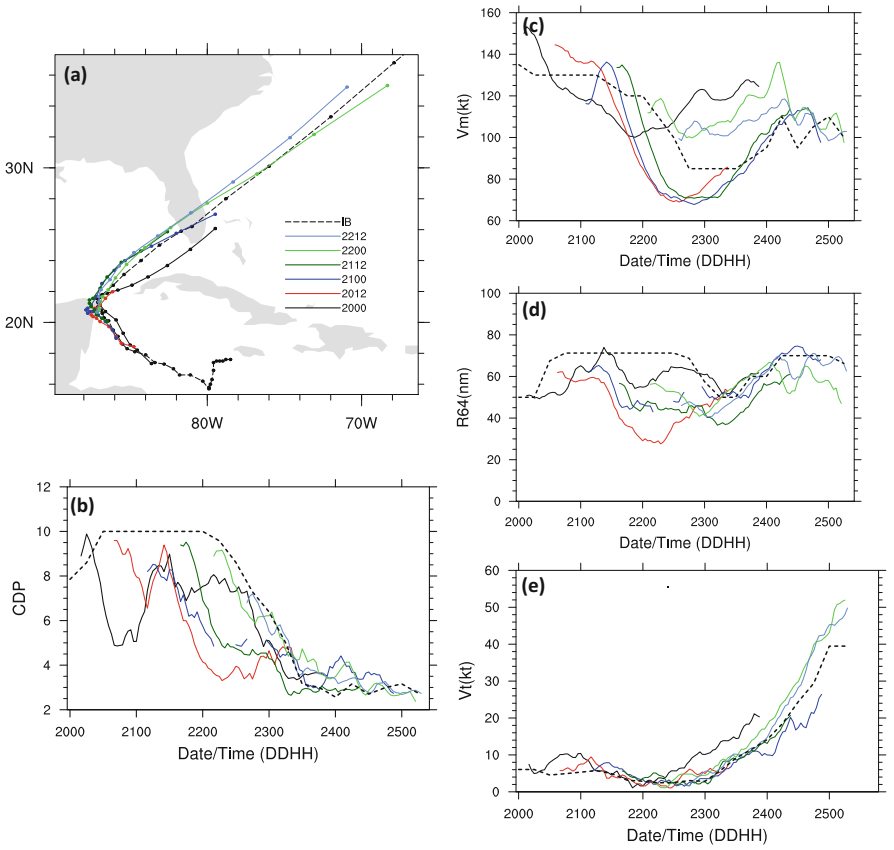

Fig. 2.5 (**a**) Hurricane Wilma tracks. The black dashed line indicates the observations (IBTrACS) and the colored lines indicate real-time forecasts initialized every 12 h from 00Z Oct 20 to 12Z Oct 22, 2005. Filled circles indicate 6-hourly track locations. (**b–e**) Observed and forecast time series of CDP, maximum wind speed, radius of hurricane force winds, and translational speed

2.5 Summary

A Cyclone Damage Potential (CDP) index has been developed that represents offshore damage. Previous studies together with physical reasoning and an analysis of limited historical cyclone and offshore loss data indicate that intensity, cyclone size, and translation speed all contribute substantially to cyclone damage. Given the importance of wind duration and fetch effects for the sea state, we expect the importance of size and translation speed to be greater for offshore losses than for onshore losses (away from the coastal surge zone). The three parameters of cyclone intensity, size, and translation speed have been combined into the CDP to provide a first order assessment of damage potential.

Because the CDP is robust to both the choice of parameters and to reasonable levels of observational uncertainty, it is therefore suitable for a variety of applications from individual events and real-time forecasts to seasonal and global summaries. An advantage of the CDP is that it can be used to provide assessments relative to other events, regions, or periods, and as an aid to interpreting and comparing historical cyclones. Actual quantitative damage assessment or prediction requires an additional step of developing a vulnerability transfer function based on a user's specific exposure and risk. This might address, for example, business vulnerability through an insurance portfolio, vulnerability of local cultural groups, and vulnerability of infrastructure.

The value of the approach developed here for cyclone damage potential has only been demonstrated using a small number of storms for a single economic sector – the offshore energy sector – whose primary exposure is offshore. It is therefore necessary to explore this potential limitation to understand the extent of its applicability. The lack of readily available spatial onshore loss data precludes a thorough analysis here, but a follow-on study using recently acquired onshore loss data will examine the applicability of CDP to onshore losses in more detail.

Potential application to landfalling storms has been explored using historical data. For landfalling storms there are cases of intense, yet small and fast moving, cyclones that have lower CDP than others that are less intense but larger and slower moving. The CDP, therefore, may provide an objective approach to assessing relative damage potential of such TCs and for use in what-if scenarios. For example, there was potential for much higher losses in the Miami area had Hurricane Andrew been larger or slower moving. For a specific cyclone impact, the CDP concept may be used in ensemble forecast mode and immediately after impact to provide a first-order damage assessment.

Climatological summaries reveal global damage potential pathways co-located with belts of recurving storms, damage potential hotspots east of the Philippines and across the north Australian coast, and the dominant contribution of the Northwest Pacific to total global damage potential. No trend in damage potential is seen for the entire North Atlantic basin, but a small (but not statistically significant) trend is found in the landfalling damage potential for North Atlantic basin landfalling storms.

The approach developed here for cyclone damage potential is transferable to developing damage potential indices for other high-impact weather and climate phenomena such as hail, floods, drought, and sea-level rise. The approach is also extendable to developing damage potential indices on large-scale environmental parameters rather than on the TC characteristics themselves. Done et al. (2015), for example, developed an index of seasonal damage potential for the North Atlantic. Using the same concept, Tippett et al. (2012, 2014) developed the Tornado Environment Index, and Allen et al. (2015) developed the Hail Environment Index. Such indices have broad societal applications, including real-time warnings and emergency management, long-term planning, providing a first order assessment of the potential for insurance claims, and cost-benefit assessments of engineering advances and adaptation measures.

Acknowledgements NCAR is funded by the National Science Foundation and this work was partially supported by NSF Award 1048829, the Willis Research Network, the Research Partnership to Secure Energy for America, and the Climatology and Simulation of Eddies/Eddies Joint Industry Project.

References

Allen JT, Tippett MK, Sobel AH (2015) An empirical model relating U.S. monthly hail occurrence to large-scale meteorological environment. J Adv Model Earth Syst 7:226–243. https://doi.org/10.1002/2014MS000397

Arnold TH, Chiltern CH (1963) New index shows plant cost trends. Chem Eng 70:143–148

Bell GD, Halpert MS, Schnell RC, Higgins RW, Lawrimore J, Kousky VE, Tinker R, Thiaw W, Chelliah M, Artusa A (2000) Climate Assessment for 1999. Bull Am Meteorol Soc 81:1328–1132

BOM (2017) Tropical cyclone severity categories. Bureau of Meteorology. http://www.bom.gov.au/cyclone/about/. Accessed 1 Oct 2017

Chavas DR, Yonekura E, Karamperidou C, Cavanaugh N, Serafin K (2013) U.S. hurricanes and economic damage: extreme value perspective. Nat Hazards Rev 14(4):237–246

Czajkowski J, Done JM (2014) As the wind blows? Understanding hurricane damages at the local level through a case study analysis. Weather Clim Soc 6:202–217

Davenport AG (1967) Gust loading factors. J Struct Div 93:11–34

Davis C, Wang W, Chen SS, Chen Y, Corbosiero K, DeMaria M, Dudhia J, Holland G, Klemp J, Michalakes J, Reeves H, Rotunno R, Snyder C, Xiao Q (2008) Prediction of land falling hurricanes with the advanced hurricane WRF model. Mon Weather Rev 136:1990–2005. https://doi.org/10.1175/2007MWR2085.1

Demuth J, DeMaria M, Knaff JA (2006) Improvement of advanced microwave sounder unit tropical cyclone intensity and size estimation algorithms. J Appl Meteor Climatol 45:1573–1581

Done JM, PaiMazumder D, Towler E, Kishtawal D (2015) Estimating tropical cyclone impacts using an index of damage potential. Clim Chang. https://doi.org/10.1007/s10584-015-1513-0

Done JM, Simmons KS, Czajkowski J (2018) Relationship between residential losses and hurricane winds: role of the Florida building code. ASCE-ASME J Risk Uncertainty Eng Syst Part A 4(1). https://doi.org/10.1061/AJRUA6.0000947

Elsner JB, Hodges RE, Jagger TH (2012) Spatial grids for hurricane climate research. Clim Dyn 39:21–36

Emanuel KA (2005) Increasing destructiveness of tropical cyclones over the past 30 years. Nature 436:686–688

Emanuel KA (2011) Global warming effects on U.S. hurricane damage. Weather Clim Soc 3:261–268

Geiger T, Frieler K, Levermann A (2016) High-income does not protect against hurricane losses. Environ Res Lett 11:084012. https://doi.org/10.1088/1748-9326/11/8/084012

Gray WM, Landsea CW (1992) African rainfall as a precursor of hurricane-related destruction on the U.S. east coast. Bull Am Meteorol Soc 73:1352–1364

Grinsted A, Moore JC, Jevrejeva S (2012) Homogeneous record of Atlantic hurricane surge threat since 1923. Proc Natl Acad Sci 109:19601–19605

Hebert C, Weinzapfel R (2006) The hurricane severity index. Impact Weather. http://impactweather.com/pdf/hsi.pdf. Accessed 1 Oct 2017

Holland GJ (1983) Tropical cyclone motion: environmental interaction plus a beta effect. J Atmos Sci 40:328–342

Holland GJ (2012) Hurricanes and rising global temperatures. Proc Natl Acad Sci 109 (48):19513–19514

Irish JL, Resio DT, Ratcliff JJ (2008) The influence of storm size on hurricane surge. J Phys Oceanogr 38:2003–2013
Jain V (2010) The role of wind duration in damage estimation. AIR currents. http://www.air-worldwide.com/Publications/AIR-Currents/2010/The-Role-of-Wind-Duration-in-Damage-Estimation/. Accessed 1 Oct 2017
Kantha L (2006) Time to replace the saffir-simpson hurricane scale? EOS Trans AGU 87(1):3
Knapp KR, Kruk MC, Levinson DH, Diamond HJ, Neumann CJ (2010) The international best track archive for climate stewardship (IBTrACS): unifying tropical cyclone best track data. Bull Am Meteorol Soc 91:363–376
Kozar ME, Misra V (2014) Statistical prediction of integrated kinetic energy in North Atlantic tropical cyclones. Mon Weather Rev 142:4646–4657
Lin N, Emanuel K, Oppenheimer M, Vanmarcke E (2012) Physically based assessment of hurricane surge threat under climate change. Nat Clim Chang 2(6):462–467
Matyas CJ (2010) Associations between the size of hurricane rain fields at landfall and their surrounding environments. Meteorog Atmos Phys 106:135–148
Miller C, Gibbons M, Beatty K, Boissonnade A (2013) Topographic speed-up effects and observed roof damage on Bermuda following hurricane Fabian (2003). Weather Forecast 28:159–174
Murnane RJ, Elsner JB (2012) Maximum wind speeds and US hurricane losses. Geophys Res Lett 39:L16707
Needham HF, Keim BD, Sathiaraj D (2015) A review of tropical cyclone-generated storm surges: global data sources, observations, and impacts. Rev Geophys 53:545–591. https://doi.org/10.1002/2014RG000477
NHC (2017) The saffir-simpson hurricane wind scale. National Hurricane Center. http://www.nhc.noaa.gov/aboutsshws.php. Accessed 1 Oct 2017
Olsen A, Porter K (2011) What we know about demand surge: brief summary. Nat Hazards Rev 12 (2):62–71
Pielke RA (2007) Future economic damage from tropical cyclones: sensitivities to societal and climate changes. Phil Trans R Soc A 365:1–13
Pita G, de Schwarzkopf MLA (2016) Urban downburst vulnerability and damage assessment from a case study in Argentina. Nat Hazards 83(1):445–463. https://doi.org/10.1007/s11069-016-2323-z
Pita G, Pinelli J, Gurley K, Mitrani-Reiser J (2015) State of the art of hurricane vulnerability estimation methods: a review. Nat Hazards Rev 16(2). https://doi.org/10.1061/(ASCE)NH.1527-6996.0000153
Powell MD, Reinhold TA (2007) Tropical cyclone destructive potential by integrated kinetic energy. Bull Am Meteor Soc 88:513–526
Proudman J (1953) Dynamical oceanography. Methuen, London Wiley, New York
Rego JL, Li C (2009) On the importance of the forward speed of hurricanes in storm surge forecasting: a numerical study. Geophys Res Lett 36:L07609
Schmidt S, Kemfert C, Hoppe P (2010) The impact of socio-economics and climate change on tropical cyclone losses in the USA. Reg Environ Chang 10:13–26
Simpson RH, Riehl H (1981) The hurricane and its impact. Louisiana State Univ Press, Baton Rouge
Smith SE (2010) Managing catastrophic risk: beyond cat bonds. In: Tang K (ed) Weather risk management: a guide for corporations, hedge funds and investors. Incisive financial publishing ltd, p 199–213
Tippett MK, Sobel AH, Camargo SJ (2012) Association of U.S. tornado occurrence with monthly environmental parameters. Geophys Res Lett 39:L02801. https://doi.org/10.1029/2011GL050368
Tippett MK, Sobel AH, Camargo SJ, Allen JT (2014) An empirical relation between U.S. tornado activity and monthly environmental parameters. J Clim 27:2983–2999. https://doi.org/10.1175/JCLI-D-13-00345.1
Vatavuk WM (2002) Updating the plant cost index. Chem Eng 109(1):62–70

Walker G, Reardon G, Jancauskas E (1988) Observed effects of topography on the wind field of cyclone Winifred. J Wind Eng Ind Aerod 28:79–88

Yu J-Y, Chou C, Chiu P–G (2009) A revised accumulated cyclone energy index. Geophys Res Lett 36:L14710

Zhai AR, Jiang JH (2014) Dependence of US hurricane economic loss on maximum wind speed and storm size. Environ Res Lett 9:064019

Chapter 3
Integrated Kinetic Energy in North Atlantic Tropical Cyclones: Climatology, Analysis, and Seasonal Applications

Michael E. Kozar and Vasubandhu Misra

Abstract Integrated Kinetic Energy (IKE) is a recently developed metric that measures the destructive potential of tropical cyclones (TCs) by integrating the square of the surface winds across these powerful storms. In this chapter, the previous literature is reviewed to provide insights on the factors that make IKE a desirable metric. IKE complements existing scales and metrics by considering a TC's entire wind field, in lieu of just focusing on the maximum intensity of a storm. Using a dataset of six-hourly IKE estimates for two decades of North Atlantic TC activity, the climatology of IKE in individual storms is explored, with emphasis on seasonal and spatial variability. The driving mechanisms for IKE variability during the lifetime of a TC are also reviewed to determine which environmental and storm-scale features promote IKE growth. The historical record of IKE can also be aggregated to a seasonal metric, called Track Integrated Kinetic Energy (TIKE), which is shown to offer a comprehensive overview of seasonal TC activity and can be used to explore interannual TC variability over the last two to three decades.

Keywords Atlantic hurricanes · Integrated kinetic energy · Tropical cyclone structure · Statistical-dynamical analysis · Seasonal activity

M. E. Kozar (✉)
Risk Management Solutions (RMS), Tallahassee, FL, USA
e-mail: Michael.Kozar@rms.com

V. Misra
Center for Ocean-Atmospheric Prediction Studies, Florida State University, Tallahassee, FL, USA

Department of Earth, Ocean and Atmospheric Science, Florida State University, Tallahassee, FL, USA

Florida Climate Institute, Florida State University, Tallahassee, FL, USA

J. M. Collins, K. Walsh (eds.), *Hurricane Risk*, Hurricane Risk 1,
https://doi.org/10.1007/978-3-030-02402-4_3

3.1 Introduction

In the first two decades of the twenty-first century, a series of North Atlantic tropical cyclones (TCs) with large wind fields made landfall in the United States. These expansive storms – including Hurricanes Ivan (2004), Katrina (2005), Ike (2008), Irene (2011), Sandy (2012), and Irma (2017) – served as further evidence that damage potential is tied to much more than just the oft-reported maximum sustained wind intensity metric. Irene and Sandy, in particular, had top wind speeds that would not rank highly on the Saffir-Simpson Hurricane Wind Scale (SSHWS) just before they came ashore (Fig. 3.1), yet both storms caused considerable wind and surge damage, exceeding what is typically expected for storms of a similar intensity.

Certainly, intensity metrics are still quite useful, as there is clear indication that wind damage from TCs is connected to inner core wind speeds (e.g. Kantha 2006; Pielke and Landsea 1998; Murnane and Elsner 2012). Specifically, Murnane and Elsner (2012) indicate that losses and maximum sustained wind speeds are exponentially related, with an increase of loss at a rate of 5% per m s^{-1} of peak winds. However, beyond these high inner core wind speeds, a common meteorological feature that is relevant to the damage caused by some of these recent landfalling hurricanes is the overall size and structure of their wind field. For instance, a wide swath of tropical storm strength winds ($\geq$17 m s^{-1}) in larger TCs contributes to an increased volume of destruction and a more widespread wind threat to the population. Zhai and Jiang (2014) indicate that using a combination of storm size and maximum wind speed explains a larger portion of the variance in losses caused by a landfalling hurricane than using intensity (or size) alone. In an illuminating example, they suggest that economic losses from the landfall of Hurricane Sandy would have been approximately 20 times smaller if its size were comparable to an average sized TC, leaving its maximum sustained winds unchanged as observed.

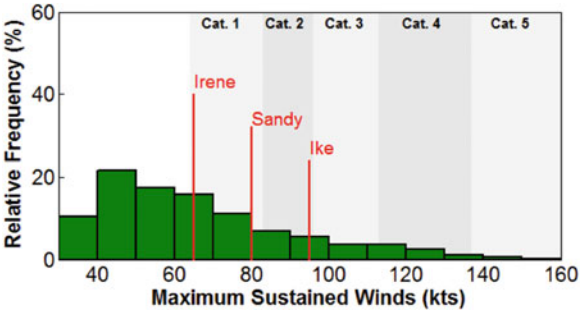

Fig. 3.1 Relative frequency distribution of six-hourly V_{max} measurements in Atlantic TCs between 1990 and 2011. This sample includes 5498 fixes from 291 storms. Vertical lines are shown to indicate V_{max} values for selected hurricanes just prior to a US landfall. The times of these V_{max} measurements are as follows: Ike 9/13/08 00Z; Irene 8/28/11 06Z; Sandy 10/29/12 18Z. The three storm points would fall in the top 45% of all TCs points in terms of V_{max} from 1990 through 2011. (Adapted from Kozar and Misra 2014)

Furthermore, storm surge from landfalling TCs continues to be a significant threat and has caused considerable damage historically (Pielke and Landsea 1998). Irish et al. (2008) found that there is a significant direct relationship between the size of a TC's wind field and the resulting peak surge, especially in regions with mildly sloping coastal bathymetry. Given that coastal developments continue to expand and become more densely populated (Crosset 2004), society is becoming more at risk to the wind and water from landfalling TCs. Given these increasing risks and the importance of storm size to the amount of lives and property exposed to the hazards associated with TCs, there is a rising interest in understanding and predicting the size and structure of TC wind fields (Cangialosi and Landsea 2016; Knaff et al. 2016).

In an effort to better evaluate the damage potential of TCs as a function of winds across the entirety of a TC, Powell and Reinhold (2007) introduced a novel, alternative metric called Integrated Kinetic Energy (IKE). This metric is proportional to a simple integration of one-half of the square of the 10-m wind field over a one-meter depth out to the radius of 34-knot winds:

$$\mathrm{IKE} = \int_v \frac{1}{2}\rho U^2 dV \tag{3.1}$$

IKE is tied to physical processes that cause damage, as it scales with wind stress on the ocean and the wind load forcing on structures (Powell and Reinhold 2007). Furthermore, given its integrated nature, IKE takes into account both inner core winds (i.e. TC intensity) and the size of hurricane wind fields, giving it potential advantages over more limiting intensity metrics which do not consider storm size at all. This is clearly demonstrated by hurricanes Irene, Ike, and Sandy, which each made landfall with IKE values that rank in the top 7.5% of historical values from 1990 to 2015, in contrast to their somewhat lower maximum sustained wind placement (Figs. 3.1 and 3.2).

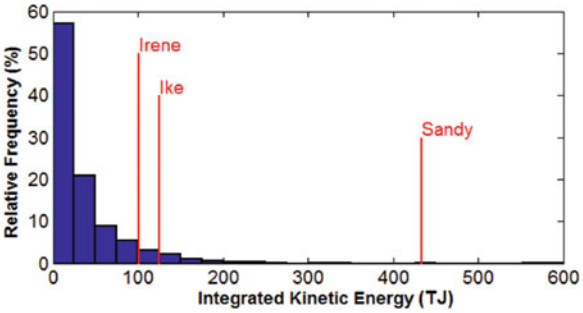

Fig. 3.2 Relative frequency distribution of six-hourly IKE measurements in Atlantic TCs between 1990 and 2011. This sample includes 5498 fixes from 291 storms. Vertical lines are shown to indicate IKE values for selected hurricanes just prior to a US landfall. The times of these IKE measurements are as follows: Ike 9/13/08 00Z; Irene 8/28/11 06Z; Sandy 10/29/12 18Z. The three storm points would fall in the top 7.5% of TCs in terms of IKE from 1990 through 2011. (Adapted from Kozar and Misra 2014)

The next section of this chapter will focus on the analysis of historical IKE values across the North Atlantic basin with a focus on how the metric can be measured or approximated, followed by a discussion on the climatology of IKE in North Atlantic tropical cyclones. Afterward, a series of sensitivity tests is presented to explore relationships between the environment, storm-scale features, and IKE, which might offer some guidance on how IKE could respond in a changing climate. Finally, an application will be presented in which IKE can be used to evaluate interannual TC activity (Sect. 3.4), with a discussion on how seasonal sums of IKE vary with changes in climate processes.

3.2 Analysis of IKE

3.2.1 Estimating Observed IKE

The biggest strength of the IKE metric is its consideration of the distribution and strength of surface winds across the entirety of a TC's wind field. However, by considering winds across such a large area, calculating IKE exactly in either a real-time or historical setting poses some potential challenges. Observations from aircraft reconnaissance serve as the most useful source of information when assessing storm size and structure. Other observational platforms such as buoys, ships, radar, and surface-based anemometers along the coast can also be of great use to measure the size and structure of TC wind fields, as demonstrated by the HRD real-time hurricane wind analysis system (H*Wind; Powell et al. 1998). When available, observationally-based gridded wind fields from analyses such as these are the preferred framework for calculating IKE directly (Powell and Reinhold 2007).

However, the critically important aircraft reconnaissance flights are not necessarily continuous in the Atlantic. For instance, Rappaport et al. (2009) reported that the coverage of these data is for only about 30% of all TC fixes in the North Atlantic. In other basins across the globe (e.g. West Pacific, Southern Hemisphere, and Indian Ocean), flight data may be absent altogether. The dearth of in situ observations in some locations has forced forecasters, analysts, and researchers alike to rely more heavily on wind field estimates from satellites (Knaff et al. 2016). These satellite-based winds may come from multiple sources, including microwave radiometers (Demuth et al. 2004, 2006), scatterometers (e.g. Atlas et al. 2011; Holmlund et al. 2001), and cloud drift winds (Velden et al. 2005). Ultimately, spaceborne retrievals are quite useful for filling gaps where surface data might not otherwise exist, but these techniques still have their own limitations. For instance, scatterometers often underestimate the inner core wind speeds within intense TCs (e.g. Brennan et al. 2009), and retrievals are susceptible to contamination from high rain rates throughout the storm (e.g. Weissman et al. 2012). As technology improves and new observation platforms become available in the coming years (e.g. GOES-16, CYGNSS, etc.), it is likely that measurements of hurricane wind structure will

improve both in quality and duration, allowing for better estimation of IKE (Morris and Ruf 2016).

In the meantime, given the inconsistent coverage and quality of hurricane wind measurements around the world, it may be difficult to compute IKE directly from observations in all cases. Other gridded datasets such as numerical reanalysis provide another option for estimating historical values of IKE across the globe in a more consistent framework. However, gridded wind reanalyses continue to show a persistent weak TC bias and often are unable to resolve smaller TCs (Manning and Hart 2007; Schenkel and Hart 2012; Buchanan et al. 2018), making them less than ideal for directly calculating the IKE of a TC's wind field in most cases.

Given the challenges of calculating IKE directly, Misra et al. (2013) offered an alternative method for approximating IKE through an empirical relationship between reported operational wind radii. Estimates of storm size are already provided by many of the TC warning centers (e.g. National Hurricane Center [NHC], Central Pacific Hurricane Center [CPHC], Joint Typhoon Warning Center [JTWC]) in their regular advisories. These operational values are often stored and/or reanalyzed after the season in research and operational datasets such as the Automated Tropical Cyclone Forecast System (ATCF) b-decks or the NHC's HURDAT2 database and the Extended Best Track (Demuth et al. 2006). Size is typically reported in datasets such as these by providing approximations of the maximum radial extent of 34-kt (tropical storm force), 50-kt (storm force by Beaufort wind scale; WMO 1970) and 64-kt (hurricane force) winds in cardinal geographic quadrants (northwest, southwest, southeast, and northeast) from available data platforms. The aforementioned data quality and coverage inconsistencies surely affect the accuracy of the operational radii metrics (e.g. Landsea and Franklin 2013). Furthermore, Vigh et al. (2012) specifically notes that some parameters such as the radius of maximum winds often do not match actual aircraft measurements particularly well in the early portions of the Extended Best Track data (i.e. pre-2001). Nonetheless, Knaff et al. (2016) indicate that the best track wind radii from the NHC provide useful estimates of TC wind radii for developing new techniques.

Table 3.1 details the algorithm to compute IKE from discretized wind radii data adapted from Misra et al. (2013). These formulas may be used in conjunction with the HURDAT2 and the Extended Best Track dataset to provide a continuous estimate of IKE for all storms in the Atlantic basin, going back almost three decades in a reasonably consistent framework. Such a dataset of IKE values, while inexact, would still be useful for analyzing the climatology of IKE in storms across the North Atlantic basin.

3.2.2 Climatology of IKE in the North Atlantic Basin

Applying the algorithm in Table 3.1 to the radii data in HURDAT2 and the Extended Best Track dataset yields a historical dataset containing IKE estimates for more than 5600 six-hourly fixes for nearly 300 storms between 1990 and 2011 in the North

Table 3.1 Algorithm to compute IKE from discretized wind radii data (e.g. Extended Best Track data Demuth et al. 2006) (From Misra et al. 2013)

Quadrant IKE contribution	Criteria	Mean wind (m s^{-1})	Area
$IKE_{18–26}$	R_{26} >0	20	1/4 π ($R_{18}{}^2$–$R_{26}{}^2$)
	No R_{26}, V_{MS}>26, R_{18}>R_{max}	20	1/4 π ($R_{18}{}^2$–(0.75R_{max}) ^{2})
	No R_{26}, V_{MS}<26, R_{18}>R_{max}	1/4 V_{MS} + 3/4 (18)	1/4 π ($R_{18}{}^2$–(0.75R_{max}) ^{2})
	No R_{26}, R_{max}=R_{18}	18	1/4 π ($R_{18}{}^2$–$(0.5R_{18})^2$)
$IKE_{26–33}$	R_{33}>0	27.75	1/4 π ($R_{26}{}^2$–$R_{33}{}^2$)
	no R_{33}, V_{MS}>33, R_{26}>R_{max}	27.75	1/4 π ($R_{26}{}^2$ −$(0.75R_{max})^2$)
	no R_{33}, V_{MS}<33, R_{26}>Rmax	.25 V_{MS}+.75 (26)	1/4 π ($R_{26}{}^2$–(0.75R_{max})^2)
	no R_{33}, R_{26}<=R_{max}	26	1/4 π [$R_{26}{}^2$–$(.5R_{26})^2$]
IKE_H	Max R_{33} Quadrant, R_{33}>R_{max}	.25V_{MS} +.75 (33)	1/4 π ($R_{33}{}^2$–(0.75R_{max})^2)
	Max R_{33} Quadrant, R_{33}= R_{max}	.25V_{MS} +.75 (33)	1/4 π ($R_{33}{}^2$–$(.75\ R_{33})^2$)
	R_{33}<R_{max}	.1V_{MS} + .9(33)	1/4 π ($R_{33}{}^2$–$(.75\ R_{33})^2$)
	Not max R_{33} Quadrant	.1V_{MS} + .9(33)	1/4 π ($R_{33}{}^2$–(0.75R_{max}) ^{2})
	R_{max} = R_{33}		

R_{18}, R_{26}, R_{33}, refer to radius of wind speeds of 18, 26, 33 ms^{-1}, R_{max} is radius of maximum winds and V_{MS} is speed of maximum sustained wind speed of the TC

Atlantic Basin. Only fixes for subtropical storms and TCs are used in this dataset, but certainly some of the included fixes will correspond to storms that are ongoing but have not completed extratropical transition. Across this wide sample of IKE fixes (of which the distribution is plotted in Fig. 3.2), the mean six-hourly IKE value is 35.4 TJs. The distribution is skewed towards lower values with more than 57% of the fixes containing less than 25 TJ of IKE. Consequently, the standard deviation of IKE values is relatively high (43.6 TJ), and there is a long tail of high IKE values in the record. Sandy in 2012 and Igor in 2010 are two recent members of this long tail, as both obtained more than ten times the mean IKE value by the end of their lifetime. Overall, the shape of the distribution for this large number of IKE samples resembles a log-normal distribution (Kozar and Misra 2014), which was also proposed as a good fit for the distribution of storm size as measured by the radius of vanishing wind (Dean et al. 2009).

Further dissection of the historical dataset reveals that over the course of a storm's lifetime, it will peak at approximately 50 TJ of IKE on average. More than a quarter of the 291 storms in the record never grow past 10 TJ of IKE at any one time, with only a fifth of the historical storms ever reaching 100 TJs during their lifetime.

The seasonal cycle of the IKE values in this record follows somewhat closely the seasonal cycle of TC frequencies in the North Atlantic, except it is skewed a little bit

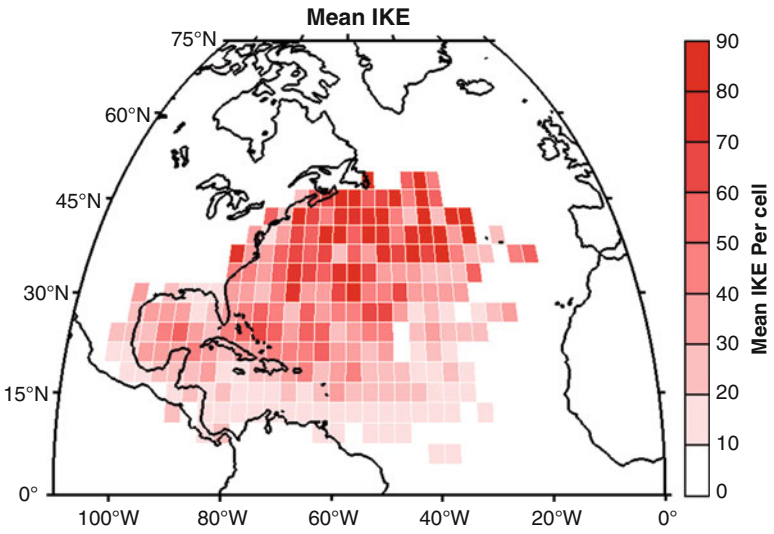

Fig. 3.3 Map showing historical mean IKE values for all fixes from 1990 to 2011 spatially across $3 \times 3°$ bins in the North Atlantic. The distribution of mean IKE suggests that storms have higher IKE on average in the northern most latitudes of the basin. Please note that the grid cells in the higher latitudes will be smaller in area than the grid cells over the deep tropics in this figure and the two that follow

more towards the end of the typical hurricane season. The mean monthly IKE value peaks in September at 44 TJ, or approximately 25% higher than the overall mean (not shown). Mean six-hourly IKE values are higher in October and November than they are in June, July, or August, indicating a preference for storms with higher IKE values later in the season.

Looking now at the spatial climatology of IKE across the Atlantic, it becomes evident that storms climatologically obtain higher IKE values as they move poleward in the northern part of the basin (Fig. 3.3). This is consistent with the higher IKE values found later in the season, as many TCs that form in October and November occur in the western half of the basin and follow a more meridional track toward the pole. Meanwhile, TCs over the main development region in the central Atlantic and Caribbean typically have less IKE, with a few other localized maxima appearing in the Gulf of Mexico and over the Bahamas. Focusing on only IKE values that exceed 100 TJ in the historical record, it becomes even more apparent that the western and northern parts of the basin are preferred regions for high IKE values (Fig. 3.4). Furthermore, storms tend to obtain their lifetime peak IKE value at the end of their tracks either in the northern part of the basin as they recurve or just before making landfall in the western edges of the basin (Fig. 3.5). This tendency for IKE to maximize in the northwest part of the basin does not necessarily overlap with where one might expect the most intense storms to be located, which would likely be further south.

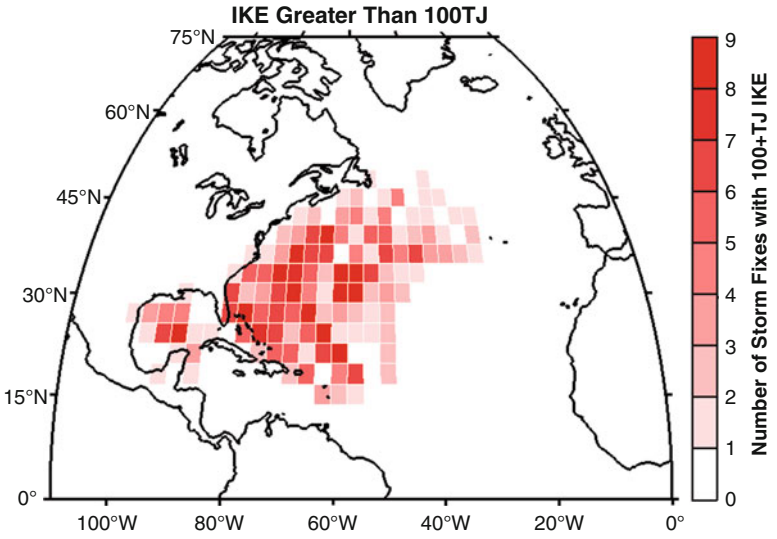

Fig. 3.4 Map showing where tropical cyclones between 1990 and 2011 had IKE exceeding 100TJ, gridded into $3 \times 3^{\circ}$ bins

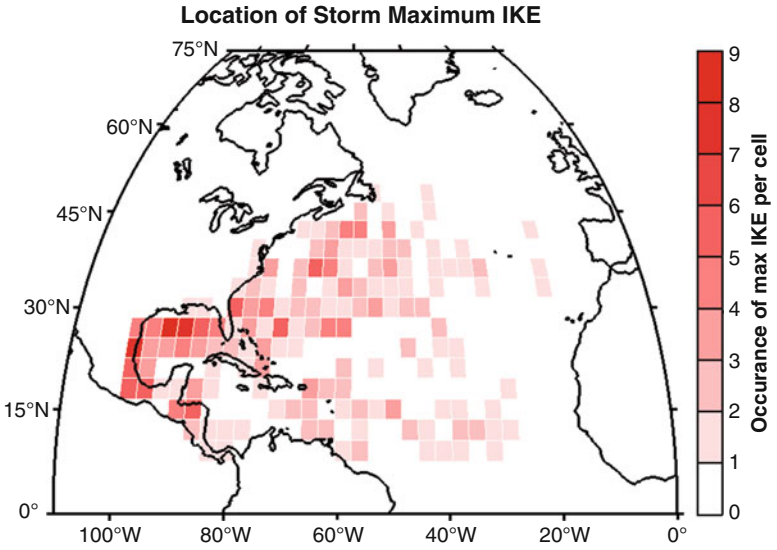

Fig. 3.5 Map showing where tropical cyclones reached their maximum lifetime IKE values from 1990 to 2011, gridded into $3 \times 3^{\circ}$ bins

Indeed, the northwestern part of the basin does not necessarily include the most favorable conditions for traditional TC development throughout most of the year. With the exception of areas along the Gulf Stream, sea surface temperatures (SSTs)

are often cooler in the northern part of the basin, and vertical wind shear also tends to be higher, suggesting that baroclinic effects or trough interactions in the mid-latitudes may be vital for creating and sustaining high IKE storms. All of this suggests that the factors that govern IKE variability are complex and likely regional, with the northern part of the basin likely impacted by more than just the processes that govern traditional intensification. Maclay et al. (2008) indicated that observed intensity and kinetic energy metrics from observations across the basin fit reasonably well to a power law function, with kinetic energy increasing by an order of $(V_{max})^{1.872}$. However, a scatter plot of intensity and IKE shows two different relationships for storms north or south of 30°N latitude (Fig. 3.6). In the southern part of the basin, IKE is tied to intensity, with the two quantities having a correlation of 0.65 (significant at the $p = 0.01$ level). In contrast, IKE and intensity are less correlated in the northern part of the basin, with the highest IKE values all occurring in an intensity sweet spot centered on the lowest Saffir-Simpson Scale category or two.

The evolution of kinetic energy and intensity has been explored at length previously. Musgrave et al. (2012) suggested that the lifecycle for a TC contains three stages—incipient, deepening, and mature—with intensification occurring in the first two phases and kinetic energy growth occurring throughout all phases. The incipient phase includes more gradual increases in kinetic energy and intensity, before intensity begins to increase more rapidly during the deepening phase. Maclay et al. (2008) found that intensifying storms over warm waters and with low shear typically saw less kinetic energy growth than would be expected by the aforementioned power law KE-V_{max} relationship, as these wind speed increases are more confined to the inner core. Putting this all together helps to explain why mean IKE values in the southern half of the basin tend to be more moderate—increasing a little bit more as storms reach the western Caribbean and Gulf of Mexico—as traditional intensification mechanisms typically only increase IKE so far.

However, as Musgrave et al. (2012) points out, kinetic energy continues to increase during the mature phase of a TC, long after the storm reaches its maximum lifetime intensity. In fact, many storms gain IKE quite rapidly as they turn poleward, which likely can be attributed to external forcing from baroclinic influences, trough interactions, and extratropical transitions, which can help to promote increased angular momentum, wind field expansion, and some inner core intensification simultaneously (e.g. Maclay et al. 2008). An IKE-V_{max} diagram of Hurricane Igor in 2010 (Fig. 3.7) serves as a good example that fits closely to the idealized lifecycle for a TC as detailed by Musgrave et al. (2013). IKE increased throughout much of the Igor's lifecycle with the most drastic increase in IKE occurring as Igor interacted with a trough in the mid-latitudes prior to becoming extratropical, causing its lifetime maximum IKE value to be at the end of its life as a tropical cyclone.

Of course, there are many additional processes that can interrupt the idealized evolution of IKE during a TC's lifecycle (and thus the climatological preferences of IKE in the basin) that have not been discussed above. Land interactions are one obvious and noteworthy event that often results in large changes across a TC's structure (e.g. potentially increasing the radius of maximum winds and the general decay of wind speeds over land), which of course will impact IKE. In addition, Sitkowski et al. (2011) found that concentric eyewall replacement cycles also greatly affect the IKE in a

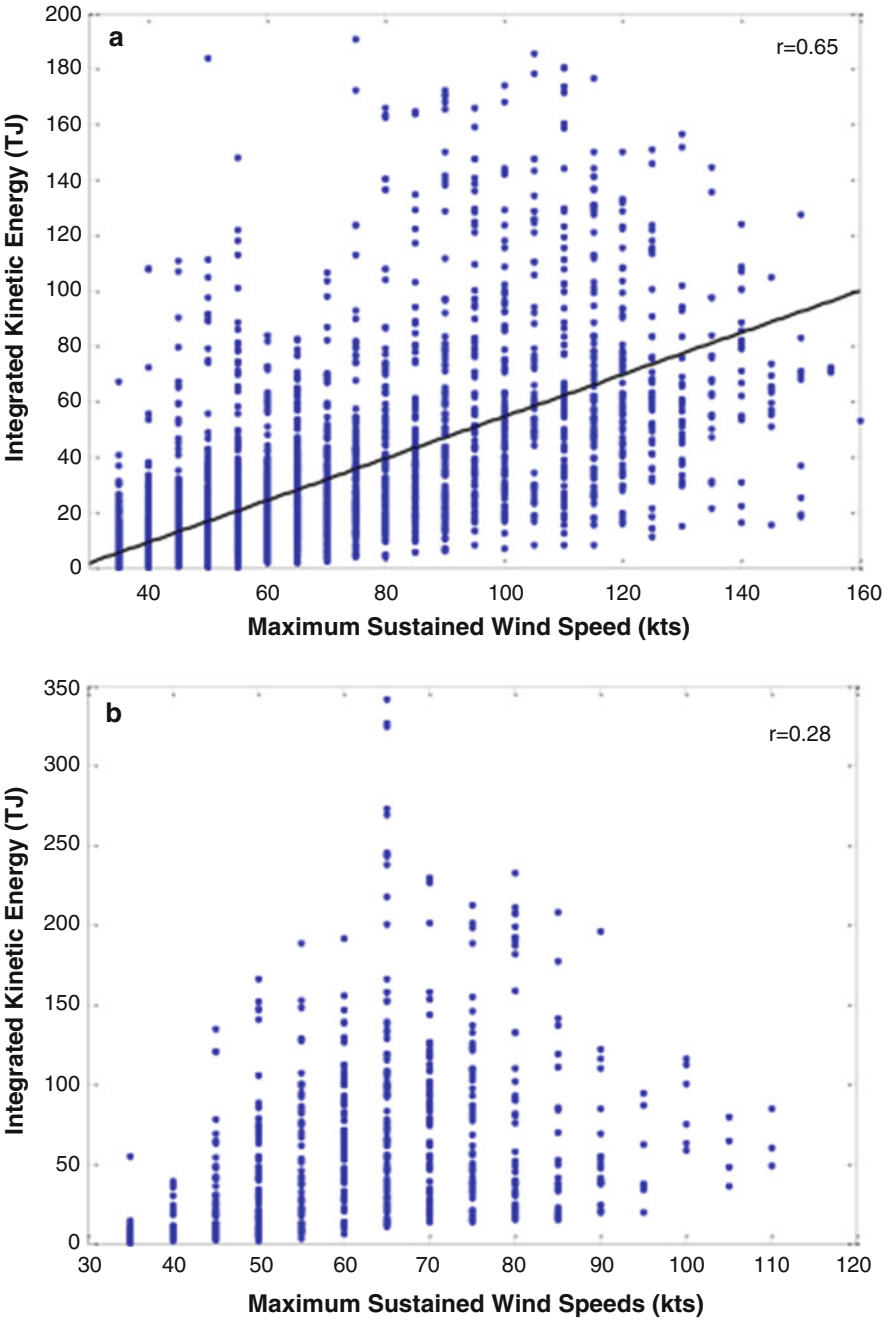

Fig. 3.6 (**a**) Plot of integrated kinetic energy (TJ) versus maximum intensity (kts) for 3896 Atlantic TCs located south of 30°N latitude between 1990 and 2011 (blue dots). The black line represents a linear regression fit for the data. Considering the large sample of storm fixes, the linear correlation is

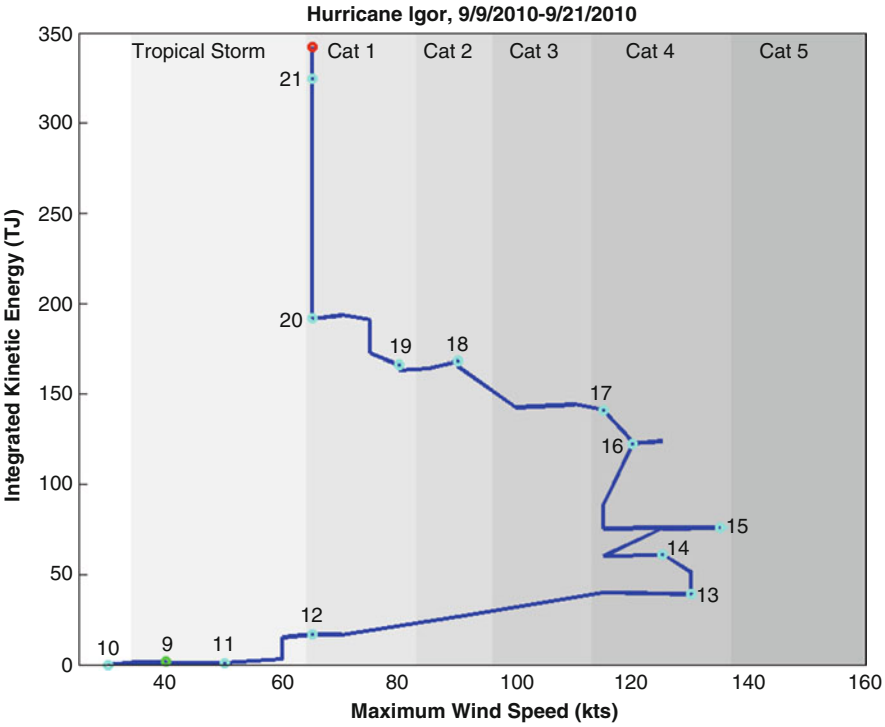

Fig. 3.7 Evolution of integrated kinetic energy (TJ) versus maximum intensity (kts) throughout the lifetime of Hurricane Igor in September of 2010 following Musgrave et al. (2012). The first point on the plot temporally (green circle) occurred on September 9, 2010, shortly after Igor obtained Tropical Storm intensity for the first time. Each of the subsequent cyan circles signals a 00Z storm fix, indicating the passage of a day's time, with the final fix occurring on September 21, 2010 (red circle) when Igor completed its extratropical transition over the North Atlantic

TC's wind field, with an average increase of 28% in a sample of 24 events. Musgrave et al. (2012) visualized these eyewall replacement cycles in the IKE-V_{max} diagram as a brief excursion to lower intensities with continued IKE growth.

3.3 Statistical-Dynamical Sensitivity Tests for Studying IKE Variability

As was summarized in the previous section, IKE has some notable climatological preferences, some strong ties to environmental conditions, and the tendency to increase throughout a TC's lifetime. All of these factors can be leveraged to model

Fig. 3.6 (continued) easily significant at the $p = 0.01$ level. (**b**) Plot of integrated kinetic energy (TJ) versus maximum intensity (kts) for 735 Atlantic TCs located north of 35°N latitude between 1990 and 2011. The correlation between VMAX and IKE in this figure is $r = 0.28$

IKE variability using a statistical-dynamical model of atmospheric and oceanic parameters. Kozar and Misra (2014) and Kozar et al. (2016) offered a proof of concept that IKE can be modeled skillfully relative to persistence and climatology. These models might be used not only for future forecasting applications (with dynamically forecasted predictors), but can also be quite useful for further analyzing the relationships between IKE and the environment, as is done here using a set of sensitivity tests.

For these sensitivity tests, we utilize the system of artificial neural networks presented by Kozar et al. (2016). This statistical-dynamical system, named the Statistical Prediction of IKE Version 2 (SPIKE2), was designed to analyze and hindcast IKE variability in North Atlantic TCs. It builds upon the linear regression techniques used in the first version of SPIKE (Kozar and Misra 2014), by incorporating the intrinsic nonlinear map of weights within the neural networks, which allowed SPIKE2 to anticipate the nonlinearities within the environment-TC system. For example, in traditional TC development, wind shear is typically negatively correlated with inner core intensity and IKE; however, in the mid-latitudes, an increase in shear (to an extent) might benefit outer wind field expansion as extratropical transition often causes wind fields to increase in size (e.g. Evans and Hart 2008). In a linear regression approach, it would be impossible to tease out these complex signals, but the neural networks used for SPIKE2 possess the flexibility to potentially anticipate these signals within the training dataset.

To best estimate how the SPIKE2 neural networks would perform in a forecast realm, Kozar et al. (2016) focused on neural networks that were calibrated and evaluated using reanalysis and hindcast data from the second generation GEFS reforecast project (Hamill et al. 2013). Despite the predictors containing some degree of modeling uncertainty and forecast error, SPIKE2 performed well and was skillful relative to both climatology and persistence out to 72 h. In fact, for a 24-h hindcast, SPIKE2 explained more than 80% of the variance in the IKE record. Despite the impressive hindcast results, this section will move the neural networks back into the perfect prognostic space using historical predictors. The historical predictors in the perfect prognostic space do not contain forecast errors and are better suited for an exercise seeking to best understand how the environment modulates IKE in observed North Atlantic TCs.

In this perfect prognostic setup, SPIKE2 is calibrated and evaluated with eighteen predictors (Table 3.2) to estimate 36-h changes of IKE. The input predictors include metrics relevant to large scale atmospheric/oceanic dynamics and thermodynamics (e.g. deep layer wind shear, upper atmospheric temperatures, relative humidity, sea surface temperatures, and upper level divergence), storm specific parameters (minimum central pressure, maximum wind speed, center position, time since genesis, etc.), and a series of persistence parameters (past 12-h change of intensity and 36-h IKE persistence). Ultimately, these parameters were chosen from a larger pool of candidate predictors based on their physical relationship to storm size and strength, and their significance for statistically modeling IKE. The neural networks were

Table 3.2 List of eighteen predictors used to calibrate the perfect prognostic version of the SPIKE2 neural networks that is used in the sensitivity tests

Variable	Definition	Units
PIKE	36 h persistence of IKE	TJ
dIKE12	Previous 12 h change of IKE	TJ
VMAX	Maximum sustained wind speed	kts
VMPI	Difference between maximum potential intensity and VMAX	kts
LAT	Latitude of storm's center	°N
LON	Longitude of storm's center	−°W
MSLP	Minimum sea level pressure	hPa
PENV	Average surface pressure *(averaged from r = 200–800 km)*	hPa
VORT	850 hPa vorticity *(r = 0–1000 km)*	10^{-7} s^{-1}
D200	200 hPa divergence *(r = 0–1000 km)*	10^{-7} s^{-1}
SHRD	850–200 hPa shear magnitude *(r = 200–800 km)*	kts
SHTD	850–200 hPa shear direction *(r = 200–800 km)*	°
RHLO	850–700 hPa relative humidity *(r = 200–800 km)*	%
RHMD	700–500 hPa relative humidity *(r = 200–800 km)*	%
T150	150 hPa temperatures *(r = 200–800 km)*	°C
SST	Sea surface temperatures	°C
SDAY	Time after tropical storm genesis	days
PDAY	Time from peak of season (Sept. 10)	days

constructed with an optimal number of nodes for these predictors to minimize the chances of overfitting. Kozar et al. (2016) offers a more complete discussion on the construction of the neural network and the selection of the predictors in greater detail. For brevity, each of these parameters will be referred to by its abbreviation in Table 3.2 throughout the remainder of this section.

Most of the eighteen parameters are extracted directly from the Statistical Hurricane Intensity Prediction Scheme (SHIPS)'s developmental dataset (DeMaria and Kaplan 1999), while others are taken from the NOAA Optimum Interpolation SST ("OI SST"; Reynolds et al. 2007) dataset and the NHC best track dataset (Jarvinen and Neumann 1979, Jarvinen et al. 1984). In the end, all predictors are normalized by the mean and standard deviation of the observed sample, which is comprised of more than 15 years of Atlantic TC data. Of course, the corresponding IKE targets used in calibration of the neural networks are taken from the wind radii-based historical record that has been described at length in the previous sections. Overall, the neural networks are trained on these 18 parameters for more than 3000 six-hourly storm fixes between 1995 and 2011.

The resulting statistical fit between SPIKE2's estimates of IKE and the historical record of IKE is a correlation greater than 0.90. The observed distribution of 36-h IKE tendency is also modeled reasonably well when given historical parameters (Fig. 3.8), albeit the modeled IKE tendency values are skewed more towards small

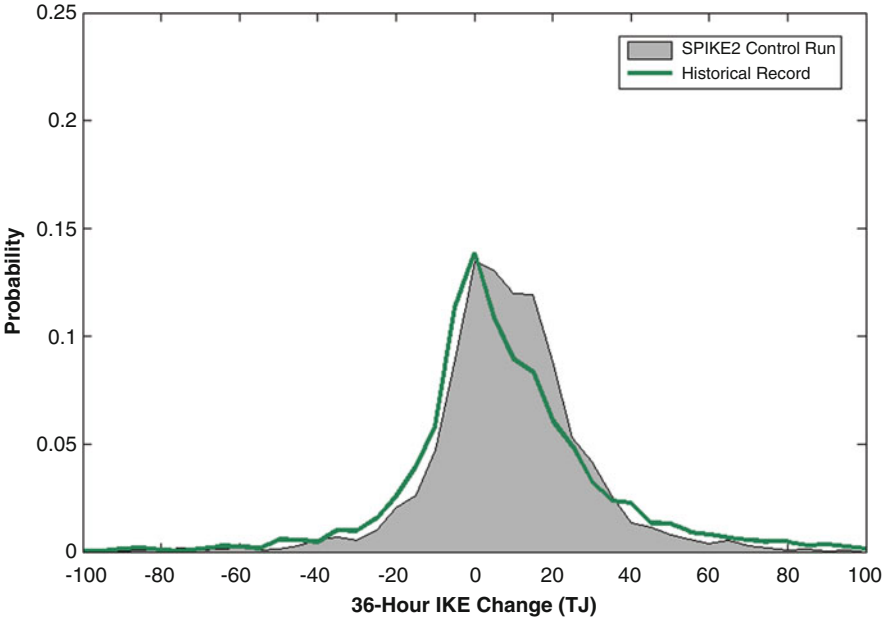

Fig. 3.8 Probability distribution of 36-h IKE change from the control run of the SPIKE2 neural network system and from the historical record. Approximately 3000 storm fixes from 1995 to 2011 are included in this distribution

increases of IKE than is observed. Given SPIKE2's ability to recreate the historical record of IKE, we are interested in learning how sensitive the modeled IKE estimates are to each predictor. As such, we will use a run of SPIKE2 with the unaltered historical parameters as the control run, and then each parameter will be perturbed one at a time by $\pm 1\sigma$ and $\pm 2\sigma$ for all of the 3000 fixes in the training dataset to examine how the nonlinear statistical model responds to perturbations in the environment. The distributions of IKE tendency as predicted by SPIKE2 in each perturbation run will be plotted against the control to best approximate how changes in the storm or the environment are likely to influence IKE tendency in an Atlantic TC (Fig. 3.9). Furthermore, the median of the distributions from each perturbation run is compared to the control run to see whether or not the distributions of IKE tendency systematically shift towards more negative or positive values (Table 3.3). The results of this sensitivity test are discussed at length by Kozar (2015), with the most significant results discussed in the remainder of this section.

Overall, the modeled distribution of IKE is most sensitive to the persistence and intensity parameters, with a few dynamical, thermodynamical, and positional parameters also having a significant impact on IKE variability. The significance of the persistence parameter is not entirely surprising. The positive shift in the distribution for the negative IKE perturbation test indicates that smaller developing TCs with less

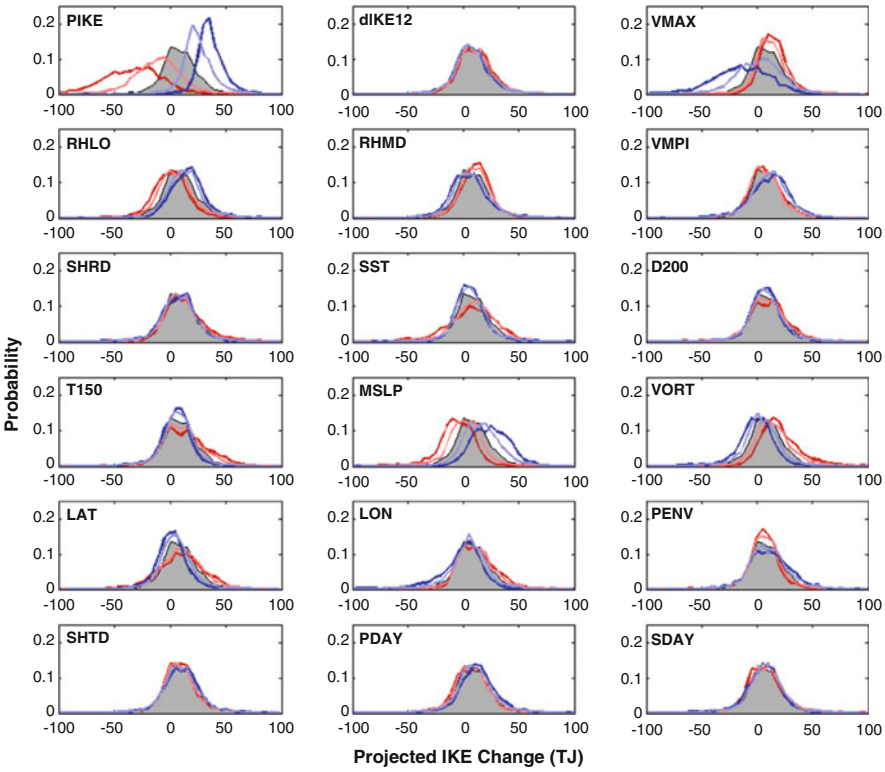

Fig. 3.9 The results of the sensitivity exercise are presented by showing how variations of each input parameter affect the probability distribution of a 36-h deterministic projection of IKE change from SPIKE2 for nearly 3000 TC fixes in the North Atlantic basin. The probability distribution for the control run is shown in each panel with a grey shaded polygon. The red curves show the distribution of projected IKE change from SPIKE2 when a single predictor is increased by one standard deviation (light red curve) or two standard deviations (dark red curve) for all historical TC fixes. The blue curves show the distribution of projected IKE change from SPIKE2 when each observed predictor is decreased by one standard deviation (light blue curve) or two standard deviations (dark blue curve) for all historical TC fixes

IKE are more likely to gain IKE, as long as other conditions are not too prohibitive, which is consistent with the theory that TCs gain IKE for most of their lifetime over the open ocean, even as intensity fluctuates, such that they obtain their maximum value of IKE prior to landfall or the completion of ET (Musgrave et al. 2012). In addition, this negative relationship between PIKE and IKE tendency is influenced by the fact that a storm with higher values of IKE obviously has more IKE to lose than does a smaller storm. Therefore, a storm with 100 TJs could theoretically lose or gain a large amount of IKE, causing the distribution of modeled IKE tendency to become broader for the positive PIKE perturbations.

Both intensity-related metrics – maximum sustained winds and minimum central pressure – have significant relationships with the modeled IKE tendency values. As

Table 3.3 Percent changes for median SPIKE2 projections of IKE tendency in each perturbation run relative to a control simulation

		Perturbations to Variables			
		−2σ	**−1σ**	**+1σ**	**+2σ**
Perturbed Input Parameter	**PIKE**	*268%*	*150%*	*−177%*	*−406%*
	dIKE12	*−13%*	*−8%*	11%	*25%*
	VMAX	*−215%*	*−61%*	*34%*	*59%*
	RHLO	*75%*	*45%*	*−39%*	*−71%*
	RHMD	*−37%*	*−20%*	*21%*	*32%*
	VMPI	*43%*	*36%*	*−17%*	−11%
	SHRD	*−2%*	*−3%*	*11%*	*31%*
	SST	*−21%*	*−16%*	*18%*	1%
	D200	*−6%*	*−4%*	10%	*26%*
	T150	*−23%*	*−9%*	*19%*	*46%*
	MSLP	*157%*	*79%*	*−62%*	*−133%*
	VORT	*−86%*	*−42%*	*49%*	*97%*
	LAT	*−62%*	*−33%*	*23%*	*12%*
	LON	*−69%*	*−25%*	*20%*	*28%*
	PENV	*23%*	*14%*	*−7%*	*−17%*
	SHTD	*24%*	*12%*	*−5%*	0%
	PDAY	*43%*	*17%*	*−4%*	*−9%*
	SDAY	*−16%*	0%	*−1%*	*−19%*

As discussed in Sect. 3.3, each perturbation run adjusts exactly one variable (leftmost column) up or down by either one or two standard deviations (topmost row). The resulting changes of IKE were tested for significance with a two-sample bootstrapping exercise. Those that are deemed significant at the two-sided 95% level are displayed in a italic font

intensity increases, IKE growth tends to be more prevalent, causing the distributions in Fig. 3.9 to shift to the right as VMAX is perturbed upward and MSLP downward. This result is not surprising, considering that Musgrave et al. (2012) showed the greatest gains in IKE to occur during the deepening and mature phases of a TCs life cycle. Despite their similarities, MSLP and VMAX interestingly affect the distribution of modeled IKE tendency values in vastly different manners. For instance, the negative VMAX perturbation runs have a broader distribution than the control run and any other VMAX or MSLP perturbation run. Therefore, a low intensity in terms of VMAX at the valid forecast time does not prevent SPIKE2 from projecting IKE to increase if other environmental parameters are favorable. In contrast, the distribution for the positive MSLP perturbation runs is shaped very similarly to the control run, albeit shifted to the left. This makes it less likely for TCs to gain an appreciable amount of IKE when its MSLP is high, as storms with higher central pressures are typically in their incipient phases (and not gaining IKE rapidly yet) or are approaching the end of their lifetime following decay in prohibitive environments (e.g. high shear or movement over land).

The differences between the distribution of the runs with negative VMAX and the distribution with positive MSLP perturbations arise because VMAX does not have a truly linear relationship with MSLP, with many operationally used pressure-wind relationships taking storm size and other environmental parameters into account (e.g. Knaff and Zehr 2007). For example, in the historical record, there are plenty of storms that have anomalously low minimum pressure levels, despite modest maximum wind speeds, especially in the mid-latitudes (e.g. Hurricane Sandy). Likewise, there are plenty of TCs that have modest values of VMAX (~50 to 70 kts) and anomalously high values of IKE (>100 TJ). As a result, it is not a surprise that the negative VMAX perturbation runs have a broader distribution to capture the possibility for high and low IKE storms depending on the other environmental and positional parameters.

On the subject of positional parameters, SPIKE2 also suggests that increasing latitude will result in IKE growth more often than not. The positive LAT perturbation runs have distributions that are skewed to the right when compared to the control run (Fig. 3.9). As a result, the median of the distribution for the $+1\sigma$ and $+2\sigma$ LAT perturbation tests is significantly greater than that of the control run at the 99% confidence level based on simple two-sample bootstrapping tests (Table 3.3). Interestingly, the distribution is not shifted quite as far away from the control run when compared with the MSLP, VMAX, and PIKE perturbation runs. This is not terribly surprising, considering that geographical positions are often overruled by the actual environmental conditions near the storm. As a result, the distribution of the positive LAT perturbation tests is somewhat broader than in the control run. This ultimately allows for a storm to have decreasing IKE when entering higher latitudes if the storm is not likely to undergo expansion from extratropical transition or trough interactions. In that regard, if a TC is over the high latitudes (LAT $= +1\sigma$), with cold oceans (SSTs $= -2\sigma$), with moderately low intensity (MSLP $= +1\sigma$; VMAX $= -1\sigma$), and its IKE has already begun to fall (dIKE $= -2\sigma$), SPIKE2 will project IKE to continue falling.

Dynamical predictors such as low-level vorticity also show some significant sensitivity to IKE variability (Table 3.3). Indeed, VORT has a strong positive relationship with modeled IKE tendency. Positive perturbations of VORT shift the distribution towards positive SPIKE2 projections, and the negative VORT perturbation runs result in a shift towards more negative IKE changes (Fig. 3.9). Overall, storm growth is projected to occur more frequently when VORT increases, and storm decay becomes more likely when a storm has either a small or weak vorticity signature, which is not surprising given that a stronger and larger circulation with high vorticity is indicative of high relative angular momentum and a strong cyclonic wind field.

Additionally, T150 also shows a significant relationship with the modeled IKE tendency distribution. The metric was used by Maclay et al. (2008) to examine kinetic energy variability, with the upper tropospheric temperatures standing in as a proxy for the tropopause height. Higher T150 values are indicative of a lower

tropopause, which is a characteristic of the higher latitudes. Given the tendency for the largest IKE changes to occur in the mid-latitudes (large gains from trough interactions, and large drops from storm decay over prohibitively cold waters), the negative T150 perturbations produce a narrower distribution, while the positive perturbations produce a wider distribution. The increase in moderate to large IKE gains in the positive T150 runs are consistent with the observed rapid growth in storms like Sandy and Igor.

On the other hand, some other predictors well known to influence TC development like SHRD and SST do not cause a systematic shift in the distribution of IKE tendency. This is likely due to the complexity of the nonlinear signals between these predictors and IKE. Through further testing it becomes clear that many of these predictors affect IKE variability in different environmental regimes. For instance, an extra perturbation test over the lower latitudes with negatively perturbed LAT and negatively perturbed T150 shows that IKE has a tendency to grow with increasing SST and decreasing SHRD, which is not true in higher latitudes where non-tropical mechanisms such as trough interactions and baroclinic forcing can allow storms to grow in size while possibly also increasing intensity briefly as storms begin to transition (e.g. Maclay et al. 2008).

Ultimately, the results presented from these sensitivity tests offer some clues on how the IKE of Atlantic TCs may respond to our changing climate. Some recent literature has suggested that stronger storms are migrating northward (e.g. Kossin et al. 2014; Baldini et al. 2016) as warm sea surface temperatures expand poleward. The sensitivity tests indicate that IKE growth is promoted when storms are more intense and in regions of higher latitude. As such, one could hypothesize that, all else being equal, a poleward shift in TC activity could promote greater increases in IKE on a per storm basis, as storms approach the Mid-Atlantic United States and interact with mid-latitude features. However, when focusing on just the North Atlantic, this poleward trend might be less significant and might even be negative in the basin (Moon et al. 2015; Kossin et al. 2016).

Other studies have also indicated that the global tropics are expanding (Lucas et al. 2014) and that baroclinicity could become weaker in the mid-latitudes, which could affect the extratropical transition process (Ito et al. 2016). All of these factors, along with long-term variability in cyclogenesis and steering currents, could have ramifications for where TCs are most likely to gain IKE. Given all of the complexities within the dynamics and thermodynamics of a changing climate, more work is clearly needed to evaluate whether or not higher IKE storms will become proportionally more common in the future, and/or whether or not the regions for IKE gain will shift across the basin at all.

3.4 Lower Frequency IKE Variability and Seasonal Applications of IKE

The six-hourly historical IKE record in the Atlantic can also be used to investigate whether or not any longer-term trends exist for IKE in the Atlantic basin. Powell and Kozar (2015) presented some initial findings that focused on interannual IKE variability. There is some slight evidence of increased IKE values for storms in the North Atlantic basin over a 25-year sample from 1990 to 2014 (Powell and Kozar 2015). Linear trend lines for the frequency of storms that exceed 25 TJs and 50 TJs are both positive during this timeframe, but they were not significant by any measure. In fact, much of this positive trend can be attributed to the lower number of TCs in the early 1990s, relative to the high annual counts seen afterwards. The peak instantaneous IKE value observed in any storm for a given year, which is less dependent on TC frequencies, also contains a positive trend (Powell and Kozar 2015). However, it is important to note that this sample is relatively short for investigating variability on interannual and longer scales, allowing for anomalous years (2005) and anomalously high-IKE storms (e.g. Igor, Sandy) to dominate the longer-term signal. As such, further work and a longer historical record are both clearly needed to better understand longer-term variability of IKE in Atlantic. tropical cyclones.

The record of IKE values can also be extended to monitor seasonal TC activity by aggregating IKE values across the lifetime of all TCs in a given year. To this end, Misra et al. (2013) proposed the Track Integrated Kinetic Energy (TIKE), the sum of IKE over the TC lifetime, which has some similarity to Accumulated Cyclone Energy (ACE; Bell et al. 2000) and Power Dissipation Index (PDI; Emanuel 2005, 2007). However, these latter indices are critically dependent on the intensity, with ACE and PDI proportional to the second and third power of the maximum sustained wind speed of a TC, and ignore the size aspect of the TC. In contrast, TIKE is comprehensive, in that it integrates the size, the wind speed, and the life span of the TC. Misra et al. (2013) computed TIKE for each named TC in the North Atlantic between 1990 and 2011 by summing the IKE values every 6 h over the lifetime of the TC.

Analysis of average monthly TIKE values reveals a peak in September (Fig. 3.10) coinciding with the corresponding peak in larger and longer-living TCs in the same month (Misra et al. 2013). Meanwhile, annual TIKE values exhibit significant interannual variations that are comparable to variations in other metrics that measure seasonal Atlantic TC activity (Fig. 3.11). The correlation over the North Atlantic between TIKE and ACE is 0.86, between TIKE and number of storms is 0.61, and between ACE and number of storms is 0.78. There are some notable differences between TIKE and the other metrics, however. Yu et al. (2009) and later Yu and Chiu (2012) noted that the differences between seasonal metrics that incorporate storm size and those that are intensity-based will grow exponentially as storm intensities increase. As such, comparisons between TIKE and ACE, as well as annual TC counts, are quite illuminating (Fig. 3.11). For example, the 2005 season,

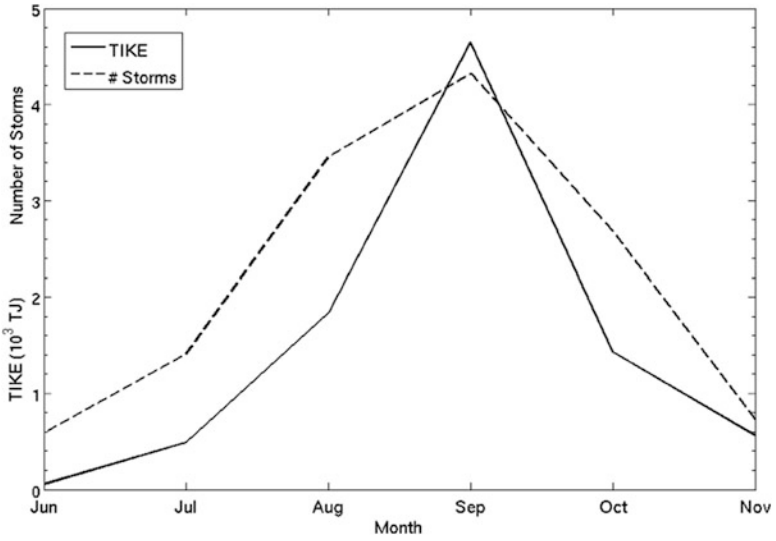

Fig. 3.10 Monthly climatology of TIKE and the number of tropical storms in the North Atlantic basin between 1990 and 2011. (From Misra et al. 2013)

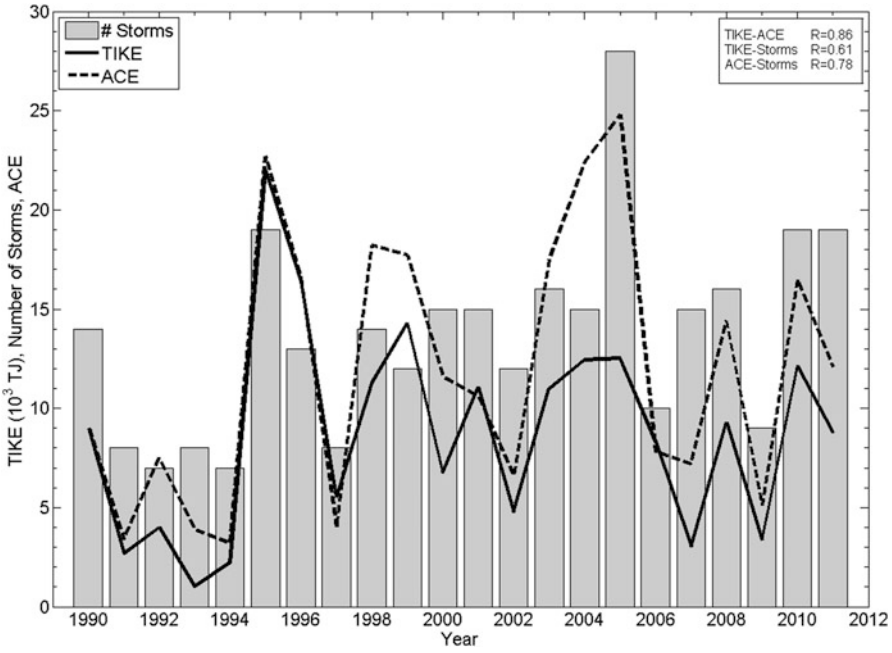

Fig. 3.11 Time series of TIKE, ACE and number of tropical storms in the North Atlantic basin from 1990 to 2011. (Adapted from Misra et al. 2013)

with its 28 named Atlantic TCs, appeared as a highly anomalous year in terms of ACE and the number of TCs in a season. However, TIKE proved to be far less anomalous in 2005. With the exception of a few notable storms such as Katrina, this comparison reveals that 2005 was not characterized by as many large-sized and long-lived TCs as other active seasons, such as 1995. Overall, the most anomalously high TIKE years were 1995 followed by 1996, 1999, and 2012, with 1993 and 2013 being the two least active years since 1990 as measured by TIKE.

Misra et al. (2013) also examined interannual variations of TIKE with global SST variations. Like most other indices of Atlantic TC activity (e.g. ACE), TIKE exhibits a robust relationship with SST variations in the equatorial Pacific associated with the El Niño Southern Oscillation (ENSO). Figure 3.12 suggests that a warm (cold) ENSO phase is associated with anomalously small (large) Atlantic TIKE. This is consistent with earlier studies which indicated that cold ENSO events are associated with not only increased TC activity as a whole, but also more recurving and landfalling TCs in the Atlantic (Bove et al. 1998; Kossin et al. 2010; Colbert and Soden 2012). In other words, cold ENSO events are associated with more TCs in the western tropical Atlantic and northern (extra-tropical) Atlantic, such that the existence of longer-lived and higher IKE storms is promoted, leading to a higher accumulation of TIKE throughout the course of a La Niña hurricane season.

Similarly, Misra et al. (2013) also investigated ties between interannual variations of TIKE and Atlantic Warm Pool (AWP) variability. The AWP is defined as the area enclosed by the 28.5 °C isotherm in the tropical-subtropical Atlantic Ocean and is a robust seasonal phenomenon that coincides with the Atlantic hurricane season (Wang and Enfield 2001). Ultimately, a positive correlation of 0.43 exists between TIKE of Atlantic TCs and the area covered by the AWP from August through October. In other words, large AWP seasons are associated with increased likelihood of larger values of TIKE and small AWP seasons are associated with smaller annual accumulations of TIKE.

Physically, this positive relationship between the size of the AWP and TIKE is consistent with the findings of earlier research. For instance, the AWP's interannual variability corresponds well with variations of the North Atlantic Subtropical High (NASH; Wang and Enfield 2001; Wang et al. 2006), which has implications for TC behavior in the entire basin. More specifically, a large (small) seasonal mean AWP is associated with a weakened (strengthened) NASH and increased (decreased) atmospheric convection and cloud cover over the AWP region. Furthermore, large seasonal AWPs correspond to weaker tropospheric vertical wind shear and a deep warm upper ocean, thus making the large-scale environment conducive for an active Atlantic TC season, with the opposite being true for small AWP seasons. Wang et al. (2011) also show that the AWP has a significant bearing on the steering flow of Atlantic TCs through its connections with the NASH, resulting in the likelihood of fewer United States landfalling TCs along the eastern seaboard during large AWP years. Putting all of this together, during large AWP years, the overall frequency of TC events is increased and storms tend to have longer life spans with larger radial

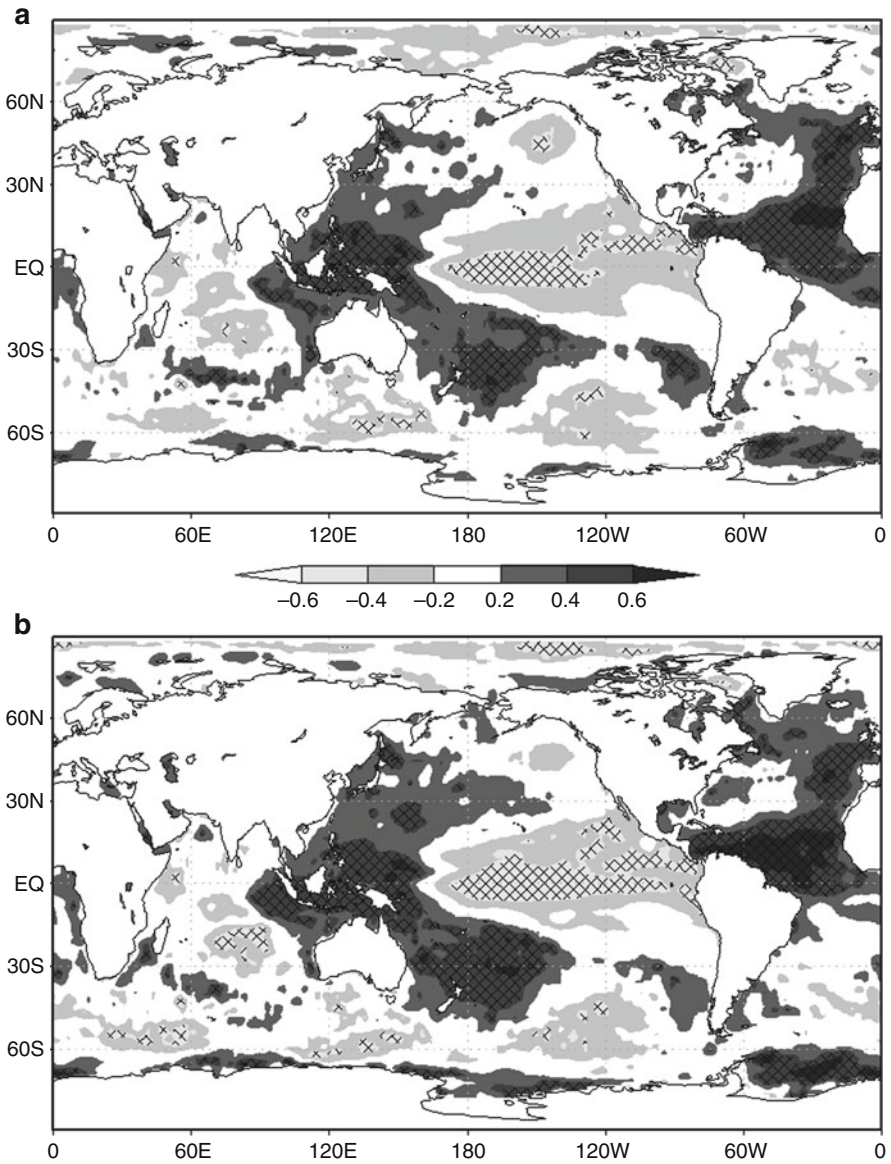

Fig. 3.12 Correlation of (**a**) TIKE and (**b**) ACE in the North Atlantic basin with contemporaneous seasonal mean SST anomalies from OISSTv2. Hashed regions show significance at the 95% confidence interval according to Student's t-test. (From Misra et al. 2013)

extents as they form further east and recurve away from the United States more frequently into an area that climatologically promotes higher IKE values. All of this ultimately ties back to an unsurprising positive relationship between interannual variations of TIKE and the AWP.

3.5 Summary and Conclusions

This chapter provides a review of IKE-related studies. The majority of these studies are confined to the North Atlantic basin, where aircraft observations are most prevalent and IKE can be consistently estimated from the historical record extending back to the 1990s. The other tropical basins are less data rich with fewer observations and more limited historical datasets. With the help of remotely sensed wind data the gaps in many of the world's oceans are being filled to some extent, and in a few years, it appears that IKE could be studied more extensively in all tropical basins.

IKE is demonstrably a very useful metric to characterize TCs. Its emphasis on size and wind structure around the azimuth of the TC provides a realistic estimate of the potential damage that TCs can cause upon landfall. IKE scales very well with wind stress over ocean and wind load forcing on structures that in turn relate to storm surge and wind damage respectively. Therefore, pursuing IKE as a complementary metric to existing practices to monitor and forecast TCs would be prudent, especially in efforts to guide in mitigating and avoiding risks from landfalling TCs.

IKE is intrinsically related to intensity metrics in a TC. The incipient, development, mature, and decay stages of a TC characterized in terms of its intensity metrics have distinct IKE tendency features as well. Although IKE typically increases through a storm's lifetime from traditional TC development mechanisms, the most rapid increase in IKE is often seen later in a storm's lifecycle as storms undergo expansion of their outer wind fields around the time of their extratropical transition. Modeling IKE and a series of environmental parameters offers some evidence regarding how the kinetic energy of a storm varies physically. As expected, IKE tends to increase with increasing lower-level vorticity and decreasing central pressure. However, the relationships between IKE and other metrics such as ocean thermodynamics and upper level winds can be more complex.

If there is a growing trend of intense TCs migrating northward over time, this could imply the potential for a corresponding growing trend in IKE across the North Atlantic, as IKE growth is promoted both when storms intensify and while storms move into the mid-latitudes. With all of the nonlinearities in the system, such as the fact that moderate shear can be both a hindrance and a supporting mechanism for storm growth, it may be difficult to estimate how IKE variability will change in a future climate, and future work is quite clearly needed. The over two decades of wind radii data for the North Atlantic with their associated uncertainties may be insufficient to conduct a rigorous trend analysis of IKE. However, statistical-

dynamical models like SPIKE2 can be integrated with model simulations of the future climate to better assess projected IKE changes in the future.

Beyond individual storms, IKE estimates can be aggregated into a seasonal metric, TIKE, which offers a unique evaluation of a season's activity level. TIKE is appealing because of its comprehensive nature to capture size, duration, intensity, and number of TCs in a particular season. Given a longer record of wind structure, these seasonal TIKE estimates can build upon the initial results presented here to better understand how climate cycles affect the interannual variability of more than just storm intensity and frequency.

Overall, the review above clearly shows that the studies on IKE are still in their infancy, and there is yet a lot to be understood and derived from them. Much of the current work is focused in utilizing IKE for operational use. In the meanwhile, the community would be well served to pursue further progress in understanding and predicting the variability of IKE and the overall TC wind field structure, given the significance of both storm size and intensity to hurricane damage. More specifically, model- and observationally-based case studies specifically focused on IKE and storm structure would be helpful to better understand how storm-specific dynamics and environmental forcings modulate IKE during the lifetime of a TC. On longer timescales, additional research clearly is needed to better understand historical interannual and multi-decadal IKE variability, since most of the work presented here is limited to just the past 20–30 years. By understanding the long-term historical trends, and by improving future climate projections, it should be possible to better understand how IKE might vary in a future climate. Finally, as mentioned earlier in this section, nearly all of the research on IKE is limited to the North Atlantic. As data quality and coverage improves around the globe, studies should expand to other basins to get a more comprehensive global perspective on IKE and its variability.

Acknowledgements We thank Drs. Frank Marks, Jonathan Vigh, and the editorial staff for their very useful reviews and comments on an earlier version of this chapter. Sections of this chapter are adapted from the Ph. D. dissertation of the first author. Thanks are also due to Drs. Robert Hart, Mark Powell, Phillip Sura, Allan Clarke, Ming Ye, and Mark Bourassa for their helpful comments and feedback. This work was supported by grants from NOAA (NA12OAR4310078) USGS (USGSG13AC00408), and South Florida Water Management District (PO 039231).

References

Atlas R, Hoffman RN, Ardizzone J, Leidner SM, Jusem JC, Smith DK, Gombos D (2011) A cross-calibrated, multiplatform ocean surface wind velocity product for meteorological and oceanographic applications. Bull Am Meteorol Soc 92:157–174. https://doi.org/10.1175/2010BAMS2946.1

Baldini LM et al (2016) Persistent northward North Atlantic tropical cyclone track migration over the past five centuries. Sci Rep 6:37522. https://doi.org/10.1038/srep37522

Bove MC, Elsner JB, Landsea CW, Niu X, O'Brien JJ (1998) Effects of El Niño on U.S. landfalling hurricanes, revisited. Bull Am Meteorol Soc 79:2477–2482. https://doi.org/10.1175/1520-0477(1998)079<2477:EOENOO>2.0.CO;2

Brennan MJ, Hennon CC, Knabb RD (2009) The operational use of QuikSCAT ocean surface vector winds at the National Hurricane Center. Weather Forecast 24:621–645. https://doi.org/10.1175/2008WAF2222188.1

Buchanan S, Misra V, Bhardwaj A (2018) Integrated kinetic energy of Atlantic tropical cyclones in a global ocean surface wind analysis. Int J Climatol 38:2651–2661. https://doi.org/10.1002/joc.5450

Cangialosi JP, Landsea CW (2016) An examination of model and official national hurricane center tropical cyclone size forecasts. Weather Forecast 31:1293–1300

Colbert AJ, Soden BJ (2012) Climatological variations in North Atlantic tropical cyclone tracks. J Clim 25:657–673. https://doi.org/10.1175/JCLI-D-11-00034.1

Crosset KM, Culliton TJ, Wiley PC, Goodspeed TR (2004) Population trends along the coastal United States: 1980–2008. National Oceanic and Atmospheric Administration, Silver Spring, p 47 https://aamboceanservice.blob.core.windows.net/oceanserviceprod/programs/mb/pdfs/coastal_pop_trends_complete.pdf

Dean L, Emanuel KA, Chavas DR (2009) On the size distribution of Atlantic tropical cyclones. Geophys Res Lett 36:L14803

DeMaria M, Kaplan J (1999) An updated statistical hurricane intensity prediction scheme (SHIPS) for the Atlantic and eastern north Pacific basins. Weather Forecast 14:326–337

Demuth J, DeMaria M, Knaff JA, Vonder Haar TH (2004) Validation of an Advanced Microwave Sounder Unit (AMSU) tropical cyclone intensity and size estimation algorithm. J Appl Meteorol Climatol 43:282–296. https://doi.org/10.1175/1520-0450(2004)043,0282:EOAMSU.2.0.CO;2

Demuth J, DeMaria M, Knaff JA (2006) Improvement of advanced microwave sounding unit tropical cyclone intensity and size estimation algorithms. J Appl Meteorol Climatol 45:1573–1581. https://doi.org/10.1175/JAM2429.1

Emanuel K (2005) Increasing destructiveness of tropical cyclones over the past 30 years. Nature 436:686–688

Emanuel K (2007) Environmental factors affecting tropical cyclone power dissipation. J Clim 20:5497–5509

Evans C, Hart RE (2008) Analysis of the wind field evolution associated with the extratropical Transition of Bonnie (1998). Mon Weather Rev 136:2047–2065

Hamill TM, Bates GT, Whitaker JS, Murray DR, Fiorino MI, Galarneau TJ, Zhu Y, Lapenta W (2013) NOAA's second-generation global medium-range ensemble reforecast dataset. Bull Am Meteorol Soc 94:1553–1565

Holmlund K, Velden C, Rohn M (2001) Enhanced automated quality control applied to high-density satellite derived winds. Mon Weather Rev 129:517–529. https://doi.org/10.1175/1520-0493(2001)129,0517:EAQCAT.2.0.CO;2

Irish JL, Resio DT, Ratcliff JJ (2008) The influence of storm size on hurricane surge. J Phys Oceanogr 38:2003–2013

Ito R, Takemi T, Arakawa O (2016) A possible reduction in the severity of typhoon wind in the northern part of Japan under global warming: a case study. SOLA 12:100–105. https://doi.org/10.2151/sola.2016-023

Jarvinen BR, Neumann CJ, (1979) Statistical forecasts of tropical cyclone intensity for the North Atlantic basin. NOAA Tech Memo NWS NHC-10, 22 pp

Jarvinen BR, Neumann CJ, Davis MAS (1984) A tropical cyclone data tape for the North Atlantic Basin, 1886–1983: contents, limitations, and uses. NOAA Technical Memorandum NWS NHC 22, Coral Gables, 21 pp

Kantha L (2006) Time to replace the Saffir-Simpson hurricane scale? Eos Trans AGU 87(1):3. https://doi.org/10.1029/2006EO010003

Knaff JA, Zehr RM (2007) Reexamination of tropical cyclone wind-pressure relationships. Weather Forecast 22:71–88

Knaff JA, Slocum CJ, Musgrave KD, Sampson CR, Strahl B (2016) Using routinely available information to estimate tropical cyclone wind structure. Mon Weather Rev 144:1233–1247. https://doi.org/10.1175/MWR-D-15-0267.1

Kossin JP, Camargo SJ, Sitkowski M (2010) Climate modulation of North Atlantic hurricane tracks. J Clim 23:3057–3076. https://doi.org/10.1175/2010JCLI3497.1

Kossin JP, Emanuel KA, Vecchi GA (2014) The poleward migration of the location of tropical cyclone maximum intensity. Nature 509:349–352. https://doi.org/10.1038/nature13278
Kozar ME (2015) Analysis and prediction of integrated kinetic energy in Atlantic tropical cyclones. Dissertation, Florida State University
Kozar ME, Misra V (2014) Statistical prediction of integrated kinetic energy in North Atlantic Tropical cyclones. Mon Weather Rev 142:4646–4657. https://doi.org/10.1175/MWR-D-14-001117.1
Kozar ME, Misra V, Powell MD (2016) Hindcasts of integrated kinetic energy in Atlantic tropical cyclones: a neural network prediction scheme. Mon Weather Rev 144:4591–4602. https://doi.org/10.1175/MWR-D016-0030.1
Landsea CW, Franklin JL (2013) Atlantic hurricane database uncertainty and presentation of a new database format. Mon Weather Rev 141:3576–3592
Lucas C, Timbal B, Nguyen H (2014) The expanding tropics: a critical assessment of the observational and modeling studies. WIREs Clim Chang 5:89–112
Maclay KS, DeMaria M, Vonder Haar TH (2008) Tropical cyclone inner-core kinetic energy evolution. Mon Weather Rev 136:4882–4898
Manning DM, Hart RE (2007) Evolution of North Atlantic ERA40 tropical cyclone representation. Geophys Res Lett 34(5):L05705. https://doi.org/10.1029/2006GL028266
Misra V, DiNapoli S, Powell M (2013) The track integrated kinetic energy of Atlantic tropical cyclones. Mon Weather Rev 141:2383–2389
Moon I-J, Kim S-H, Klotzbach P, Chan JCL (2015) Roles of interbasin frequency changes in the poleward shifts of the maximum intensity location of tropical cyclones. Environ Res Lett 10:104004. https://doi.org/10.1088/1748-9326/10/10/104004
Morris M, Ruf CS (2016) Estimating tropical cyclone integrated kinetic energy with the CYGNSS satellite constellation. J Appl Meteorol Climatol 56:235–245. https://doi.org/10.1175/JAMC-D-16-0176.1
Murnane RJ, Elsner JB (2012) Maximum wind speeds and US hurricane losses. Geophys Res Lett 39:L16707. https://doi.org/10.1029/2012GL052740
Musgrave KD, Taft RK, Vigh JL, McNoldy BD, Schubert WH (2012) Time evolution of the intensity and size of tropical cyclones. J Adv Model Earth Syst 4:M08001
Pielke RA Jr, Landsea CW (1998) Normalized hurricane damages in the United States: 1925–1995. Weather Forecast 13(3):621–631. https://doi.org/10.1175/1520-0434(1998)013<0621:NHDITU>2.0.CO;2
Powell M, Kozar M, (2015) Tropical cyclone integrated kinetic energy in the Atlantic basin. 5th Int. Summit on Hurricanes and Clim Change, Crete, Greece, Aegean Conferences, 24
Powell MD, Reinhold TA (2007) Tropical cyclone destructive potential by integrated kinetic energy. Bull Am Meteorol Soc 88:513–526
Powell MD, Houston SH, Amat LR, Morisseau-Leroy N (1998) The HRD real-time hurricane wind analysis system. J Wind Eng Ind Aerodyn 77–78:53–64
Rappaport EN et al (2009) Advances and challenges at the National Hurricane Center. Weather Forecast 24:395–419. https://doi.org/10.1175/2008WAF2222128.1
Schenkel BA, Hart RE (2012) An examination of tropical cyclone position, intensity, and intensity life cycle within atmospheric reanalysis datasets. J Clim 25(10):3453–3475
Sitkowski M, Koss JP, Rozoff CM (2011) Intensity and structure changes during hurricane eyewall replacement cycles. Mon Weather Rev 139:3829–3847
Velden C et al (2005) Recent innovations in deriving tropospheric winds from meteorological satellites. Bull Am Meteorol Soc 86:205–223. https://doi.org/10.1175/BAMS-86-2-205
Vigh JL, Knaff JA, Schubert WH (2012) A climatology of hurricane eye formation. Mon Weather Rev 140:1405–1426. https://doi.org/10.1175/MWR-D-11-00108.1
Wang C, Enfield DB (2001) The tropical Western Hemisphere warm pool. Geophys Res Lett 28:1635–1638. https://doi.org/10.1029/2000GL011763

Wang C, Enfield DB, Lee S-K, Landsea CW (2006) Influences of the Atlantic warm pool on Western Hemisphere summer rainfall and Atlantic hurricanes. J Clim 19:3011–3028. https://doi.org/10.1175/JCLI3770.1

Wang C, Liu H, Lee S-K, Atlas R (2011) Impact of the Atlantic warm pool on United States landfalling hurricanes. Geophys Res Lett 38:1635–1638. https://doi.org/10.1029/2011GL049265

Weissman DE, Stiles BW, Hristova-Veleva SM, Long DG, Smith DK, Hilburn KA, Jones WL (2012) Challenges to satellite sensors of ocean winds: addressing precipitation effects. J Atmos Ocean Technol 29:356–374. https://doi.org/10.1175/JTECH-D-11-00054.1

World Meteorological Organization (1970) The Beaufort Scale of wind force. WMO Commission for Maritime Meteorology, Marine Sciences Affairs Report No. 3, WMO, 22 pp

Yu J-Y, Chiu P-G (2012) Contrasting various metrics for measuring tropical cyclone activity. Terr Atmos Ocean Sci 23:303–316

Yu J–Y, Chou C, Chiu P-G (2009) A revised accumulated cyclone energy index. Geophys Res Lett 36:L14710. https://doi.org/10.1029/2009GL039254

Zhai AR, Jiang JH (2014) Dependence of US hurricane economic loss on maximum wind speed and storm size. Environ Res Lett 9. https://doi.org/10.1088/1748-9326/9/6/064019

Chapter 4
Mapping Tropical Cyclone Energy as an Approach to Hazard Assessment

Yi-Jie Zhu and Stephen G. Evans

Abstract Tropical cyclones (TCs), specifically their higher energy equivalents of hurricanes or typhoons, are the focus of great concern over their destructive impacts on coastal regions; this concern was enhanced as the trio of hurricanes (Harvey, Irma, and Maria) imposed spectacular damage and economic losses to parts of the United States and the Caribbean in 2017. We investigated historical TC events from the Western North Pacific and North Atlantic basins and introduced a new energy-based approach to mapping and spatially assessing TC hazards in both basins. By combining the energy index (EI) simplified from the power dissipation index (PDI) with a weighted density mapping tool, we defined a spatial energy cell which delineated a zone of intense TC energy loss. The energy cell we identified from the TC hazard map represents historical hot spots of TC events with reference to both frequency and intensity. We show that as TCs in Western North Pacific move westward from the source energy cell, energy is dissipated very rapidly over the Philippine land mass forming a dramatic energy discontinuity which we term an energy cliff. The migration of energy cells in the North Atlantic reflects inter-decadal variations of TC activity. Finally, the concept of energy dissipation discussed in this paper could be employed as a basis for the energy-based comparison of the magnitudes of all categories of natural hazards and help illuminate the nature of hazard-impact relationships.

Keywords Tropical cyclones · Energy mapping · Hazard assessment · North Atlantic · Western North Pacific · Philippines

Y.-J. Zhu (✉)
Natural Disaster Systems, Department of Earth and Environmental Sciences, University of Waterloo, Waterloo, ON, Canada

School of Geosciences, University of South Florida, Tampa, FL, USA
e-mail: yijiezhu@mail.usf.edu

S. G. Evans
Natural Disaster Systems, Department of Earth and Environmental Sciences, University of Waterloo, Waterloo, ON, Canada
e-mail: sgevans@uwaterloo.ca

J. M. Collins, K. Walsh (eds.), *Hurricane Risk*, Hurricane Risk 1,
https://doi.org/10.1007/978-3-030-02402-4_4

4.1 Introduction

Tropical cyclones (TCs) are known as one of the most destructive natural hazards in the world (Emanuel 2005a). They are common phenomena and have caused extensive damage and significant life loss in many regions of the tropics encountered in their path (e.g., Jonkman et al. 2009; Zhang et al. 2009; Peduzzi et al. 2012; Lin et al. 2013). A TC system reaching 65 knots is generally termed a *Typhoon* in the Western North Pacific, or a *Hurricane* in the North Atlantic (definition in NOAA: http://www.aoml.noaa.gov/hrd/tcfaq/A1.html). In the North Atlantic (NA), the trio of major hurricanes in 2017 (Harvey, Irma, and Maria) have re-awakened the awareness of the power conveyed by such natural hazards in causing tragic life loss and massive economic impacts along the US coastline and in Puerto Rico (Oldenborgh et al. 2017; Shuckburgh et al. 2017; Halverson 2018; Pullen 2018). In the Western North Pacific (WNP), Typhoon Haiyan caused considerable damage to the central Philippines and brought at least 6200 deaths (Esteban et al. 2015; Nakamura et al. 2015; Takagi et al. 2017) in 2013.

In recent decades, an increasing amount of research has explored the linkage between the potential destructiveness and the characteristics of powerful TC systems (e.g., Emanuel 2005b; Kubota and Chan 2009; Wing et al. 2007; Misra et al. 2013; Pun et al. 2013). With regards to hazards assessment and emergency preparations, the intensity and frequency are two key components of defining hazard characteristics that reflect either how destructive a typical hurricane could be or how frequently a place could suffer from cyclone hazards during a given period.

Typically, a quantitative hazard assessment involves an analysis of magnitude and temporal frequency. We note that hazard assessment is best developed in relation to earthquakes where earthquake magnitude is well constrained by an instrumental measure of magnitude, an expression of the amount of energy released during the seismic event, and a well-developed magnitude-frequency relation. Our view of catastrophic natural hazards as being energy-release events provides a convenient framework for hazard assessment based on magnitude, but also in terms of evaluating destructiveness. From the perspective of TC hazard impact assessment, wind speed, storm surges, and extremely heavy rainfall are three main factors of the destructiveness. The maximum sustained surface wind speed defined by the highest 1-min average wind has been used as the dominant metric for the TC intensity measurement since 1974 when Saffir-Simpson scale (SS) was proposed for potential destructive level of TCs under five wind speed categories (Simpson and Saffir 1974). Bister and Emanuel (1998) has given an estimate of the power dissipated by a TC using a maximum wind speed function. The energy function of the TC was then simplified to the power dissipation index (PDI) with assumptions of constant environmental factors (Emanuel 2005b).

This study explores a new approach to assessing TC hazards in the WNP and the NA by translating PDI as an energy function of TCs into an energy cell with a newly defined energy index in an attempt to spatially visualize TC hazard. We also make a

hypothetical comparison of the magnitude of energy dissipation between TCs and earthquakes as a step toward understanding the relationship between hazard characteristics and the type and magnitude of impacts.

4.2 The Energy Function of a Tropical Cyclone

In 1974, the SS described hurricane wind speed by five categories of potential destructiveness (Simpson and Saffir 1974). Climatologists in the next few decades developed alternative measures such as Accumulated Cyclone Energy (ACE; Bell et al. 2000) and the PDI (Emanuel 2005b) to quantitatively define hurricane intensity on a wind speed basis over the storm lifetime. In other work, Integrated Kinetic Energy (IKE; Powell and Reinhold 2007) and Track Integrated Kinetic Energy (TIKE; Misra et al. 2013) are two interpretations of the energy function of TCs that takes storm size into account to indicate potential damage that could be inflicted by storms' impact area. Due to the fact that fewer factors are required to calculate the value of ACE and PDI (ACE using the square and PDI using the cube of the maximum sustained wind speed at 6 h intervals), they are routinely used to describe seasonal hurricane activities in terms of intensity and frequency in response to, for example, changes in sea surface temperatures (Camargo and Sobel 2005; Villarini and Vecchi 2012).

While both ACE and PDI have been used to investigate seasonal TC intensities with correlations and responses to environmental factors, the PDI reanalyzed by Emanuel (2007) showed empirical and statistical relationships with environmental factors that help simulate future TC activity in a changing climate. The PDI also shows significant correlations with sea surface temperature in the NA between Africa and the Caribbean Sea during the hurricane season (Emanuel 2005b, 2007).

Related studies applying PDI to hurricane analysis are mostly concerned with temporal statistical trends and correlations with environmental change (e.g., Wu et al. 2008; Murakami et al. 2014; Liu and Chan 2017), but lack any component of spatial analysis with reference to hazard mapping. Hence, we employed PDI as our TC intensity index (Kn^3) in this study for energy cell mapping in the WNP and the NA basin. The PDI in the original form is defined as (Emanuel 2005b)

$$PDI = \int_0^{\tau} {V_{max}}^3 dt \tag{4.1}$$

where ($V_{\max}$) is the maximum sustained wind speed (in knots) measured in any given period (which in this study is taken as 6 h); and (τ) denotes the duration of the TC event (in hours). For the purpose of mapping historical TC tracks from an energy approach, we disaggregated the PDI function by the storm lifetime, defining an Energy Index (EI) as

$$EI = {V_{max}}^3 \tag{4.2}$$

where it is used for the weight coefficient in the Kernel density algorithm of historical TC track points as explained in details in Sect. 4.2.

For the purpose of energy comparisons among different categories of geohazards, the Power Dissipation function (PD) expressing the amount of dissipated energy, which integrates more factors, is also used in this study. The PD was proposed by Emanuel (2005b) as follows:

$$PD = 2\pi \int_0^{\tau_0} dt \int_0^{r_0} \rho C_D V^3 r dr \tag{4.3}$$

where the drag coefficient $(C_D) = 2 \times 10^{-3}$ is assumed to be constant, regardless of the variability induced by sea surface roughness and wind speed (Powell et al. 2003); air density (ρ)=1 kg/m^3. and (V) is the 6-h maximum sustained wind speed. Since accurate storm dimensions (r_0) in meters are sometimes difficult to obtain, we assumed the average radius of maximum wind speed to be 50 km for this paper (cf. Emanuel 2005b) and assume that the wind speed is constant over this radius at its maximum value.

4.3 Hybrid Complexity of Tropical Cyclones: Multi-hazard Systems

The impact assessment of TC hazards concerns destructive wind, storm surge, and extremely heavy rainfall as the physical processes that generate damage that cumulatively may produce disaster events. A typical landfall of a TC usually generates all three hazard components in some degree, the effects of which may be amplified by steep topography (that could generate landslides) or the failure of defensive infrastructure by storm surge loading (exceedance of design loads) that could cause coastal flooding. Multi-hazards, or hybrid hazards, is a useful term that describes TC threats and which addresses the complexity of TC hazards in terms of impact assessment. A conceptual expression of TC's impact (I) from a physical perspective could be:

$$I = a_1 W + a_2 S + a_3 R \tag{4.4}$$

where W, S, and R denote elements of wind speed, storm surge, and rainfall brought by a TC to a region respectively. The three components (Eq. 4.4) are not evenly distributed in TC events but are potentially higher in summation from stronger TCs. (a_1), (a_2) and (a_3) are three response factors describing the degree of impacts that the corresponding components (W, S, R) could actually impose on an impacted region. The three components (W, S, R) are TC dependent while response factors $(a_{1\ -\ 3})$ are region dependent and may reflect geography and topography. The combination of

TC's physical properties, together with variations of regional response, form the complexity of hybrid TC hazards.

4.4 Data and Method

4.4.1 Data Sources for North Atlantic and Western North Pacific Tropical Cyclones

The NA basin TC data source for this study is the International Best Track Archive for Climate Stewardship (IBTrACS) maintained by the National Centers for Environmental Information[1] (Knapp et al. 2010). The maximum wind speed obtained from this data set is the 10-min average sustained value measured in 6-h intervals. The data set is pre-filtered for TC events that occurred in the NA basin. Only TC events between 1982 and 2017 are employed due to having a sufficient number of data points available (a 36 year period) but lower uncertainties of V_{max} (Eq. 4.1) recordings after the 1980s. The filter of the V_{max} is set to equal or larger than 35 knots (-17 ms^{-1}) to meet the minimum threshold of the tropical storm intensity as suggested by the National Hurricane Center (see more details on https://www.nhc.noaa.gov/aboutgloss.shtml).

Data for the TCs in the WNP basin are obtained from the Annual Tropical Cyclone Report published by US Navy Joint Typhoon Warning Center (JTWC)[2] spanning a 55-year period from 1959 to 2013, with the data available for downloading from http://weather.unisys.com/hurricane/index.php. Table 4.1 gives a summary of wind speed data by TCs that have been employed in this study. The wind speed catalogue is constructed following the SS (Simpson and Saffir 1974).

Table 4.1 Fact sheet of investigated wind speed data sets

	Data point count		Avg. (Knots)		Annual frequency of data points	
SS wind speed catalogue	NA	WNP	NA	WNP	NA	WNP
Tropical storm (<65 Knots)	6688	15,909	45.50	46.00	186	289
Category 1 (65 – 85 Knots)	2302	7219	72.35	73.26	64	131
Category 2 (90 – 100 Knots)	671	2970	94.28	94.16	19	54
Category 3 (105 – 115 Knots)	417	1806	110.22	110.20	12	33
Category 4 (120 – 135 Knots)	281	1617	125.07	126.21	8	29
Category 5 (>135 Knots)	79	654	146.33	146.61	2	12

[1]National Center for Environmental Information is operated by the National Oceanic and Atmospheric Administration https://www.ncdc.noaa.gov

[2]Joint Typhoon Warning Center (JTWC) is a combined Air Force/Navy organization operating under the command of the Commanding Officer, U.S. Naval Pacific Meteorology and Oceanography Center West /Joint Typhoon Warning Center, Guam.

4.4.2 *Delineation of Spatial Clusters*

The Weighted Density Map (WDM), also called the 'weighted heat map' tool, is utilized in this study for the cluster analysis that is the basis for mapping the energy dissipation topography of TCs. The open-source geographic information system QGIS version 2.18 is used for mapping purposes. We applied quartic Kernel density estimating algorithm for generating concentration values of historical TC tracks. The number of TC track point occurrences is counted in a designated searching radius where in this study we used $1.2 \times 1.2°$ for mapping Hurricane Maria and $4 \times 4°$ for the NA and WNP basin. The search radius parameter in the Kernel density algorithm decreases the output values by the distance from the center and thus depicts the approximate profile of the storm radius. The EI value is defined as a weighted input where, for example, a geospatial point representing an EI value of 1×10^6 (Kn^3) counts 1×10^6 times when conducting the density calculation.

4.5 Energy Cell Detection and Tracking: The Example of Hurricane Maria in the Vicinity of Puerto Rico, 2017

Hurricane Maria was first recognized as a tropical depression on 16 September 2017, but rapidly intensified from SS Category 1 to Category 5 in the next 24 h. During the morning on 20 September, the massive storm system made landfall on the island of Puerto Rico with wind speeds reaching SS Category 4. Maria ran across the island of Puerto Rico during the next 12 h accompanied by fierce wind, extreme rainfall, and flash flooding. Maria caused catastrophic property damage and significant life loss until the hurricane degraded after moving offshore (NOAA 2017). The Maria event illustrated the manner in which hurricane intensity changes before, during, and after landfall. By combining the EI with the spatial clustered weighted density map tool, the energy-based approach to Maria's activity/behaviour is mapped in Fig. 4.1.

A rapid intensification that occurred near Dominica indicated a process of strong energy sink within the hurricane system. After a series of repeated pulse-like energy gain and energy dumping processes that formed a distended rod-like red cell, a parcel of energy (see details in zoomed-in inset in Fig. 4.1) moved toward the east coast of Puerto Rico and rapidly dissipated after landfall. This implies the occurrence of energy transformation during the landfall process that converted heat energy into another form of mechanical energy such as wind and precipitation. The structure and formation of TCs are well understood by physicists and meteorologists, wherein a mature hurricane can be compared to an idealized heat engine (Emanuel 1986, 1991; Willoughby 1999). In the case of Hurricane Maria, the land surface of Puerto Rico acted as a trigger for sudden energy loss. To develop the idea further, the conceptual

energy cell approach is now applied to broader regions to describe the spatial density of historical energy parcels and dissipation phenomena.

4.6 Application of Energy Cell Mapping to Tropical Cyclone Basins (North Atlantic and Western North Pacific)

The NA and WNP frequently generate TCs; it is of importance to visualise the distribution of TCs in these breeding oceans. The energy function PDI has been used to quantitatively summarize the annual TC activities due to its advantages of expressing both TC lifetime and magnitude (e.g., Mestre and Hallegatte 2009). Here, we use the energy-cell-based conceptual approach developed above with reference to Hurricane Maria (Fig. 4.1) to shed light on the spatial characteristics of TC intensity and frequency.

Energy cells in the NA are spread unevenly and are concentrated along the southeast – northwest corridors of prevailing TC tracks (Fig. 4.2). Regions with a relatively higher value of EI density correspond to those with more frequent and intense TC activities during the period 1982–2017.

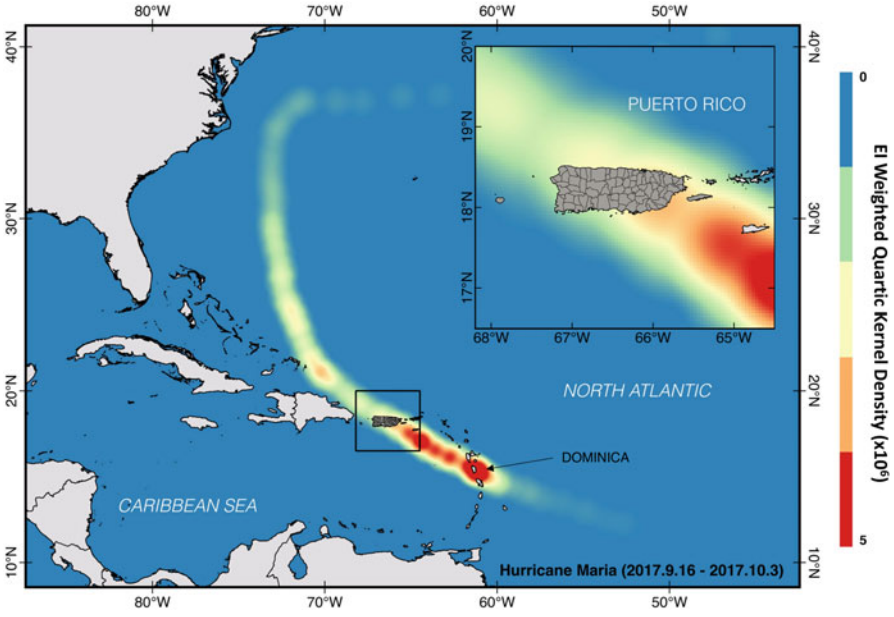

Fig. 4.1 Conceptual energy map of Hurricane Maria by EI weighted density. Search radius is set to $1.2 \times 1.2°$ with the Kernel Quartic Shape Density applied

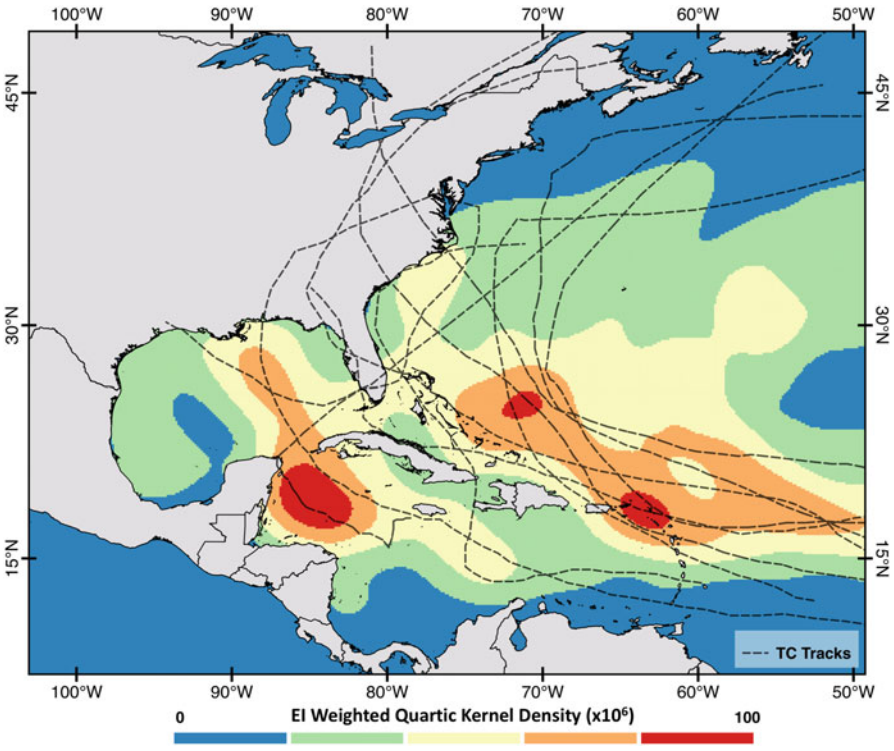

Fig. 4.2 Distribution of conceptual TC energy cells in the North Atlantic by EI weighted Kernel density algorithm with $4 \times 4^{\circ}$ search radius ($N_{TC} = 439$, $N_{Points} = 10{,}081$). Dash lines in black show TC tracks as a reference with top ten greatest lifetime PDI during the year 1982–2017. PDI calculated with wind speed of 35 knots and above

Puerto Rico is shown immediately to the west (down track) of an energy hot spot (the Anguilla energy cell) and lies in a vast area of energy concentration (Fig. 4.2). Areas of Central America such as East Mexico, Honduras, Belize, and Nicaragua are exposed to a hot spot cell margin (the Belize cell), and have suffered major impacts from historical TCs. Notably, Hurricane Mitch passed through this region in 1998, when houses and their inhabitants were swept away in torrents, floods, and landslides; Mitch claimed over 11,000 deaths in Honduras and Nicaragua (NOAA 2009). The Belize cell extends northward to the Gulf of Mexico shoreline of the United States; the 2005 hurricane season was the main contributor to the energy concentration on coast of Louisiana.

By using 55 years of TC track data from 1959 to 2013, the energy cell in the WNP can be identified as a well-defined cluster of dissipation parcels immediately to the east of the central and north Philippine archipelago, and Taiwan (Fig. 4.3).

The parcels of energy release represent a relatively high frequency of high intensity TCs that have passed through the area (Fig. 4.3).

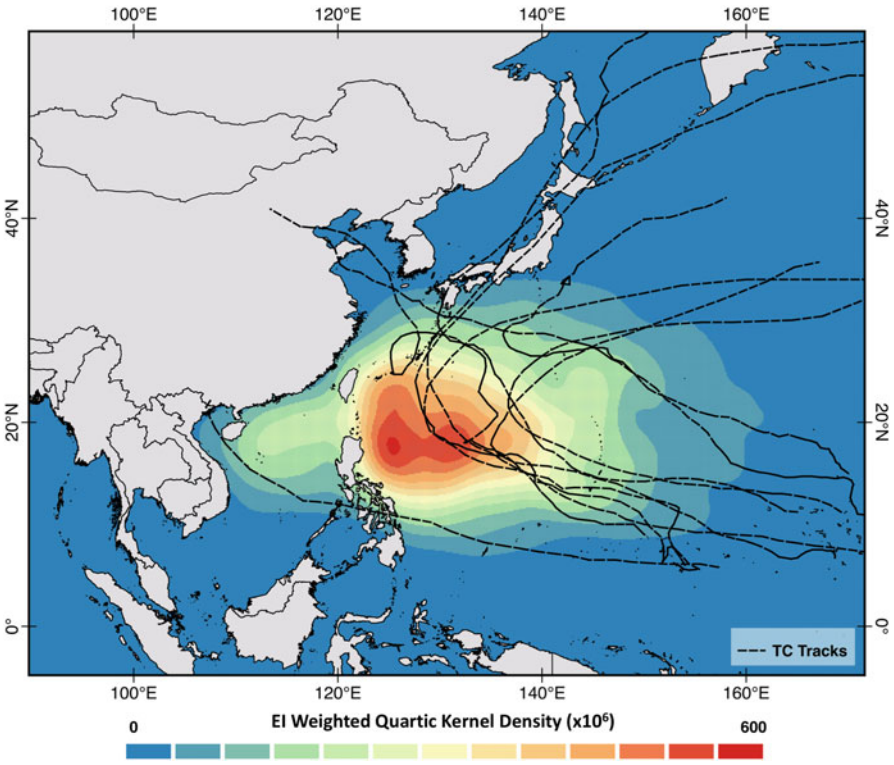

Fig. 4.3 Distribution of conceptual TC energy cells in the Western North Pacific by EI weighted Kernel density algorithm with $4 \times 4°$ search radius ($N_{TC} = 1411$, $N_{Points} = 30{,}175$) Dash lines in black show TC tracks as a reference with top ten greatest lifetime PDI during the year 1959–2013. PDI calculated with wind speed of 35 knots and above

4.7 Interpretation of the Energy Cell and Implication for Hazard Assessment

The theoretical description of a TC event can be conceptualized as a Carnot heat engine (as first suggested by Emanuel (1986)), in which the system is a transformation of the thermal energy and the mechanical energy. The warm sea surface temperature together with favorable environmental factors, such as low vertical wind shear, are the recipe for TC formation. The heat brought into the TC system by water vapor from a warm sea surface is a major energy source, while the wind force is a form of energy dissipation. The greater the maximum wind speed recorded, the larger amount of energy that has been transferred.

By mapping the energy cell using EI density, the energy dissipation stage of the TC mechanism is spatially visualized by the form and distribution of the energy cell topography formed by the contours of energy dissipation. High values from the

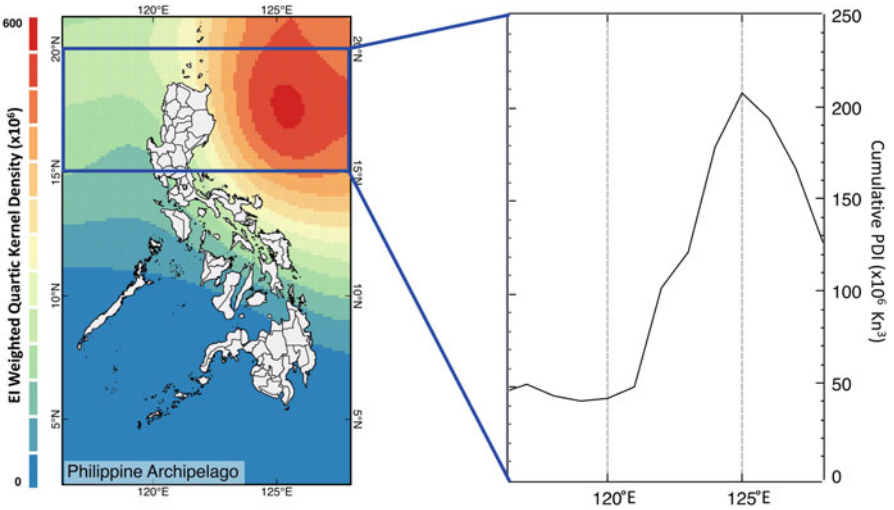

Fig. 4.4 Regional map of conceptual energy cell surrounding the Philippine archipelago. $4 \times 4°$ searching radius on EI weighted density. The energy profile shows the cumulative EI value with 1° increment of longitude from 15°N to 20°N

energy cell mapping locate areas of large (cumulative) but also frequent energy sinks that occurred during the designated time period. Energy cell mapping using EI density opens up the opportunity of visualizing hazard hot spots from historical TC occurrence and characteristics. In the WNP, Luzon, the largest island in the Philippines in the north region of the archipelago, is found immediately west of the Philippine energy cell, where the dissipation of energy was at its maximum crossing 125°E, but is seen to decrease sharply when passing over the island (Fig. 4.4).

The rapid loss of energy from TCs (which we term an energy cliff; Fig. 4.4) implies a lack of energy transfer from the landmass to the TC system. i.e., the land surface represents an empty energy source. The topography of the energy surface thus provides insight into TC hazard.

The distribution of TC wind speed is shown in Fig. 4.5; similar to the PDI weighted density map (Fig. 4.4), wind speeds recorded over 120 knots are clustered to the east of Luzon. The annual frequency does decrease with increasing wind speed, but shows a turning point at 140 knots as indicated by the locally weighted curve (LOESS; Fig. 4.5). This implies the existence of a physical threshold that limits the maximum value of the surface wind speed (Fig. 4.5).

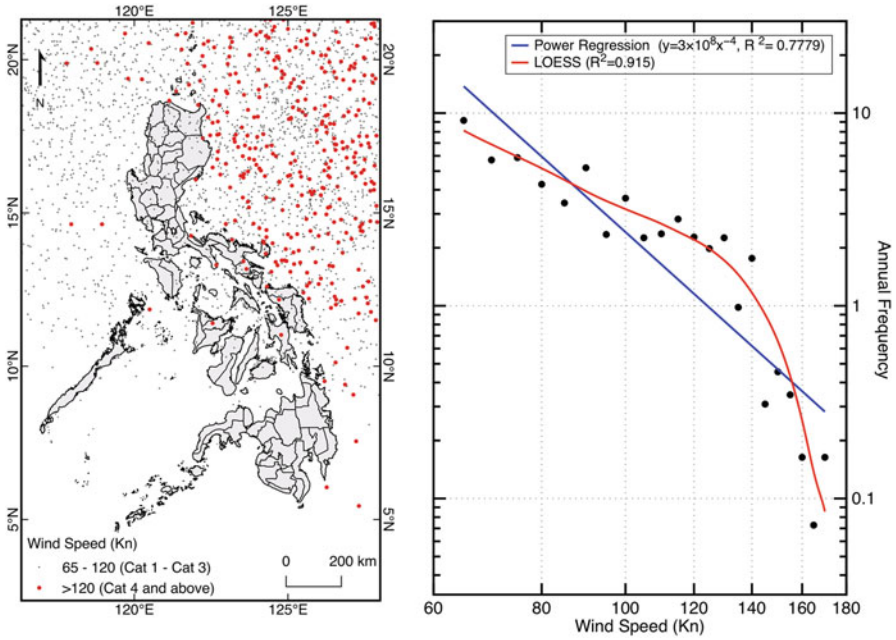

Fig. 4.5 Spatial distribution of Philippines TC tracking points over 65 knots from 1959 to 2013. Annual frequency profile of 6-h wind speed points in log-log scale

4.8 Migration of Energy Cell, Changing Climate and Energy Cell Mobility

The change in the frequency and intensity of TCs with time, especially with respect to climate change, has been much discussed in recent research (e.g., Knutson et al. 2010; Walsh et al. 2016; Collins and Roache 2017; Scoccimarro et al. 2017). The sea surface temperature (SST) as an ingredient of TC formation has been suggested as an indicator of potential TC occurrence and is shown to increase in high-resolution models of climate change (e.g., Yoshimura et al. 2006; Johnson and Xie 2010). A practical threshold of cyclone formation globally was suggested to lie between 25.5 and 26.5 °C, without a detected shift through the years (Dare and McBride 2011). Emanuel (2005b) showed an increasing destructiveness potential of hurricanes since 1970 by warming SSTs, while some other studies provide evidence of an oscillation of annual and decadal variations of TC occurrence and intensity (e.g., Chen et al. 1998; Camargo and Sobel 2005; Webster et al. 2005). However, research on the convection theory basis suggests the deviation between local and tropical mean SST would be a much more precise approach to examine TC responses to SST changes. He et al. (2015)

spatially analyzed and discussed the TC track density from the WNP in the late 1990s, where a decadal increasing trend of the genesis and track densities is shown in the north region of the WNP, while a decreasing trend is present in the south region of the WNP. The northward migration of TC genesis in the WNP together with SST changes implies a potential northward expansion of the Philippine energy cell, contributing a much wider impact area of the TC and its stronger phase, the typhoon.

In the NA, the TCs in the period 1982–2017 from our study also showed non-constant conditions from the energy approach and spatial perspectives. We split 36 years into three time slices of 12 years in width (1982–1993, 1994–2005, and 2006–2017), and generated EI weighted density of each slice (Fig. 4.6). The energy cell as expressed by EI weighted density, migrated with changing intensity through the 36 years. The years 1982–1993 (Fig. 4.6a) was the quietest period regarding the EI density when comparing to the other two time periods (1994–2005 in Fig. 4.6b, and 2006–2017 in Fig. 4.6c). Decadal variations of TC activity are indicated, with the years 1994 to 2005 the strongest.

By employing a statistical box plot for all three time slices (Fig. 4.6d), the major contribution to high energy dissipation for years 1994–2005 and 2006–2017 is the

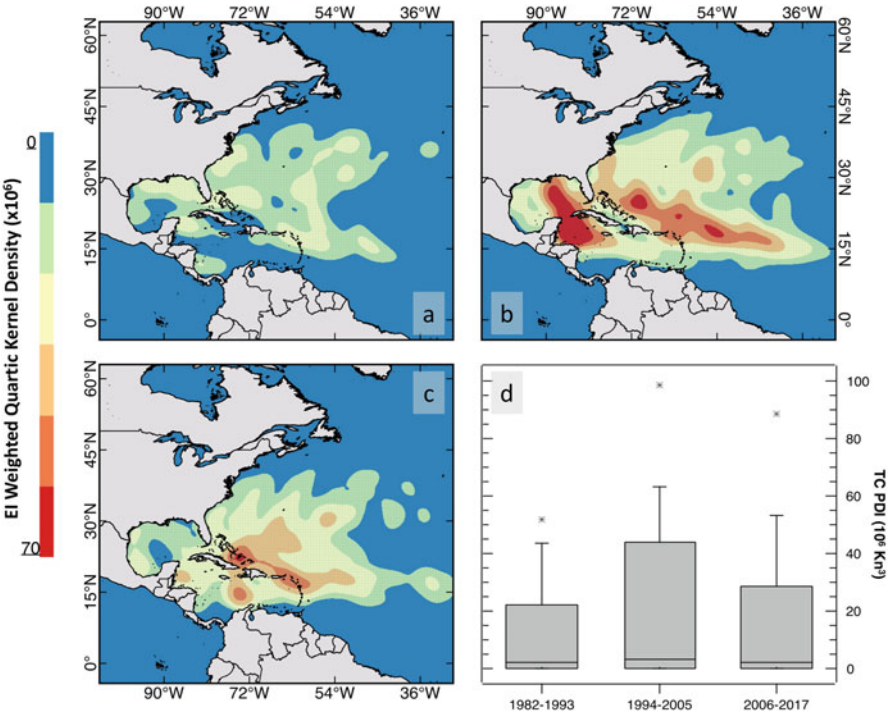

Fig. 4.6 EI weighted density map with $4 \times 4°$ search radius for years from 1982 to 1993 (**a**), 1994–2005 (**b**), and 2006–2017 (**c**). The statistical box plot for TC incidents from three time slices (**d**), with the box set from 5% to 95%, whiskers to 99%, and asterisks denote maximum value

occurrence of mega hurricanes with extremely high wind speed and long-lasting lifetime; frequency plays a subordinate role. The total number of TCs with maximum wind speed over 35 knots for 1982–1993, 1994–2005, and 2006–2017 is 109, 176, and 173, respectively. However, the corresponding total PDI is rounded to 658, 1670, and 1188 ($\times 10^6$ Kn^3); note that in 1994–2005 and 2006–2017, almost the same number of TCs occurred, but the differences in intensity resulted in a huge difference in total PDI. The energy dissipation topography derived from our energy-based approach is thus mainly controlled by the occurrence of TCs reaching high levels of wind speed that is sustained over long time periods.

4.9 Discussion: Energy and Impact

The dissipation of energy from TCs reflects the degree of potential destructiveness from the dynamic TC system. In 2013, Typhoon Haiyan, with a maximum wind speed of 170 knots, lashed the Philippines and brought about extensive devastation on its pathway through the archipelago, largely by a massive storm surge that contributed to a high death toll (Lagmay et al. 2015). By employing the PD equation (Eq. 4.3), the 2013 Typhoon Haiyan involved approximately 6.5×10^{13} watts of energy dissipation, which, if integrated over the storm lifetime, is equal to 6.8×10^{19} joules.

We compared the energetics of Typhoon Haiyan with that of a major Philippine earthquake in 1976; an earthquake's energy can be expressed as a function of a measured magnitude (Gutenberg and Richter 1942, 1956a, b; Kanamori 1977). The M 8.0 Mindanao earthquake in 1976 according to the National Geophysical Data Center,[3] caused over 8000 fatalities in the Philippines from its devastating structural damages and tsunamis. The corresponding energy release in this fatal event was 6.3×10^{16} joules. Thus, the comparison of the two most destructive hazard events in recent decades in the Philippines shows that the magnitude of energy dissipation in Typhoon Haiyan is three orders of magnitude greater than 1976 Mindanao Earthquake.

Although a greater energy capacity exists for the typhoon, this does not directly contribute to a greater number of fatalities as a number of other factors are at play. For example, in the case of typhoons, a buffer exists during the onset of development (preparation time) of the hazard that typically does not occur for earthquakes. Genesis of TCs, in most cases, occurs within some distance from the mainland. TCs move landward at a speed that allows adequate time for the prediction of potential track and storm intensity, and in the event of a direct threat, allows preparation time for evacuation. Fatalities are also related to population density and emergency preparedness. The population exposed to the hazards is a key factor

[3]National Geophysical Data Center/World Data Service (NGDC/WDS): Significant Earthquake Database. National Geophysical Data Center, NOAA. doi:https://doi.org/10.7289/V5TD9V7K

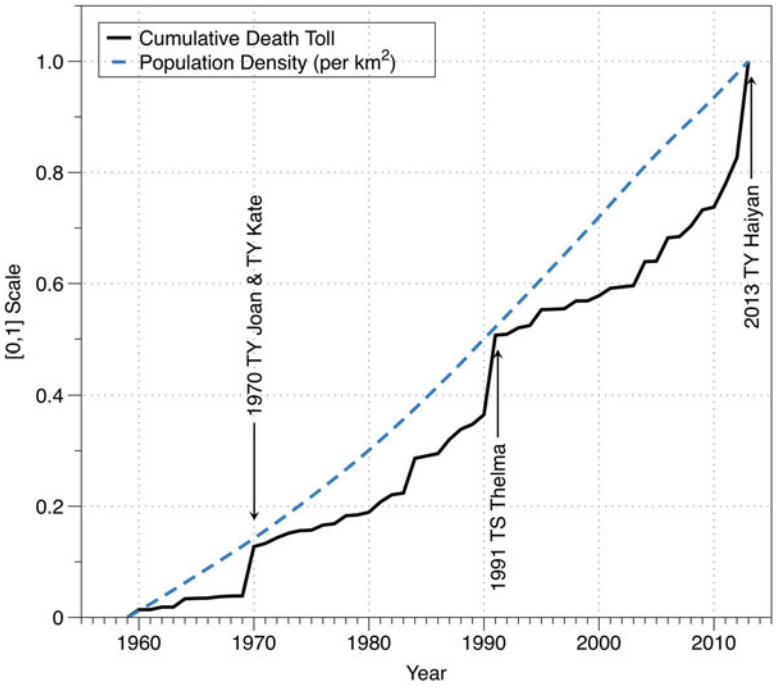

Fig. 4.7 Cumulative death toll by TCs in the Philippines with reference to the population density from 1959 to 2013. Fatality data source accessed from EM-DAT Database (EM-DAT: The Emergency Events Database – Université catholique de Louvain (UCL) – CRED, D. Guha-Sapir, www.emdat.be, Brussels, Belgium); Population density from the World Bank Database (Food and Agriculture Organization and World Bank population estimates. Population density is midyear population divided by land area in square kilometers. https://data.worldbank.org/country/philippines)

in mortality. At a constant natural hazard magnitude, the larger exposure is expected to bring greater fatalities to the residents. The growth of population in the world will result in an increase of exposure to TCs (Peduzzi et al. 2012). Under the circumstances of a steady growth in population density, the total death toll by TC hazards in the Philippines experienced three major increases in the three calamitous years (1970, 1991, and 2013) (Fig. 4.7). Tropical Storm Thelma in 1991, as an example, scourged the Philippines leaving the death toll over 6000 (JTWC report 1991). The storm's slow movement was accompanied by torrential rains (150 mm in 24 h over the central Philippines) that were concentrated in a narrow area, resulting in landslides, dam failure, and unprecedented flash flooding (JTWC report 1991). The potential destructiveness was underestimated and low preparedness resulted in high fatalities.

4.10 Conclusions

In this paper, we introduced a new energy-based approach to historical TC activity as a visualization tool for hazard impact assessment. The mapping of energy cells by the weighted density of the EI spatially illustrates the dissipation of energy from a TC system and identifies hotspots of TC activity in both the NA and WNP basins. The spatial distribution of energy cells is a response to both TC historical frequency and intensity. Energy cells migrate in time and are not static features of the energy dissipation topography in a region. Results from the 12-year time-slice analysis in the NA show variations in the spatial distribution, and the density of energy cells is determined by the occurrence of those TCs with large PDI values (high wind speeds sustained for long periods). Migration of energy cells in the NA basin indicates the changing environment between the 12-year time slices; however, a significant signal of a continuous increase in cell density, indicating a greater magnitude and frequency of TCs, was not detected.

We compared the energy-impact relations of TCs and earthquakes in the Philippines. In the archipelago, for a given magnitude of energy dissipation, typhoons obtain a higher annual frequency. By considering the fatalities induced by the two hazards, there is no simple relationship between the energy released and the death toll, but greater energy release by TCs is offset by a lower dissipation rate which acts as a hazard buffer providing for effective warning, preparation time, and evacuation.

References

Bell GD, Halpert MS, Schnell RC et al (2000) Climate assessment for 1999. Bull Am Meteorol Soc 81(6):s1–s50. https://doi.org/10.1175/1520-0477(2000)81[s1:CAF]2.0.CO;2

Bister M, Emanuel KA (1998) Dissipative heating and hurricane intensity. Meteorolog Atmos Phys 65(3-4):233–240

Camargo SJ, Sobel AH (2005) Western North Pacific tropical cyclone intensity and ENSO. J Clim 18(15):2996–3006. https://doi.org/10.1175/JCLI3457.1

Chen TC, Weng SP, Yamazaki N et al (1998) Interannual variation in the tropical cyclone formation over the western North Pacific. Mon Weather Rev 126(4):1080–1090. https://doi.org/10.1175/1520-0493(1998)126<1080:IVITTC>2.0.CO;2

Collins JM, Roache DR (2017) The 2016 North Atlantic hurricane season: a season of extremes. Geophys Res Lett 44(10):5071–5077. https://doi.org/10.1002/2017GL073390

Dare RA, McBride JL (2011) The threshold sea surface temperature condition for tropical cyclogenesis. J Clim 24(17):4570–4576. https://doi.org/10.1175/JCLI-D-10-05006.1

Emanuel KA (1986) An air-sea interaction theory for tropical cyclones. Part I: steady-state maintenance. J Atmos Sci 43(6):585–605. https://doi.org/10.1175/1520-0469(1986)043<0585:AASITF>2.0.CO;2

Emanuel KA (1991) The theory of hurricanes. Annu Rev Fluid Mech 23(1):179–196. https://doi.org/10.1146/annurev.fl.23.010191.001143

Emanuel KA (2005a) Divine wind: the history and science of hurricanes. Oxford University Press, Oxford

Emanuel KA (2005b) Increasing destructiveness of tropical cyclones over the past 30 years. Nature 436(7051):686–688. https://doi.org/10.1038/nature03906

Emanuel KA (2007) Environmental factors affecting tropical cyclone power dissipation. J Clim 20 (22):5497–5509. https://doi.org/10.1175/2007JCLI1571.1

Esteban M, Valenzuela VP, Yun NY et al (2015) Typhoon Haiyan 2013 evacuation preparations and awareness. Int J Sustain Futur Hum Secur 3(1):37–45. https://doi.org/10.24910/jsustain/3.1/3745

Gutenberg B, Richter C (1942) Earthquake magnitude, intensity, energy, and acceleration. Bull Seismol Soc Am 32(3):163–191

Gutenberg B, Richter C (1956a) Earthquake magnitude, intensity, energy, and acceleration (second paper). Bull Seismol Soc Am 46(2):105–145

Gutenberg B, Richter C (1956b) Magnitude and energy of earthquakes. Ann Geophys 9(1):1–15

Halverson JB (2018) The Costliest hurricane season in US history. Weatherwise 71(2):20–27. https://doi.org/10.1080/00431672.2018.1416862

He H, Yang J, Gong D et al (2015) Decadal changes in tropical cyclone activity over the western North Pacific in the late 1990s. Clim Dyn 45(11–12):3317–3329. https://doi.org/10.1007/s00382-015-2541-1

Johnson NC, Xie SP (2010) Changes in the sea surface temperature threshold for tropical convection. Nat Geosci 3(12):842. https://doi.org/10.1038/ngeo1008

Jonkman SN, Maaskant B, Boyd E et al (2009) Loss of life caused by the flooding of New Orleans after Hurricane Katrina: analysis of the relationship between flood characteristics and mortality. Risk Anal 29(5):676–698. https://doi.org/10.1111/j.1539-6924.2008.01190.x

JTWC (1991) Annual tropical cyclone report. Joint Typhoon Warning Center, Pearl Harbor

Kanamori H (1977) The energy release in great earthquakes. J Geophys Res 82(20):2981–2987. https://doi.org/10.1029/JB082i020p02981

Knapp KR, Kruk MC, Levinson DH et al (2010) The international best track archive for climate stewardship (IBTrACS) unifying tropical cyclone data. Bull Am Meteorol Soc 91(3):363–376. https://doi.org/10.1175/2009BAMS2755.1

Knutson TR, McBride JL, Chan J et al (2010) Tropical cyclones and climate change. Nat Geosci 3 (3):157. https://doi.org/10.1038/ngeo779

Kubota H, Chan JC (2009) Interdecadal variability of tropical cyclone landfall in the Philippines from 1902 to 2005. Geophys Res Lett 36(12):1–4. https://doi.org/10.1029/2009GL038108

Lagmay AMF, Agaton RP, Bahala MAC et al (2015) Devastating storm surges of Typhoon Haiyan. Int J Disaster Risk Reduct 11:1–12. https://doi.org/10.1016/j.ijdrr.2014.10.006

Lin II, Black P, Price JF et al (2013) An ocean coupling potential intensity index for tropical cyclones. Geophys Res Lett 40(9):1878–1882. https://doi.org/10.1002/grl.50091

Liu KS, Chan JC (2017) Variations in the power dissipation index in the East Asia region. Clim Dyn 48(5–6):1963–1985. https://doi.org/10.1007/s00382-016-3185-5

Mestre O, Hallegatte S (2009) Predictors of tropical cyclone numbers and extreme hurricane intensities over the North Atlantic using generalized additive and linear models. J Clim 22 (3):633–648. https://doi.org/10.1175/2008JCLI2318.1

Misra V, DiNapoli S, Powell M (2013) The track integrated kinetic energy of Atlantic tropical cyclones. Mon Weather Rev 141(7):2383–2389. https://doi.org/10.1175/MWR-D-12-00349.1

Murakami H, Li T, Hsu PC (2014) Contributing factors to the recent high level of accumulated cyclone energy (ACE) and power dissipation index (PDI) in the North Atlantic. J Clim 27 (8):3023–3034. https://doi.org/10.1175/JCLI-D-13-00394.1

Nakamura R, Takahiro O, Shibayama T et al (2015) Evaluation of storm surge caused by Typhoon Yolanda (2013) and using weather-storm surge-wave-tide model. Procedia Eng 116:373–380. https://doi.org/10.1016/j.proeng.2015.08.306

NOAA (2009) Mitch: the deadliest Atlantic hurricane since 1780. https://web.archive.org/web/20120717103126/http://lwf.ncdc.noaa.gov/oa/reports/mitch/mitch.html#TOP. Accessed 10 Feb 2018

NOAA (2017) Major hurricane Maria – September 20, 2017.http://www.weather.gov/sju/maria2017. Accessed 8 Feb 2018

Oldenborgh GJ, Wiel K, Sebastian A et al (2017) Attribution of extreme rainfall from Hurricane Harvey, August 2017. Environ Res Lett 12(12):124009. https://doi.org/10.1088/1748-9326/aa9ef2

Peduzzi P, Chatenoux B, Dao H et al (2012) Global trends in tropical cyclone risk. Nat Clim Chang 2(4):289–294. https://doi.org/10.1038/nclimate1410

Powell MD, Reinhold TA (2007) Tropical cyclone destructive potential by integrated kinetic energy. Bull Am Meteorol Soc 88(4):513–526. https://doi.org/10.1175/BAMS-88-4-513

Powell MD, Vickery PJ, Reinhold TA (2003) Reduced drag coefficient for high wind speeds in tropical cyclones. Nature 422(6929):279–283. https://doi.org/10.1038/nature01481

Pullen LC (2018) Puerto Rico after Hurricane Maria. Am J Transplant 18(2):283–284. https://doi.org/10.1111/ajt.14647

Pun IF, Lin II, Lo MH (2013) Recent increase in high tropical cyclone heat potential area in the Western North Pacific Ocean. Geophys Res Lett 40(17):4680–4684. https://doi.org/10.1002/grl.50548

Scoccimarro E, Villarini G, Gualdi S et al (2017) Tropical cyclone rainfall changes in a warmer climate. In: Collins J, Walsh K (eds) Hurricanes and climate change. Springer, Cham, pp 243–255. https://doi.org/10.1007/978-3-319-47594-3_10

Shuckburgh E, Mitchell D, Stott P (2017) Hurricanes Harvey, Irma and Maria: how natural were these 'natural disasters'? Weather 72(11):353–354. https://doi.org/10.1002/wea.3190

Simpson RH, Saffir H (1974) The hurricane disaster potential scale. Weatherwise 27(8):169

Takagi H, Esteban M, Shibayama T et al (2017) Track analysis, simulation, and field survey of the 2013 Typhoon Haiyan storm surge. J Flood Risk Manag 10(1):42–52. https://doi.org/10.1111/jfr3.12136

Villarini G, Vecchi GA (2012) North Atlantic Power Dissipation Index (PDI) and Accumulated Cyclone Energy (ACE): statistical modeling and sensitivity to sea surface temperature changes. J Clim 25(2):625–637. https://doi.org/10.1175/JCLI-D-11-00146.1

Walsh KJ, McBride JL, Klotzbach PJ et al (2016) Tropical cyclones and climate change. WIREs Clim Change 7(1):65–89. https://doi.org/10.1002/wcc.371

Webster PJ, Holland GJ, Curry JA et al (2005) Changes in tropical cyclone number, duration, and intensity in a warming environment. Science 309(5742):1844–1846. https://doi.org/10.1126/science.1116448

Willoughby HE (1999) Hurricane heat engines. Nature 401(6754):649

Wing AA, Sobel AH, Camargo SJ (2007) Relationship between the potential and actual intensities of tropical cyclones on interannual time scales. Geophys Res Lett 34(8):L08810. https://doi.org/10.1029/2006GL028581

Wu L, Wang B, Braun SA (2008) Implications of tropical cyclone power dissipation index. Int J Climatol 28(6):727–731. https://doi.org/10.1002/joc.1573

Yoshimura J, Sugi M, Noda A (2006) Influence of greenhouse warming on tropical cyclone frequency. J Meteorol Soc Jpn Ser II 84(2):405–428. https://doi.org/10.2151/jmsj.84.405

Zhang Q, Wu L, Liu Q (2009) Tropical cyclone damages in China 1983–2006. Bull Am Meteorol Soc 90(4):489–496. https://doi.org/10.1175/2008BAMS2631.1

Chapter 5
Overview of Potential Hurricane Death and Damage in the Tampa Bay Region

Charles H. Paxton

Abstract The Tampa Bay area has not been impacted by a direct major hurricane landfall since 1921, but nearly every year the Tampa Bay region suffers effects from tropical storms and weak hurricanes brushing by the area. These weaker storms, like Hurricane Irma in 2017, still create significant damage. A stronger storm would be catastrophic. This chapter draws comparisons between past storms in the Tampa Bay area and elsewhere that have caused death and destruction, and discusses potential ecological, sociological, and human health disasters within the Tampa Bay area during a major hurricane landfall.

Keywords Tampa Bay · Hurricane · Storm surge · Evacuation · Hazardous materials

5.1 Introduction

This chapter describes a potentially disastrous situation. Tampa Bay has not been impacted by a direct major hurricane landfall since 1921, but nearly every year the Tampa Bay region suffers effects from tropical storms and weak hurricanes brushing by the area. These weaker storms, like Hurricane Irma in 2017, still create significant damage. A stronger storm would be catastrophic. This chapter draws comparisons between past storms in the Tampa Bay area and elsewhere that have caused death and destruction, and discusses potential ecological, sociological, and human health disasters within the Tampa Bay area during a major hurricane landfall.

C. H. Paxton (✉)
Channelside Weather LLC, Tampa, FL, USA
e-mail: charlie@channelsideweather.com

J. M. Collins, K. Walsh (eds.), *Hurricane Risk*, Hurricane Risk 1,
https://doi.org/10.1007/978-3-030-02402-4_5

5.2 Tampa Bay Area Characteristics

The five coastal counties of Pasco, Pinellas, Hillsborough, Manatee, and Sarasota, (Fig. 5.1) encompass an area about 9500 km^2 (3700 mi^2) and have a population of 3.6 million (Census 2015). Within that population lies vulnerability. About 30% of the population is at least 65 years old (1 million people) with a similar percentage living in the FEMA floodplain (28 %), and around 800,000 (23 %) living in poverty.

Tampa Bay (Fig. 5.2) is Florida's largest open-water estuary at 1010 km^2 (390 mi^2) (TBEP 2017) and over four million people reside in the watershed. The northern part of Tampa Bay has several distinct areas that include Old Tampa Bay to the west and Hillsboro Bay to the east, of which McKay Bay is in the northeast reaches. Tampa Bay was designated an "Estuary of National Significance" in 1990. Tampa Bay and other coastal waters are home to fish, birds, mangroves, and charismatic megafauna that

Fig. 5.1 Map of Florida and counties of interest

Fig. 5.2 A view of the Tampa Bay region looking from southwest to northeast. (Tihansky et al. 2011)

include manatees, dolphins, and sea turtles. Sea grass areas, noted within the Tampa Bay Water Atlas (2018), grow around the shores within Tampa Bay with the greatest coverage within the nearshore gulf waters north of Tampa Bay.

5.3 Past Storms Affecting the Tampa Bay Area

The area has had many close brushes with tropical cyclones through the years. In the historical record that goes back to the mid-1800s, three major hurricanes stand out.

The Great Gale of 1848, when the population of the Tampa Bay region was around 1000, occurred from a hurricane that was in the area roughly from September 23 to 28. Upon landfall it was estimated to be in the Category 3–4 range with winds around 215 kph (134 mph). This hurricane created a storm tide of 4.6 m (15 ft) with a rise and fall in 6–8 h (NWS 1848 2017).

In 1921, the Tampa Bay area population was only 135,000 when a hurricane moved ashore near Tarpon Springs. The hurricane was weakening from a Category 3 to a Category 2 at landfall but had been a Category 4 only 24 h prior (NWS 1921 2017). At landfall the winds were 180 kph (100 mph). The storm surge was estimated at 3–3.5 m (10–12 ft) in the northern part of Tampa Bay with major flooding, and the most notable damage, along the populated Bayshore Boulevard and downtown Tampa. The hurricane caused three confirmed fatalities. In Pinellas County the hurricane flooded Pass-a-Grille, destroyed the wooden Casino in

Gulfport, and damaged the Municipal Pier in St. Petersburg. Honeymoon Island was split in two, forming what was to become Caladesi Island (Davis and Elko 2003). The hurricane caused between 5 and 10 million dollars in damages to crops, including a thriving citrus industry in Pinellas County, throughout the state's midsection.

More recently, Hurricane Elena caused a major disruption to life in 1985. Elena stalled for 30 h about 160 km (100 miles) northwest of Tampa beginning early Saturday, August 31. Elena's sustained Category 3 winds were 200 kph (125 mph) (NHC 1985). Elena never came closer than 80 miles to Tampa Bay but still produced tides 2.1 m (7 ft) above normal. Around 300,000 people evacuated the Tampa Bay Area and about 1.25 million evacuated statewide. At the time, it was the largest evacuation in Florida's history. Pinellas County took most of the impact, where Elena destroyed 256 homes and damaged 7707 homes, and nearly 120,000 people were situated in shelters (Pinellas EOC 2008). By Saturday evening, all escape routes out of the county were closed due to flooding or debris. After Elena was nearly stationary offshore for 30 h, the storm turned westward, away from the coast on Sunday. The storm resulted in no direct fatalities, but four victims died of indirect causes.

5.4 Storm Surge Potential

The Tampa Bay region is now a disaster waiting to happen. Storm surge estimates are astounding when considering the highly populated, low-lying land areas. A Category 1 storm can create a surge up to 3 m inside Tampa Bay. According to the Tampa Bay Regional Planning Council (TBRPC 2006), the impacts of a 3 m (10 ft) rise in water level in the Tampa Bay region, similar to the surge from a Category 1 hurricane, would inundate almost 18% of the land within Pasco, Pinellas, Hillsborough, and Manatee Counties. This would impact 805,000 people in 428,000 dwelling units. A Category 2 hurricane (Fig. 5.3) could generate this 3 m (10 ft) storm surge, which would begin to cut off Pinellas County from the mainland as the Lake Tarpon area is inundated in the northern part of Tampa Bay. Pinellas County is also cut in two across Cross Bayou that runs across the central county from Tampa Bay to the Gulf barrier islands.

Figure 5.4 shows the surge evacuation zones based on different hurricane categories. Those major hurricanes could potentially create these surge heights: Category 3 up to 6.5 m (21 ft), Category 4 up to 9 m (29.5 ft), Category 5 greater than 9 m (29.5 ft). As the surge increases, the waters inside the bay get deeper and can support larger wind-driven battering waves that create more damage.

5.5 Demographics

The population density is highest (1000–10,000 people per 2.59 km^2 per mi^2) near the coast where the greatest storm surge threat exists (Fig. 5.5). The median age of the population within the area (Fig. 5.6) is notably older, more than 65 years of age, within some of the

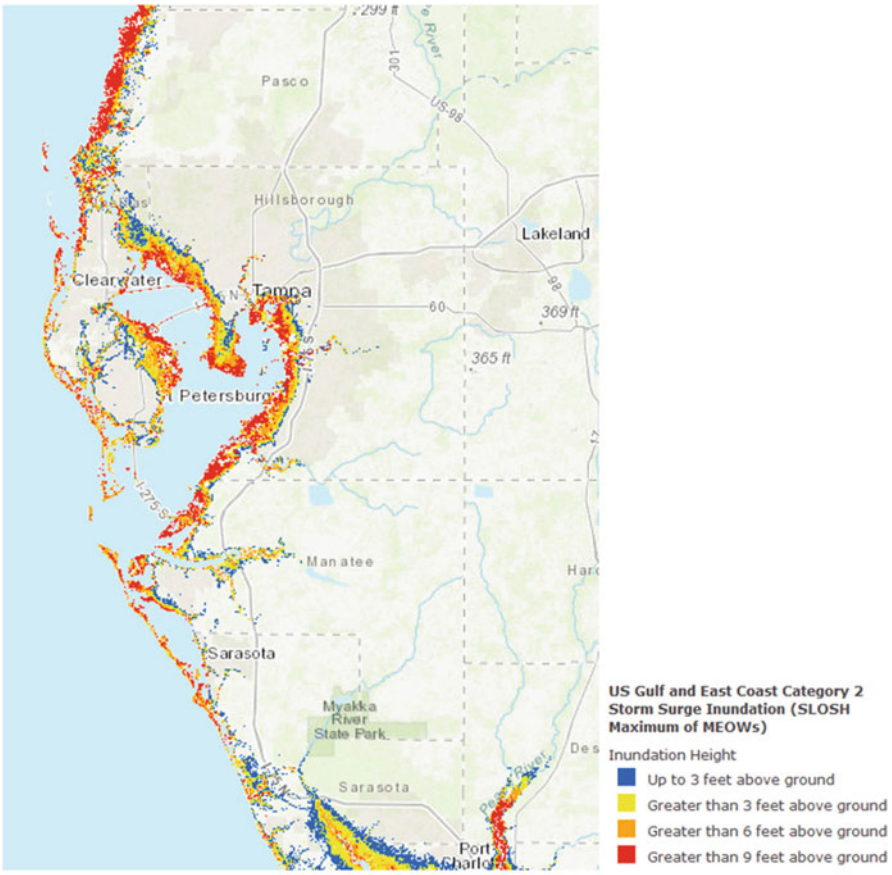

Fig. 5.3 Maximum surge heights expected with a Category 2 storm. (FDEM 2018)

more vulnerable areas near the gulf coast, particularly along the barrier islands and coastal Sarasota County. The youngest populations are most noticeable in inland areas to the east and typically over higher ground (U.S. Census 2010).

5.6 Housing

Figure 5.7 shows the age of houses in the area, with the oldest homes ranging from those built before 1950 to those built after 2000. The oldest home sites in Pinellas County were mostly built in the two sections of the county with high ground. More recent construction has been in some of the most vulnerable areas, including the barrier islands and near Cross Bayou. The Shore Acres area of northeast St. Petersburg has a network of dredged canals and low-lying fingers of land exposed to Tampa Bay, where nuisance rainfall flooding at high tide is common and storm

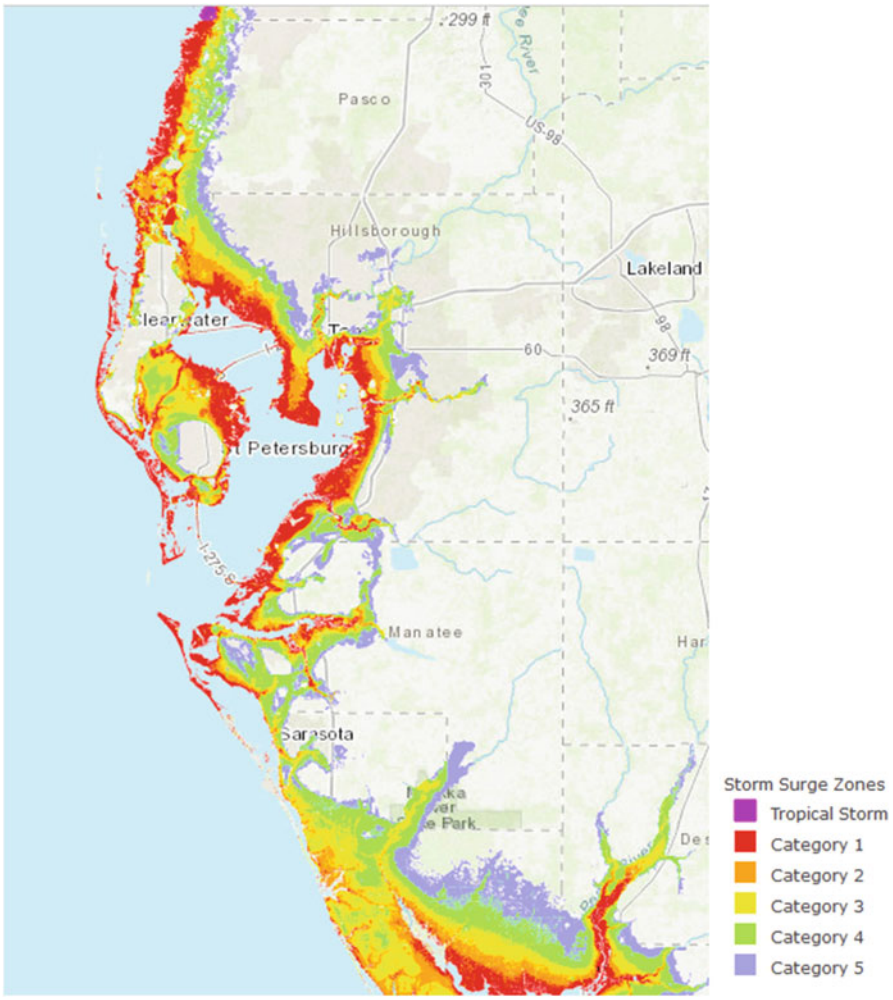

Fig. 5.4 Surge zones for hurricane Categories 1–5. (FDEM 2018)

surge flooding from minor storm systems is not uncommon. In Tampa, some of the older upscale neighborhoods such as Seminole Heights were built on high ground, but much of the older housing in both richer and poorer areas was built on lower ground on the Interbay Peninsula. In Manatee County, the oldest homes were built along and near low-lying parts of the Manatee River where storm surge flooding can be a problem. In Sarasota County, much of the early development was in lower lying coastal locations on the mainland side of Sarasota Bay.

Much of the housing in the Tampa Bay region is modest. Over 120,000 mobile homes are spread through the area, mostly clustered in trailer parks. The newer mobile homes are typically stronger than the older models. The older models are

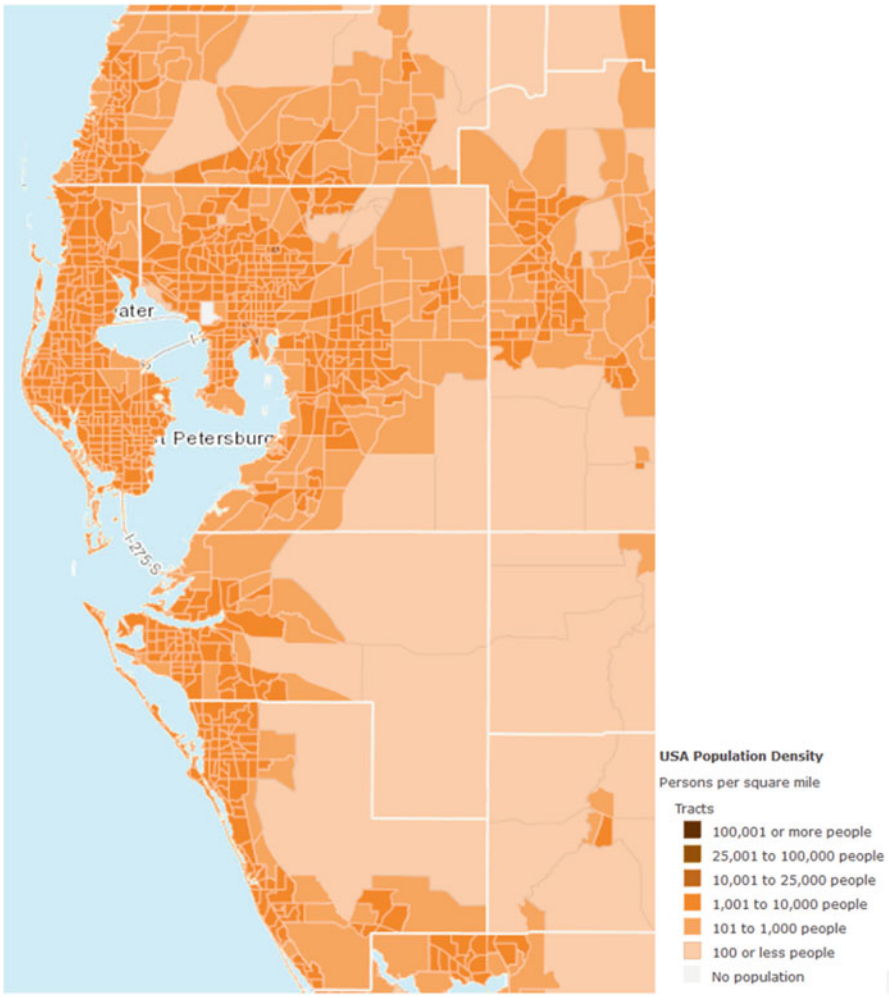

Fig. 5.5 Population density per square mile. (U.S. Census 2010)

sometimes not secured by straps that hold the mobile home to the ground. Most mobile homes have flimsy aluminum attachments such as awnings and carports that tend to fly and cause supplemental roof damage when the winds reach over 80 kph (50 mph). The median home value by zip code (Fig. 5.8) within the five-county area is greatest, over $600k, along the vulnerable barrier islands and near the downtown areas of Tampa, St. Petersburg, Bradenton, and Sarasota – much of which is on low ground.

The barrier islands are also where repetitive losses due to flooding from rainfall or surge or sometimes a combination have occurred (Fig. 5.9). These areas are mainly along the gulf coastal barrier islands along and south of Tampa Bay and within salt

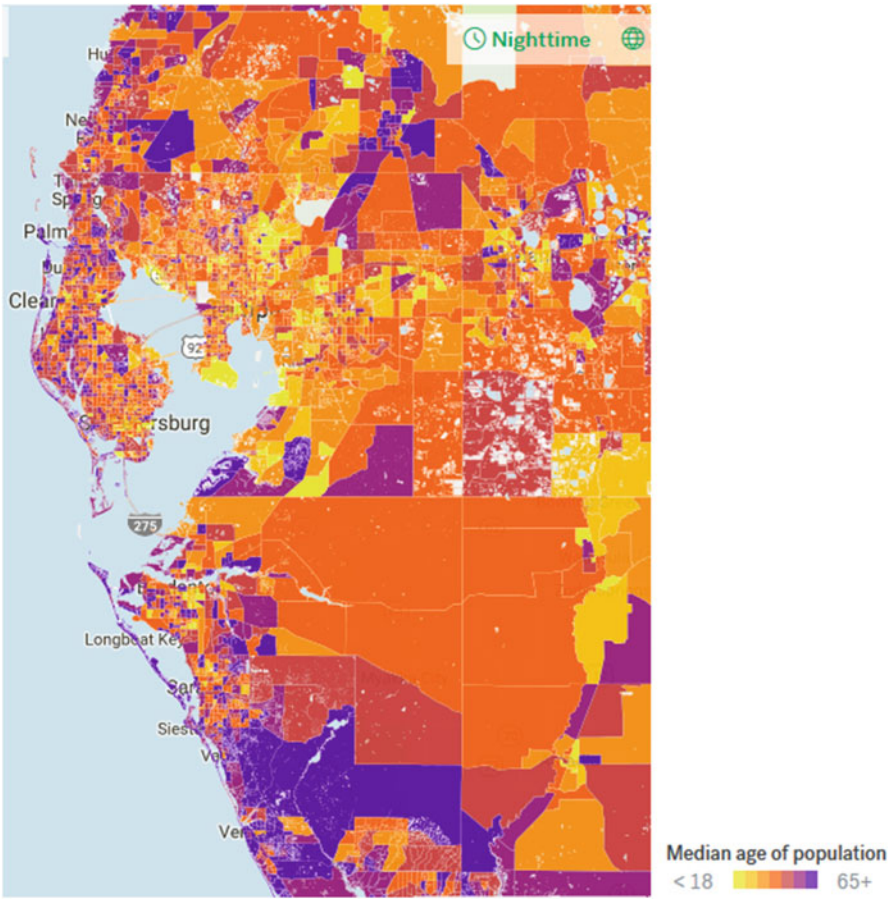

Fig. 5.6 Median age of population. (Trulia 2018)

marsh areas north of Tampa Bay. Other repetitive loss locations are along the inside of Tampa Bay and along the several surge and freshwater flooding prone rivers that feed into Tampa Bay.

5.7 Reconstruction Costs

According to Corelogic (2018), the Tampa metropolitan area, which is comprised of Hillsborough and Pinellas counties, ranks number 3, behind Miami and New York, in the top 15 metropolitan areas for storm surge risk from Category 1–5 storms. In the metropolitan area, 459,082 total homes are at risk of storm surge flooding with a total estimated reconstruction cost value of $79.2 billion. At the south end of Tampa Bay, the Bradenton metropolitan area, comprised of Manatee and Sarasota counties,

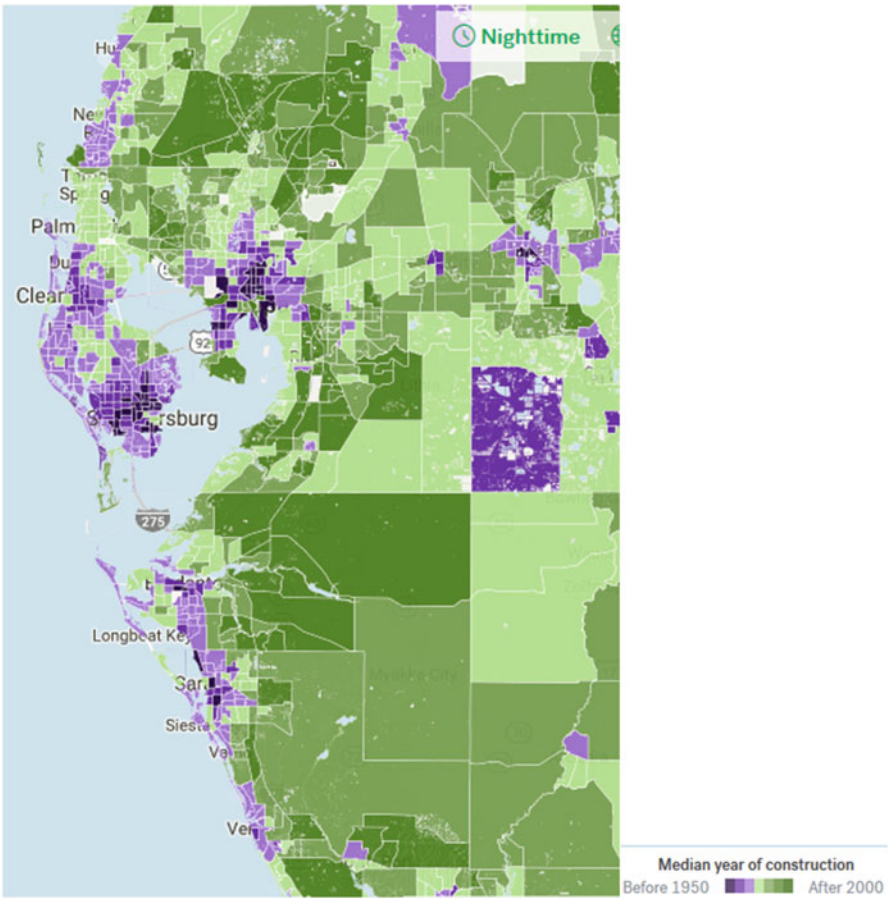

Fig. 5.7 Median year of construction. Older areas denoted in purple shades. (Trulia 2018)

ranks number 8. This area has 254,535 homes in Category 1–5 storm surge zones with a reconstruction cost value of $49.2 billion.

5.8 Evacuation Routes

The main north-south evacuation route is Interstate 75 with a segment, I-275, passing over the Sunshine Skyway Bridge across the southern part of Tampa Bay directly through the St. Petersburg area and across the northern part of Tampa Bay over the Howard Frankland Bridge and through Tampa (Fig. 5.10). Most evacuees on I-275 will be travelling in the northbound lanes – away from any storm coming from a southerly direction. Evacuees from around the Tampa Bay area will likely be merging with evacuees from the Naples and Fort Myers metro areas. North of Tampa

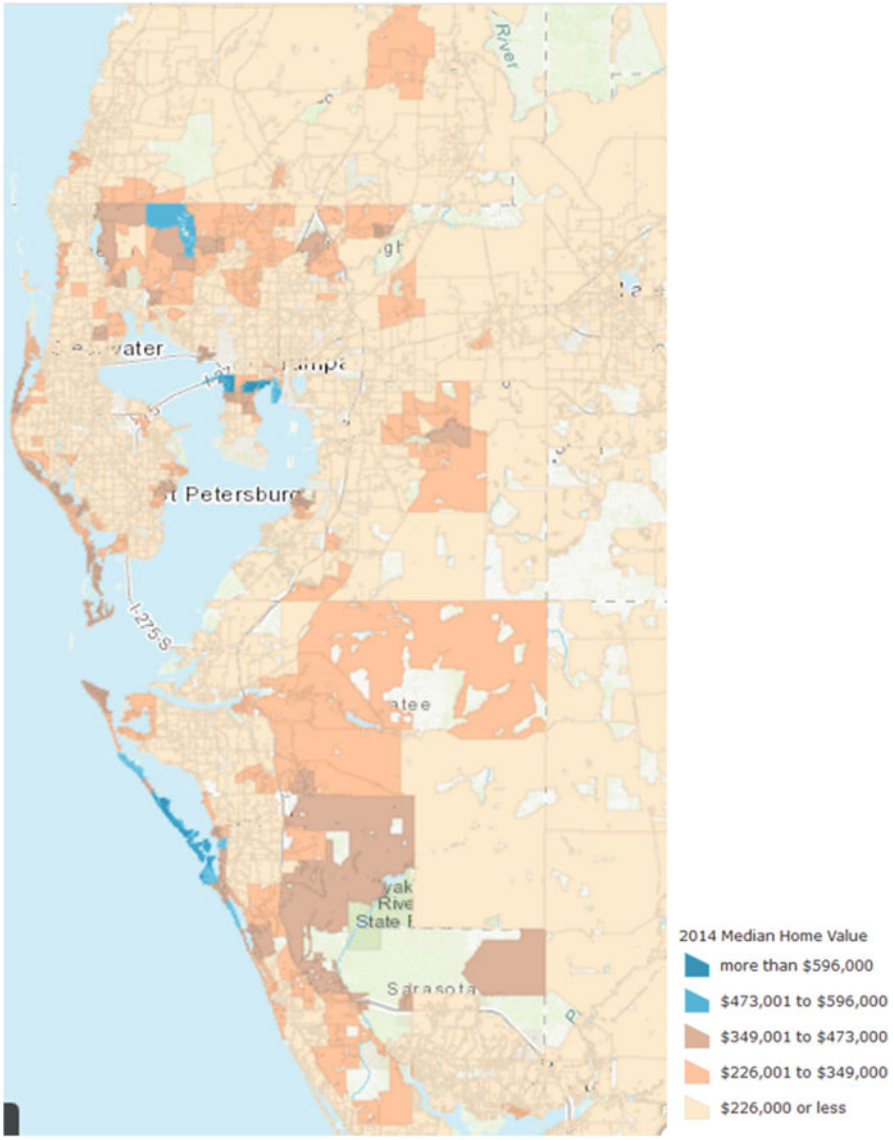

Fig. 5.8 Median home value by zip code 2014. (ESRI 2014)

Bay I-75 goes from three northbound lanes to two, which could create a bottleneck at the merge point. During Hurricane Irma, the inside shoulder lane was used to limit the congestion through that stretch. The primary east-west evacuation route is Interstate 4, which would be used for people evacuating to Orlando or to the Florida east coast.

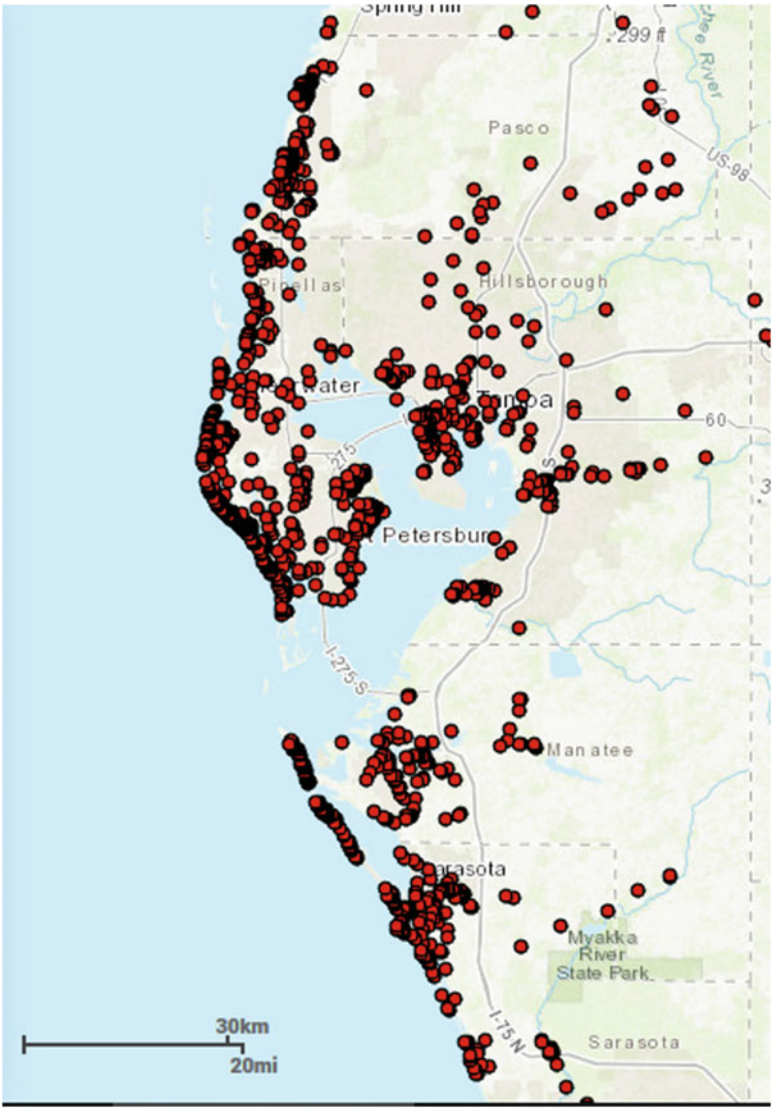

Fig. 5.9 Repetitive loss properties. (Coastal Resilience 2018)

When the time comes to evacuate, Pinellas County by far will have the most difficulty with the longest evacuation times. Pinellas County is on a peninsula with a narrow strip of land on the north end that connects to the mainland. Pinellas County evacuees will first be evacuating, mostly over bridges, into counties that are also facing evacuation. People from those counties will likely be merging onto I-75 or I-4 with evacuees from counties to the south, including Manatee and Sarasota,

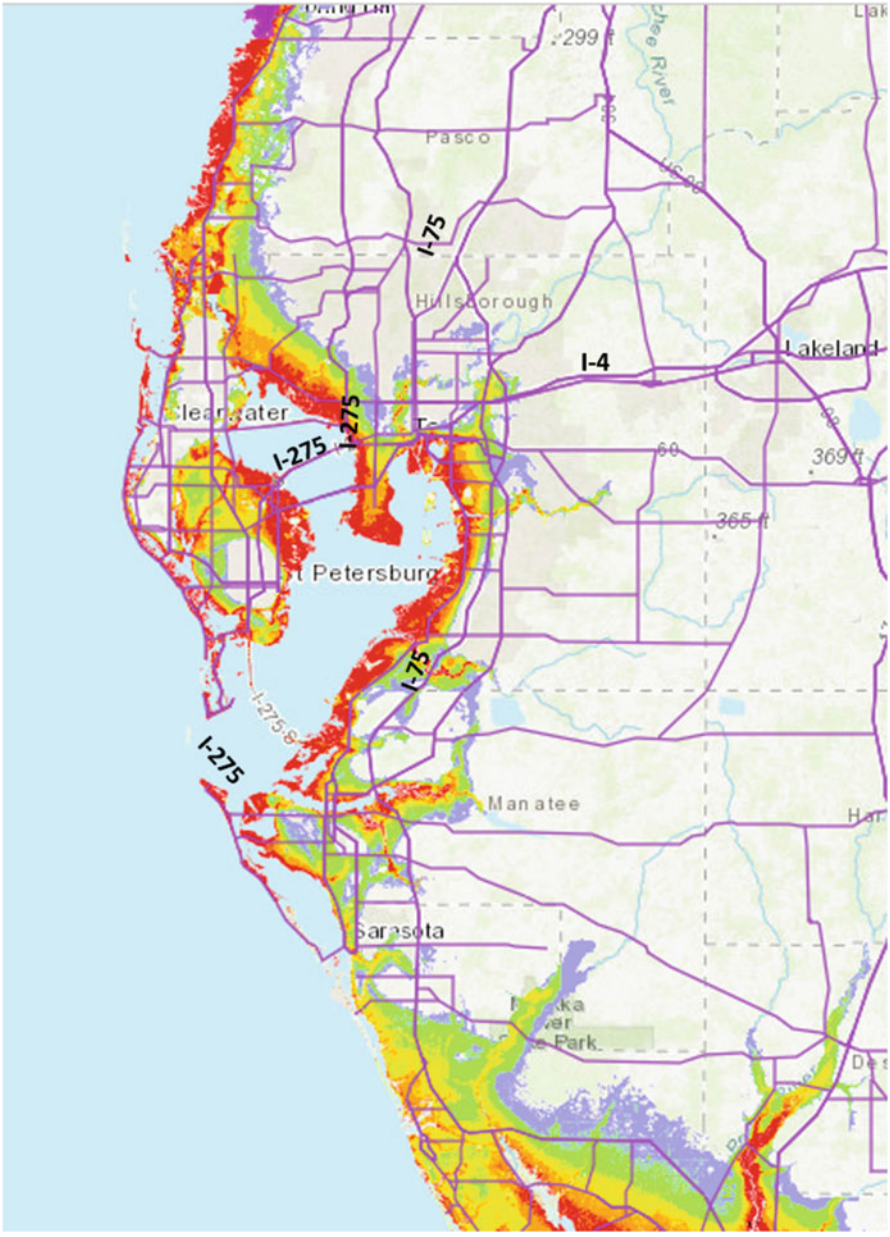

Fig. 5.10 Tampa Bay area primary evacuation routes over evacuation zones. (FDEM 2018)

particularly if the storm is coming from the south along the coast. According to TBPRC (2010), with the approach of a Category 3 hurricane, 70% of the Pinellas population in evacuation zones would evacuate. This evacuation would take 30 h just to leave Pinellas County into one of three adjacent counties that would also be evacuating. One major traffic incident would increase evacuation times even further. During the worst of Hurricane Irma in 2017, the county only cared for about 24,000 residents and 2000 pets in shelters (Pinellas EOC 2018). It is unknown how many evacuated out of the county as Irma approached.

Pinellas evacuees that leave too late may be following evacuation route signs that lead to flooded roads or low-lying bridges that may already be closed. Bridges across Tampa Bay are closed when winds are expected to reach tropical storm force, so the four major bridges across Tampa Bay from Pinellas County to the mainland will be closed. This will cause significant problems for those people hoping to evacuate late in the game. The evacuation signs, which are fixed in place, will still lead to the closed bridges.

Interestingly, the Sunshine Skyway Bridge that crosses the southern part of Tampa Bay is not considered an evacuation route. With a roadway nearly 200 ft above the bay, the Skyway Bridge is typically closed due to high winds sooner than the other three bridges that span the northern realms of Tampa Bay. The general rule that emergency managers state is for evacuees to go to the closest safest location.

5.9 Roadways and Evacuation Scenarios

Nearly every hurricane evacuation scenario seems nightmarish. Emergency management officials wonder how a region with daily backed up rush-hour traffic even in good weather will deal with the realities of a major hurricane evacuation, particularly for a storm that has either developed or intensified nearby giving little time to prepare or evacuate.

5.10 Emergency Services

Important infrastructure (Fig. 5.11), such as police stations and fire stations, and Fig. 5.12 showing hospitals, are laced among the housing areas and often built in surge-prone areas. In a major storm situation, this will limit the access and response time to resident emergencies. In advance of a major storm, resources will need to be repositioned to safer areas.

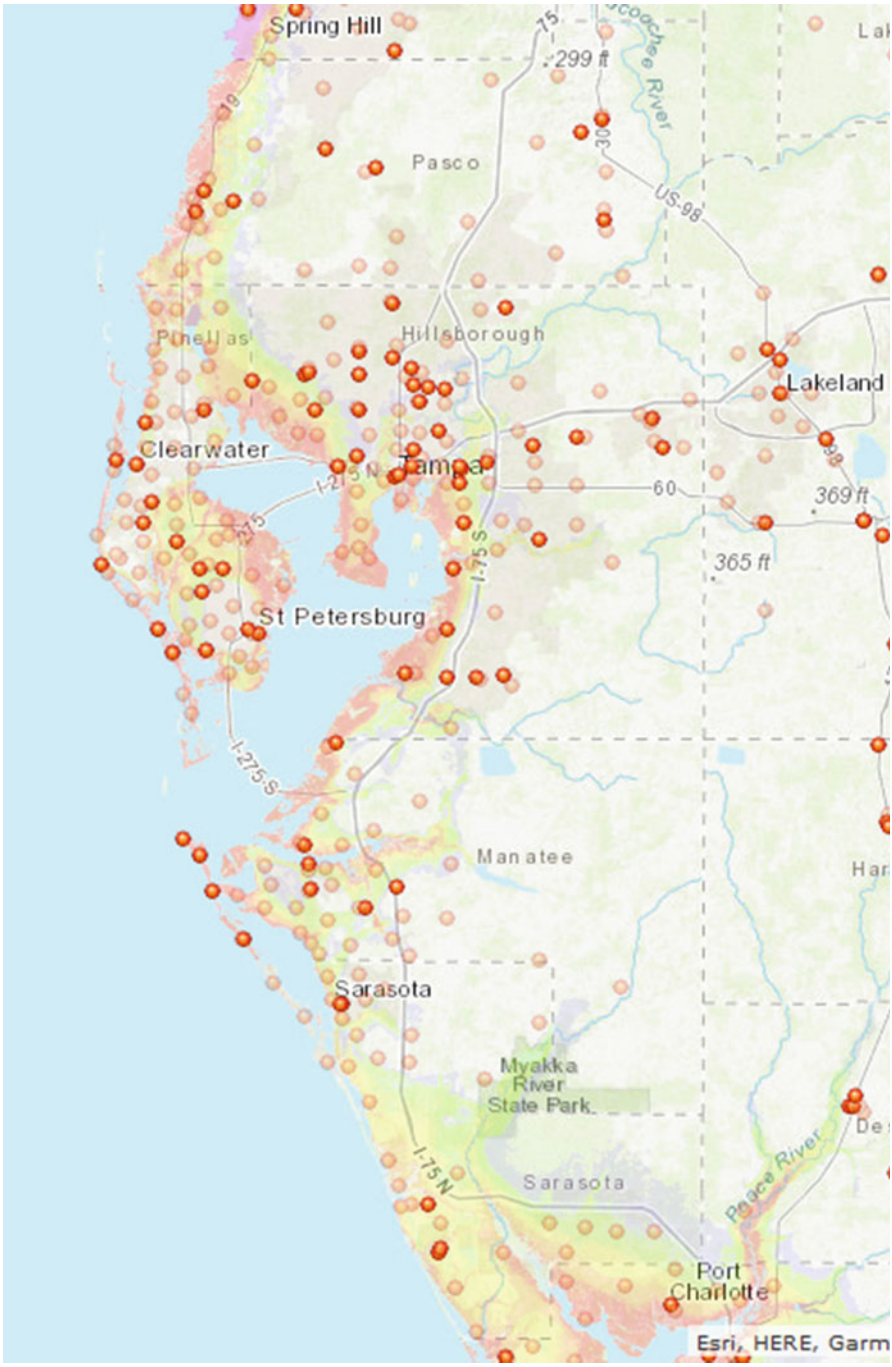

Fig. 5.11 Law enforcement offices (bold) and fire stations (faded). (FDEM Geoportal 2018). Evacuation zones as in Fig. 5.10

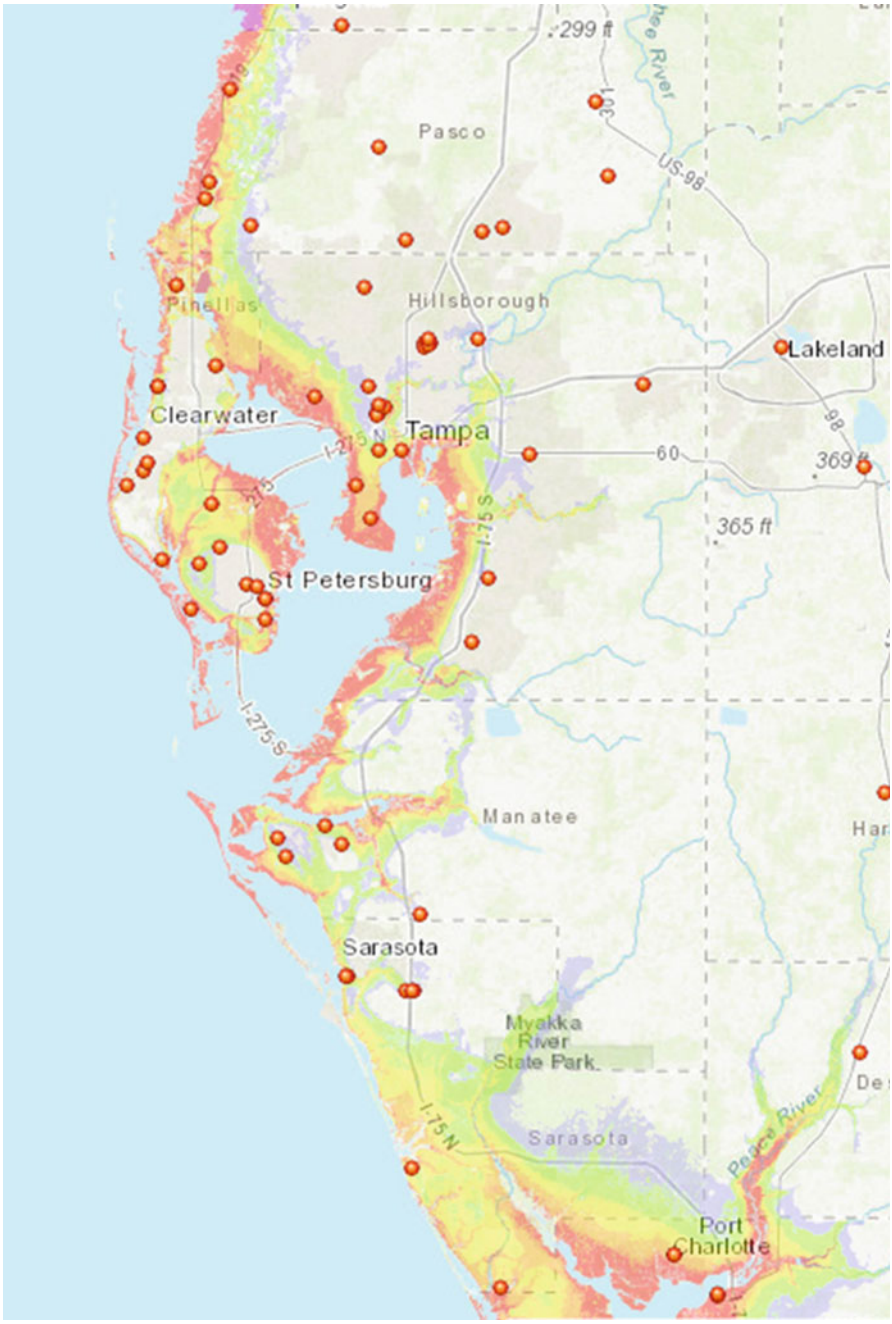

Fig. 5.12 Hospitals and trauma centers. (FAHCA 2018)

5.11 Medical Facilities

Figure 5.12 shows locations of Agency for Health Care Administration (FAHCA 2018) licensed hospitals and trauma center facilities. Many of the major medical facilities are within the surge zone, which will limit or exclude their use during and after a major hurricane. Tampa General Hospital and Manatee Memorial Hospital are two where access will be impacted by surge even from weaker hurricanes. TBRPC (2010) suggests that after a Category 5 storm, most bay area medical facilities will be unusable for up to or over 1 year.

5.12 Bridges

Hurricanes in other places along the Gulf of Mexico coast have revealed what could be potential problems for the bridges and causeways across Tampa Bay. In 2004, Hurricane Ivan's storm surge and wave action, upon landfall near Mobile, Alabama, displaced sections of the I-10 bridge roadway in the east- and west-bound lanes that only had a 4 m (12 ft) clearance above the mean water level. A temporary steel bridge was erected, and two new three-lane bridges were built during the next 32 months to replace the old bridges. The total cost to replace the I-10 bridges that stretched for 4.2 km (2.6 mi) was $243M or $93M per mile (Road Traffic Technology 2018).

The total cost of all bridges damaged by Hurricane Katrina in 2005 was around $1 billion and included two three-lane bridges along I-10 that were 9.1 m (30 ft) above Lake Ponchartrain. More than $2.4 billion was spent to rebuild the region's infrastructure (Lee and Hall 2011). Padgett et al. (2008) studied 44 bridges damaged by Hurricane Katrina and found high storm surge contributed the most to damage, but some bridges where storm surge was less were damaged by debris impact.

Four bridges stretch across Tampa Bay (Fig. 5.13) and include the 4.8 km (3.0 mi) I-275 Howard Frankland Bridge, the 4.5 km (2.8 mi) Gandy Bridge, and the 1 km (0.6 mi) Courtney Campbell Bridge that add up to around 10 km (6.5 mi). A rough estimate based on construction coasts after Katrina is around $160M per km ($100M per mile) to rebuild if the bridges in Tampa Bay are destroyed.

The I-275 Howard Frankland Bridge center spans are 13.1 m and 14.9 m (43 and 49 ft) while the roadway approaches on the causeway are at an elevation about 2.1 m (7 ft) (NAVD88), while the 100-year floodplain is at about 2.7 m (9 ft) (NAVD88) elevation (HFBS 2017). The low member elevation on the approach spans of the existing northbound bridge is about 3.0 m (10 ft). The Gandy and Courtney Campbell Bridge center spans are also elevated above potential storm surges, so it is unlikely that they would be destroyed by roadway displacement, but the approach bridge sections and low-lying causeways at each end of the bridges are vulnerable. The fourth bridge, the 9 km (5.6 mi) Skyway Bridge, is elevated well above the water level, but again, the low-lying causeways at each end of the bridge would suffer significant damage from storm surge.

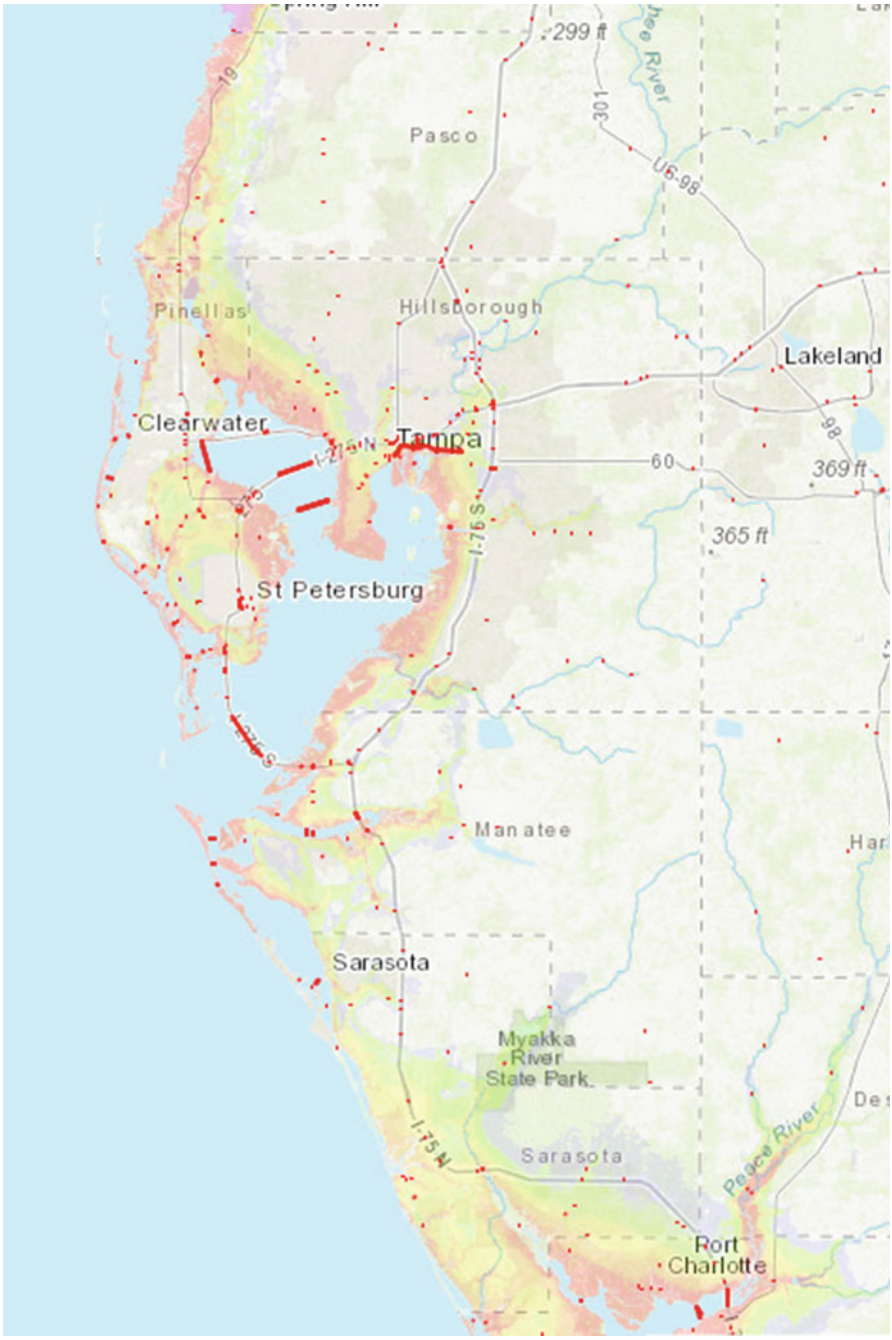

Fig. 5.13 Florida Department of Transportation bridges. Each red dot or red line is a bridge. (FDOT 2017)

5.13 The Power Grid

Figure 5.14 shows the locations of electric generation plants and main transmission lines to distribute the electricity (HIFLD 2017). A major hurricane could impact most of the area's electric generation plants, which are typically in surge evacuation zones. One critical impact would be the inability of workers to return to the plants due to road closures or obstructions. Most of the plants run on natural gas, but the Big Bend power plant on the east side of Tampa Bay is one of the few coal powered plants in operation in Florida. A major hurricane, either local or distant, could impact barge delivery of coal to the plant. Although a conversion of this plant to natural gas is planned, it could take 10 years to complete (McGrory and Danielson 2018). In 2009, a 60-megawatt natural gas- and fuel oil-fired peaking unit was installed at the Big Bend plant. This unit can provide power during periods of peak customer demand and can be used when catastrophic weather causes the electric grid to lose power. It is the only peaking unit deployed in the Tampa Bay region. The peaking unit can start the Big Bend's larger generating units in a blackout when power from the grid is not available (TECO 2018).

Suspended power lines are vulnerable to wind, and particularly wind-felled trees. On the local level, many new communities have underground electrical utilities, but older communities do not. After the 2004 hurricane season, electrical utilities made an effort to keep trees near power lines trimmed to minimize damage during the next storm. The tree trimming continued even though hurricane activity subsided for 10 years after Hurricane Wilma (TECO 2017; FPL 2018). Ultimately, though, when a major hurricane impacts the Tampa Bay region, some residents will be without power for weeks or longer.

5.14 Waste Water Facilities

Thirty percent of the residents live in surge zones, so it is not surprising that 30% of water treatment facilities are also in the surge zone (Fig. 5.15). Storm surge can inundate wells and water mains, creating breakage and contamination. Electricity loss prevents water and sewage pumping, interrupting the supply of fresh drinking water and leaving waste to accumulate. Human and pet water will require boiling before consumption following a major storm.

After Hurricane Hermine passed the region in 2016, the ground was saturated with rain water and St. Petersburg's aging and cracked pipes allowed water into the sanitary sewer system. The combined impacts from Hermine created a scenario where over 110 million liters (29 million gallons) of sewage spilled into Tampa Bay (Frago 2016). Hurricane Irma created a similar scenario, but this time in Hillsborough County, where 1.3 million liters (329,000 gal) of sewage spilled into the bay (Frago and Danielson 2017).

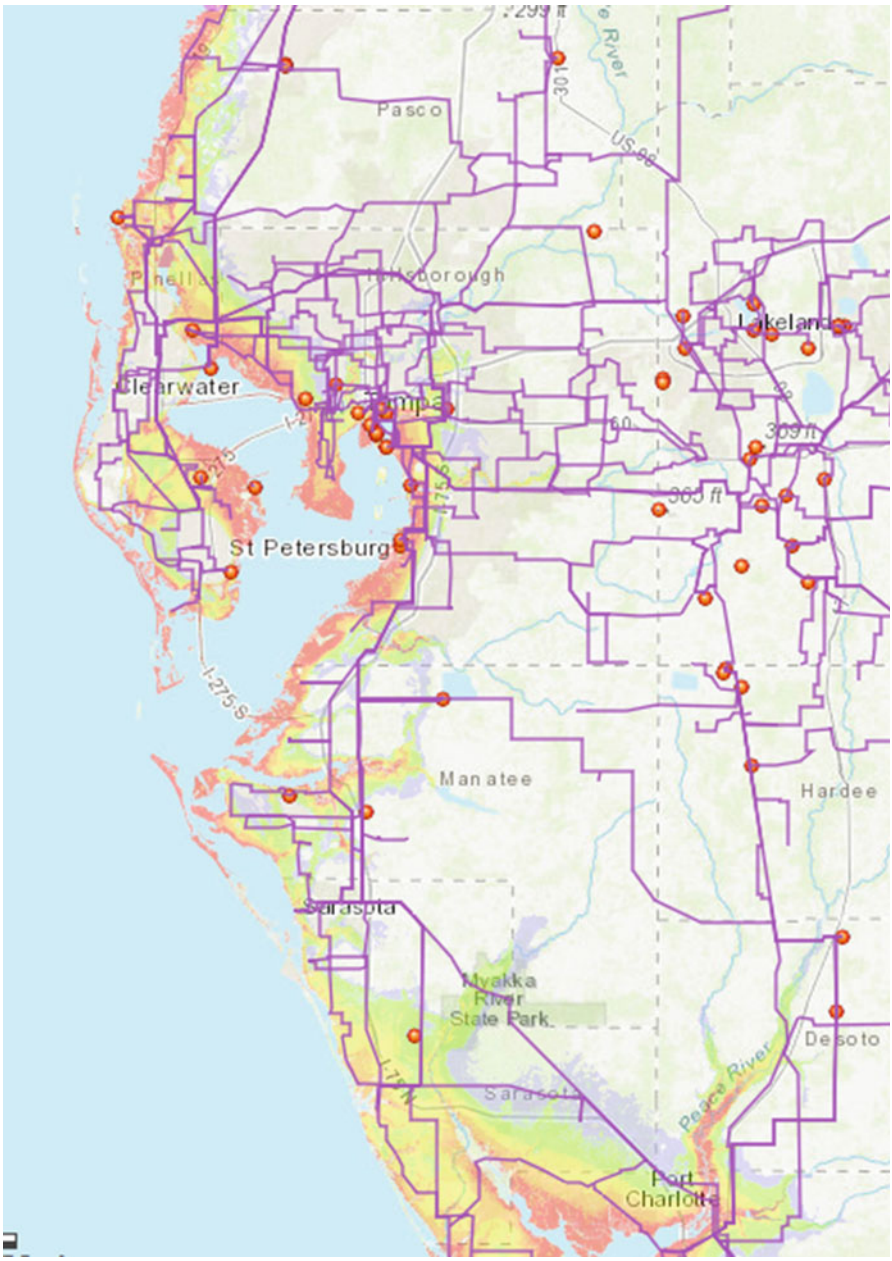

Fig. 5.14 Electrical power generating plants and main transmission lines. (HIFLD 2017)

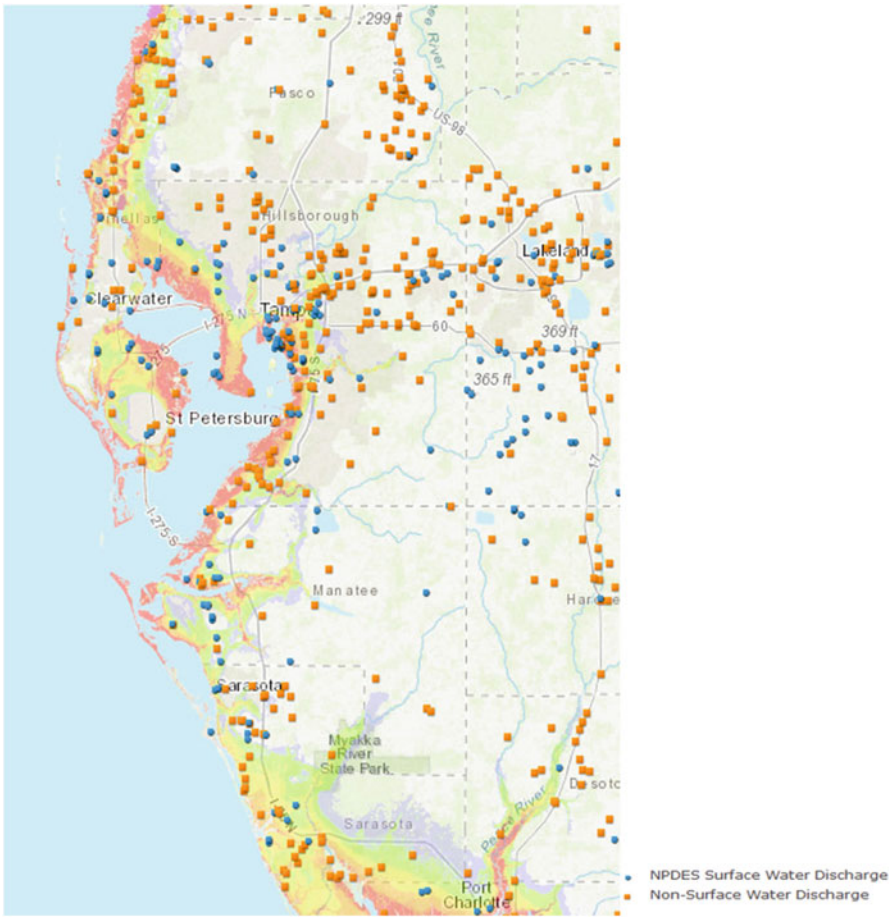

Fig. 5.15 National Pollutant Discharge Elimination System wastewater facilities. (WAFR 2017)

5.15 Port Tampa Bay

Port Tampa Bay is Florida's largest port by tonnage, handling over 33.6 mt (37 million tons) of cargo per year, and Florida's largest port in terms of physical size, encompassing over 20.2 km^2 (5000 acres). The port activity ranges from cruise ships to bulk cargo. To gain insight into potential problems at Port Tampa Bay, we consider circumstances from the past and from other ports in the region. Port Manatee in Manatee County, which is closer to the Gulf of Mexico, is a smaller but growing facility and shares the risk of storm impact.

After Hurricane Katrina ripped through Empire, Louisiana on August 29, 2005, many vessels became unmoored drifting battering rams that came to rest on land after the surge retreated. Vessels Sea Wolf and Sea Falcon were found in the middle

Fig. 5.16 Vessels Sea Wolf and Sea Falcon in the middle of a major roadway following Hurricane Katrina in 2005. (U.S. Coast Guard photo by Petty Officer 2nd Class Jennifer Johnson)

of a major roadway and presented a removal problem (Fig. 5.16). Large barges were also pushed well inland which made removal difficult. Loose vessels are a major problem in a busy port, particularly where hazardous materials such as gasoline and ammonia are offloaded or stored.

In the past, ships have had serious accidents within the narrow channel that stretches for 64 km (40 mi) from Port Tampa Bay to the open waters of the Gulf of Mexico. In 1980, a major ship collision occurred near the Sunshine Skyway Bridge when the USCG Blackthorn collided with the vessel Capricorn, leaving 23 sailors dead. Also in 1980, another catastrophe occurred when the vessel Summit Venture hit the original Sunshine Skyway Bridge and knocked out the center span, leaving 35 dead from vehicles plummeting off the bridge. Thirteen years later, in 1993, three vessels, the freighter Balsa, and barges Bouchard and Ocean 255, collided near the Sunshine Skyway Bridge. The Bouchard spilled an estimated 1.3 million liters (336,000 gal) of No.6 fuel oil into Tampa Bay. All these collisions had an impact on vessel traffic in and out of Tampa Bay. Since then, vessel tracking systems have make collisions less likely.

To limit damage to port structures, vessels larger than 454 mt (500 tons) moored in Port Tampa Bay must leave 24 h prior to hurricane-force winds. Keep in mind, though, the ship channel is long and narrow. Any ship hastily leaving port through the ship channel that runs aground has the potential to block other vessels from leaving. If ships cannot evacuate and are stuck in port during a major storm, they can become a peril to port facilities that store dangerous materials.

Several businesses refurbish vessels on dry docks that operate within the port boundaries. This creates a more difficult scenario with an approaching storm because the vessels cannot be relocated. Scuttling or sinking the ship and drydock could be required to reduce the chance of a loose vessel from acting as a battering ram within the port.

More refined petroleum comes through Port Tampa Bay than any other Florida port. The storage tanks hold about 5–7 days of fuel, so they are constantly refueled by ship and barges carrying petroleum. Prior to tropical impacts, the demand for fuel resources increases as people top off the fuel in their vehicles. During the 2004 hurricane season, the rapid succession of four different tropical systems interrupted petroleum deliveries and created a fuel shortage along the west coast of Florida. Petroleum storage units have been damaged as the result of storm surge in other locations. Godoy (2007) found that wind pressures damaged tanks along the path of Hurricane Katrina and Hurricane Rita. He found that most of the damage was due to flooding that caused tanks to dislodge from their foundations. If the fuel depots at Port Tampa Bay are compromised during a storm, then recovery will be significantly hampered. State and U.S. Coast Guard authorities have placed the highest priority on filling the fuel tanks prior to the storm and opening the ship channel post storm to keep fuel flowing (Mark Luther, personal communication, 6 April 2018).

5.16 Hazardous Materials in the Surge Zone

Some of Tampa Bay's thriving commerce uses hazardous materials or creates hazardous waste. This is a particular concern when those industries are in the surge zone. Hazardous waste and used oil facilities that are vulnerable and noted as Hurricane Facilities of Concern by the Florida Department of Environmental Protection (FDEP 2005) are shown in Fig. 5.17. This includes treatment, storage, and disposal facilities (TSDs) that are permitted to manage hazardous waste; hazardous waste transfer facilities where hazardous waste may be stored or staged for up to 10 days; used oil transfer facilities where used oil may be stored or staged for up to 35 days; and large quantity generators (LQGs) of hazardous waste that generate more than 1000 kg (2200 lb) of hazardous waste in any 1 month and may store their hazardous waste on-site for up to 90 days. Most of these entities in the counties of interest are within surge evacuation zone locations.

5.17 The Phosphate Industry

The phosphate industry digs phosphate rock from the ground in interior Florida as one of the key ingredients to manufacture fertilizer. Fertilizers added to soil contain three key nutrients used by plants: nitrogen, phosphorus, and potassium. The phosphate rock is processed with sulfuric acid, producing phosphoric acid. The

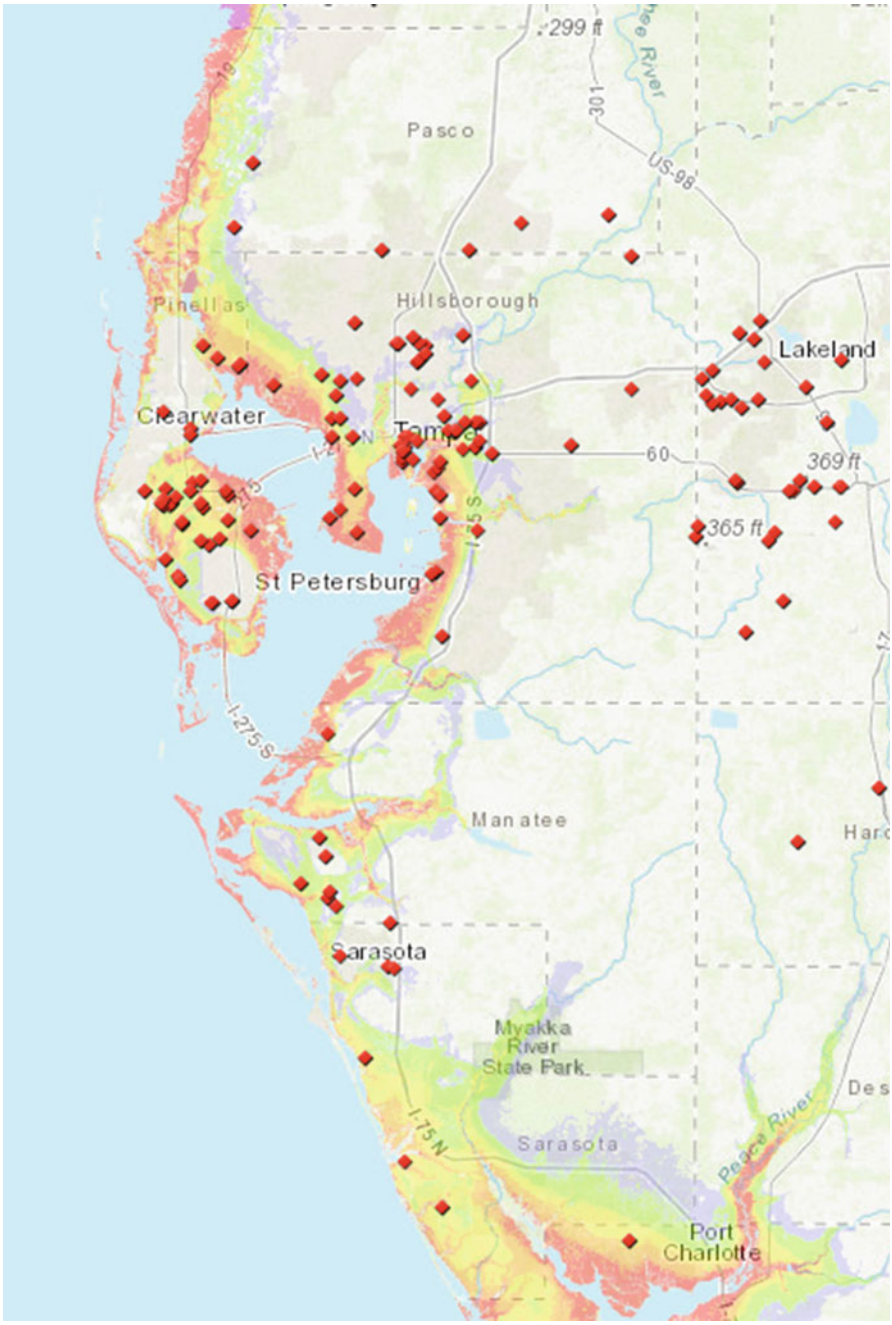

Fig. 5.17 Facilities that are permitted to manage hazardous waste; hazardous waste transfer facilities, used oil transfer facilities, and large quantity hazardous waste generators. (FDEP 2018)

Fig. 5.18 Two gypsum stacks (indicated by yellow arrows) situated adjacent to Tampa Bay and the Alafia River. (Google Maps)

phosphoric acid is then combined with ammonia to create ammonium phosphate, and is then typically blended and granulated with ammonium nitrate, potassium chloride, and triple superphosphate (madehow.com 2018). The accumulated byproduct of fertilizer processing called phosphogypsum, a slightly radioactive waste material, is then dumped into massive wide piles up to 67 m (200 ft) in height over an area up to 2.6 km^2. The surface of these stacks is slightly depressed. In these depressions atop the gypsum stacks are large pools, up to 1.6 km^2 (400 acres) of very acidic mineralized water (about pH 1.5) for processing ore (Pittman 2017). The processing plants are mostly located inland near the mines, but one processing plant exists next to Tampa Bay along the Alafia River (Fig. 5.18). Another processing plant near Tampa Bay (to the south in Manatee County) that belonged to a defunct processing operation was removed and partially cleaned up with 140 million in taxpayer dollars.

Figure 5.19 shows the large extent of the mining in inland areas adjacent to the Tampa Bay region, indicated by the teal blue manmade polygonal water areas. The figure also shows the phosphate processing facilities and gypsum stacks in red (FDEM 2011), most of which are located at the headwaters of several major Florida Rivers, shown in yellow.

Phosphate processing disasters have occurred on a somewhat regular basis, sometimes related to moderate weather systems. A major, slow-moving hurricane, similar to Hurricane Harvey (2017) that dumped more than 1.3 m (50 in.) of rain near Houston, Texas, or Hurricane Easy (1950) that dropped over 1 m (38 in.) of rain in just 24 h north of Tampa Bay in Yankeetown, Florida, could create a scenario where

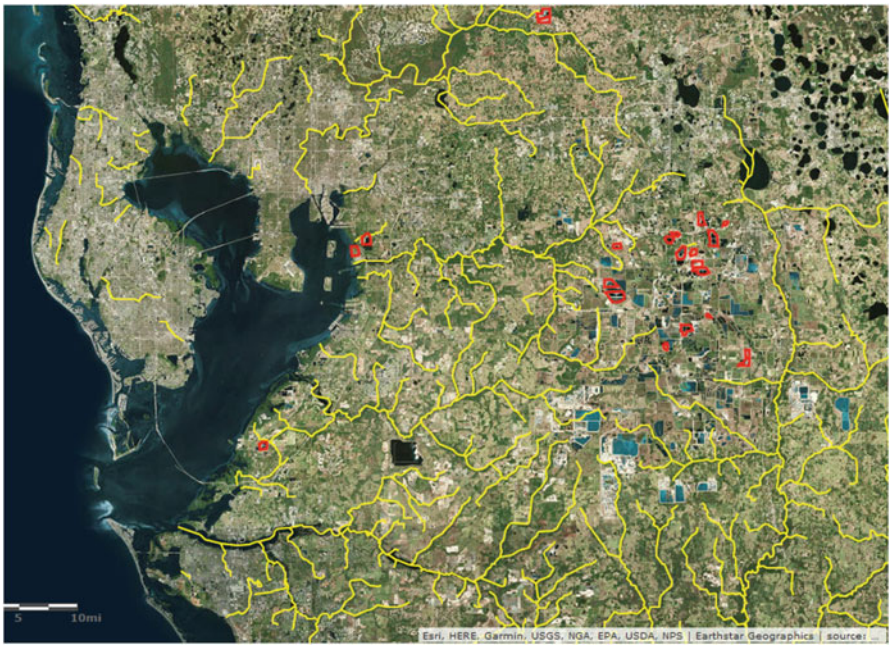

Fig. 5.19 Phosphate mining areas (blue), waterways (yellow) and gypsum stacks (red). (FDEP 2011)

phosphate processing facilities have simultaneous failures. When a facility has a gypsum stack failure, it has been repeatedly shown that any secondary containment, such as earthen berms, is inadequate, and the release goes into one of the rivers, and eventually into bays and the Gulf of Mexico. These releases are particularly deadly to life in the rivers. These past phosphate-related disaster scenarios indicate the magnitude of the problem with containment failures:

- Mar. 1, 1967, Polk County, Florida, USA Mobil Chemical. A phosphate retention failure released 250,000 m^3 of phosphatic clay slimes which reached the Peace River creating a fish kill. (Patagonia Alliance 2014). Over 125 mm (5 in.) had fallen in the previous 30 days.
- Dec. 3, 1971, Polk County, Florida, Cities Service Co. A phosphate pond dam failure released 9 million m^3 of clay water tailings that traveled 120 km downstream on the Peace River, creating a large fish kill (Patagonia Alliance 2014). Upwards of 175 mm (7 in.) of rain had fallen in the vicinity during the since the beginning of November.
- Mar. 30, 1987 Hillsborough County, Florida, during heavy rains Gardinier phosphate processing leaked 13.7 million gallons of acidic waste from a gypsum stack into the Alafia River and Tampa Bay. The leak resulted in a massive fish kill (Paulson et al. 1991). Upwards of 100 mm (4 in.) of rain had fallen in the previous 24 h

- May 1, 1988: Hillsborough County, Florida, Gardinier phosphate. Three hundred five metric tons (336 tons) of PFS fertilizing solution of 75% phosphoric acid (Patagonia Alliance 2014) was released from one of Gardinier's 4990 mt (5500-ton) tanks. The release killed an unknown number of fish in the Alafia River that feeds into Tampa Bay. Weather is not suspected as a contributor to this release.
- Oct. 12, 1993: Hillsborough County, Florida, Cargill phosphate. Fish were killed when acidic water spilled into Archie Creek and into Tampa Bay (Patagonia Alliance 2014). Over 254 mm (10 in.) of rain had fallen from the beginning of September up to that date.
- Jan. 2, 1994: Polk County, Florida, USA Cargill phosphate. Seventy six thousand cubic meter of water spilled into the Peace River near Fort Meade (Patagonia Alliance 2014). Precipitation was only moderate leading up to the spill.
- Jun. 15, 1994: Polk County, Florida, IMC-Agrico phosphate. A sinkhole opens in phosphogypsum stack resulting in a release of acidic water into groundwater (Patagonia Alliance 2014). Upwards of 254 mm (10 in.) of rainfall had fallen during the previous 30 days.
- Oct. 2, 1994: Polk County, Florida, USA IMC-Agrico phosphate. Payne Creek Mine dam failed releasing 6.8 million m^3 of water from a clay settling pond. The majority of the spill was contained on the adjacent mining area but 500,000 m^3 escaped into Hickey Branch, a tributary of Payne Creek (Patagonia Alliance 2014). Over 280 mm (11 in.) of rain had fallen in the previous month over the area.
- Nov. 19, 1994: Hillsborough County, Florida, USA IMC-Agrico. A phosphate dam failure at the Hopewell Mine with nearly 1.9 million m^3 of water from a clay settling pond spilled into nearby wetlands and the Alafia River, (Patagonia Alliance 2014). Upwards of 125 mm (5 in.) of rain had fallen during the previous 2 weeks.
- Dec. 7, 1997: Mulberry Phosphates. A rainstorm compromised a gypsum stack and 56 million gallons of highly acidic wastewater containing phosphoric acid escaped. This release killed all fish and marine life along 42 mi of the Alafia River before flowing into Tampa Bay (Pittman 2017). Some nearby locations had received over 254 mm (10 in.) of rain during the previous month and up to the event.
- Sep. 5, 2004: Hillsborough County, Florida, Cargill Crop Nutrition. As 178–254 mm (7–10 in.) of rain fell, a dike at the top of a 30 m (100-ft)- high gypsum stack holding 5.7 million liters (150-million gallons) of polluted water broke after waves driven by Tropical Storm Frances bashed the dike's southwest corner causing a gypsum stack breach released 60 million gallons (227,000 m^3) of acidic liquid into Archie Creek and Tampa Bay (Patagonia Alliance 2014). Cargill Crop Nutrition and IMC Global Inc. merged in October 2004 and operated as Mosaic.
- Dec. 14, 2005: A leaky pipeline at Mosaic's Riverview, Florida plant spills 40,000 gal of hazardous waste material. Hundreds of small fish die in Archie Creek. (Stein 2006). This occurrence did not appear to be weather related.

- Aug. 27, 2016: Polk County, Florida, Mosaic Inc. A sinkhole developed under a gypsum stack and drained 215 million gallons of contaminated water into the aquifer. A similar occurrence happened in 1994 at the same facility (Pittman 2017). During the month of August 2016 several locations in the vicinity received upwards of 254 mm (10 in.) of rain.

Ammonia is used in the production of fertilizer and a pipeline transporting ammonia stretches from Port Tampa Bay through the populated parts of eastern Hillsborough County to the inland processing plants. The pipeline has typically been operating without incident except for the following two human-caused breaches:

- In 2003, a person compromised the pipeline near the upscale Fish Hawk Ranch subdivision and two schools. The school officials moved 2000 elementary and middle school students to other schools. The ammonia was strong enough where a work crew was "throwing up". Nearly 100 firefighters used hoses to help disperse the plume of vapors (Firehouse.com 2003).
- In 2007, A 16-year-old male drilled into the ammonia pipeline along the Alafia River bridge at U.S. Highway 301. It took almost 2 days to stop the gas leak as hundreds of residents were evacuated (Catalanello 2008).

The scenario in a major hurricane could be worse than anything previously encountered if the Port Tampa Bay storage facilities, or the pipeline attached to the Alafia River bridge, is compromised by battering hurricane debris or loose vessels carried by the storm surge. Other incidents below provide a hint at what could happen in association with wind or surge from a major hurricane. The extreme wind, rain, and water currents could also help to disperse any releases.

- In 2005 a molten sulfur storage tank ruptured at the Port of Tampa and leaked about 4082 mt (4500 tons) of molten sulfur, of which, 2.7–3.6 mt (3–4) tons went into the Sparkman Canal at the port (Sulphuric-acid.com 2008).
- In 2008 sulfur dioxide leaked at Mosaic Phosphates in Mulberry, Florida causing injury to 29 workers, of which, 18 contractors were hospitalized with respiratory problems with one person admitted in serious condition. A company spokeswoman said the plant routinely emits sulfur dioxide, but weather conditions during this release caused the noxious cloud to hug the ground instead of drifting away (Sulphuric-acid.com 2008).
- In 2013, another sulfur dioxide release occurred at Port Tampa Bay when a fire started during "routine maintenance" to a sulfur storage silo. The sulfur is kept warm by a system of heated coils that are installed around the tank. As firefighters sprayed water onto the fire, it created sulfur dioxide. In less than a week another fire occurred at the same sulfur tank. After the second fire the tank was thoroughly inspected (Sulphuric-acid.com 2008).
- In 2013, a train carrying thousands of gallons of ethanol derailed tipping 11 rail cars – 3 of which contained 30,000 gal of highly flammable ethanol. Wind and rain complicated efforts to contain the spill and 4500 gal leaked out. (no citation?)

5.18 Deadly Cyclones of the Past Around the World

Impacts of tropical cyclones in other places around the world can provide insight into potential impacts in the Tampa Bay area. Every location is different by geographical factors, building standards, industry, historical factors, culture, and governmental response. This is a look at tropical cyclones that have impacted areas around the world, and lessons to be learned for future impacts to the Tampa Bay area. The list is organized by the number of deaths for the storms presented.

- Hurricane Andrew struck south Florida and then Louisiana in 1992 and caused 26 direct and 43 indirect deaths. The surge was up to 5.2 m (16.9 ft). Although the number of deaths was relatively low for a Category 5 storm striking a populated area, Andrew destroyed 28,066 homes and damaged 107,380 homes, leaving 180,000 people homeless. Livelihoods were also taken away with 82,000 businesses destroyed or damaged and 32,900 acres of farmland were damaged. Other damage included: 31 public schools destroyed/damaged, 59 health facilities damaged, 9500 traffic signs and signals, 3300 miles of power lines destroyed, 3000 water mains damaged, 1.4M residents without electric power and 80,000 without phone service (Godschalk 1999). Since then, building codes in Florida have been strengthened but in the Tampa Bay region many structures are older and have not been tested by major hurricane winds.
- Hurricane Audrey struck the Texas/Louisiana border in 1957 leaving 416 people dead. It was the seventh deadliest hurricane in the U.S. with a storm surge of up to 3.7 m (12 ft). In Cameron Louisiana, with a population of 3000, 370 perished – 12% of the population. In the 35 km (22 mi) from Cameron to Grand Chenier, 60–80 % of the buildings were destroyed or significantly damaged (Hurricane Science Audrey 2017). Twelve percent of the population dying in any one of the Tampa Bay area counties would be devastating.
- Hurricane Katrina was a large Category 3 storm at landfall and created a storm surge of up to 8.5 m (27.8 ft) in 2005. The storm created $81 billion in property damages. The surge was largely responsible for the death toll of 1836 people. Sadly, more than half of the deaths in Louisiana were senior citizens over the age of 75 (Brunkard et al. 2008). The Tampa Bay region has a large population of elderly people that is mostly situated in coastal areas.
- Super Typhoon Haiyan struck the city of Tacloban, Leyte province, Philippines in 2013 with 230 kph (145 mph) winds and gusts to 315 kph (195 mph) pushing a storm surge up to 7 m (23 ft). The storm surge tore eight ships from their moorings that created more damage onshore. The storm resulted in 7361 dead or missing (Masters 2014). Historically, residents faced impacts from typhoons several times per year but were not prepared for this worst-case scenario.
- The Galveston Hurricane storm surge in 1900, estimated at 15 ft, killed upwards of 10,000 people (Murname 2017). The storm came at a time when communication, construction, and response was primitive by today's standards. The lack of warning and location left the population vulnerable.

- Cyclone Nargis, a Category 3 or 4 storm with 209 kph (130 mph) winds and gusts to 258 kph (160 mph), struck Myanmar in 2008, killing over 140,000 people after a 24-h intensification from Category 1 to a Category 4 storm. The landfall was at the mouth of the Irrawaddy River with a surge of up to 3.7 m (12 ft) and inundated the flat land up to 40 km (25 mi) inland. Between 400 and 500 mm (15.7–19.7 in.) of rain fell. To exacerbate a dire situation, after the storm struck, foreign aid was declined by the governmental regime. The rapid intensification was due to a transient, deep, warm ocean feature in the Bay of Bengal increasing energy available to the cyclone (Yu and McPhaden 2011). Similar features in the Gulf of Mexico influenced the rapid intensification of Hurricanes Katrina and Rita in 2005 and could occur within hurricanes destined for the Tampa Bay area.
- Super Cyclonic Storm BoB (Bay of Bengal) 1 struck Bangladesh in 1991 with 258 kph (160 mph) winds that created a storm surge of up to 6 m (20 ft) with 80–90 % of all structures destroyed resulting in the deaths of 140,000 people, most of whom drowned (USAID 2017). Chowdhury et al. (1993) mentioned that elderly and socioeconomically disadvantaged were at greater risk and the death toll could have been 20% more without shelters. A similar 6 m storm surge would devastate a huge portion of the Tampa Bay region.
- The Bhola Cyclone in 1970 was the deadliest recorded tropical cyclone with up to 500,000 fatalities in the part of then Pakistan, which became Bangladesh. The storm's highest winds were estimated at 240 kph (150 mph) creating a surge of up to 6 m (20 ft). This was a poor country with poor communication, where 35% of the area is less than 6 m (20 ft) above sea level (Hurricane Science Bhola 2017). At the time, the governmental junta delayed relief to the stricken country.

5.19 Deaths After the Storm

In the past, many of the fatalities occurred after the storms. In 2004 and 2005, the eight hurricanes that struck Florida in 2004 led to 59 direct deaths and 85 deaths after the storm. In 2005, 27 people succumbed to the direct storm influences and 42 died after the storm. Therefore, about 60% of the deaths occurred after each storm. The bulk of the post-storm causes of death were linked to trauma, drowning, electrocution, and carbon monoxide poisoning (Ragan et al. 2008).

5.20 Project Phoenix

The Tampa Bay Regional Planning Council Tampa Bay Catastrophic Plan (2010) described the potential effects from "Hurricane Phoenix", a Category 5 storm that hits the Tampa Bay area. The damage assessment from the 258 kph (160 mph) winds, 8 m (26 ft) storm surge, was a $250 billion-dollar price tag. The human toll was calculated with these assumptions: no evacuation by 10% of the barrier islands

population and an additional 30% of the vulnerable population leaving two million people in a surge zone. It was suggested that 2000 people (1/1000) would lose their lives as a direct result of the storm (primarily due to non-evacuation of storm surge areas and mobile homes). It was also suggested that an additional 200 people (1/10,000) could lose their lives following the storm. Based on the significant storms that struck Florida during 2004 and 2005, where 60% of the deaths occurred after the storm, those estimates seem far too low. The Phoenix scenario would leave two million people displaced from dwellings that are not habitable and could take weeks or months to rebuild. The study also estimated that over one million pets would be displaced.

5.21 Concluding Remarks

Tampa Bay area residents are vulnerable to storm surge but have no experience with a significant storm. There is little difference between outcomes of those people who do not receive a warning to those who receive a warning and ignore it. The net result is the potential for a greater loss of life. Those that do not understand the potential threat will eventually face the reality of a horrific event, but not until they run out of excuses. With over 30 years as a meteorologist in the Tampa Bay area, the author has heard various versions of these excuses for complacency as storms approach, including:

- We never get it that bad.
- I don't live near the coast.
- I don't want to leave my pets.
- I evacuated for Charley (Irma) and I will never do that again!
- If I leave I won't be able to come back home and take care of damage for several days to weeks.
- I'll wait to see what the storm is doing before I evacuate.

The storm itself, is just the beginning of a post-storm survival story, followed by the long road to restoration or, potentially, total abandonment of a home or community.

References

Brunkard J, Namulanda G, Ratard R (2008) Hurricane Katrina deaths, Louisiana, 2005. Disaster Med Public Health Prep 2(4):215–223. https://doi.org/10.1097/DMP.0b013e31818aaf55

Catalanello R (2008) Teen charged in Tampa ammonia pipeline leak. Accessed 16 Feb 2018. http://www.tampabay.com/news/publicsafety/crime/teen-charged-in-tampa-ammonia-pipeline-leak/503817

Chowdhury AMR, Bhuyia AU, Choudhury AY, Sen R (1993) The Bangladesh cyclone of 1991: why so many people died. Disasters 17:291–304
Coastal Resilience (2018) Mapping portal. Accessed 12 March 2018. http://maps.coastalresilience.org
Corelogic (2018) 2018 CoreLogic Storm Surge Report. Accessed 30 May 2018. https://www.corelogic.com/downloadable-docs/storm-surge-report-2018.pdf
Davis RA, Elko NA (2003) Geology and morphodynamics of Caladesi and Honeymoon Islands, Florida. Accessed 25 Apr 2018. https://www.pinellascounty.org/environment/coastalMngmt/Appendices/GeolMorphodynamics.pdf
ESRI (2014) Median home value. Accessed 15 Feb 2018. http://www.arcgis.com/home/webmap/viewer.html
FAHCA (2018) Florida agency for healthcare administration data collection. Accessed 19 Jan 2018. http://ahca.myflorida.com/schs/DataCollection/DataCollection.shtml
FDEM (2018) Storm surge zones from statewide regional evacuation studies. Accessed 23 Jan 2018. http://floridadisaster.org/res
FDEP (2005) Hurricane facilities of concern. Accessed 14 Jan 2018. http://geodata.dep.state.fl.us/
FDEP (2011) Florida gypsumstacks. Accessed 14 Jan 2018. http://geodata.dep.state.fl.us/datasets/florida-gypsumstacks
FDOT (2017) Bridges. Accessed 14 Jan 2018. https://www.arcgis.com/home/item.html?id=a8cbcdaba463422db465e4a8032700cc
FDEM Geoportal, 2018 Law enforcement and fire stations, Accessed 28 Jan 2018. http://geodata.floridadisaster.org/
Firehouse.com (2003) Hillsborough county Fla – ammonia leak force evacuation. Accessed 20 Jan 2018. https://forums.firehouse.com/forum/firehouse-direct/fire-wire/33958-hillsborough-county-fla-ammonia-leak-force-evacuation
FPL (2018) Line clearing program. Accessed 19 Jan 2018. https://www.fpl.com/reliability/trees/line-clearing.html
Frago C (2016) Tampa Bay's sewage mess: 29 million gallons spilled into the bay and rising. Accessed 15 Feb 2018. http://www.tampabay.com/news/environment/water/tampa-bays-sewage-mess-29-million-gallons-spilled-into-the-bay-and-rising/2292477
Frago C, Danielson R (2017) 329,000 gallons of sewage spills in Tampa during storm; St. Petersburg has smaller spill. Accessed 15 Feb 2018. http://www.tampabay.com/news/environment/water/329000-gallons-of-wastewater-spill-in-tampa-during-monday-nights-storm/2335537
Godoy LA (2007) Performance of storage tanks in oil facilities damaged by hurricanes Katrina and Rita. J Perform Constr Facil 21:6 https://doi.org/10.1061/(ASCE)0887-3828(2007)21:6(441)
Godschalk D (1999) Natural hazard nitigation: recasting disaster policy and planning. Island Press, Washington, DC 1999. 575 p
HFBS (2017) Project Development & Environment (PD&E) study for replacement of the Northbound Howard Frankland Bridge (I-275/SR 93). Accessed 24 Jan 2018. http://hfbs.fdotd7studies.com/pdf/HFB_Draft_PER_With_Appendix_20171023.pdf
HIFLD (2017) Homeland infrastructure foundation level database. Accessed 9 Feb 2018. https://gii.dhs.gov/HIFLD
Hurricane Science Audrey (2017) Audrey. Accessed 28 May 2017. http://hurricanescience.org/history/storms/1950s/audrey
Hurricane Science Bhola (2017) Bhola. Accessed 28 May 2017. http://hurricanescience.org/history/storms/1970s/greatbhola
Lee LJ, Hall B (2011) Louisiana's Recovery. FHWA-HRT-11-005, 75:1
Madehow (2018) Accessed 18 Jan 2018. http://www.madehow.com/Volume-3/Fertilizer.html#ixzz56LmsSH2M
Masters J (2014) Super typhoon Haiyan storm surge survey finds high water marks 46 feet high. Accessed 28 May 2018. https://maps.wunderground.com/blog/JeffMasters/comment.html?entrynum=2676&page=38

McGrory Danielson R (2018) Tampa electric planning to convert big bend power plant where five died in June from coal to natural gas. Accessed 12 Feb 2018. http://www.tampabay.com/news/business/energy/Tampa-Electric-planning-to-convert-Big-Bend-power-plant-where-five-died-in-June-from-coal-to-natural-gas_164449729

Murname K (2017) As terrible as harvey is, the Galveston hurricane of 1900 was much, much worse. Accessed 25 Nov 2017. https://www.forbes.com/sites/kevinmurnane/2017/08/27/as-terrible-as-harvey-is-the-galveston-hurricane-of-1900-was-much-much-worse/#5db5cd972594

NHC (1985) Hurricane Elena. Accessed 24 May 2017. https://www.nhc.noaa.gov/archive/storm_wallets/atlantic/atl1985-prelim/elena/

NWS 1848 (2017) The 1848 hurricane. Accessed 2 Jun 2017. https://www.weather.gov/media/tbw/paig/PresAmHurricane1848.pdf

NWS 1921 (2017) The 1921 hurricane. Accessed 2 Jun 2017. http://www.crh.noaa.gov/Image/tbw/paig/PresAmHurricane1921.pdf

Padgett, J., R. DesRoches, B. Nielson, M. Yashinsky, O. Kwon, N. Burdette; E. Tavera, 2008: Bridge damage and repair costs from hurricane Katrina, J Bridge Eng, 13:1, https://doi.org/https://doi.org/10.1061/(ASCE)1084-0702(2008)13:1(6)

Patagonia Alliance (2014) Accessed 14 Jan 2018. http://www.patagoniaalliance.org/wp-content/uploads/2014/09/Chronology-of-major-tailings-dam-failures.pdf

Paulson RW, Chase EB, Roberts RS, Moody DW (1991) National water summary 1988–89. U.S. Government Printing Office. P.23

Pinellas EOC (2008) Accessed 15 Feb 2018. http://www.pinellascounty.org/newsletters/e-lert/images/sept2008/Hurricane_&_Safety_News.pdf

Pinellas EOC (2018) Hurricane Irma after-action report. Accessed 24 Apr 2018. https://www.pinellascounty.org/emergency/PDF/Irma/after_action_report.pdf

Pittman C (2017) The clock is ticking on Florida's mountains of hazardous phosphate waste. Accessed 21 Feb 2018. https://www.sarasotamagazine.com/articles/2017/4/26/florida-phosphate

Ragan P, Schulte J, Nelson SJ, Jones KT (2008) Mortality surveillance: 2004 to 2005 Florida hurricane-related deaths. Am J Forensic Med Pathol. 2008 Jun 29(2):148–153. https://doi.org/10.1097/PAF.0b013e318175dd5e

Road Traffic Technology (2018) I-10 bridges, Escambia Bay, FL. Accessed 5 Feb 2018. https://www.roadtraffic-technology.com/projects/i-10/

Stein L (2006) A 40,000-gallon wakeup call. Accessed 13 Feb 2018. http://www.sptimes.com/2006/01/27/Brandontimes/A_40_000_gallon_wakeu.shtml

Sulphuric-acid.com (2008) Sulphuric acid plant safety – accidents (Archive). Accessed 15 Feb 2018. http://www.sulphuric-acid.com/techmanual/Plant_Safety/safety_accidents-Archive.htm

Tampa Bay Water Atlas (2018) Seagrass. Accessed 21 Apr 2018. http://www.tampabay.wateratlas.usf.edu/news/details/15159/

TBEP (2017) A portrait of the Tampa Bay Estuary. Accessed 25 Oct 2017. http://www.tbep.org/a_portrait_of_the_tampa_bay_estuary.html

TBRPC (2006) Sea level rise in the Tampa Bay Region. Accessed 20 Oct 2017. http://www.tbrpc.org/mapping/pdfs/sea_level_rise/Tampa%20Bay%20-%20Sea%20Level%20Rise%20Project%20Draft%20Report%20without%20maps.pdf

TBRPC (2010) Tampa Bay catastrophic plan: project phoenix. Accessed 20 May 2017. http://www.tbrpc.org/tampabaycatplan/pdf/Project_Phoenix_Scenario_Info.pdf

TECO (2017) Tree trimming. Accessed 24 Nov 2017. http://www.tampaelectric.com/company/ourpowersystem/treetrimming/

TECO (2018) Big bend power station. Accessed 27 Jan 2018. http://www.tampaelectric.com/company/ourpowersystem/powergeneration/bigbend/

Tihansky AB, Dadisman SV, Dwyer B (2011) Better than a bird's eye view. Accessed 22 May 2017. http://baysoundings.com/legacy-archives/spring2011/Stories/Better-Than-Birds-Eye-View.php

Trulia (2018) Trulia maps. Accessed 11 Jan 2018. https://www.trulia.com/local/tampa-fl/type:median_age_demographics

U.S. Census 2010 (2010) Accessed 24 May 2017. https://www.census.gov/

U.S. Census 2015 (2015) Accessed 24 May 2017. https://www.census.gov/

USAID (2017) The Bangladesh cyclone of 1991. Accessed 2 June 2017. http://pdf.usaid.gov/pdf_docs/Pnadg744.pdf

WAFR (2017) Wastewater sites from WAFR IMS wastewater facilities from WAFR IMS. Accessed 20 Jan 2018. https://ca.dep.state.fl.us/arcgis/rest/services/OpenData/WAFR/MapServer

Yu L, McPhaden MJ (2011) Ocean preconditioning of cyclone Nargis in the Bay of Bengal: interaction between rossby waves, surface fresh waters, and Sea surface temperatures. J Phys Oceanogr 41:1741–1755

Chapter 6
The 2015 Hurricane Season in the North Atlantic: An Analysis of Environmental Conditions

Jennifer M. Collins and David R. Roache

Abstract The 2015 North Atlantic hurricane season was particularly inactive, this inactivity occurring in the presence of a near-record El Niño, the strongest since 1997. When analyzing large-scale environmental conditions utilizing NCEP/NCAR Reanalysis 2, we show that the Caribbean was particularly inactive under very strong wind shear and positive Omega conditions. While conditions generally were not conducive in the North Atlantic, there were conducive conditions present at specific times and specific locations, and these tended to be when and where we saw tropical cyclone activity. Vorticity in particular showed large intraseasonal variability with the location of the positive vorticity relating to storms such as Ana in May, Claudette in July, multiple storms in August and September, and Joaquin in October. We assess how the active and inactive periods observed during the 2015 hurricane season were related to this month to month atmospheric variability.

Keywords Hurricanes · North Atlantic · 2015 season

6.1 Introduction

The North Atlantic is one of the most widely studied basins with regards to hurricane activity, particularly due to a hurricane's typical west-north -west track and the basin's location next to the densely populated eastern sea-board. There is therefore much attention from various groups including the research community, reinsurance, emergency management, and the public.

Several authors have provided explanations of why hurricanes form (Palmén 1948; Namias 1954; Gray 1979). Such explanations focus on both dynamic (e.g. low wind shear and positive relative vorticity) as well as thermodynamic (e.g. warm sea-surface temperatures and high mid-level relative humidity) factors.

J. M. Collins (✉) · D. R. Roache
School of Geosciences, University of South Florida, Tampa, FL, USA
e-mail: collinsjm@usf.edu

J. M. Collins, K. Walsh (eds.), *Hurricane Risk*, Hurricane Risk 1,
https://doi.org/10.1007/978-3-030-02402-4_6

Table 6.1 2015 tropical cyclone statistics

Tropical storms	Tropical storm days	Hurricanes	Hurricane days	Major hurricanes	Major hurricane days	ACE ($\times 10^4$ kt^2)
11	43.50	4	12	2	4	62.6850

Some studies have examined particularly active or inactive seasons in different basins. For instance, Collins and Roache (2010) examined the 2009 below normal season in the North Atlantic and the unconducive conditions surrounding that season. Collins et al. (2016) and Murakami et al. (2017) considered the hyperactive season of the Eastern North Pacific in 2015 and the environmental variables contributing to this activity. Considerable interannual variability occurs in the North Atlantic and Knaff (1997), Elsner and Kara (1999), and Lupo et al. (2008) each highlight the relationship between El Niño – Southern Oscillation (ENSO) and North Atlantic tropical cyclone activity. This paper also focuses on the 2015 season of the North Atlantic and the intraseasonal levels of activity that occurred there.

As shown in Table 6.1, in 2015, the North Atlantic had a total of 11 named storms (maximum 1-min, 10-m sustained winds >= 34 knots), 4 of which reached hurricane strength (maximum sustained winds >= 64 knots) and only 2 of which reached major hurricane strength (maximum sustained winds >= 96 knots). The average for the period 1981–2010 is 12.1, 6.4 and 2.7 respectively. The 2015 hurricane season in the North Atlantic was the 18th weakest year in terms of Accumulated Cyclone Energy (ACE; Bell et al. 2000), with 62.6850×10^4 kt^2 being generated. This marked the third consecutive below average season in the North Atlantic, and witnessed the continuation of the record streak of days since a major hurricane made landfall in the United States, the last being Hurricane Wilma in 2005.

6.2 Data

Tropical cyclone data were collected from the HURDAT2 (HURricane DATa 2nd generation) database (Landsea and Franklin 2013) for 1900–2015. These data are available online at http://www.aoml.noaa.gov/hrd/hurdat/Data_Storm.html with tropical cyclone records available at six-hourly intervals. Tropical cyclone numbers, tropical cyclone days and ACE are used to access the season storm activity and ACE, used as an overall measure of activity, is used for a comparison to past seasons as well as a monthly comparison within the 2015 season. Bell et al. (2000) defines ACE as the sum of the squares of the maximum sustained surface wind speed (knots) measured every 6 h for all named systems while they are at least tropical storm strength and not extratropical in phase.

For environmental variables examined, the National Centers for Environmental Prediction/National Center for Atmospheric Research (NCEP/NCAR) reanalysis 2 is utilized (Kanamitsu et al. 2002). The global data are available from https://www.esrl.noaa.gov/psd/data/gridded/data.ncep.reanalysis2.html. In the reanalysis, the data are

available from 1979-present, on a 2.5° by 2.5° latitude-longitude grid for six-hourly and monthly time resolution, and for several vertical levels in the atmosphere (the number of which depends on the examined variable). The NCEP/NCAR reanalysis 2 is suitable for this study due to the period covered and the comprehensive observational database. Confidence in these data have previously been addressed (Collins and Mason 2000; Kalnay et al. 1996). The climatology period of 1981–2010 was used for all environmental datasets. The monthly environmental data were averaged over August to October to correspond with peak North Atlantic tropical cyclone activity.

6.3 Analysis of the 2015 North Atlantic TC Season

Table 6.2 shows ACE by month. It can be seen that the ACE at the beginning of the season in May came entirely from the one storm, Tropical Storm Ana. The peak in ACE occurred in October, again entirely from one storm, Hurricane Joaquin, only one of two major hurricanes of the season. The next highest months by ACE were August and September. This is expected that August – October would yield the highest ACE as these are the peak months historically. June was the least active month by ACE.

A moderate and strengthening El Niño event was in place at the start of the hurricane season, becoming a strong El Niño by the peak of the hurricane season. Examining the Multivariate ENSO Index (MEI; Wolter and Timlin 1998), which considers sea surface temperatures, surface pressure, cloud fraction, and meridional and zonal winds, the July-October-averaged MEI was at its second highest level since 1979, surpassed only by the 1997 El Niño event. Levine and McPhaden (2016) discuss the factors which led up to the strong 2015 El Niño.

Considerable intraseasonal variability occurred, not only in terms of ACE, but also in terms of the environmental factors known to influence the formation of tropical cyclones. The location where hurricanes formed can be linked to the location of these conducive factors, likewise we see no activity in locations where these factors are unconducive. Figures 6.1, 6.2, 6.3, 6.4, 6.5, 6.6, and 6.7 displays

Table 6.2 2015 Accumulated Cyclone Energy (ACE) by month, and the named storms (*TS* tropical storm, *H* hurricane, *MH* major hurricane) that contributed to it

Month	ACE ($\times 10^4$ kt^2)	Named storms
May	2.12	TS Ana
June	1.065	TS Bill
July	1.13	TS Claudette
August	15.8275	MH Danny, TS Erika, H Fred
September	12.3075	H Fred, TS Grace, TS Henri, TS Ida, MH Joaquin
October	26.58	MH Joaquin
November	3.655	H Kate

Storms listed in multiple months formed in the first and lasted into the second

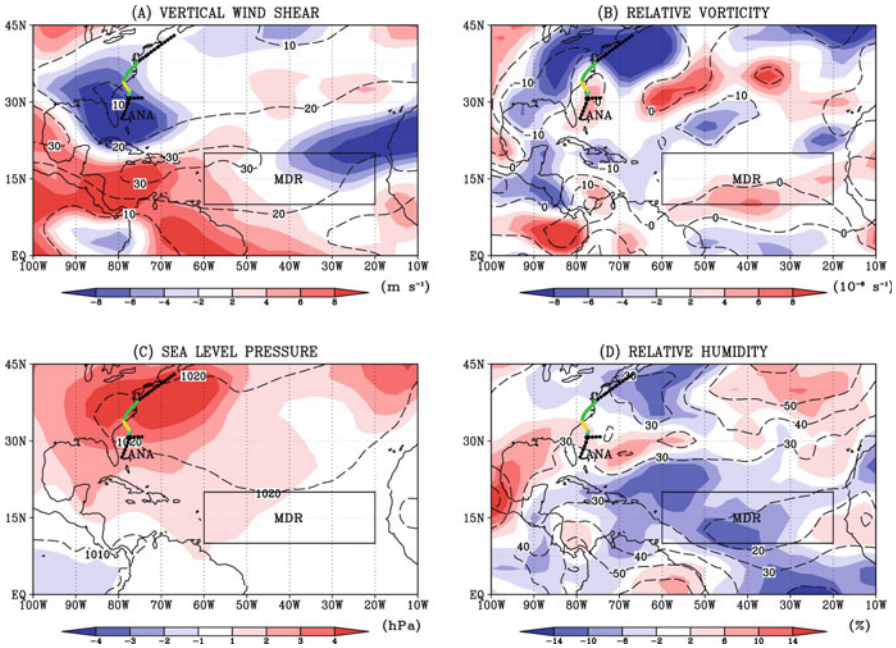

Fig. 6.1 Mean atmospheric conditions in the North Atlantic basin during May 2015. Tropical cyclone tracks plotted: a low depicted by black dots, a tropical depression by solid green, tropical storm by solid yellow, sub-tropical storm by solid aqua, hurricane by solid orange, major hurricane by solid purple, data from a previous month by solid grey

conditions throughout the basin. Anomalies in these environmental factors are presented relative to the 1981–2010 climatology period.

6.3.1 May Activity

As noted, the total ACE in May was generated by Tropical Storm Ana which formed on May 8. Figure 6.1 shows the strong positive vorticity (panel B) present in the location of Ana's development. It also shows a large area of strong negative wind shear (panel A). The Main Development Region (MDR) of north Atlantic tropical cyclones is identified on this and subsequent plots as bounded from 10 to 20° North and 20 to 60° West.

6.3.2 June and July Activity

While June and July achieved the lowest ACE values of the season, this is to be expected as these are not usually active months. Activity in 2015 in these months

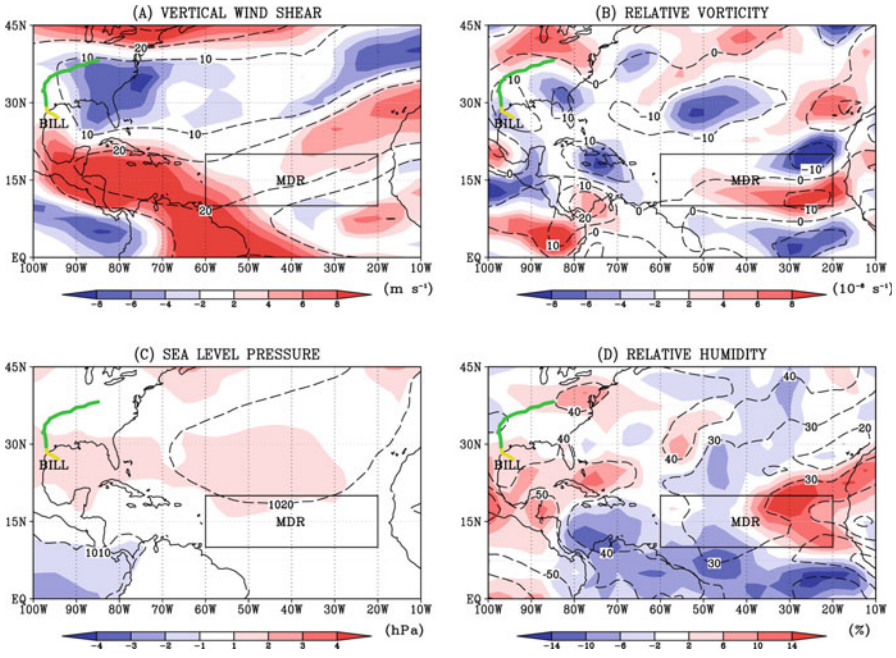

Fig. 6.2 Mean atmospheric conditions in the North Atlantic basin during June 2015. Tropical cyclone tracks plotted: a low depicted by black dots, a tropical depression by solid green, tropical storm by solid yellow, sub-tropical storm by solid aqua, hurricane by solid orange, major hurricane by solid purple, data from a previous month by solid grey

was average with one named storm each month. In June (Fig. 6.2), the Northwest Caribbean exhibited particularly high vertical wind shear, a feature typical of an El Niño year. These conditions are unconducive to storm development. In July (Fig. 6.3), humidity is particularly low and unconducive in the MDR, and shear in the Caribbean is likewise unfavorable for development. Where Claudette formed off the eastern coast of the US, conditions were fairly conducive.

6.3.3 August Activity

August saw multiple storms form in the North Atlantic including Category 3 Hurricane Danny. Figure 6.4 shows that there is strong positive vorticity (panel B) in the Main Development Region (MDR). Hurricane Fred formed near the end of the month, and was impacted by conditions during both August and September. Its track during August only is shown in Fig. 6.4.

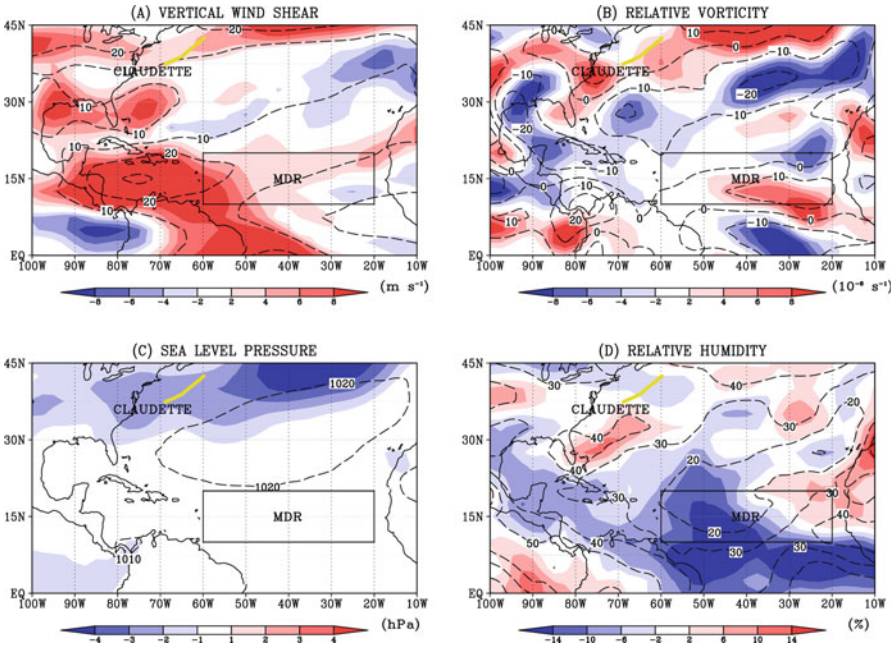

Fig. 6.3 Mean atmospheric conditions in the North Atlantic basin during July 2015. Tropical cyclone tracks plotted: a low depicted by black dots, a tropical depression by solid green, tropical storm by solid yellow, sub-tropical storm by solid aqua, hurricane by solid orange, major hurricane by solid purple, data from a previous month by solid grey

6.3.4 September Activity

Several storms formed in September. It can be observed from Fig. 6.5 that there is strong positive vorticity (panel B) in the Central North Atlantic. There is also strong positive vorticity in the eastern MDR where Fred, Grace, and Ida formed. The absence of strong shear (panel A) where these storms formed was also a positive contributor to their formation. Joaquin and Henri formed in a region of negative sea level pressure (panel C). Joaquin formed in late September, although the majority of this storm's lifecycle was in early October when environmental conditions were very different.

6.3.5 October Activity

Again strong positive vorticity marks the area of Joaquin's presence (Fig. 6.6, panel b). There is also negative SLP (panel C) off the Eastern Seaboard which is important for Joaquin. While the atmosphere was dry all season (see Figs. 6.1, 6.2, 6.3, 6.4, 6.5, 6.6, and 6.7d), October was the least dry month and actually had some positive

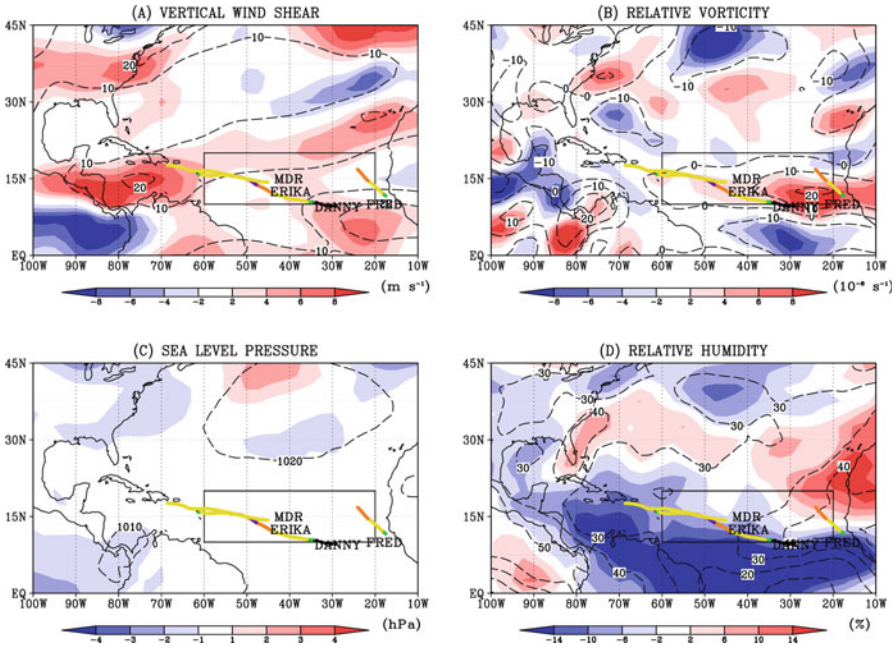

Fig. 6.4 Mean atmospheric conditions in the North Atlantic basin during August 2015. Tropical cyclone tracks plotted: a low depicted by black dots, a tropical depression by solid green, tropical storm by solid yellow, sub-tropical storm by solid aqua, hurricane by solid orange, major hurricane by solid purple, data from a previous month by solid grey

relative humidity anomalies in Joaquin's path (panel D). This change to favorable environmental conditions from September to October was critical in Joaquin's development into a major hurricane. Despite strong positive vorticity anomalies (panel B) in the MDR in October, no storms formed there largely due to the dry atmospheric conditions (panel D), including some areas up to 10% more dry than average.

6.3.6 November Activity

While the official hurricane season in the North Atlantic extends to November 30, it is still rare to get a storm of hurricane force. Hurricane Kate however occurred in November in an environment of strong negative wind shear (Fig. 6.7, panel a). Furthermore, while the basin was particularly dry all season (Figs. 6.1, 6.2, 6.3, 6.4, 6.5, 6.6, and 6.7d), Hurricane Kate also formed in an environment of positive relative humidity (panel D).

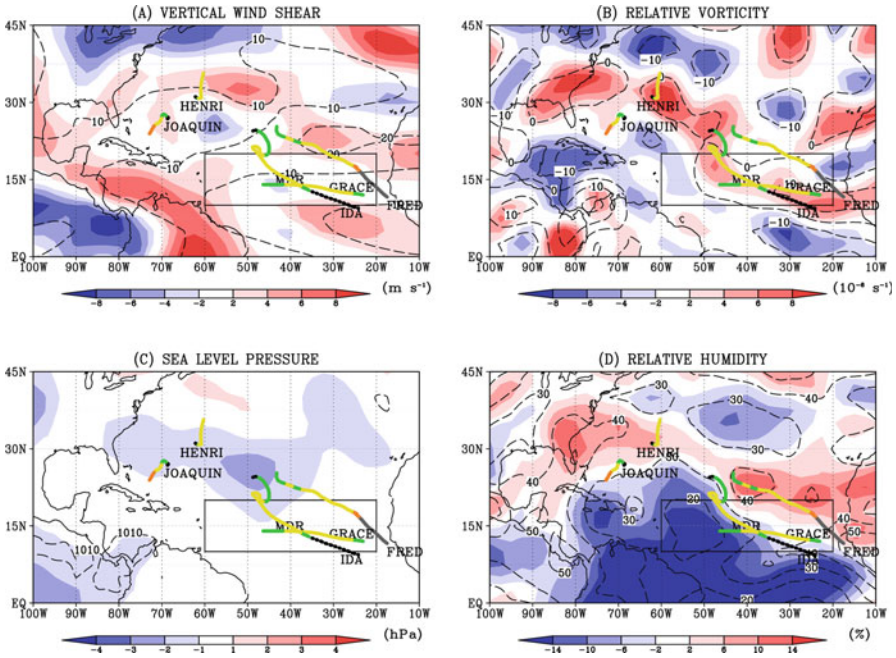

Fig. 6.5 Mean atmospheric conditions in the North Atlantic basin during September 2015. Tropical cyclone tracks plotted: a low depicted by black dots, a tropical depression by solid green, tropical storm by solid yellow, sub-tropical storm by solid aqua, hurricane by solid orange, major hurricane by solid purple, extra tropical by dotted magenta, data from a previous month by solid grey

6.4 The Caribbean

No storms formed in the Caribbean and only one went into it as a tropical storm (Erica). Erica then dissipated while in this region. The lack of storms in the Caribbean contributes to the lack also observed in the Gulf of Mexico. The particularly high vertical wind shear throughout the Caribbean in the 2015 season, as shown in Fig. 6.8b, explains the inactivity, and is responsible for the rapid dissipation of Erica as it moved into the Northern Caribbean. Such high shear is common here in an El Niño due to the atmospheric circulation anomalies associated with El Niño (Gray and Sheaffer 1991).

6.5 Conclusions

This article examines the large-scale environment that led to the 2015 North Atlantic hurricane season. The focus of this manuscript was on the intraseasonal variation in ACE and conducive and non-conducive conditions for hurricanes to form. It was

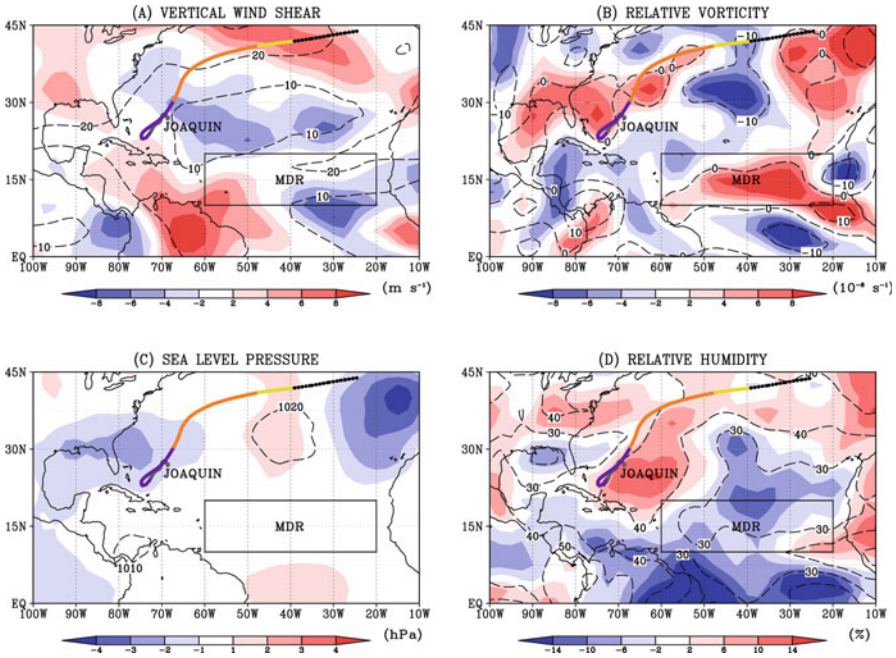

Fig. 6.6 Mean atmospheric conditions in the North Atlantic basin during October 2015. Tropical cyclone tracks plotted: a low depicted by black dots, a tropical depression by solid green, tropical storm by solid yellow, sub-tropical storm by solid aqua, hurricane by solid orange, major hurricane by solid purple, extra tropical by dotted magenta, data from a previous month by solid grey

shown that vorticity was a big player in the month to month variability in 2015. Other studies, such as Collins and Roache (2011), have likewise shown the importance of vorticity on intraseasonal hurricane activity. A very strong El Niño event generated an environment of particularly strong shear in the Caribbean, resulting in no tropical cyclones forming in this region for the entire season. This also impacted storms in the Gulf. Storms in the MDR were weak and short-lived.

Other studies have noted the role of the Madden-Julian Oscillation (MJO) on intraseasonal variability of hurricane activity (Maloney and Hartmann 2000; Collins and Roache 2011; Klotzbach and Blake 2013). Indeed, it was shown to be an important influence of intraseasonal variability for the 2015 season in the Eastern North Pacific (Collins et al. 2016). However, an examination of a Hovmöller diagram of 850-hPa zonal wind anomalies averaged from 7.5°S to 7.5°N (not shown) indicates no discernable MJO influence for the intraseasonal variability noted in 2015 for the North Atlantic basin, so the MJO was ruled out in this study as a major factor for the 2015 tropical cyclone activity.

Knowledge of the state of ENSO appears to allow for predictability of active vs. inactive seasons. The 2015 season in the North Atlantic behaved as expected due to the El Niño event. However, it is worth noting that even in a suppressed year, storms of substantial magnitude can form when local conditions

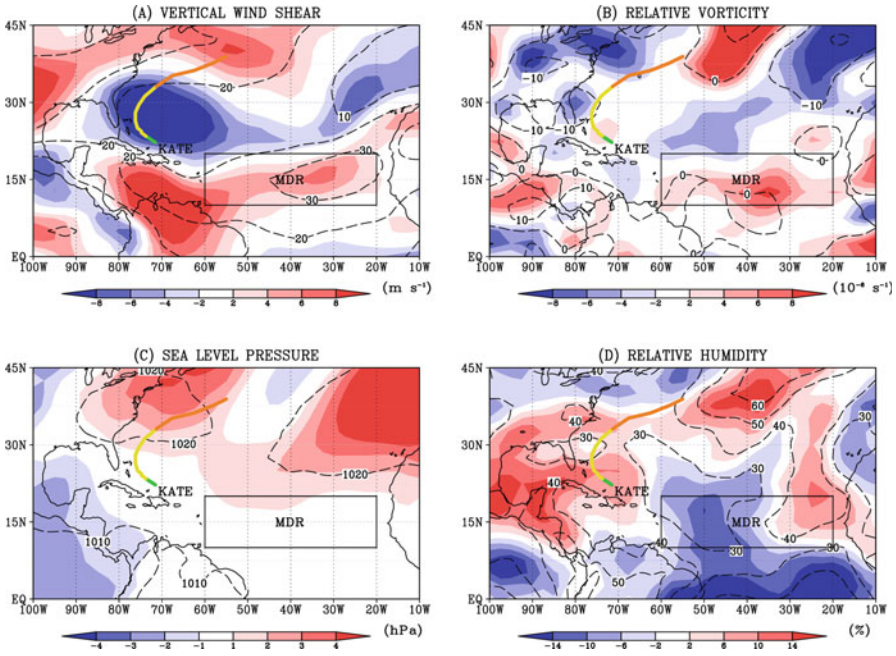

Fig. 6.7 Mean atmospheric conditions in the North Atlantic basin during November 2015. Tropical cyclone tracks plotted: a low depicted by black dots, a tropical depression by solid green, tropical storm by solid yellow, sub-tropical storm by solid aqua, hurricane by solid orange, major hurricane by solid purple, extra tropical by dotted magenta, data from a previous month by solid grey

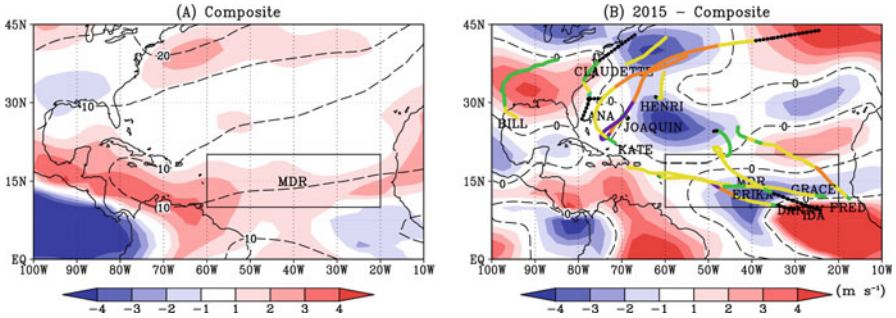

Fig. 6.8 (**a**) Mean vertical wind shear (m s^{-1}) from a composite of El Niño years (1965, 1972, 1982, 1987, 1997) and (**b**) mean vertical wind shear in 2015 compared to mean vertical wind shear from a composite of El Niño years

conducive to that happening coincide, and that even in such weaker seasons vigilance is needed because all it takes is one hurricane, as exemplified by Hurricane Andrew in 1992.

Acknowledgments We thank the reviewers of this paper.

References

Bell GD, Halpert MS, Schnell RC, Higgins RW, Lawrimore J, Kousky VE, Tinker R, Thiaw W, Chelliah M, Artusa A (2000) Climate assessment for 1999. Bull Am Meteorol Soc 81:S1–S50

Collins JM, Klotzbach PJ, Maue RN, Roache DR, Blake ES, Paxton CH, Mehta CA (2016) The record-breaking 2015 hurricane season in the eastern North Pacific: an analysis of environmental conditions. Geophys Res Lett 43(17):9214–9224. https://doi.org/10.1002/2016GL070597

Collins JM, Mason IM (2000) Local environmental conditions related to seasonal tropical cyclone activity in the NE Pacific basin. Geophys Res Lett 27(23):3881–3884

Collins JM, Roache DR (2010) The inactive 2009 hurricane season in the North Atlantic basin: an analysis of environmental conditions. Natl Weather Dig 34:117–128

Collins JM, Roache DR (2011) The 2009 hurricane season in the eastern North Pacific basin: an analysis of environmental conditions. Mon Weather Rev 139:1673–1682

Elsner JB, Kara AB (1999) Hurricanes of the North Atlantic. Oxford University Press, New York 488pp

Gray WM (1979) Hurricanes: their formation, structure and likely role in the tropical circulation. In: Shaw DB (ed) Meteorology over tropical oceans, royal meteorological. Society Press, Bracknell, pp 155–218

Gray WM, Sheaffer JD (1991) In: Glantz MH, Katz RW, Nicholls N (eds) El Niño and QBO influences on tropical cyclone activity. Teleconnections linking worldwide climate anomalies: scientific basis and societal impact. Cambridge University Press, Cambridge, UK

Kalnay et al (1996) The NCEP/NCAR 40-year reanalysis project. Bull Am Meteorol Soc 77:437–470

Kanamitsu et al (2002) NCEP-DOE AMIP-II reanalysis (R-2). Bull Am Meteorol Soc 83:1631–1643

Klotzbach PJ, Blake ES (2013) North-Central Pacific tropical cyclones: impacts of El Niño-Southern Oscillation and the Madden-Julian oscillation. J Clim 26:7720–7733

Knaff JA (1997) Implications of summertime sea level pressure anomalies in the tropical Atlantic region. J Clim 10:789–804

Landsea CW, Franklin JL (2013) Atlantic hurricane database uncertainty and presentation of a new database format. Mon Weather Rev 141:3576–3592. https://doi.org/10.1175/MWR-D-12-00254.1

Levine AFZ, McPhaden MJ (2016) How the July 2014 easterly wind burst gave the 2015-6 El Niño a head start. Geophys Res Lett 43. doi:https://doi.org/10.1002/2016GL069204

Lupo AR, Latham TK, Magill T, Clark JV, Melick CJ, Market PS (2008) The interannual variability of hurricane activity in the Atlantic and East Pacific regions. Natl Weather Dig 32(2):119–133

Maloney ED, Hartmann DL (2000) Modulation of eastern North Pacific hurricanes by the Madden-Julian oscillation. J Clim 13:1451–1460

Murakami et al (2017) Dominant role of subtropical Pacific warming in extreme eastern Pacific hurricane seasons: 2015 and the future. J Clim 30:243–264

Namias J (1954) Long range factors affecting the genesis and paths of tropical cyclones, Proc UNESCO Symp on Typhoons. UNESCO, Tokyo, pp 213–219

Palmén E (1948) On the formation and structure of tropical hurricanes. Geophysica 3:26–38

Wolter K, Timlin MS (1998) Measuring the strength of ENSO events – how does 1997/1998 rank? Weather 53:315–324. https://doi.org/10.1002/j.1477+8696.1998.tb06408x

Chapter 7
Impact of Aerosols and Ocean Temperature on Tropical Cyclone Days Near Australia

Rupsa Bhowmick and Jill C. Trepanier

Abstract Tropical cyclones (TCs) devastate nations around the world. Many different variables influence TC intensification or decay. Near Australia, one of those influences may stem from the arid interior of the landmass. The influences of aerosol optical depth (AOD), sea surface temperature (SST) and upper ocean temperature (UOT) on monthly TC days over eastern Australia and the southwest Pacific Ocean are examined using data from 1985 to 2015. The area experiences TCs in November (Nov) through June with a peak in March. Variables occurring together in time are considered as possible predictors of TC days, as well as lagged relationships between them. Spearman rank correlation tests showcase the significant relationships between all pairs of variables during a variety of months. A Poisson multiple regression model is applied on TC-SST-AOD and TC-UOT-AOD to find the most significant relationships between the variables throughout the season. Four significant models are found without violating statistical assumptions. An increase in Nov AOD and Dec SST leads to a significant increase in Jan TC days. Dec UOTs are found to be negatively related to TC days in Jan. The difference in directions is related to the difference in heating mechanisms associated with the surface conditions and the lower subsurface in environments of relatively higher AOD. Probabilities of monthly days during unfavorable and favorable conditions are found. Low to moderate TC days are expected in Jan when both Nov AOD and Dec SSTs are low. There is a chance of a higher number of Jan TC days in both high Nov AOD and Dec SSTs. This study provides scenarios between the variables to aid in forecasting.

Keywords Tropical cyclone · Aerosol optical depth · Sea surface temperature · Southwest Pacific · Poisson regression · Frequency

R. Bhowmick (✉) · J. C. Trepanier
Department of Geography and Anthropology, Louisiana State University, Baton Rouge, LA, USA
e-mail: rbhowm1@lsu.edu; jtrepa3@lsu.edu

J. M. Collins, K. Walsh (eds.), *Hurricane Risk*, Hurricane Risk 1,
https://doi.org/10.1007/978-3-030-02402-4_7

7.1 Introduction

The northern half of eastern Australia (EA) is subjected to devastating tropical cyclones (TCs) generated over the southwest Pacific Ocean (SWPO). The SWPO spreads over an area of approximately 10 million square nautical miles from the Gulf of Carpentaria (130°E) to 180°. The main cyclogenesis region exists over the Coral Sea, adjacent to the northeastern and eastern coasts of Australia (Diamond et al. 2013). EA is considered one of the most populated and developed regions of the country while also experiencing the fastest growth (Hall et al. 2001). TCs cause 76% of the disasters in the EA/SWPO region and other nearby small islands (Bettencourt et al. 2006), with total insured losses of $16.1 billion ($US) accumulating from 2000 to 2012 (Deloitte Economics 2013).

McBride and Keenan (1982) find that 49% of EA events form in the Coral Sea within 300 km of the Australian coast. TC intensity, longevity of life cycle, and dissipation largely depend on underlying sea surface temperature (SST) and the temperature of the ocean's mixed layer. During the past decade, research shows aerosols can substantially influence the shortwave radiation and cloud microphysics of an area and, consequently, the nearby SST and upper ocean temperature (UOT) (Church et al. 2005; Foltz and McPhaden 2008). The SWPO has experienced increasing temperatures in recent decades, and the trend might be related to atmospheric temperature increases or changes in oceanic circulation (Salinger et al. 1993, 1995; Cortese et al. 2013; Barrows et al. 2007; Cai et al. 2005). Another possible cause of SST variability is a change in the relationship between SSTs and atmospheric aerosol, here defined by aerosol optical depth (AOD). Atmospheric aerosol is a complex and dynamic mixture of solid and liquid particles from natural and anthropogenic sources. AOD is a measure of the extinction of solar radiation by aerosol particles. It is a dimensionless number related to the amount of aerosols in the vertical column of the atmosphere over any observed location (Augustine et al. 2008).

Compared to other ocean basins around the world, this region is the most understudied, possibly due to its relatively isolated location in the South Pacific Ocean. The aim of this study is to estimate the influence of AOD on SST, UOT, and the number of days in a month occupied by named TCs (at least 17 ms^{-1}) over the SWPO affecting EA and other nearby regions from 1985 to 2015. These variables are assessed with time series analyses to identify trends through time. The results presented can be used to better understand the range of past and present TC variability related to atmospheric aerosols. This information is useful for the advancement in seasonal TC forecasting, hazard assessment, and risk management strategies by incorporating atmospheric aerosols as a cause of TC variability. Researchers may be able to use real-time or predicted AOD levels (Abish and Mohanakumar 2013) in forecast models to help better understand the expected ocean temperature response and the resultant number of TC days.

7.2 Study Area

The SWPO study region extends from the Gulf of Carpentaria, Australia (130°E) to 180°W and from the equator to 30°S. This includes the Gulf of Carpentaria and Coral Sea. The Coral Sea is the marginal sea located in the SWPO adjacent to the northeast coast of Queensland, Australia (142°E), bordered by the Solomon Islands and Papua New Guinea to the north (9°S), New Caledonia and Vanuatu to the east (170°E) and the Tasman Sea to the south (30°S) (see Fig. 7.1) (Jaffrés 2013). The Coral Sea is the focus of this study as it is considered the main cyclogenesis location for TCs affecting EA (Hall et al. 2001; Diamond et al. 2013).

Figure 7.1 shows the study region highlighting northeastern and eastern cities heavily influenced by TCs and southeastern cities influenced by TC-induced precipitation. Also included are the major dust source areas throughout the continent, which contribute to the aerosol amount over the SWPO (130°E to 180°). The largest

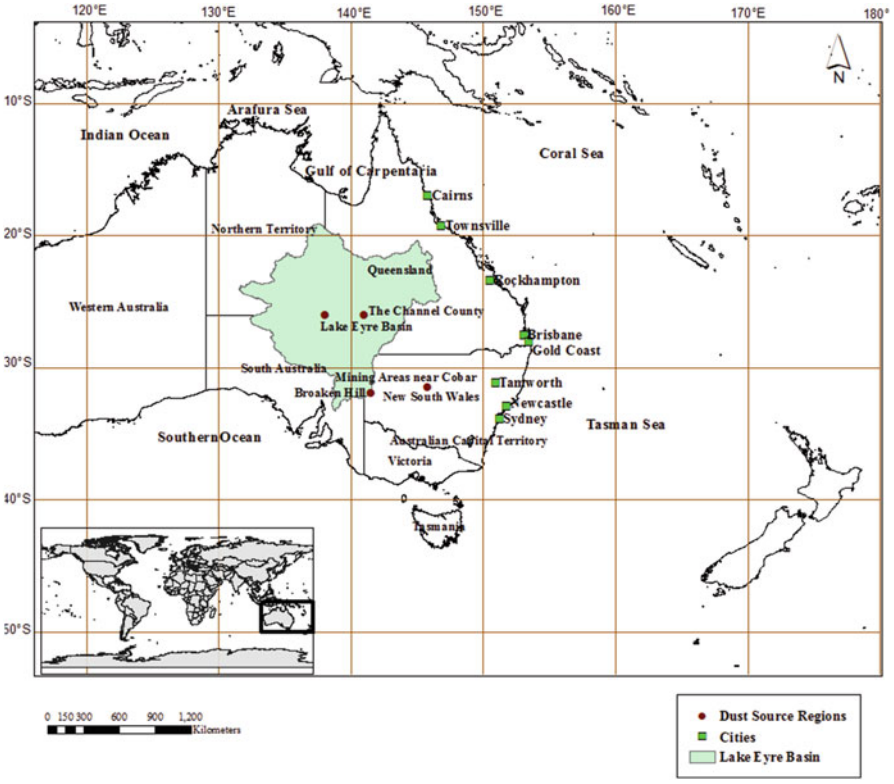

Fig. 7.1 Study region: EA and the SWPO (130°E to 180°, 0° to 30°S). Circles indicate major AOD source regions, which contribute to the aerosol concentration over the SWPO. Squares indicate major cities along the coast of EA. The region highlighted over central Australia is the Lake Eyre Basin, the largest AOD source in Australia

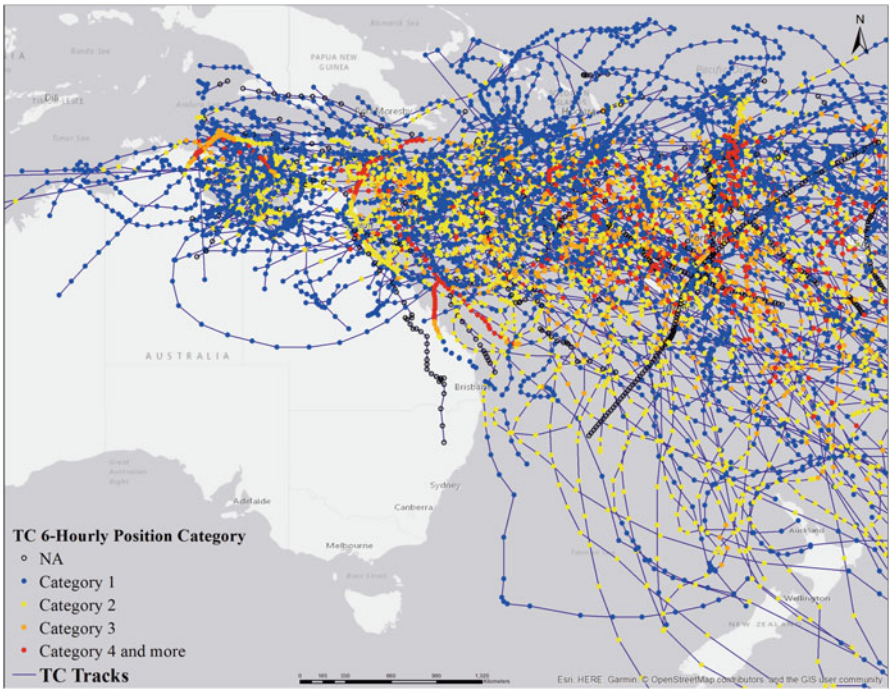

Fig. 7.2 Track map showing the TCs included in this study (winds >17 ms^{-1}) from 1985 to 2015. Tracks are colored based on the Australian intensity categories

of these is the Lake Eyre Basin. TCs considered for this study are those originating over the SWPO (west of 180°) following the path over the Coral Sea, Gulf of Carpentaria, and Tasman Sea that both do or do not make landfall over northeastern and eastern Australia. This study also includes TCs affecting New Zealand and other smaller islands in the south, east and southeastern directions away from mainland Australia (Fig. 7.2). The tracks in Fig. 7.2 are plotted with the available six-hourly TC data from the Southwest Pacific Enhanced Archive for Tropical Cyclones (SPEArTC) (Diamond et al. 2013). The tracks are color-coded based on the intensity at the six-hourly observation point. Those in red are the most intense wind speeds.

Australian AOD is smaller in amount compared to Saharan AOD and contributes an emission rate of around 100 Tg/year, or about 5% in the global AOD amount (Mitchell et al. 2010). It is the largest source of AOD aerosols in the Southern Hemisphere and an important atmospheric aspect modifying regional climate through radiative impacts (Choobari et al. 2013). Australia contributes nearly 70% of the atmospheric AOD load in the Southern Hemisphere (Rotstayn et al. 2009). The Lake Eyre Basin extends 1.2 million km^2 in the interior arid and semi-arid region of the landmass and is one of the largest sources of AOD (Fig. 7.1) (Mitchell et al. 2010).

Weather Research and Forecasting (WRF)-Chem model simulations and Moderate Resolution Imaging Spectroradiometer (MODIS) data indicate the Lake Eyre Basin as a major AOD path toward Northern Australia, the Coral Sea, Gulf of Carpentaria, Arafura Sea and Tasman Sea due to post-frontal southwesterly winds and associated anticyclonic circulation (Alizadeh Choobari et al. 2012). Bigg et al. (1984) notes a seasonal cycle of biogenic AOD concentration over the SWPO originating from Australia and identifies a summer maximum. PROSPERO and UEMATSU (1989) found the highest AOD concentration in the SWPO simultaneously occurs with the maximum number of dust storms, also during summer in Australia. Kristament et al. (1993) states the northeast and EA receive their peak of rainfall in the summer away from the center of the landmass due to the placement of the Hadley cell.

SST is one of the most important factors for tropical cyclogenesis. Evans (1993) suggested SST provides the upper limit for TC intensity by supplying the available energy in the system. Although Palmen (1948) set 26–27 °C as the threshold SST for TC formation, Dare and McBride (2011) present a global climatology of SST thresholds and find 7% of TCs form below 26.5 °C. The 27 °C isothermal line has a mean position in the Coral Sea between 10 and 20°S providing the necessary energy supply above the threshold for TC genesis.

The role of UOT in forcing TC variability is one of the critical areas to be addressed by this study. Lin et al. (2013) states in order to explore more of the ocean's role in TC intensification, it is necessary to consider the upper ocean column apart from SST because TCs also interact with upper ocean layers typically from the surface down to 100–200 m. TC intensification, dissipation, and track direction also closely depend upon UOT and the depth of the mixed layer. Over the Coral Sea, the mixed layer depth (MLD) associated with UOT experiences a seasonality as a result of larger seasonal variations and wind stress (Jaffrés 2013). MLDs are relatively homogenous throughout the Coral Sea during summer and are the thickest during July–August (Jaffrés 2013).

7.3 Data

Monthly TC days are derived from the SPEArTC (Diamond et al. 2013). SPEArTC provides a complete list of TCs in the SWPO from 135°E (west of the Gulf of Carpentaria) to 120°W and from the equator to 40° S. This record consists of the six-hourly TC locations for individual storms back to 1841. The major benefits of SPEArTC data are: (1) it integrates TC track information from various sources (e.g., the Australian Bureau of Meteorology and the Regional Specialized Meteorological Centers in Nadi and Wellington); (2) it includes digitization of new tracks and any post-1969 satellite era tracks; and (3) the data are readily available at a centralized, secure location in line with the work of the International Best Tracks for Climate Stewardship (IBTrACS) (Knapp et al. 2010). The SPEArTC dataset also was not constrained by the World Meteorological Organization's 160°E boundary as in

IBTrACS (Diamond et al. 2013). In this way, SPEArTC provides a robust, holistic TC data archive for the SWPO.

Storms included into one individual TC season are those that formed within the EA/SWPO region between 1 November and 30 June of the following calendar year, as the official Australian TC season spans over the passing of a new year. In the data record, the beginning year of the season is used as the code (e.g., season 1985 spans from November 1985 to June 1986) (Ramsay et al. 2017). For this present study, TCs are included that exceeded 17 ms^{-1} (10-min) maximum sustained wind speed (MSW). There are 329 TCs considered for this study. Any single day having at least one TC is considered as one active TC day in this study. Computation of a monthly TC day's statistic was done by summing the total number of days when any named SWPO TC was present over the study region.

A variety of satellite data is used in this study for the independent variables. The monthly mean AOD is derived from the Advanced Very High Resolution Radiometer (AVHRR) onboard a National Oceanic and Atmospheric Administration (NOAA) satellite. It estimates AOD from backscatter radiation at a wavelength of 0.63 μm (Prospero 1997) at 0.1 * 0.1 degree spatial resolution. AVHRR AOD retrieved from the NOAA PATHFINDER Atmospheres Extended (PATMOS-x) satellite is one of the most reliable sources of satellite data, offering more than 30 years of daytime satellite aerosol data in cloud-free conditions on a monthly basis with high spatial resolution.

As climatological trend analysis requires a minimum 30-year period, monthly mean SST (°C) data products are derived from three different satellite sensors to complete the period of record. The three datasets are the Pathfinder AVHRR, Tropical Rainfall Measuring Mission (TRMM) Microwave Imager (TMI), and Advanced Microwave Scanning Radiometer-2 (AMSR2). NOAA/NASA AVHRR Ocean Pathfinder SST products provide gridded data with 0.08 * 0.08 degree spatial resolution from November 1985 to May 2003. The data are considered a reliable source of SST measurement as it has three SST measurement suitable infrared channels (Vazquez et al. 1998). TMI provides gridded monthly mean microwave SST (MWSST) data from June 2003 to June 2012 at 0.25 * 0.25° spatial resolution. AMSRE2 provides microwave SST from 2012 to 2015 based on brightness temperature (Gentemann and Hilburn 2015).

It is notable the combination of three SST data sets may present bias into the study. As an attempt to check for this, two sample t-tests have been performed between each different SST data set to confirm whether the data are significantly different from one another. Non-significant p-values from each t-test support the null hypothesis of no difference between three SST datasets.

Monthly mean gridded UOT (°C) values are derived from the Simple Ocean Data Assimilation (SODA) version 3.3.1 reanalysis data set with 0.5 * 0.5° spatial resolution taken over the upper 110 m of the ocean (Carton and Giese 2008). The monthly and annual averages of AOD, SST, and UOT data over the study region are considered as possible predictors of the number of TC days near EA.

7.4 Descriptive Statistics

The analysis of AOD influence on TCs near EA begins with descriptive statistics about the observed variables since 1985. Figure 7.3 shows the monthly occurrence of TCs originating over the SWPO. TCs occur in this region from November (Nov) to May with a maximum in March (Mar) and a minimum in June (Jun). Over 63% of all TCs in this region occur from January (Jan) to Mar. During these months, the conditions are most favorable and produce the most TC days influencing EA. The northeast and east coastal land areas have such a close proximity to the main cyclone development region (i.e., the Coral Sea) they are most vulnerable toward TC associated wind damage, extreme rainfall, storm surge and coastal flooding during these months (McBride and Keenan 1982).

Figure 7.4a shows the frequency distribution of SSTs in the SWPO region for the entirety of the TC season. From Nov to May, SSTs are warm enough to support cyclone formation, being very near or above the 26 °C threshold. The bulk of the days have values between 27 and 28 °C. The highest values of SSTs are typically found during February (Feb) and Mar, corresponding to the months with the highest number of TC days. From Feb to April (Apr), the main development region for TCs shifts toward the Coral Sea (Diamond et al. 2013), and the mean position of the 27 °C isothermal line falls between 10 and 20°S.

Figure 7.4b shows the frequency distribution of UOT in the SWPO region at the 110-m depth. Most UOT values are 24 °C or greater and the peak values occur in Apr, May, then Jun, and are between 25 and 26 °C. It is interesting to note the highest UOT months do not coincide with the highest SST months, perhaps due to the barrier layer. The barrier layer is the layer between the mixed layer and the

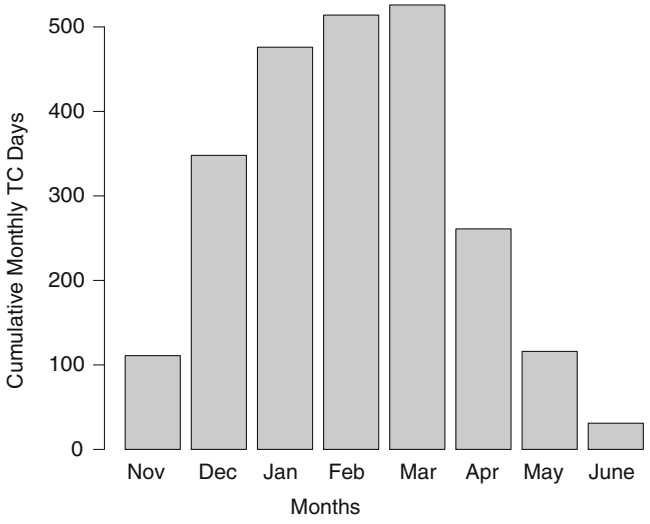

Fig. 7.3 Cumulative TC days per month for events occurring in the SWPO (1985–2015)

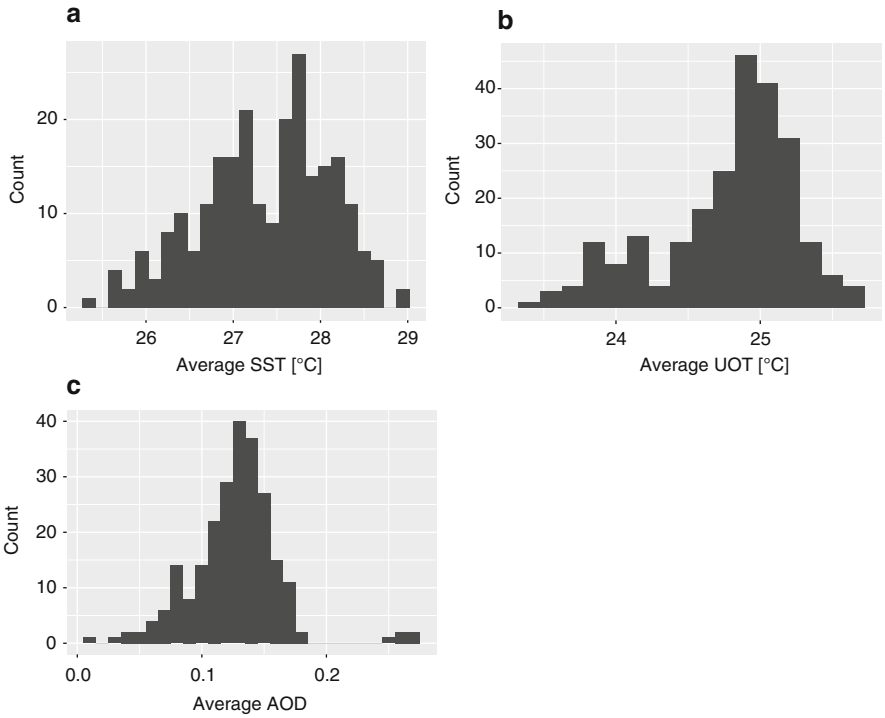

Fig. 7.4 Frequency distribution of the covariates. (a) SST (°C) frequency distribution over study region. (b) UOT (°C) frequency distribution over the study region. (c) AOD frequency distribution over the study area. AOD is a unit-less variable with ranges from 0 to 0.4 (1985–2015)

isothermal layer (Katsura et al. 2015). Here, the barrier layer can lead to high UOT during the late summer and early winter months. This layer has a tendency to thicken in the Coral Sea region during cooler months, leading to high UOT in the late TC season while not in the middle (Jaffrés 2013).

The distribution of AOD over the SWPO region is shown in Fig. 7.4c. This is the average AOD over the Gulf of Carpentaria, Coral Sea, and portions of the Arafura and Tasman Seas. Much of the distribution falls between 0.1 and 0.17. The adjacent arid and semi-arid portions of EA supply the dust leading to the recorded AOD values over the SWPO. The months with the highest AOD levels coincide with the months of highest SST and highest TC days (i.e., Feb and Mar).

To illustrate the change in the variables over time, seasonally averaged time series of TC, SST, UOT, and AOD are included. Stationarity of the individual time series' and trend direction are determined using the Kwiatkowski–Phillips–Schmidt–Shin (KPSS) test, where p-values <0.05 indicate non-stationarity. The KPSS test is based on ordinary least squares regression, which defines the direction and stationarity of linear trend. The time series' are decomposed and the trends in each variable are plotted in Fig. 7.5. The test results show three variables (TC days, SST, and AOD)

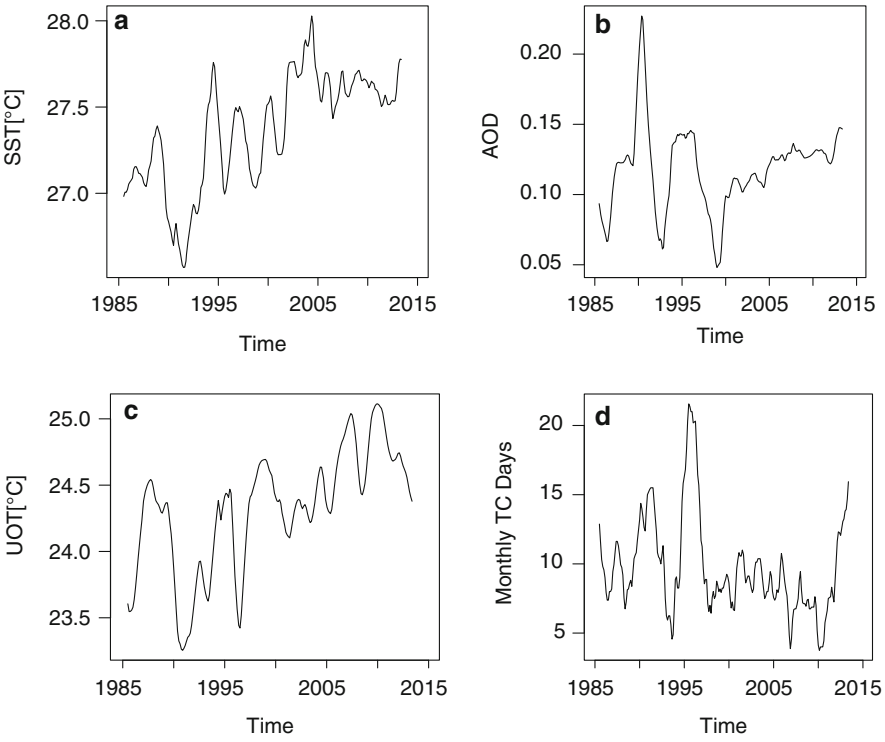

Fig. 7.5 Time series plots. (**a**) Time series of SST (°C). (**b**) Time series of AOD (**c**) Time series of UOT (°C). (**d**) Time series of TC days (1985–2015)

have positive trends and UOT has a neutral trend (TC Days = 0.17, SST = 0.20, UOT = 0, and AOD = 0.24).

Figure 7.5a shows SST has a significant, positive change over time (p-value = 0.01), while also showing decadal variability. The change in SST over time is likely a result of the El Niño Southern Oscillation (ENSO). SWPO SST is largely dominated by ENSO phases on both sides of the temperature gradient. During El Niño years, positive SST anomalies occur eastward in the South Pacific. In La Niña years, these anomalies shift toward the West Pacific. Based on the Ocean Niño Index, El Niño years have lower SST than La Niña years in the SWPO. Research suggests the SWPO has experienced a decadal increase in SST, possibly due to more La Niña like conditions, which may be the cause of the significant increase in SST (DeLong et al. 2012). Figure 7.5b shows the AOD trend in the SWPO region. The change in AOD over time is not statistically significant. The UOT time series in Fig. 7.5c shows a significant, positive trend over time (p-value = 0.01). This could also be related to ENSO, similar to SSTs in the region. Figure 7.5d shows the positive, but insignificant trend in TC days (p-value = 0.1).

7.5 Correlation Between the Variables

Initial relationships between seasonal averages of AOD, SST, UOT, and the number of TC days are estimated using correlation tests. Monthly averages are also considered to identify temporal variability in the relationships. Variables concurrently occurring are compared as well as lagged relationships between them. For example, Nov AOD is related to December (Dec) SST.

The variables are identified as not normally distributed using a Shapiro-Wilks test, thus the Spearman Rank Correlation Coefficient test is used. The rank correlation coefficient (r_s), is generally expressed as,

$$r_s = 1 - \frac{6\Sigma d_i^2}{n(n^2 - 1)}, \tag{7.1}$$

where n is the number of observations in each of the two variables in the correlation and d_i is the ranked difference between the i^{th} measurements for the two variables. Monthly lagged relationships are considered to describe the predictive capability of one variable on another. The lagged relationships might prove helpful to understand feedback and interactions in complex climate systems (Elsner 2007).

The correlation coefficient of the seasonally averaged SST and AOD is 0.15 (p-value = 0.00). However, there are no statistically significant relationships when instead considering monthly pairs of SST and AOD. The relationship between AOD and UOT proves to be insignificant on the seasonal and monthly level. In contrast, Evan et al. (2009) found a strong negative relationship between AOD and MLD temperature over the tropical North Atlantic Ocean because of scattering and reduction in surface solar radiation associated with AOD. The relatively lower AOD amount over the SWPO is one of the possible causes of the insignificant relationship between AOD and UOT.

Table 7.1 shows the monthly lagged relationships between AOD and TC days. The simultaneous correlation coefficient between seasonally averaged AOD and TC days is 0.34 (p-value = <0.00). Increased Feb AOD leads to a significant increase in May TC days. Both indicate a higher AOD concentration leads to higher TC days. Table 7.2 shows correlation statistics between lagged monthly SST values and TC

Table 7.1 Correlation statistics between lagged monthly AOD and TC days. Significant relationships are shown in bold (0.05 level)

Months		Results	
AOD	TC days	ρ	p-value
Nov	Jan	0.28	0.13
Dec	Feb	0.33	0.07
Jan	Mar	0.33	0.08
Feb	Apr	0.02	0.93
Mar	May	0.16	0.41
Feb	**May**	**0.36**	**0.05**
Apr	June	0.11	0.56

Table 7.2 Correlation statistics between lagged monthly SST and TC days

Months		Results	
SST	TC	ρ	p-value
Nov	Nov	−0.17	0.38
Dec	Dec	−0.19	0.31
Dec	Jan	0.30	0.11
Jan	Feb	0.09	0.64
Feb	Mar	0.07	0.72
Mar	Apr	0.04	0.82
Apr	May	−0.21	0.27

Table 7.3 Correlation statistics between lagged monthly UOT and TC days. Significant months at the 0.1 level are shown in bold

Months		Results	
TC	UOT	ρ	p-value
Nov	Nov	−0.30	0.11
Dec	**Dec**	**−0.33**	**0.08**
Jan	Dec	−0.22	0.24
Feb	Jan	−0.07	0.69
Mar	Feb	−0.09	0.63
Apr	Mar	0.13	0.49
May	Apr	−0.16	0.41
June	May	−0.12	0.52

days indicating no statistical significance. Table 7.3 shows correlation statistics for UOT and TC days. There is no statistically significant relationship between monthly pairs of UOT and TC days.

7.6 Poisson Model

To estimate the influence of AOD, SST, and UOT on the count of monthly TC days, a multivariate Poisson regression model is employed. A Poisson regression model is a form of generalized linear regression where the response variable is count data and follows a Poisson distribution. This model is based on the assumption that the response variable has a discrete, Poisson distribution defined on the non-negative integers (Elsner and Jagger 2006). The logarithm of the expected value of the response variable is modeled upon the linear combination of the independent variables (Elsner and Jagger 2013). In a Poisson model, the probability distribution, i.e., the probability of occurrence of exactly y (here, TC days) is given by:

$$\Pr(Y_i = y) = \frac{\mu_i^y \exp^{-\mu_i}}{y!}, \mathrm{y} = 0, 1, 2, \ldots, \infty, \tag{7.2}$$

where μ_i is

$$\mu_i = \exp^{\beta_0 + \Sigma_j \beta_j X_{ij}}, \tag{7.3}$$

where X_{ij} is the data value for predictor j on observation i, and β_j is the corresponding Poisson regression coefficient for predictor j. It can be shown theoretically the expected number of monthly TC days $E(Y) = \text{Var}(Y) = \mu$, when Y has a Poisson distribution (McDonnell and Holbrook 2004). The method to fit a Poisson regression model is to use the Poisson model formulation to derive the maximum likelihood function. It means for a given β (vector of Poisson regression coefficients), μ is calculated for each set of predictors and the likelihood of the observed number of TC days is estimated using Eq. (7.2).

Application of Poisson regression over a linear model is beneficial for modeling discrete events such as the frequency of TC days in a month or in a season. Solow and Nicholls (1990) used Poisson regression to build a statistical model of the relationship between TC frequency and the Southern Oscillation Index near Australia. A Poisson regression model was used by Elsner et al. (2001) to estimate the statistical relationship between annual U.S. hurricane activity and the ENSO. Poisson regression models are used to assess low-level relative vorticity, vertical wind shear, ocean thermal energy, the saturated equivalent potential temperature gradient, and the middle-tropospheric humidity as potential predictors of tropical cyclogenesis over the EA/SWPO region (McDonnell and Holbrook 2004). Elsner and Jagger (2006) used Poisson regression to model seasonal U.S. hurricane counts. Most recently, Ellis et al. (2015) use a Poisson distribution to model annual extreme hurricane frequency over the North Atlantic Basin.

Multivariate Poisson regression models are used to model the count of monthly TC days over lagged monthly values of SST, UOT, and AOD. The model's goodness of fit is tested using an ANOVA and a chi-square test of the residual deviance. Lagged correlation coefficients between SST and UOT show statistically significant multicollinearity during the early and late TC season, thus they are not both considered in the same regression model. Two different multivariate Poisson models are considered, (1) the effect of monthly SST and AOD on TC days and (2) the effect of monthly UOT and AOD on TC days.

7.6.1 Monthly Counts

Figure 7.6 shows the frequency of monthly TC days through time (first in each monthly set) and the number of years with varying TC day amounts per month (second in each monthly set). There are 329 individual TCs. The year-to-year variability and the distribution of count appear to be consistent with a random count process, thus supporting the use of Poisson regression. Nov, May, and Jun have zero TC days for more than 15 years. These months are at the beginning and end of the season, respectively. In the primary TC months, starting from Jan to Mar, many of the years have over 15 TC days. Feb is the only month where TC days are

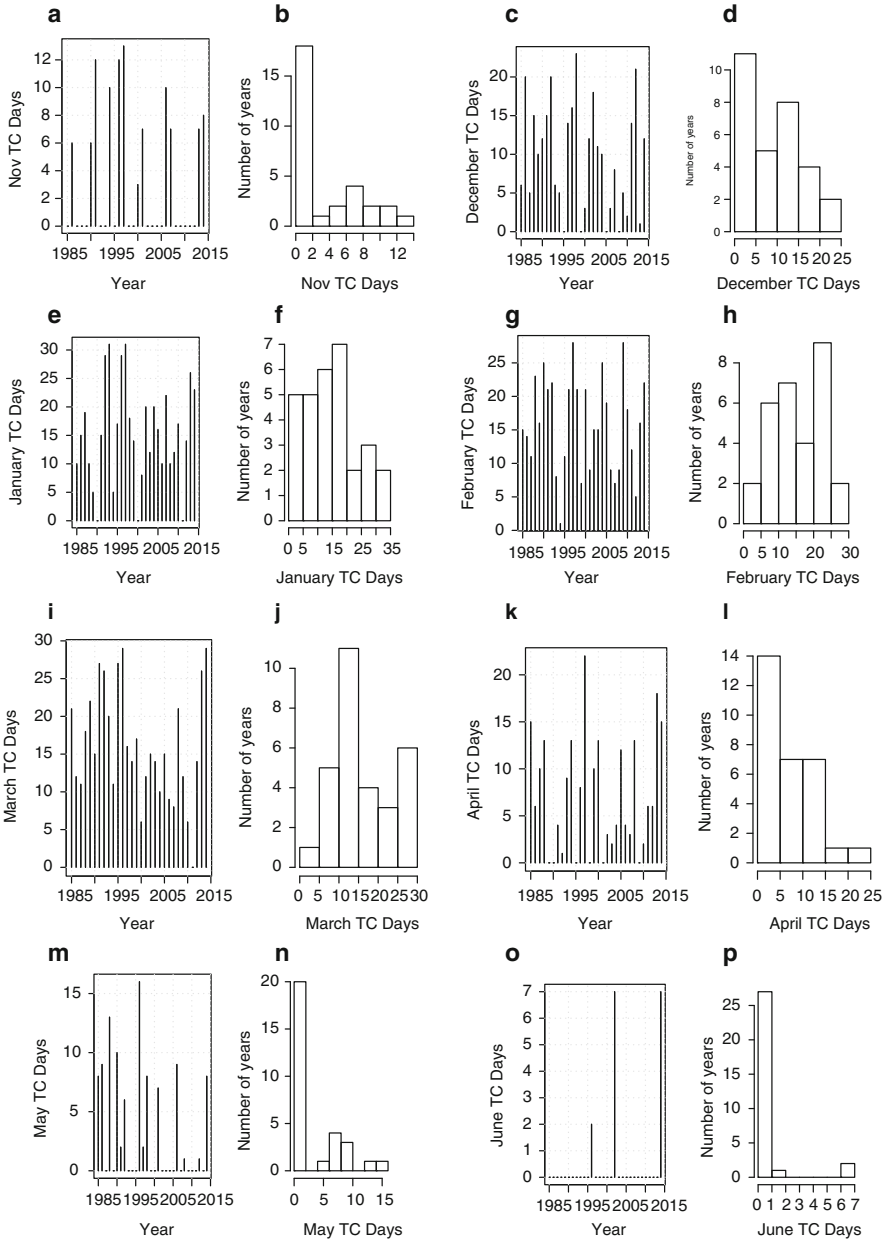

Fig. 7.6 Frequency of monthly TC days through time (first in pair) and the number of years with varying TC day amounts (second in pair) over the SWPO region. (**a**, **b**) Nov. (**c**, **d**) Dec. (**e**, **f**) Jan. (**g**, **h**) Feb. (**i**, **j**) Mar. (**k**, **l**) Apr. (**m**, **n**) May. (**o**, **p**) June

Table 7.4 Top eight most and least active years by cumulative TC days from Nov to Jun

Active years		Non-active years	
Years	TC days	Year	TC days
1986	106	1987	59
1988	93	1994	50
1991	107	1999	60
1992	124	2001	58
1996	171	2008	54
1997	139	2009	57
2013	98	2011	32
2014	131	2012	61

always recorded. Table 7.4 shows the years with TC days during the most active and least active seasons. The highest number of TC days (171) occurred in 1996, and the lowest (32) occurred in 2011. The time series and distribution of count plots provide a clear picture of how TC days vary over the season.

7.6.2 Bivariate Relationships

Figures 7.7 and 7.8 show the summaries of the covariate distributions for each TC count. These plots show the mean, median, range, and quartile division of the covariate for the particular month against TC days. The circles represent medians and lines represent the length from the first/third quartile to the minimum/maximum value. Each plot shows AOD is likely to be important in statistically explaining the variability of monthly TC days as the variation is more systematic in counts across their range of values. As the correlation coefficient shows a strong lagged relationship between TC days and the covariates, the Poisson model should be appropriate to define a particular month's TC count based on one previous month's SST and two previous month's AOD. The bivariate plot shows Nov AOD with Dec TC count, Nov AOD with Jan TC count, and Feb AOD with Apr TC count have the clearest variation across their range of values. SST and UOT have less clear variation for the entire TC season. Although bivariate relationships do not necessarily explain the exact relationship, they can indicate the strongest match between the response and covariates to guide the model choices.

7.6.3 Model Results

Table 7.5 provides the Poisson regression model coefficients for the count of monthly TC days with SST and AOD as covariates. The table also provides the p-value of the model's coefficients to determine statistical significance. A variety of possible lagged combinations of the variables were tested. Only significant

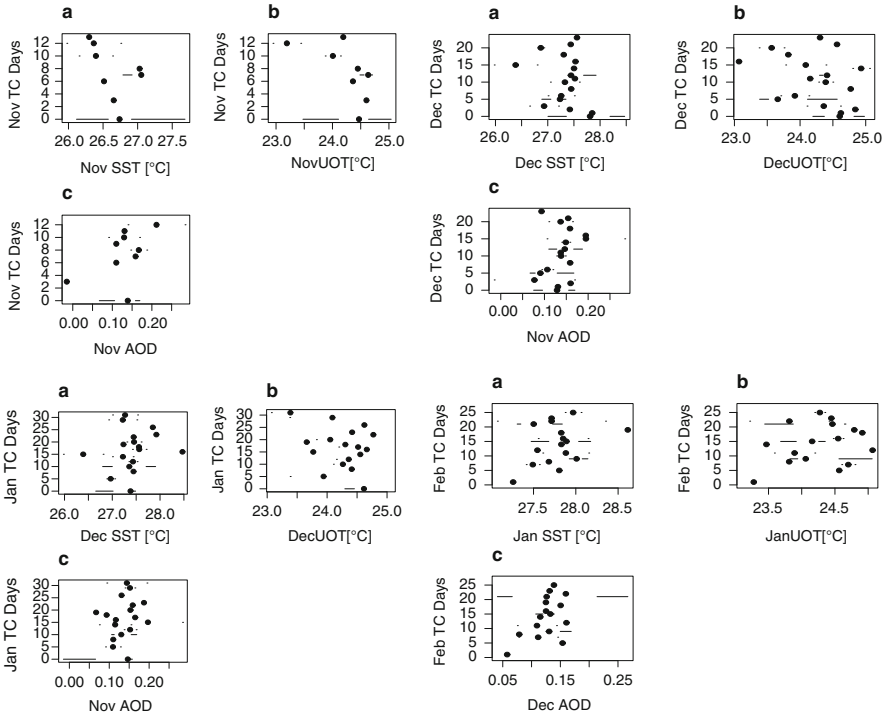

Fig. 7.7 Bivariate relationships between covariates and Nov, Dec, Jan, and Feb TC days. Plots show the five number summary values of all months and all covariates, including the mean, median, range, and quartile division of the covariate for the particular month against TC days. The circles represent medians and lines represent the length from the first/third quartile to the minimum/maximum value. First set of (**a**, **b**, **c**) Nov SST, UOT, and AOD on Nov TC days. Second set of (**a**, **b**, **c**) Dec SST-Dec UOT Nov AOD – on Dec TC days. The third set of (**a**, **b**, **c**) Dec SST-Dec UOT- Nov AOD on Jan TC days. The fourth set of (**a**, **b**, **c**) Jan SST-Jan UOT- Dec AOD on Feb TC days

relationships are discussed. Nov AOD-Dec SST-Dec TC days and Nov AOD-Dec SST-Jan TC days display robust, statistically significant scenarios of lagged relationships between variables. In either model, the direction of the relationship between SST and TC days differs. In the first scenario, Dec SST is negatively related to Dec TC days whereas Dec SST is positively correlated with Jan TC days. This showcases a lagged thermal response of TC occurrence to surface ocean temperature. The negative relationship during Dec could be due to a lack of available energy so early in the season. A Shapiro-Wilk's test is applied on the residuals of the monthly Poisson regression models to test the adequacy of the models. P-values greater than 0.05 indicate normally distributed residuals and adequate models. These two model combinations are used for predicting the number of Dec and Jan TC days in differing conditions.

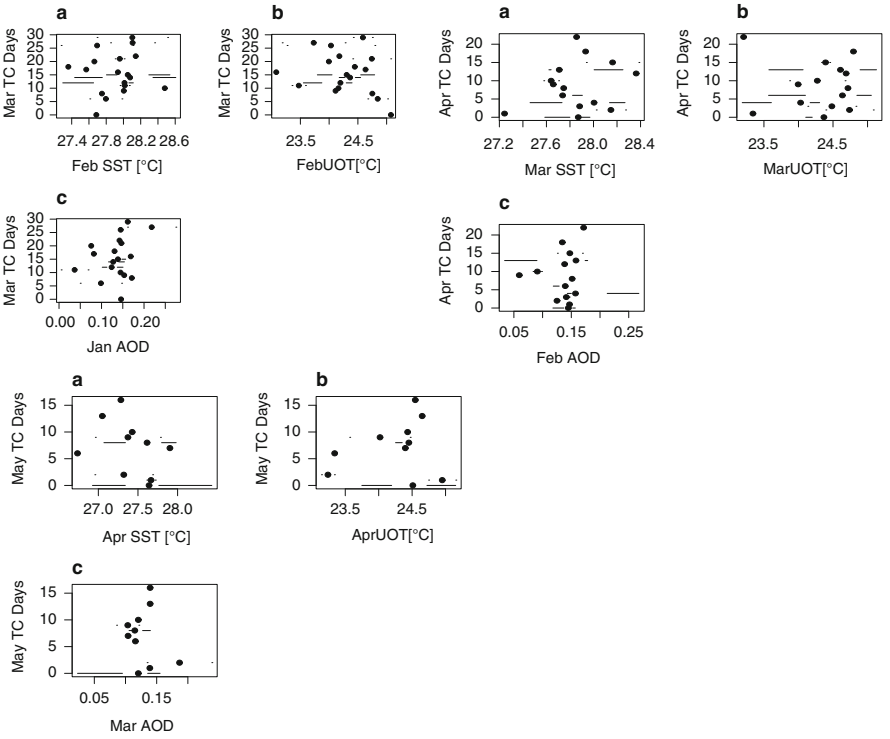

Fig. 7.8 Remaining bivariate relationships between covariates and Mar, Apr, and May TC days. First set of (**a**, **b**, **c**) Feb SST-Feb UOT- Jan AOD on Mar TC days. Second set of (**a**, **b**, **c**) Mar SST-Mar UOT- Feb AOD on Apr TC days. The third set of (**a**, **b**, **c**) Apr SST-Apr UOT- Mar AOD on May TC days

Table 7.5 Poisson regression coefficients and residual p-values for lagged TC-SST-AOD models. The bold highlights those used for prediction

Months			Results				
TC	SST	AOD	SST estimate	AOD estimate	SST p-value	AOD p-value	Residual p-value
Nov	Nov	Nov	−0.67	6.48	0.03	0.00	0.00
Dec	**Dec**	**Nov**	**−0.33**	**2.89**	**0.01**	**0.01**	**0.49**
Jan	**Dec**	**Nov**	**0.25**	**3.56**	**0.01**	**0.00**	**0.67**
Feb	Jan	Dec	0.16	3.64	0.22	0.00	0.46
Mar	Feb	Jan	0.03	3.66	0.81	0.00	0.09
Apr	Mar	Feb	0.51	−1.97	0.06	0.29	0.18
May	Apr	Mar	−1.00	2.55	0.00	0.28	0.00
June	May	Apr	0.97	−6.61	0.15	0.61	0.00

Table 7.6 Poisson regression coefficients and residual p-values for lagged TC-UOT-AOD models. The bold highlights those used for prediction

Months			Results				
TC	UOT	AOD	UOT estimate	AOD estimate	UOT p-value	AOD p-value	Residual p-value
Nov	Nov	Nov	−0.66	6.63	0.00	0.00	0.00
Dec	**Dec**	**Nov**	**−0.38**	**3.02**	**0.00**	**0.01**	**0.83**
Jan	**Dec**	**Nov**	**−0.33**	**2.56**	**0.00**	**0.01**	**0.52**
Feb	Jan	Dec	−0.02	3.44	0.85	0.00	0.43
Mar	Feb	Jan	−0.12	3.46	0.15	0.00	0.22
Apr	Mar	Feb	−0.03	−1.73	0.81	0.34	0.15
May	Apr	Mar	−0.24	1.58	0.21	0.57	0.00
June	May	Apr	−0.08	−8.61	0.89	0.47	0.00

Table 7.7 Poisson regression coefficients and residual p-values for lagged SST-TC model. Bold models indicate significant results (0.05) in adequate models

Months		Results		
TC	SST	SST estimate	SST p-value	Residual p-value
Nov	Nov	−1.11	0.00	0.00
Dec	**Dec**	**−0.40**	**0.00**	**0.35**
Jan	**Dec**	**0.24**	**0.02**	**0.27**
Feb	Jan	0.13	0.33	0.47
Mar	Feb	0.10	0.42	0.34
Apr	Mar	0.48	0.07	0.11
May	Apr	−0.98	0.00	0.00
June	May	1.02	0.13	0.00

Table 7.6 lists the coefficients of the Poisson regression model for the count of monthly TC days with UOT and AOD as covariates and includes the same information as Table 7.5. Similar significant monthly combinations of AOD-UOT-TC days exist as compared to the SST covariate. The major difference is all concurrent and lagged monthly UOT are negatively related to the count of monthly TC days. Nov AOD is significantly, positively related to Dec and Jan TC days when Dec UOT is held constant, and Dec UOT is significantly, negatively related to Dec and Jan monthly TCs. This result suggests as AOD increases in NOV and UOT decreases in Dec, TC days in both Dec and Jan increase.

To test whether large positive coefficients of AOD might influence the coefficients of SST, Poisson regression models using the single predictors SST and UOT were run. Table 7.7 lists the coefficients of the Poisson regression model for the count of monthly TC days with SST as the covariate. Model results represent similar relationships, supporting the use of the multivariate Poisson model. The same is true of the relationship between TC days and UOT (see Table 7.8).

The two above-mentioned tables provide a systematic description of the relationships between the count of monthly TC days and the nearby SST, UOT, and AOD

Table 7.8 Poisson regression coefficients and residual p-values for lagged UOT-TC model. Bold models indicate significant results (0.05) in adequate models

Months		Results		
TC	UOT	UOT estimate	UOT p-value	Residual p-value
Nov	Nov	−0.79	0.00	0.00
Dec	**Dec**	**−0.43**	**0.00**	**0.19**
Jan	**Dec**	**−0.37**	**0.00**	**0.28**
Feb	Jan	−0.03	0.68	0.36
Mar	Feb	−0.14	0.08	0.57
Apr	Mar	0.00	0.98	0.08
May	Apr	−0.27	0.16	0.00
June	May	−0.01	0.98	0.00

covariates. Only four models (two from model 1, and two from model 2) provide statistically significant relationships between all variables.

The models show a difference in the direction of the results. In one case, positive SST leads to more TC days. On the other hand, decreasing UOT leads to more TC days. The first relationship is shown frequently in the literature, where increasing SSTs lead to more TCs (Trepanier 2014). However, the UOT relationship requires further explanation. Subsurface ocean water is typically colder than the surface. During the forward movement of a TC, the intense wind mixes the colder subsurface water with the warmer surface to reduce overall upper ocean temperature. This is referred to as the TC-induced ocean cooling (coupling) effect (OCE). The stronger the OCE during a TC's intensification, the colder the resultant SST is during the TC's lifespan, and the smaller the available air-sea sensible and latent heat fluxes for TC intensification (Huang et al. 2015). This suggests a TC may mix enough subsurface cold water to lead to a relationship showing more TC days in a cooler UOT environment.

However, quantitatively adding AOD can reduce the surface ocean warming by blocking solar radiation. Additional AOD in the atmosphere can reduce insolation, but the existing heat remaining between the surface and AOD layer may provide a temperature change to the subsurface waters and provide available energy for TC genesis (Delworth et al. 2005). This could provide the positive relationship between AOD and TC days when accounting for a decreasing UOT.

In contrast, considering the SST condition, when the season is becoming more active, the relationships are positive between Nov AOD, Dec SST, and Jan TC days. Based on the Poisson model results, these four pairs have been used for making predictions and discussing the physical relationship in those concurrent and lagged months.

Figure 7.9 plots the significant models with the plotmo package in R (Milborrow 2018). Figure 7.9a shows an increase in Dec SST causes a decrease in Dec TC days, but the rate increases with Nov AOD. Figure 7.9b shows Jan TC days increase with increasing Dec SST and with increasing Nov AOD. Figure 7.9c shows Dec TC days decrease with increasing Dec UOT and increase with increasing Nov AOD. Figure 7.9d shows Jan TC days decrease with increasing Dec UOT and increase with increasing Nov AOD.

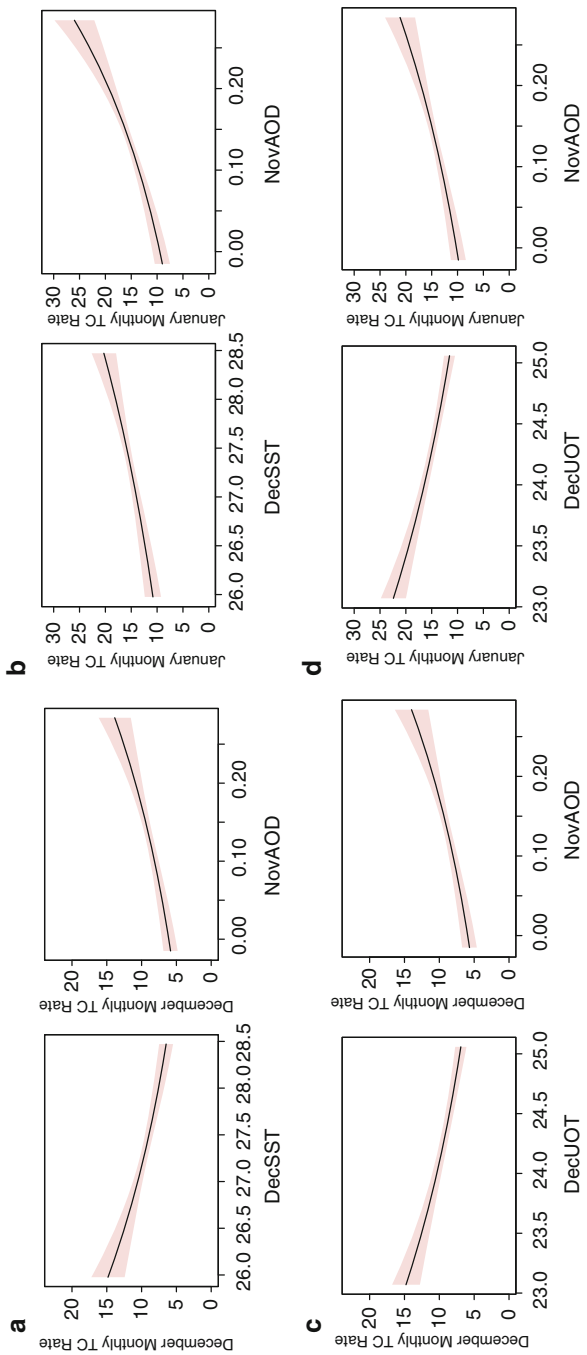

Fig. 7.9 Monthly TC rate based on the covariates. Ninety-five percent confidence levels about the line are shown in pink shading. (**a**) Dec TC days based on Dec SST and Nov AOD. (**b**) Jan TC days based on Dec SST and Nov AOD. (**c**) Dec TC days based on Dec UOT and Nov AOD. (**d**) Jan TC days based on Dec UOT and Nov AOD

Table 7.9 Exponential coefficients of covariates (SST and AOD)

Exponential (exp) of coefficients				
Months		Results		
TC	SST	AOD	SST	AOD
Dec	Dec	Nov	0.72	18.04
Jan	Dec	Nov	1.29	35.03

Table 7.10 Exponential coefficients of covariates (UOT and AOD)

Exponential (exp) of coefficients				
Months		Results		
TC	UOT	AOD	UOT	AOD
Dec	Dec	Nov	0.68	20.52
Jan	Dec	Nov	0.72	12.91

Interpretation of the Poisson regression coefficients is different than the interpretation of ordinary least squares regression. Given the other covariates in the model are held in constant, exponentiations of one covariate's coefficient provides a ratio of the TC days for a unit change in the particular covariate. The results in Table 7.9 show that for every one-degree increase in December SST while holding Nov AOD constant, Dec TC count decreases by a factor of 28%. Similarly, for every one-unit increase in Nov AOD while holding Dec SST constant, Dec TC count will increase and multiply by 18. For every one-degree increase in Dec SST, Jan TC count increases by 29%, and for every one-unit increase in AOD in November, Jan TC count increases and multiplies by 35. Similarly, in Table 7.10, for every one-degree increase in Dec UOT while holding Nov AOD constant, Dec TC count decreases by 32%. For every one-unit increase in Nov AOD while holding Dec UOT constant, Dec TC count will increase and multiply by 20.5.

A goodness of fit test has been conducted on the significant Poisson regression models' deviance residuals to see how much the observed outcome supports the expected outcome. A chi-square test of the deviance of the residuals gives a low p-value, providing strong evidence to reject the null hypothesis of no difference between the expected and observed outcome. The validity of the model also depends on the sample size. Models with large samples tend to provide a better fit than those with small samples. To validate the chi-square test, another goodness of fit test is considered: the ANOVA. The ANOVA test gives a large p-value, supporting the acceptance of the null of no difference. Based on the outcome of the ANOVA chi-square goodness of fit test, the Poisson regression models above are used for TC monthly count prediction.

7.6.4 Predicting TC Count

Model predictions have been made using the months in the statistically significant models. The prediction models can be used to change the amount of AOD, SST, and UOT to see how much each can contribute to the change in TC days.

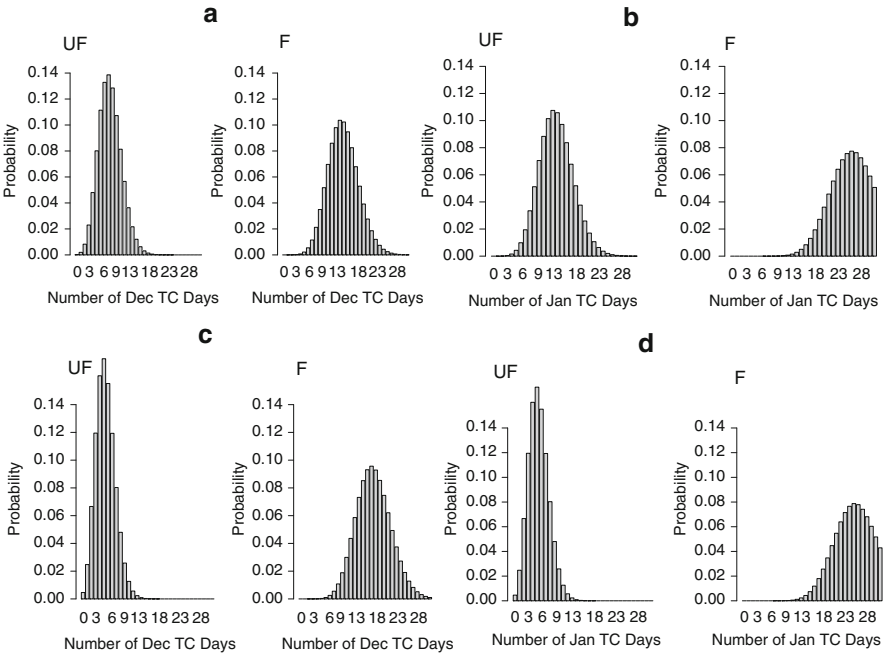

Fig. 7.10 Prediction of TC counts based on Poisson models in unfavorable (UF) and favorable (F) conditions. SST models are shown in (**a**, **b**). UF/F is a low/high AOD, low/high SST environment. UOT models are shown in (**c**, **d**). UF/F is a high/low UOT and a low/high AOD environment. (**a**) Dec TC prediction based on Dec SST and Nov AOD. (**b**) Jan TC prediction based on Dec SST and Nov AOD. (**c**) Dec TC prediction based on Dec UOT and Nov AOD. (**d**) Jan TC prediction based on Dec UOT and Nov AOD

Figure 7.10 shows bar plots for each significant model discussed above. Figure 7.10a–d shows a probability estimate of the monthly days during unfavorable (UF) and favorable (F) conditions. Defining UF and F conditions depends on each model. It is important to note that all references to low SST values are still values well above the threshold for TC formation. The model may support a negative, concurrent Dec relationship, but the values in these months are never below the cyclogenesis threshold. F and UF conditions differ between the SST and UOT models. UF/F conditions in the model using SST include low/high AOD and low/high SST. UF/F conditions in the model using UOT include high/low UOT and low/high AOD. Figure 7.10a–c shows the model for Dec TC days based on Dec SST/UOT and Nov AOD. Figure 7.10b–d shows the model for Jan TC days based on Dec SST/UOT and Nov AOD.

In Fig. 7.10a-UF, it shows a higher likelihood of fewer Dec TC days. In 10a-F conditions, the expected probability of 15 or more Dec TC days is higher than 8%. In Fig. 7.10b-UF conditions, there is moderate probability of more Jan TC days with low SST and low AOD. In 10b-F conditions, there is an 8% probability of a higher

number of Jan TC days in a high SST and high AOD environment. In Fig. 7.10c-UF conditions, the expected probability of 10–13 Dec TC days is more than 14% but then begins to decline. In 10c-F conditions, the expected probability of 24–28 Dec TC days is between 6% and 8%. In Fig. 7.10d-UF conditions, low to moderate numbers of TC days have higher than 14% probability. The 10d-F conditions show more days of the month with TCs. Overall, the model predictions show an increasing trend of monthly TC days in the F conditions for all models.

7.7 Discussion and Concluding Remarks

The statistical relationships between monthly mean SST, UOT, AOD, and TC days were investigated for the period 1985–2015 in the SWPO TC development region near EA (the Coral Sea and portions of the Gulf of Carpentaria). A Poisson generalized linear model was used to determine the statistically significant links between oceanic variables, AOD, and TC days over the SWPO.

A positive significant link has been found between AOD and TC days for the entire TC season. Two different relationships were found regarding AOD, SST, and TC days. In one instance, high Nov AOD and low Dec SST lead to increased Dec TC days. In this instance, the temporal lag between the ocean temperature and the atmospheric response is more apparent. High Nov AOD and high Dec SSTs lead to high Jan TC days. In the first model, an increase in AOD causes an increase in the heating of the lower troposphere by absorbing solar radiation, as well as cooling off the surface by negative radiative forcing. A negative surface radiative forcing results in a decrease in the meridional SST gradient. It results in a cooling down of SST but the SST remains above the threshold level and high enough to contribute necessary energy to the development or maintenance of a TC. As argued by Evan and Allen (1992) and Evan et al. (2011), influences of AOD on ocean temperature through surface radiative forcing would weaken the monsoon circulation, and reduce the strength of vertical wind shear and ultimately promote TC development and activity. The negative relationship between concurrent Dec TC days and Dec SST is similar to the result presented in Zhao et al. (2018), where they found similar results over the Western North Pacific.

The lagged positive relationship between SST and TC days explains the complex ocean atmospheric interactions taking place over time. This lagged relationship suggests time is needed for the sea surface to influence the thermodynamic and dynamic factors required for TC genesis. Over the Australia region, Rotstayn et al. (2011) found AOD-induced radiative heating can enhance ascent and moisture convergence, leading to increased convection and precipitation in some situations. These arguments support the findings of this study. Chiacchio et al. (2017) finds a positive link between sea salt, organic aerosol, and TC frequency over the South Pacific, which can be related to the increase in surface heat exchange between the ocean's surface and atmosphere, leading to larger latent and sensible heating. Higher TC days associated with higher AOD could be explained by an increasing rate of

clouds with increasing AOD over northern coastal Australia (Small et al. 2011). Higher amounts of aerosols can act as cloud condensation nuclei (CCN). CCN directly affect an initial environment of a pre-TC vortex through release of latent heat and indirectly through rainband development (Zhang et al. 2009).

Eastern Australia, the adjoining Coral Sea, and Gulf of Carpentaria experience seasonal AOD outbreaks from the arid and semi-arid regions of Australia. Major AOD outbreaks typically occur from Sep to Mar. In contrast, starting from Apr to July, the AOD outbreaks remain low. The Poisson model results show earlier TC months have a more significant relationship with AOD than the later months. Lower AOD activity during later months in the TC development region is one of the possible causes of the insignificant relationships. Evans and Allan (1992) found an increasing likelihood of tropical cyclogenesis over north Australia related to equatorward shifting of the monsoon trough. A weak monsoon trough coupled with an upper-level anticyclone causes weak vertical wind shear, which increases TC development (Meywerk and Ramanathan 1999; Evans et al. 2011).

UOT has a negative, significant relationship in the two earlier lagged monthly combinations in the TC season. The relationships shown between UOT and the frequency of TC days indicate a lack of direct interaction between subsurface ocean temperature and the energy required for TC development. High positive coefficients of AOD throughout the season may cancel out the UOT coefficients, or the high amount of AOD loading may cause a decline of UOT through surface radiative forcing. This may be leading to the minor role UOT plays in modulating the count of monthly TC days.

The impact of aerosols on TC development, intensification, weakening, and associated precipitation is widely studied over different ocean basins of the world (Dunion and Velden 2004; Shu and Wu 2009; Gong et al. 2006; Zhang et al. 2007; Evan et al. 2011; Levin et al. 2005). Evan et al. (2006) found North Atlantic TC activity is strongly inversely correlated with mean AOD coverage. Shu and Wu (2009) found AOD can affect TC intensity in both favorable (initial development) and unfavorable (subsequent development) manners. Based on these previous findings, this study was designed to identify the relationship between AOD and TC activity over the EA/SWPO region. The results here do not indicate as strong a relationship between these variables as over the North Atlantic. Some of the possible reasons for this difference are the Coral Sea and Gulf of Carpentaria receive considerably lower amounts of aerosols compared to the North Atlantic main TC development region, which is adjacent to the Sahara Desert. In addition, Australian aerosol particles more frequently travel to the southeast by prefrontal northwesterly winds and to the northwest by southeasterly trade winds.

Rainfall is also one of the major factors for low AOD aerosol concentration over the Coral Sea and northern Australia. The presence of the South Pacific Convergence Zone during summer months causes a maximum in rainfall, which leads to a low AOD over the region (Kristament et al. 1993). The SWPO region is also greatly influenced by ENSO, where ENSO has a different influence on the SWPO compared to any other basin around the world. The Madden Julian Oscillation also modulates aerosol loading and TC development activity by modulating precipitation and cloud

cover conditions. Each of these teleconnections and their influence on rainfall, AOD, and TC genesis will be explored in future research.

This study is one of the first to establish a statistically significant relationship between AOD, ocean temperature variables, and TC frequency over the EA/SWPO region. The above models help to explain some of the variability in TC activity influenced by AOD, SST, and UOT. However, there are many additional thermodynamic and dynamic factors dictating the ultimate formation of TCs in this area. Future research will focus on including other dynamic variables required for TC development (e.g., relative humidity and vertical wind shear) and how AOD may influence their modulation on TC variability. The benefit from this study is the finding of a significant positive relationship between AOD and TC days with cooler but above the threshold SST and UOT conditions in the month of, and warmer SSTs in the month prior, to TC formation. This study provides scenarios that can be used to better understand the range of past, present, and future TC day variability influenced by AOD, SST, and UOT.

References

Abish B, Mohanakumar K (2013) A stochastic model for predicting aerosol optical depth over the north Indian region. Int J Remote Sens 34(4):1449–1458

Alizadeh Choobari O, Zawar-Reza P, Sturman A (2012) Atmospheric forcing of the three-dimensional distribution of dust particles over Australia: a case study. J Geophys Res: Atmos 117(D11):D11206

Augustine JA, Hodges GB, Dutton EG, Michalsky JJ, Cornwall CR (2008) An aerosol optical depth climatology for NOAA's national surface radiation budget network (SURFRAD). J Geophys Res Atmos 113(D11):D11204

Barrows TT, Juggins S, De Deckker P, Calvo E, Pelejero C (2007) Long-term sea surface temperature and climate change in the Australian–New Zealand region. Paleoceanography 22 (2):1–17

Bettencourt S, Croad R, Freeman P, Hay J, Jones R, King P, Lal P, Mearns A, Miller G, Pswarayi-Riddihough I (2006) Not if but when: Adapting to natural hazards in the Pacific Islands region. The World Bank, Washington, DC

Bigg E, Gras J, Evans C (1984) Origin of Aitken particles in remote regions of the southern hemisphere. J Atmos Chem 1(2):203–214

Cai W, Shi G, Cowan T, Bi D, Ribbe J (2005) The response of the Southern Annular Mode, the East Australian Current, and the southern mid-latitude ocean circulation to global warming. Geophys Res Lett 32 (23) L23706

Carton JA, Giese BS (2008) A reanalysis of ocean climate using Simple Ocean Data Assimilation (SODA). Mon Weather Rev 136(8):2999–3017

Chiacchio M, Pausata FS, Messori G, Hannachi A, Chin M, Önskog T, Ekman AM, Barrie L (2017) On the links between meteorological variables, aerosols, and tropical cyclone frequency in individual ocean basins. J Geophys Res Atmos 122(2):802–822

Choobari OA, Zawar-Reza P, Sturman A (2013) Simulation of the spatial distribution of mineral dust and its direct radiative forcing over Australia. Tellus B 65:19856

Church JA, White NJ, Arblaster JM (2005) Significant decadal-scale impact of volcanic eruptions on sea level and ocean heat content. Nature 438(7064):74

Cortese G, Dunbar G, Carter L, Scott G, Bostock H, Bowen M, Crundwell M, Hayward B, Howard W, Martínez JI (2013) Southwest Pacific Ocean response to a warmer world: insights from marine isotope stage 5e. Paleoceanography 28(3):585–598

Dare RA, McBride JL (2011) The threshold sea surface temperature condition for tropical cyclogenesis. J Clim 24(17):4570–4576

Deloitte Access Economics (2013) Building our nation's resilience to natural disasters. ACT Deloitte Access Economics, Barton

DeLong KL, Quinn TM, Taylor FW, Lin K, Shen C-C (2012) Sea surface temperature variability in the southwest tropical Pacific since AD 1649. Nat Clim Chang 2(11):799

Delworth TL, Ramaswamy V, Stenchikov GL (2005) The impact of aerosols on simulated ocean temperature and heat content in the 20th century. Geophys Res Lett 32(24):L24709

Diamond HJ, Lorrey AM, Renwick JA (2013) A southwest Pacific tropical cyclone climatology and linkages to the El Niño–Southern Oscillation. J Clim 26(1):3–25

Dunion JP, Velden CS (2004) The impact of the Saharan air layer on Atlantic tropical cyclone activity. Bull Am Meteorol Soc 85(3):353–365

Ellis Kelsey N, Sylvester LM, Trepanier JC (2015) Spatiotemporal patterns of extreme hurricanes impacting US coastal cities. Nat Hazards 75(3):2733–2749

Elsner JB (2007) Granger causality and Atlantic hurricanes. Tellus A 59(4):476–485

Elsner JB, Jagger TH (2006) Prediction models for annual US hurricane counts. J Clim 19 (12):2935–2952

Elsner JB, Jagger TH (2013) Hurricane climatology: a modern statistical guide using R. Oxford University Press, Oxford

Elsner JB, Bossak BH, Niu XF (2001) Secular changes to the ENSO-US hurricane relationship. Geophys Res Lett 28(21):4123–4126

Evan AT, Dunion J, Foley JA, Heidinger AK, Velden CS (2006) New evidence for a relationship between Atlantic tropical cyclone activity and African dust outbreaks. Geophys Res Lett 33(19): L19813

Evan AT, Vimont DJ, Heidinger AK, Kossin JP, Bennartz R (2009) The role of aerosols in the evolution of tropical North Atlantic Ocean temperature anomalies. Science 324(5928):778–781

Evan AT, Kossin JP, Ramanathan V (2011) Arabian Sea tropical cyclones intensified by emissions of black carbon and other aerosols. Nature 479(7371):94–97

Evans JL (1993) Sensitivity of tropical cyclone intensity to sea surface temperature. J Clim 6 (6):1133–1140

Evans JL, Allan RJ (1992) El Nino/Southern oscillation modification to the structure of the monsoon and tropical cyclone activity in the Australasian region. Int J Climatol 12(6):611–623

Foltz GR, McPhaden MJ (2008) Impact of Saharan dust on tropical North Atlantic SST. J Clim 21 (19):5048–5060

Gentemann CL, Hilburn KA (2015) In situ validation of sea surface temperatures from the GCOM-W1 AMSR2 RSS calibrated brightness temperatures. J Geophys Res Oceans 120(5):3567–3585

Gong S, Zhang X, Zhao T, Zhang X, Barrie L, McKendry I, Zhao C (2006) A simulated climatology of Asian dust aerosol and its trans-Pacific transport. Part II: interannual variability and climate connections. J Clim 19(1):104–122

Hall JD, Matthews AJ, Karoly DJ (2001) The modulation of tropical cyclone activity in the Australian region by the Madden–Julian oscillation. Mon Weather Rev 129(12):2970–2982

Huang P, Lin II, Chou C, Huang RH (2015) Change in ocean subsurface environment to suppress tropical cyclone intensification under global warming. Nat Commun 6:7188

Jens M, Ramanathan V (1999) Observations of the spectral clear?sky aerosol forcing over the tropical Indian Ocean. J Geophys Res Atmos 104(D20):24359–24370

Jaffrés JB (2013) Mixed layer depth seasonality within the Coral Sea based on Argo data. PLoS One 8(4):e60985

Katsura S, Oka E, Sato K (2015) Formation mechanism of barrier layer in the subtropical Pacific. J Phys Oceanogr 45(11):2790–2805

Knapp KR, Kruk MC, Levinson DH, Diamond HJ, Neumann CJ (2010) The international best track archive for climate stewardship (IBTrACS) unifying tropical cyclone data. Bull Am Meteorol Soc 91(3):363–376

Kristament I, Harvey M, Liley J (1993) A seasonal cycle in the southwest Pacific free tropospheric aerosol concentration. J Geophys Res Atmos 98(D9):16829–16837

Levin Z, Teller A, Ganor E, Yin Y (2005) On the interactions of mineral dust, sea-salt particles, and clouds: a measurement and modeling study from the Mediterranean Israeli dust experiment campaign. J Geophys Res Atmos 110(D20):D20202

Lin I-I, Goni GJ, Knaff JA, Forbes C, Ali MM (2013) Ocean heat content for tropical cyclone intensity forecasting and its impact on storm surge. Nat Hazards 66(3):1481–1500

McBride J, Keenan T (1982) Climatology of tropical cyclone genesis in the Australian region. J Climatol 2(1):13–33

McDonnell KA, Holbrook NJ (2004) A Poisson regression model of tropical cyclogenesis for the Australian–Southwest Pacific Ocean region. Weather Forecast 19(2):440–455

Milborrow S (2018) Plotmo: plot a model's residuals, response, and partial dependence plots. R package version 3.5.0. https://CRAN.R-project.org/package=plotmo

Mitchell R, Campbell S, Qin Y (2010) Recent increase in aerosol loading over the Australian arid zone. Atmos Chem Phys 10(4):1689–1699

Palmen E (1948) On the formation and structure of tropical hurricanes. Geophysica 3(1):26–38

Prospero JM (1997) Characterization of tropospheric aerosols over the oceans with the NOAA advanced very high resolution radiometer optical thickness operational product. J Geophys Res 102(D14):16,889–816,909

Prospero JM, Uematsu M (1989) Mineral aerosol transport to the Pacific Ocean. In: Prospero JM, Uematsu M, Savoie DL (eds) Chemical oceanography, vol 10. Academic Press, London, p 187

Ramsay H, Richman M, Leslie L (2017) The modulating influence of Indian Ocean Sea surface temperatures on Australian region seasonal tropical cyclone counts. J Clim 30(13):4843–4856

Rotstayn LD, Keywood MD, Forgan BW, Gabric AJ, Galbally IE, Gras JL, Luhar AK, McTainsh GH, Mitchell RM, Young SA (2009) Possible impacts of anthropogenic and natural aerosols on Australian climate: a review. Int J Climatol 29(4):461–479

Rotstayn L, Collier M, Mitchell R, Qin Y, Campbell S, Dravitzki S (2011) Simulated enhancement of ENSO-related rainfall variability due to Australian dust. Atmos Chem Phys 11 (13):6575–6592

Salinger MJ, Hay J, McGann R, Fitzharris B (1993) Southwest Pacific temperatures: diurnal and seasonal trends. Geophys Res Lett 20(10):935–938

Salinger MJ, Basher R, Fitzharris B, Hay J, Jones P, MacVeigh J, Schmidely-Leleu I (1995) Climate trends in the South-West Pacific. Int J Climatol 15(3):285–302

Shu S, Wu L (2009) Analysis of the influence of Saharan air layer on tropical cyclone intensity using AIRS/aqua data. Geophys Res Lett 36(9):L09809

Small JD, Jiang JH, Su H, Zhai C (2011) Relationship between aerosol and cloud fraction over Australia. Geophys Res Lett 38(23):L23802

Solow A, Nicholls N (1990) The relationship between the southern oscillation and tropical cyclone frequency in the Australian region. J Clim 3(10):1097–1101

Trepanier JC (2014) Hurricane winds over the North Atlantic: spatial analysis and sensitivity to ocean temperature. Nat Hazards 71(3):1733–1747

Vazquez J, Perry K, Kilpatrick K (1998) NOAA/NASA AVHRR Oceans Pathfinder sea surface temperature data set user's reference manual. Jet Propulsion Laboratory Tech Rep D-14070

Zhang R, Li G, Fan J, Wu DL, Molina MJ (2007) Intensification of Pacific storm track linked to Asian pollution. Proc Natl Acad Sci 104(13):5295–5299

Zhang H, McFarquhar GM, Cotton WR, Deng Y (2009) Direct and indirect impacts of Saharan dust acting as cloud condensation nuclei on tropical cyclone eyewall development. Geophys Res Lett 36(6):L06802

Zhao H, Wu L, Raga G (2018) Inter-decadal change of the lagged inter-annual relationship between local sea surface temperature and tropical cyclone activity over the western North Pacific. Theor Appl Climatol 134: 1–14

Chapter 8
Climate Theory and Tropical Cyclone Risk Assessment

Kevin Walsh

Abstract The links between the ability of general circulation models to simulate tropical cyclones and the development of a climate theory of tropical cyclone formation are explored, with an emphasis on the potential of general circulation models (GCMs) and theory for tropical cyclone hazard and risk assessment. While GCMs can now generate a reasonable simulation of the observed tropical cyclone formation rates and intensity distributions, they are very expensive to run. Simpler methods involving statistical relationships between climate variables and tropical cyclone formation have been developed and have been used for hazard assessment, but like other methods used for projections, such as downscaling or GCMs, they do not constitute a theory of tropical cyclone formation. An outline is given of some of the possible characteristics of such a theory and its potential utility for climate science and risk.

Keywords Tropical cyclone · Tropical climate · Tropical cyclone formation

8.1 Introduction

Climate science and climate models are increasingly being used as tools for tropical cyclone (TC) risk assessment. Recent reviews on this general topic are those of Cobb and Done (2017) and Wehner et al. (2017). In principle, the main advantage of climate models over the statistical models that have typically been used in hazard estimation is that climate models are physically based and therefore can generate climate conditions and TC characteristics that are outside the extremes in the observed record. Statistical models can also do this, but the extreme tails of their distributions outside of the observed record must be estimated. While climate models still have considerable room for improvement, the current state of the art indicates

K. Walsh (✉)
School of Earth Sciences, The University of Melbourne, Parkville, VIC, Australia
e-mail: kevin.walsh@unimelb.edu.au

J. M. Collins, K. Walsh (eds.), *Hurricane Risk*, Hurricane Risk 1,
https://doi.org/10.1007/978-3-030-02402-4_8

that many aspects of TC climatology can be reasonably well simulated by fine resolution climate models. Nevertheless, Cobb and Done (2017) recently concluded that the use of general circulation model (GCM)-simulated TC climate output as a direct input to risk models was unlikely at this stage, given the biases in climate model simulations and the considerable cost in computer time of generating them. Thus, the main use of GCMs at present is to make physical inferences of the possible effects of climate variations that can then be used to constrain and modify the predictions of risk models; that is, for the construction of climate variability and climate change scenarios that might be applied to risk assessment methods (e.g. TCRM, http://geoscienceaustralia.github.io/tcrm/).

Another method that could be used to constrain risk models is an improved theoretical understanding of the relationship between climate and TC characteristics. Initial advances in this field have included the successful theory of TC potential intensity (PI; Emanuel 1986, 1988; Holland 1997; Bister and Emanuel 2002), whereby well-tested concepts in the theory of thermodynamics are applied to the problem of estimating the maximum energy available for TC intensification. Modifications to this theory have included the dynamic effects of vertical wind shear (Tang and Emanuel 2012) and ocean coupling (Miyamoto et al. 2014), as these processes can inhibit TCs from reaching their PI. Indeed, most TCs do not reach their theoretical PI during their lifetimes (e.g. Emanuel 2000). In addition to helping to constrain the maximum climatological intensity, the PI theory has been successfully used as a component of short-term statistical forecasts of TC intensity (DeMaria and Kaplan 1994).

Much less advanced is a climate theory of TC formation. The initial work of Gray (1968, 1975, 1979) established statistical relationships between climate variables and TC formation, termed by Gray as the Seasonal Genesis Parameter (SGP). The SGP provided the foundation for the later development of a considerable number of such statistical relationships, now known collectively as genesis potential indices (GPIs; Menkes et al. 2012). These indices are based on environmental parameters that are known to be important controls of TC activity, and thus in principle can be used for diagnosing the relationship between climate and TC formation. However, being based on statistical relationships rather than equations that represent physical processes, they do not constitute a theory of TC formation. Nevertheless, it can be easily argued that a strong statistical relationship between a climate variable and TC formation rates is an indicator that this variable might be part of such a theory, if it were to be constructed.

The general aim of this chapter is to draw links between GCM-based hazard assessments and climate theory. Some of the arguments made in this chapter are speculative, as one of the goals of this paper is to try to make suggestions regarding productive areas of research that might give us more information on the fundamental ways in which climate and TC formation are related. Section 8.2 discusses recent developments in physical modeling of the climatology of TCs and its relation to risk assessment. Section 8.3 discusses how GPIs can be used to illustrate the relationship between climate and TC formation and gives an example of their use in risk assessment. Finally, Sect. 8.4 considers the role of theory in this process.

8.2 Recent Developments in Physical Modeling of Tropical Cyclone Climatology

To be used as a credible tool for both hazard assessment and as a means of better understanding the relationship between climate and TC formation, a GCM must have a good simulation of both mean climate and TC formation. A recent review of the capability of GCMs and regional climate models (RCMs) to simulate the observed TC climatology is given in Camargo and Wing (2016). One of the main uses of GCMs in this context is to simulate the possible effects of climate change on TCs; a recent review is that of Walsh et al. (2016). Developments in this field can be summarized by reference to a couple of key recent papers. Knutson et al. (2015) used a GCM with a fine horizontal resolution (50 km), with each individual storm then resimulated (or "downscaled") with the GFDL hurricane model at a horizontal resolution of 9 km. The combined modeling system is able to give a good simulation of TC numbers and even a reasonable simulation of the total annual global number of very intense TCs (Saffir-Simpson categories 4 and 5; Simpson and Saffir 1974), a task that had previously been challenging for most modeling systems. These results are very encouraging but a cautionary note is that such simulations are computationally expensive, requiring considerable resources on large supercomputers. Another approach is taken by Yoshida et al. (2017), who run a moderately fine-resolution (60 km) climate model in a large number of "ensembles", simulations that use slightly different initial conditions to capture the effect of stochastic variability on the resulting climate state. In addition, due to known differences in the projections of future sea surface temperatures (SSTs) by different GCMs, they simulate ensembles using different future SST patterns from different GCMs. Contrary to a number of other studies, they project a future decline in the number of very intense TCs, although the native horizontal resolution of this study is considerably coarser than that of Knutson et al. (2015). The use of ensembles enables this work to estimate the uncertainty in future projections that might be due simply to the internal variability of the climate system (see also Villarini and Vecchi 2012).

These fine-resolution GCM simulations usually use specified SSTs as lower boundary conditions, with the SST fields being derived from lower-resolution coupled ocean-atmosphere GCM simulations of changed climate conditions. Thus, these simulations do not have two-way interaction between the atmosphere and the ocean. Ideally, such coupling needs to be included in simulations of future TC activity because it is well known that there are strong interactions between the atmosphere and the ocean in TCs (e.g. Lin et al. 2013). For instance, TCs can cool the ocean surface through increased mixing at the base of the mixed layer, and to a lesser extent through large surface heat and moisture fluxes. A modest number of GCM studies have used a high-resolution coupled ocean-atmosphere GCM to simulate future TC behavior (Murakami et al. 2015; for a recent review, see Camargo and Wing 2016). In general, the main results of the fixed-SST models – the decrease in total TC models combined with an increase in intensities of the strongest storms – are similar in the coupled model experiments, although more

coupled model simulations are needed to make this conclusion more robust. With increases in computing power, coupled model experiments will probably become routine and replace the fixed SST experiments as the model system of choice for simulating the effect of climate change on TCs (see also Haarsma et al. 2016).

A method of downscaling that is computationally efficient is that of Emanuel (2017). In his method, weak tropical lows (or "seeds") simulated by an economical hurricane model are allowed to evolve in the climate conditions provided by a coarse-resolution model. The ones that survive to intensify to TC strength constitute the model's simulated TC climatology. Emanuel (2017) describes a new, simplified statistical dynamical model (the FAST model) that is a development of the CHIPS model that was previously employed using a similar methodology (Emanuel 2006). The FAST model relies on simpler equations for TC intensity. Both models include the effect of air-sea interaction, shear and PI. The FAST model produces a reasonable simulation of current climate tropical genesis rates and even of intensity distributions over the North Atlantic, with the notable exception of genesis rates in the main development region in this basin. The reason for this is unclear at present.

One issue with this method is that it requires a seeding rate to be specified so the number of TC "survivors" is similar to the number of TCs in observations. The maximum wind speed of the seeds is about 12 ms^{-1}, or of tropical depression strength, although note that the quantitative intensity lower threshold of "tropical depression" is poorly defined. Nevertheless, the results of Tory et al. (2017; see the next section) indicate that these tropical depressions share many of the relationships to climate variables that TCs do. This poses the question of whether using them as a starting point for a climate simulation is bypassing the initial and potentially important stages of TC genesis. This is a potential issue for accurate simulation of TC genesis in a different climate using this method. In contrast, this initial genesis phase is not bypassed in GCMs, which generate their own TCs, although of course given their relatively coarse resolution compared with physical processes that are important in TCs, they have their own uncertainty issues for projections. In particular, the limited resolution of GCMs means that important aspects of the formation process, such as aggregation (see Sect. 8.4), are poorly represented. It is not known at present how important is a representation of these small-scale processes in any climate theory of TC formation.

Downscaling is not the only way to compensate for the biases inherent in GCM-based simulations of TC climatology. Increasingly, statistical bias correction is being used as a method to extract information from GCMs, particularly for intense TCs at the extreme upper end of the intensity distribution. Bias correction of GCM-based TC climatology simulations has been used for some time. For instance, some studies (e.g. Murakami et al. 2012) use a methodology where the threshold values used in their TC detection scheme are tuned to guarantee that the number of TCs generated globally equals that observed. This is a reasonable technique for perturbation experiments, where one is more interested in the response of the simulation of a climate model to, for instance, higher carbon dioxide content or changed SSTs. The method is admittedly less justifiable as a means of determining if the GCM is actually generating the correct number of TCs. Recent bias correction

methods include that of Sugi et al. (2016), who correct the intensity distribution of the TCs simulated by the GCMs to enable some inferences to be made about the high intensity (Saffir-Simpson categories 4 and 5) TCs. This is the method used by Yoshida et al. (2017) in their ensemble simulations. Note that this model's ability to simulate very intense TCs relies on this bias correction technique rather than the native ability of the model to generate such intense TCs spontaneously. It could therefore be argued that this result, while useful, is less confident than similar predictions made by models that are able to simulate very intense TCs directly, such as the results of Knutson et al. (2015). Another recent bias correction approach is that of Gettelman et al. (2017), who input GCM-generated TCs directly into a wind damage model, with the GCM winds scaled to obtain a wind-pressure relationship similar to observations. They find comparable damage results to those calculated using input from the IBTrACS best track TC observations.

8.3 GPIs and a Climate Theory of Tropical Cyclone Formation

An even more economical approach is to use GPIs, statistical relationships between climate variables and TC formation rates. A considerable amount of the progress in our understanding of the relationship between climate and TC formation has come from the formulation and development of GPIs. The pioneering work of Gray (1968, 1975, 1979) has been followed by updated formulations that more realistically represent the relationship between variations of their constituent variables and TC formation through the inclusion of more physically-based predictors. For instance, the original SGP developed by Gray relied on an excessively strong relationship between SST variations and TC formation, and SST has typically been replaced in subsequent GPIs by PI. Nevertheless, despite considerable work on this topic, consensus has not yet been reached on the best formulation for a GPI. While GPIs, by definition, give good results when applied to observed fields, when applied to the large-scale climate fields produced by climate models, competing GPI formulations give conflicting results for future climate conditions. For instance, Camargo et al. (2014) compared the number of TCs generated directly by a fine-resolution climate model to the GPI values diagnosed from the climate model's simulated climate variables under current and future climate conditions. They noted that few of the GPIs that they used captured the future decrease in TC numbers directly simulated in the GCMs. Since a decrease in the future numbers of TCs is a result produced by the overwhelming majority of climate models, this may represent an issue for the credibility of GPIs as a true representation of the relationship between climate variables and TC formation. Another possibility is contamination of the climate fields by the TCs themselves, due to (for instance) their very strong wind fields (Swanson 2008).

Alternatively, it is always possible that the GCMs are all incorrect due to a common missing factor; e.g. model resolution, which is a crucial factor in the realistic simulation of TCs. We speculate that the result of Camargo et al. (2014) would also make sense if there were a stochastic, short timescale component to formation that occurs in observations, is captured at least partially by direct GCM simulation, and that responds differently to climate forcings than the relatively intense TCs, since they have already travelled some way down the path of intensification. Camargo et al. (2014) also noted, though, that there was a combination of GPI parameters, including saturation deficit (a quantity related to atmospheric moisture content) and PI, that did give a decrease in TC numbers in future climate simulations, which is in agreement with the results of direct GCM simulation. Thus, there is reason to believe that a consistent response to future climate change forcing between GPIs and GCMs may be achieved and that a consensus between GPI and GCM climate responses might be developed.

GPIs have also been used in simulations of past climate, noting the important reservation that GPIs tuned to the current climate will not necessarily give the correct response in a considerably changed climate (of course, the same could be said about climate models, but their representation of the relevant physical processes is more comprehensive that those of GPIs). Korty et al. (2012a, b) addressed this issue for simulations of the climate of the Holocene and the last Glacial Maximum by examining the individual components of the GPIs to determine their response as well. The rationale here is that presumably, even in a changed climate, an increase in vertical wind shear or a decrease in atmospheric moisture content should not lead to an increase in TC numbers unless there were a large change in another variable in a direction expected to be favorable for TC formation. In general, their analysis supported this argument. Note that TC formation is not necessarily expected to decrease in a cooler climate; in fact, during the Last Glacial Maximum (about 26,000 years ago), GCM simulations suggest the opposite (Merlis 2014). The reason is likely related to a general decrease in tropical stability with the lower surface temperatures that occurred then (see Sect. 8.4 below). Yan et al. (2017) attempted to diagnose TC formation from past climate simulations over about the past 1000 years and compared variations in the formation rate with detailed historical records of typhoon incidence from east Asia, but found discrepancies in Taiwan and southern China, illustrating the current limitations of this technique.

Recent research using these tools has even examined the likelihood of TCs on extrasolar planets. Bin et al. (2018) used an atmospheric GCM combined with a slab ocean to simulate the climate of a synchronously-rotating ocean world, similar to conditions for the ocean planets expected to be found in considerable numbers orbiting the small but very numerous M-type stars. Bin et al. (2018) used the GPI approach of Emanuel and Nolan (2004) instead of directly simulating the TCs due to the coarse resolution of their GCM. One could argue again that the statistical parameters for this GPI, being based on Earth's climate, might not be completely valid for the very different climate of a tidally-locked M-star ocean world. It would be preferable to re-run their experiments using a GCM at much finer horizontal resolution so that TCs could be generated directly, and then the analysis would not

have to rely on the GPI technique working well in a different climate. Even so, their approach is novel and shows another potential application of this type of experiment. The relevance for terrestrial climate is that this type of result could be potentially used to say something about the relationship of climate variations or differences in planetary orography to TC formation, although the observations of TCs on extrasolar planets required to confirm these experiments will not be available for many decades, if ever.

Another potential application of the GPI approach is illustrated by Lavender et al. (2018). Here, very long (>1000 year) current climate GCM simulations are analyzed to determine the distribution in the current climate of year-to-year variations in TC formation over the Atlantic basin. Since the GCMs are relatively coarse resolution, their TC climatology is diagnosed using several different GPI representations. An example of this kind of result is shown in Fig. 8.1, for three different GPIs (see Appendix for technical details of several GPIs). Before comparison to the 2005 observations, the variance of these GPIs is rescaled to match the variance and mean of the best track formation rate over the Atlantic, excluding the year 2005, an event that is a clear outlier in the observed record. The results are then compared with the record high year of TC formation in the well-observed recent period since 1944 in the Atlantic, the year 2005 when there were 27 TCs in that basin. The results show that it is unlikely that the TC numbers observed in 2005 would be considerably exceeded over a period of more than 1000 years. This suggests that the year 2005 could be used as a benchmark for the potential maximum TC formation in the Atlantic basin, for risk management purposes.

A recent model that combines the Emanuel seeding method with a GPI approach is that of Lee et al. (2018). Here, the seeding rate for an Emanuel-type seed model is set by the Tippett et al. (2011) GPI, and the seeding locations are randomly specified. The model uses a similar method for generating tracks as Emanuel (2006) but uses a different intensity model, using an efficient autoregressive equation that uses meteorological variables such as PI as inputs (Lee et al. 2015). The model is able to generate a good simulation of many characteristics of observed TC formation patterns and intensity distributions in the current climate. Of interest to the relationship between climate and TCs is that this model is able to simulate the observed bi-modal TC intensity distribution, which further analysis ascribes to the presence of a percentage of TCs that undergo rapid intensification. Note that it is possible that the bimodal distribution may be an artifact of the Dvorak TC intensity estimation technique (Dvorak 1975), which has low resolution at higher TC intensities (Torn and Snyder 2012; Kossin et al. 2013). Nevertheless, the ability of the Lee et al. (2018) model to simulate the bimodal distribution argues for a physical explanation of the bimodality, although this is a considerable modeling challenge.

One potential issue with the GPI approach is that since a GPI is calculated from climate means, it is implicitly assumed that the distribution of formation probability around that mean is known. Presumably, a climate theory of TC formation that related formation to climate mean fields would also implicitly assume such a distribution. This is a potential issue for such a theory because of the stochastic nature of TC formation that takes place at small spatial and time scales. Even so,

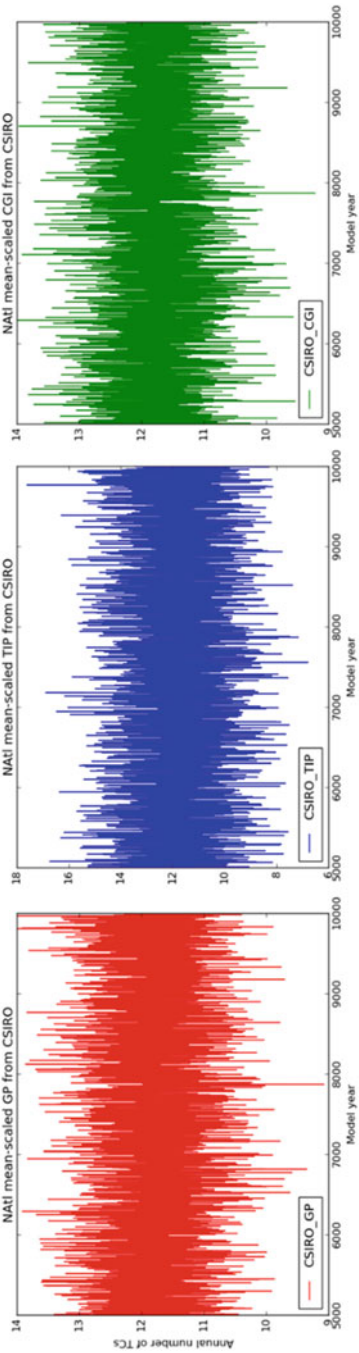

Fig. 8.1 Interannual variability of (left) the Emanuel and Nolan (2004) Genesis Potential (GP), (centre) the Tippett et al. (2011) index (TIP) and (right) the Bruyere et al. (2012) Cyclone Genesis Index (CGI) calculated over a period of 5000 model years

GPIs can capture both the interannual variation of TC numbers in the formation basins as well as the spatial patterns of formation, despite being tuned on global numbers (e.g. Camargo et al. 2007).

Tory et al. (2017) tried a different approach, using climate parameters to investigate the geographical limits on regions of TC formation (see also McGauley and Nolan 2011). Tory et al. (2017) established good relationships between geographical boundaries of TC formation regions and various threshold parameters of climate variables, as expected from previous work, but they also examined the performance of a novel parameter, the south-north (i.e. meridional) gradient of absolute vorticity. The rationale for the use of this variable is its relationship to the onset of barotropic instability, a known criterion for TC formation that refers to the generation of unstable waves by horizontal differences in wind speed and direction (e.g. Ferreira and Schubert 1997; Frank 2008). They combined this with the 850 hPa absolute vorticity, and this new combination was found to be important for defining the equatorward boundary of TC formation. The method of Tory et al. (2017) can both be used as an evaluation method for climate simulations and also for suggesting combinations of variables that might be important in a climate theory of TC formation based on the concept that, for instance, land distribution and amount must be an important factor in determining annual mean TC formation and that variations in land amount and location will cause changes in TC formation rates.

Parenthetically, the influence of land amount could change TC formation rates in unexpected ways. For example, the number of TCs that form annually in the Northern Hemisphere is about double the number in the Southern Hemisphere, despite the fact that the Northern Hemisphere has about five times as much land as the Southern Hemisphere. Naively, one would expect this relationship to be the other way around, since TCs form only over the ocean. One factor that is related to land amount, however, is climatological vertical wind shear in the summer season in each hemisphere, which is when the great majority of TCs form. In the Northern Hemisphere, climatological vertical shear is lower in this season than in the corresponding summer season in the Southern Hemisphere due to the presence of large land masses in the Northern Hemisphere that heats the mid-latitude regions of the Northern Hemisphere. This reduces the meridional temperature gradient and thereby the summer climatological vertical wind shear through the thermal wind relationship. This relationship between Northern Hemisphere land amount and TC formation has not yet been tested in a series of GCM simulations to our knowledge, however. Land regions can also generate precursor disturbances for TCs, such as easterly waves in the Atlantic (e.g. Daloz et al. 2012), thus affecting the climatology of TC formation.

8.4 Theoretical Techniques in Support of Risk Assessment

A discussion of GPIs leads naturally on to the search for more fundamental theoretical concepts that might assist us in understanding and better constraining the relationship between climate and TC formation rates and their geographical

distribution. For example, PI is a well-accepted theory that has been used not only for climate science but also for weather forecasting (DeMaria and Kaplan 1994). There is, however, no equivalent climate theory for TC formation. One possible reason may relate to the processes by which TCs form. TC formation is likely a two-stage process, broadly termed here as aggregation and intensification (see, for instance, Frank 1987). In the aggregation (or genesis) stage, the convective elements undergo a process of merging that creates a larger, more coherent tropical low. In the intensification stage, the tropical low intensifies to a TC. Note that it is likely that the defined observed low-level wind speed threshold for TC formation (about 17 ms^{-1} for winds at an altitude of 10 m) occurs after the start of the intensification stage, so numbers of TCs are likely dictated, to a degree, by PI. In this context, for the 17 ms^{-1} threshold to have a special meaning for a climate theory of TC formation, there would ideally need to be some kind of difference in kind between tropical lows with intensities less than 17 ms^{-1} and TCs with higher intensities. In contrast, there is actually nothing climatologically special about 17 ms^{-1} as a wind speed threshold; this threshold was originally set purely due to the fact that storms with at least this wind speed are defined to have winds of gale force or stronger. Thus, there is likely a need for identification and analysis of tropical depressions (TDs) at an earlier stage of development, during their initial intensification, to gain a more complete picture of the effect of climate on TCs.

Tory et al. (2017) tried doing this but was hampered by the lack of an objective threshold definition for TDs. For instance, the standard Dvorak technique (Dvorak 1975) for deducing TC intensity from the appearance of a circulation feature in a satellite image is vague when defining the various stages of TD development (see also Duvel et al. 2017). Tory et al. (2017) calculate that their TD threshold corresponds roughly to a 10 m wind speed of 12 ms^{-1}, versus about 17 ms^{-1} for the observed TC threshold. Note that this 12 ms^{-1} intensity threshold is the same as that used in the Emanuel seeding methodology discussed above. Tory et al. (2017) investigate the variation in the "failure rate" of these TDs, the percentage of TDs that fail to reach TC status, and find some variations in failure rates between basins. The main variation in failure rate, though, is with latitude; TDs are much more likely to fail to reach TC status poleward of 15° latitude than equatorward of this latitude. At latitudes closer to the equator than 15°, 65–80% of TDs intensify to TCs. Since the interannual and seasonal variation of TDs is also well correlated with that of TCs, this suggests that these TDs are not actually different in kind from TCs, rather just different in intensity. It is important to note, however, that there appears to be clear differences in the effect of vertical wind shear on TDs versus TCs, with shear having a greater effect on TC numbers than on TD numbers. In summary, Tory et al. (2017) found that shear, PI and their barotropic instability diagnostic were related to the TD failure rate, while 850 hPa absolute vorticity and 700 hPa relative humidity were not. They point out that this is consistent with Bruyère et al. (2012), who considered these latter two quantities to be threshold parameters only.

What aspects of TC formation should a climate theory explain? Clearly, any climate theory must have consistent relationships between climate variables and TC formation between basins. This idea was recently investigated by Sharmila and

Walsh (2017), who found that vertical shear has the most consistent relationship to TC formation during the times of the year in each basin where TC formation is a maximum. Low-relative vorticity was also important, whereas relative humidity and potential intensity have more inconsistent relationships between basins. This emphasizes, again, the likely role of relative humidity as only being a threshold parameter for formation. Given the numerous issues yet to be addressed, it is possibly easier at this stage to say what a climate theory of TC formation will not contain. For instance, it will likely not involve a specific tropical wave mechanism, as TCs appear to be able to gain the convection required for formation from many different types of waves and convective disturbances (e.g. Tory and Frank 2010; Patricola et al. 2018).

Insight into the relative roles of aggregation versus intensification can be obtained from idealized simulations of climatological TC formation, whereby models are run with simplified geography or climate to restrict the number of variables that might affect TC formation. Khairoutdinov and Emanuel (2013) show that, in their idealized "TC-world" simulations, the number of TCs decreases with increasing SSTs. Their proposed mechanism is that the convective mass flux decreases due to the fact that precipitation increases considerably slower with SST than does the atmospheric water vapor content, a mechanism that is well accepted (e.g. Held and Soden 2006). Since the TCs become larger and more intense as SST increases, they have more convective mass flux per cyclone, thus leading to a decrease in total numbers due to the decrease in total convective mass flux (see also Sugi et al. 2002; Merlis et al. 2016). This is also accompanied by an increase in tropical stability, a mechanism likely related to a climate theory of TC formation. The "TC-world" experiments of Khairoutdinov and Emanuel (2013) take place in an environment where there are essentially no constraints on TC formation, but even in the real world where such constraints exist (e.g. land, regions of high vertical wind shear, regions of low relative humidity over the oceans), a decrease in overall convective mass flux should still lead to a decrease in TC numbers.

The results of Khairoutdinov and Emanuel (2013) show that self-aggregation of convection, the tendency of large convective systems to agglomerate from smaller ones, is clearly a relevant issue for TC formation in its initial stages (see also Wing et al. 2017). At present, the relative contributions of the likely contributing factors to self-aggregation rates – radiation, surface fluxes, clouds and water vapor – are currently unknown. The fluid mechanical process of vortex merger also clearly plays a role (Montgomery and Smith 2017), but again a quantitative theory related to TC formation rates is lacking.

Some insight into quantitative relationships between these mechanisms and TC formation rate may be obtained from idealized GCM simulations, whereby aspects of terrestrial planetary characteristics are retained but variations in certain climate variables are removed. The results of coordinated experiments (e.g. Walsh et al. 2015) suggest some systematic responses to changes in SSTs and atmospheric CO_2 concentration that are in general agreement with the role of the vertical circulation in changes in TC numbers established by Sugi et al. (2002) and Held and Soden (2006).

A more radical approach, in which all land is removed in the GCM simulation and various SST values are specified, is the "aquaplanet" simulation (Hayashi and Sumi

1986). Ballinger et al. (2015) used some aquaplanet simulations at 50 km resolution to show that the poleward extent of the region of maximum SST was important for rates of TC formation: if this region were further poleward, more TCs were generated. Viale and Merlis (2017) show that the typical response to increase CO_2 alone is a decrease in TC numbers due to weaker vertical circulation and drier air. Chavas et al. (2017) show that for an aquaplanet with uniform tropical-like SSTs and non-zero rotation, TCs migrate towards the poles, giving a much larger incidence of TCs there than in the latitudinally-defined "tropical" regions of such a simulation.

Snapshots from the same time interval of two different aquaplanet runs using the UK Met Office Unified Model, V8.5 are shown in Fig. 8.2 (Pope et al. 2007). Here, the SSTs are specified at 30 °C everywhere (top panel) or 25 °C everywhere (bottom panel). In this simulation, the rotation rate is the same as that of the observed Earth, so the resulting poleward beta drift (Holland 1983) causes a strong concentration of TCs in the higher latitudes. There are noticeably more TCs in the run with the lower SSTs, in agreement with the paleoclimate results of Korty et al. (2012a, b) and Khairoutdinov and Emanuel (2013). These simulations are part of a project that aims to constrain the effects of climate and orography on TC formation rates, through a systematic series of experiments that vary such quantities as SST, land fraction, and vertical stability. Analysis of these simulations is ongoing.

Some more basic theoretical insights might be obtained by contrasting baroclinic instability, the well-established theory of mid-latitude cyclone formation (Charney 1947; Eady 1949), with barotropic instability (a limiting case of baroclinic instability), whose relationship to TC formation is likely (but much less quantitatively) established. Mid-latitude lows act to gradually reduce the meridional temperature gradient via meridional heat transport, and the period of time for this to occur (known as the limit cycle) dictates the lifetime of mid-latitude cyclones. The theory of baroclinic instability also gives the spatial dimensions of mid-latitude cyclones, where the most unstable mode typically is of wavenumber 7 or 8 (that is, a cyclone diameter of 1000–2000 km). Mid-latitude lows form much more frequently than TCs, suggesting a much stronger relationship between formation rate and the available instability in the extratropics than in the tropics. Thus, if we knew a threshold criterion for mid-latitude cyclone formation, since we already know their typical spatial scale, their typical energy production (based on their size and typical integrated wind speeds), and their lifetimes, the annual number of mid-latitude cyclones could be estimated approximately from the current climate conditions in the midlatitudes. No calculation at present is possible for TCs because, although we have some idea of the available energy (as indicated by PI), and we know their typical spatial scales, energy production, and lifetimes, there is no known sufficient climate-related threshold condition for TC formation, whereby satisfaction of this condition would lead to TC formation most of the time. If that were known, it is possible that an estimate of the annual number of TCs could be made from climate conditions. This could be done by noting that the lifetimes of TCs are dictated by the length of time that they typically stay within climatically hospitable regions (Tory et al. 2017), a quantity that can be estimated from their typical speed of movement as dictated by steering winds, beta drift, and the geographical extent of those regions.

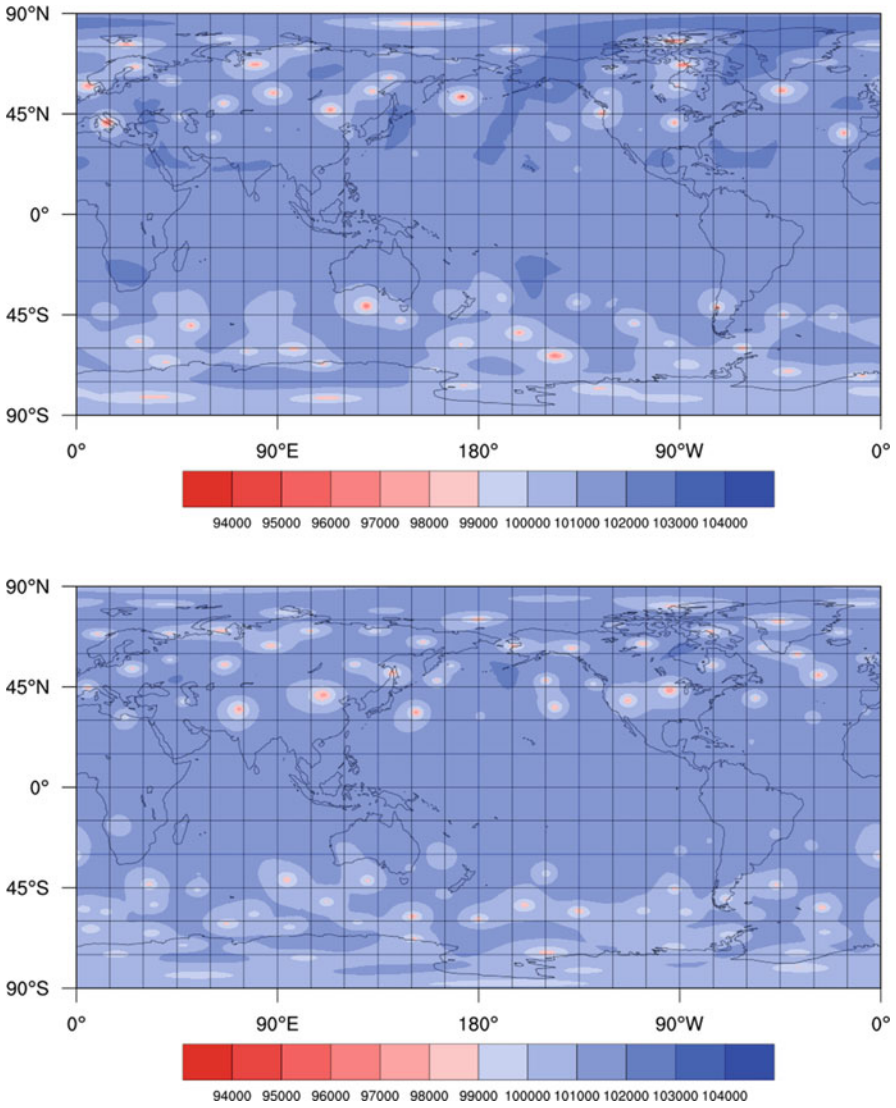

Fig. 8.2 Snapshot of tropical aquaplanet simulations of mean sea level pressure (in Pa) for (top) constant SST of 30 °C; and (bottom) 25 °C. Continental outlines are indicative only and do not represent the actual orography

Discussion of this topic might seem quite esoteric, except for the fact that it has relevance to TC hazard assessment. Developments in a climate theory of TC formation have the potential to provide a more fundamental explanation of year-to-year variations in TC numbers than might be gained purely from statistical relationships, with obvious implications for prediction and analysis.

8.5 Conclusion

The current state of climate models indicates that they can simulate the climatology of intense TCs, but they are very expensive to run. Downscaling approaches can show considerable skill while being more economical to produce results, but they have only been tested against historical storms and there is no guarantee that they can handle global climate change. Statistical methods such as bias correction and the use of GPIs are even more economical and can be useful, but are approximations and have their own uncertainties. While GPIs give a good indication of what climate variables are important for TC formation and have been applied to TC hazard assessment, they do not constitute a theory (neither do GCM simulations). In addition, to be useful in a changed climate, GPIs need to give the same climate response as very high-resolution GCM experiments, and the exact formulation of a GPI required to guarantee that is presently unknown. GCM experiments also need finer resolution, improved model physics, and coupled ocean-atmosphere interaction to improve our confidence that they are achieving the correct response for the effects of climate change on TCs. GCM experiments can be used to gain insight into the relationship between climate and TC formation and, given the recent improvement in the ability of GCMs to simulate the climatology of TCs, this area of research is promising. However, GCMs still do not have simulations of TC climate that are good enough to feed directly into risk models. An analytical theory of TC formation analogous to the established analytical theory of mid-latitude cyclone formation does not exist but would be useful for risk analysis if it were to be developed.

Acknowledgments The author would like to acknowledge funding from Australian Research Council Discovery Projects DP150102272. Funding also has been supplied by the Bermuda Institute of Ocean Sciences' Risk Prediction Initiative (RPI).

Appendix: Formulation of GPIs

Emanuel and Nolan (2004):

$$GP = \left|10^5\eta\right|^{\frac{3}{2}}\left(\frac{H}{50}\right)^3\left(\frac{V_{pot}}{70}\right)^3(1+0.1V_{shear})^{-2}$$

η = absolute vorticity at 850 hPa (s^{-1})
H = Relative humidity at 700 hPa (%)
V_{pot} = potential intensity (m s^{-1}) calculated using a routine provided by Emanuel (http://eaps4.mit.edu/faculty/Emanuel/)
V_{shear} = vertical shear from 850 to 200 hPa (m s^{-1})

Emanuel (2010):

$$GP = |\eta|^3 \chi^{-\frac{4}{3}} \max\left(\left(V_{pot} - 35\right), 0\right)^2 (25 + V_{shear})^{-4}$$

χ = saturation deficit
Tippett et al. (2011):

$$TCS = \exp\left(b + b_\eta \eta + b_H H + b_T T + b_V V + \log(cos\phi)\right)$$

η = clipped absolute vorticity at 850 hPa in 10^5 s^{-1} ($\eta =$ min $(\eta, 3.7)$)
$T = SST - \overline{SST}^{[20^\circ S - 20^\circ N]}$ in °C
ϕ = latitude
H = Relative humidity at 600 hPa (%)
V = vertical shear from 850 to 200 hPa (m s^{-1})

The constants used are those from line 6 of Tippett et al. (2011)'s Table 1 and are those used by Menkes et al. (2012):

$$b = -5.8; b_\eta = 1.03; b_H = 0.05; b_T = 0.56; b_V = -0.15$$

Bruyere et al. (2012):

$$CGI = \left(\frac{V_{pot}}{70}\right)^3 (1 + 0.1 V_{shear})^{-2}$$

Since the CGI does not include a vorticity term to remove TCs that form close to the equator, its values are set to zero between 0 and 5°N.

References

Ballinger AP, Merlis TM, Held IM, Zhao M (2015) The sensitivity of tropical cyclone activity to off-equatorial thermal forcing in aquaplanet simulations. J Atmos Sci 72:2286–2302
Bin J, Tian F, Lin Y, Wang Y (2018) Low probability of tropical cyclones on ocean planets in the habitable zones of M dwarfs. Icarus 299:364–369
Bister M, Emanuel KA (2002) Low frequency variability of tropical cyclone potential intensity 1. Interannual to interdecadal variability. J Geophys Res Atmos 107:4801
Bruyère CL, Holland GJ, Towler E (2012) Investigating the use of a genesis potential index for tropical cyclones in the North Atlantic Basin. J Clim 25:8611–8626
Camargo SJ, Wing AA (2016) Tropical cyclones in climate models. WIRES Clim Chang 7:211–237
Camargo SJ, Emanuel KA, Sobel AH (2007) Use of a genesis potential index to diagnose ENSO effects on tropical cyclone genesis. J Clim 20:4819–4834
Camargo SJ, Tippett MK, Sobel AH, Vecchi GA, Zhao M (2014) Testing the performance of tropical cyclone genesis indices in future climates using the HIRAM model. J Clim 27:9171–9196
Charney JG (1947) The dynamics of long waves in a baroclinic westerly current. J Meteorol 4:136–162

Chavas DR, Reed KA, Knaff JA (2017) Physical understanding of the tropical cyclone wind-pressure relationship. Nat Commun 8:1360
Cobb A, Done J (2017) The use of global climate models for tropical cyclone risk assessment. In: Collins J, Walsh K (eds) Hurricanes and climate change, vol 3. Springer, Dordrecht, pp 167–186
Daloz A-S, Chauvin F, Walsh K, Lavender S, Abbs D, Roux F (2012) The ability of GCMs to simulate tropical cyclones and their precursors over the North Atlantic Main Development Region. Clim Dyn 39:1559–1576
DeMaria M, Kaplan J (1994) A statistical hurricane intensity prediction scheme (SHIPS) for the Atlantic basin. Weather Forecast 9:209–220. https://doi.org/10.1175
Duvel JP, Camargo SJ, Sobel AH (2017) Role of the convection scheme in modeling initiation and intensification of tropical depressions over the North Atlantic. Mon Weather Rev 145:1495–1509
Dvorak VF (1975) Tropical cyclone intensity analysis and forecasting from satellite imagery. Mon Weather Rev 103:420–430
Eady ET (1949) Long waves and cyclone waves. Tellus 1:33–52
Emanuel KA (1986) An air–sea interaction theory for tropical cyclones, part I: steady-state maintenance. J Atmos Sci 43:585–605
Emanuel KA (1988) The maximum intensity of hurricanes. J Atmos Sci 45:1143–1155
Emanuel K (2000) A statistical analysis of tropical cyclone intensity. Mon Weather Rev 128:1139–1152
Emanuel K (2006) Climate and tropical cyclone activity: a new model downscaling approach. J Clim 19:4797–4802
Emanuel KA (2010) Tropical cyclone activity downscaled from NOAA-CIRES reanalysis, 1908–1958. J Adv Model Earth Syst 2. https://doi.org/10.3894/JAMES.2010.2.1
Emanuel K (2017) A fast intensity simulator for tropical cyclone risk analysis. Nat Hazards 88:779–796
Emanuel K, Nolan DS (2004) Tropical cyclone activity and the global climate system. In: Proceedings of 26th AMS Conference on Hurricanes and Tropical Meteorology, No. 10A.2, pp 240–241
Ferreira RN, Schubert WH (1997) Barotropic aspects of ITCZ breakdown. J Atmos Sci 54:261–285
Frank WM (1987) Tropical cyclone formation. In: Elsberry RL (ed) A global view of tropical cyclones. Office of Naval Research, Washington, DC, pp 53–90
Frank WM (2008) What role do tropical cyclones play in the general circulation? In: Proceedings of the 28th Conference on Hurricanes and Tropical Meteorology, 28 April–2 May 2008, Orlando, FL, American Meteorological Society
Gettelman A, Bresch DN, Chen CC, Truesdale JE, Bacmeister JT (2017) Projections of future tropical cyclone damage with a high-resolution global climate model. Clim Chang 7:496
Gray WM (1968) Global view of the origin of tropical disturbances and storms. Mon Weather Rev 96:669–700
Gray WM (1975) Tropical cyclone genesis. Colorado State University, Colorado
Gray WM (1979) Hurricanes: their formation, structure and likely role in the tropical circulation. In: Shaw DB (ed) Meteorology over the tropical oceans. Royal Meteorolgical Soc, Bracknell, pp 155–218
Haarsma RJ, Roberts MJ, Vidale PL, Senior CA, Bellucci A, Bao Q, Chang P, Corti S, Fuckar NS, Guemas V, Von Hardenberg J (2016) High resolution model intercomparison project (HighResMIP v1. 0) for CMIP6. Geosci Model Dev 9:4185–4208
Hayashi Y-Y, Sumi A (1986) The 30–40 day oscillations simulated in an “aqua planet” model. J Meteorol Soc Jpn 64:451–467
Held IM, Soden BJ (2006) Robust responses of the hydrological cycle to global warming. J Clim 19:5686–5699
Holland GJ (1983) Tropical cyclone motion: environmental interaction plus a beta effect. J Atmos Sci 40:328–342

Holland GJ (1997) The maximum potential intensity of tropical cyclones. J Atmos Sci 54:2519–2541
Khairoutdinov M, Emanuel K (2013) Rotating radiative-convective equilibrium simulated by a cloud-resolving model. J Adv Model Earth Syst 5:816–825
Knutson TR, Sirutis JJ, Zhao M, Tuleya RE, Bender M, Vecchi GA, Villarini G, Chavas D (2015) Global projections of intense tropical cyclone activity for the late twenty-first century from dynamical downscaling of CMIP5/RCP4.5 scenarios. J Clim 28:7203–7224
Korty RL, Camargo SJ, Galewsky J (2012a) Variations in tropical cyclone genesis factors in simulations of the Holocene Epoch. J Clim 25:8196–8211. https://doi.org/10.1175/JCLI-D-12-00033.1
Korty RL, Camargo SJ, Galewsky J (2012b) Tropical cyclone genesis factors in simulations of the Last Glacial Maximum. J Clim 25:4348–4365. https://doi.org/10.1175/JCLI-D-11-00517.1
Kossin JP, Olander TL, Knapp KR (2013) Trend analysis with a new global record of tropical cyclone intensity. J Clim 26:9960–9976
Lavender SL, Walsh KJE, Caron L-P, King M, Monkiewicz S, Guishard M, Hunt B, Zhang Q (2018) Estimation of the maximum annual number of North Atlantic tropical cyclones using climate models. Sci Adv 4:eaat6509. Submitted to Science
Lee CY, Tippett MK, Camargo SJ, Sobel AH (2015) Probabilistic multiple linear regression modeling for tropical cyclone intensity. Mon Weather Rev 143:933–954
Lee CY, Tippett MK, Sobel AH, Camargo SJ (2018) An environmentally forced tropical cyclone hazard model. J Adv Model Earth Syst. https://doi.org/10.1002/2017MS001186
Lin II, Black P, Price JF, Yang CY, Chen SS, Lien CC, Harr P, Chi NH, Wu CC, D'Asaro EA (2013) An ocean coupling potential intensity index for tropical cyclones. Geophy Res Lett 40:1878–1882
McGauley MG, Nolan DS (2011) Measuring environmental favorability for tropical cyclogenesis by statistical analysis of threshold parameters. J Clim 24:5968–5997
Menkes CE, Lengaigne M, Marchesiello P, Jourdain NC, Vincent EM, Lefèvre J, Chauvin F, Royer JF (2012) Comparison of tropical cyclogenesis indices on seasonal to interannual timescales. Clim Dyn 38:301–321
Merlis TM (2014). Tropical cyclone frequency in simulations of the Last Glacial Maximum. Available at: https://ams.confex.com/ams/31Hurr/webprogram/Paper244915.html.
Merlis TM, Zhou W, Held IM, Zhao M (2016) Surface temperature dependence of tropical cyclone-permitting simulations in a spherical model with uniform thermal forcing. Geophys Res Lett 43 (6):2859–2865
Miyamoto Y, Bryan GH, Rotunno R (2014) An analytical model of maximum potential intensity for tropical cyclones incorporating the effect of ocean mixing. Geophys Res Lett 107:4801
Montgomery MT, Smith RK (2017) Recent developments in the fluid dynamics of tropical cyclones. Ann Rev Fluid Mech 49:541–574
Murakami H, Wang Y, Yoshimura Y, Mizuta R, Sugi M, Shindo E, Adachi Y, Yukimoto S, Hosaka M, Kusunoki S et al (2012) Future changes in tropical cyclone activity projected by the new high-resolution MRIAGCM. J Clim 25:3237–3260
Murakami H, Vecchi GA, Underwood S, Delworth TL, Wittenberg AT, Anderson WG, Chen JH, Gudgel RG, Harris LM, Lin SJ, Zeng F (2015) Simulation and prediction of category 4 and 5 hurricanes in the high-resolution GFDL HiFLOR coupled climate model. J Clim 28:9058–9079
Patricola CM, Saravanan R, Chang P (2018) The response of Atlantic tropical cyclones to suppression of African easterly waves. Geophys Res Lett 45:471–479. https://doi.org/10.1002/2017GL076081
Pope V et al (2007) The Met Office Hadley Centre climate modelling capability: the competing requirements for improved resolution, complexity and dealing with uncertainty. Philos Trans R Soc A365:2635–2657
Sharmila S, Walsh KJE (2017) Impact of large-scale dynamic versus thermodynamic climate conditions on contrasting tropical cyclone genesis frequency. J Clim 30:8865–8883
Simpson RH, Saffir H (1974) The hurricane disaster potential scale. Weatherwise 27:169

Sugi M, Noda A, Sato N (2002) Influence of the global warming on tropical cyclone climatology: an experiment with the JMA global model. J Meteorol Soc Jpn 80:249–272
Sugi M, Murakami H, Yoshida K (2016) Projection of future changes in the frequency of intense tropical cyclones. Clim Dyn 49:619–632. https://doi.org/10.1007/s00382-016-3361-7
Swanson KL (2008) False causality between Atlantic hurricane activity fluctuations and seasonal lower atmospheric wind anomalies. Geophys Res Lett 35:L18807
Tang B, Emanuel K (2012) Sensitivity of tropical cyclone intensity to ventilation in an axisymmetric model. J Atmos Sci 69:2394–2413
Tippett MK, Camargo SJ, Sobel AH (2011) A Poisson regression index for tropical cyclone genesis and the role of large-scale vorticity in genesis. J Clim 24:2335–2357
Torn RD, Snyder C (2012) Uncertainty of tropical cyclone best-track information. Weather Forecast 27:715–729
Tory KJ, Frank WM (2010) Tropical cyclone formation. In: JCL C, Kepert JD (eds) Global perspectives on tropical cyclones; from science to mitigation. World Scientific, Singapore, pp 55–92
Tory KJ, Ye H, Dare RA (2017) Understanding the geographic distribution of tropical cyclone formation for applications in climate models. Clim Dyn 50:2489–2512
Viale F, Merlis TM (2017) Variations in tropical cyclone frequency response to solar and CO2 forcing in aquaplanet simulations. J Adv Model Earth Syst 9:4–18
Villarini G, Vecchi GA (2012) Twenty-first-century projections of North Atlantic tropical storms from CMIP5 models. Nature Clim Chang 2:604
Walsh KJE, Camargo SJ, Vecchi GA, Daloz AS, Elsner J, Emanuel K, Horn M, Lim Y-K, Roberts M, Patricola C, Scoccimarro E, Sobel AH, Strazzo S, Villarini G, Wehner M, Zhao M, Kossin J, LaRow T, Oouchi K, Schubert S, Wang H, Bacmeister J, Chang P, Chauvin F, Jablonowski C, Kumar A, Murakami H, Ose T, Reed KA, Saravanan R, Yamada Y, Zarzycki CM, Vidale P-L, Jonas JA, Henderson N (2015) Hurricanes and climate: the U.S. CLIVAR working group on hurricanes. Bull Am Meteorol Soc 96:997–1017
Walsh KJE, McBride JL, Klotzbach PJ, Balachandran, Camargo SJ, Holland G, Knutson TR, Kossin J, Lee TC, Sobel A, Sugi M (2016) Tropical cyclones and climate change. WIRES Clim Chang 7:65–89. https://doi.org/10.1002/wcc.371
Wehner M, Reed KA, Zarzycki CM (2017) High-resolution multi-decadal simulation of tropical cyclones. In: Collins J, Walsh K (eds) Hurricanes and climate change, vol 3. Springer, Dordrecht, pp 187–212
Wing AA, Emanuel K, Holloway CE, Muller C (2017) Convective self-aggregation in numerical simulations: a review. Surv Geophys 38:1173–1197
Yan Q, Wei T, Zhang Z (2017) Variations in large-scale tropical cyclone genesis factors over the western North Pacific in the PMIP3 last millennium simulations. Clim Dyn 48:957–970
Yoshida K, Sugi M, Mizuta R, Murakami H, Ishii M (2017) Future changes in tropical cyclone activity in high-resolution large-ensemble simulations. Geophys Res Lett 44:9910–9917

Chapter 9
Global Tropical Cyclone Damages and Fatalities Under Climate Change: An Updated Assessment

Laura A. Bakkensen and Robert O. Mendelsohn

Abstract Although it is well known that climate change will alter future tropical cyclone characteristics, there have been relatively few studies that have measured global impacts. This paper utilizes new insights about the damage caused by tropical cyclones from Bakkensen and Mendelsohn (J Assoc Env Res Econ 3:555–587, 2016) to update the original methodology of Mendelsohn et al. (Nat Clim Change 2:205–209, 2012). We find that future cyclone losses are very sensitive to both adaptation and development. Future development (higher income) is predicted to sharply reduce future fatalities. However, damage may take two distinct paths. If countries follow the United States and adapt very little, damage is predicted to increase proportionally with income, rising 400% over the century. However, if development follows the remaining OECD countries, which have done a lot of adaptation, future cyclone damage will only increase slightly.

Keywords Tropical cyclone damage and fatalities · Adaptation

9.1 Motivation

Tropical cyclones (hurricanes, typhoons) cause significant damage to many coastal communities across the globe (Shultz et al. 2005; World Bank 2010; IPCC 2012) with average losses of $26 billion per year (Mendelsohn et al. 2012). It is well acknowledged that future cyclones will be affected by climate change (Emanuel 2005; Ranson et al. 2014). Although the number of hurricanes may not increase, it is expected that the intensity of the largest storms may well increase (Emanuel 2005;

L. A. Bakkensen (✉)
University of Arizona School of Government and Public Policy, Tucson, AZ, USA
e-mail: laurabakkensen@email.arizona.edu

R. O. Mendelsohn
Yale University School of Forestry and Environmental Studies, New Haven, CT, USA
e-mail: robert.mendelsohn@yale.edu

J. M. Collins, K. Walsh (eds.), *Hurricane Risk*, Hurricane Risk 1,
https://doi.org/10.1007/978-3-030-02402-4_9

IPCC 2012; Ranson et al. 2014). This may have especially harmful consequences because damage increases nonlinearly with intensity (Hallegatte 2007; Pielke 2007; Narita et al. 2009; Nordhaus 2010; Bakkensen et al. 2018). The potential impacts of tropical cyclones can be a major factor in the social cost of carbon depending on how quickly tropical cyclone damage rises (Pearce 2003; Stern 2007; Tol 2008). Ranson et al. (2014) provides an excellent review of the current state of future tropical and extra-tropical cyclone damage estimates.

Many initial studies of tropical cyclone damage assumed that global cyclones would uniformly increase in intensity (Pielke 2007; Narita et al. 2009; Nordhaus 2010). However, climate change is likely to lead to much more complicated changes in future tropical cyclones (Emanuel et al. 2008; IPCC 2013; Walsh et al. 2016). There is some evidence that only larger storms will get stronger (Emanuel et al. 2008). There is also evidence that storm intensity may vary by ocean basin (Emanuel et al. 2008; IPCC 2012). One advantage of the Tropical Cyclone Integrated Assessment Model (TCIAM) is that the model captures alternative predictions of how cyclones might change in each basin (Mendelsohn et al. 2012). This model used simulated cyclone data to track cyclone intensity, position, and frequency in each basin in alternative climate scenarios so that it could predict how these changes might affect human communities.[1]

However, an important weakness of the TCIAM is that the damage function was heavily dependent on outcomes in the United States (Nordhaus 2010; Dinan 2017). At the time the model was built, the only available damage functions were based on American damage. New empirical research has broadened damage estimates to capture tropical cyclone impacts on not just the United States, but also other wealthy countries and the rest of the world (Bakkensen and Mendelsohn 2016). This paper explores how these new damage estimates alter the results of the original TCIAM.

The new damage research examines how tropical cyclone damage depends not only on storm intensity, but also on the income and the population density of the place that is struck by each storm (Bakkensen and Mendelsohn 2016). The results reveal that the damage caused by storms that hit the United States increase proportionally with income and increase very rapidly with intensity. The storms that hit other wealthy countries, in contrast, increase very slowly with income and are much less sensitive to intensity. Holding everything else constant, a storm that hits the United States causes ten times more damage than a storm that hits other wealthy countries. Looking across all countries, higher income monotonically decreases fatalities but has a hill-shaped effect on damage. As countries go from poor towards middle class, damage rises, but as they enter middle class, damage starts to fall (with the exception of the United States). Damage also depends on whether the region that is hit by the storm is urban or rural. Surprisingly, damage and fatalities do not rise

[1]Hallegatte (2007) also utilizes simulation data to estimate future cyclone damages, thereby capturing sophisticated underlying distribution dynamics.

with population density because most urban centers do more to protect themselves. Additional literature on damage and fatality determinants identifies the importance of factors including institutions and economic growth (see reviews by Cavallo and Noy 2011; Kousky 2014). Similar to the climate change analyses, there are also many country-specific studies on damage and fatality determinants that we do not review here.

The chapter proceeds as follows: the theoretical foundations are explained in Sect. 9.2. Section 9.3 describes the empirical methodology followed by a list of data sources in Sect. 9.3.1. Section 9.4 presents and discusses the results, and Sect. 9.5 offers concluding remarks. The References and Appendix sections are presented at the end.

9.2 Theoretical Foundation

The theoretical foundation is based on Mendelsohn et al. (2012). In this paper, the authors note that the economic damage from a tropical cyclone (D) is equal to the total of all property losses caused by the tropical cyclone. A parallel theory follows for fatalities as well. The expected value of damages from tropical cyclones can be calculated by:

$$E[D] = \sum_j \sum_j \pi\left(X_{ij}, C\right) D\left(X_{ij}, Z_i\right) \tag{9.1}$$

where $\pi(X_{ij}, C)$ is the probability that tropical cyclone j will make landfall at location i, given tropical cyclone characteristics X and climate conditions C. $D(X_{ij}, Z_i)$ represents the damages from tropical cyclone j at location i, given tropical cyclone characteristics X_{ij} and local socioeconomic conditions Z_i. Expected damages are a summation of the probability of a landfall at a given location multiplied by the damages from the tropical cyclones, summed across all locations and tropical cyclones. Atmospheric experts are key to estimating the probability function, while economists specialize in the damages portion (Mendelsohn et al. 2012).

The impact of socioeconomic change, or a change in human communities from current socioeconomic conditions, $Z_{0,}$ to new socioeconomic conditions, Z_1, while holding climate fixed at level C_0, on tropical cyclone damages can be calculated by:

$$SC = E[D(Z_1, X(C_0))] - E[D(Z_0, X(C_0))] \tag{9.2}$$

which is the difference between the expected damage of each society, holding all other factors constant.

The impact of climate change, or a change in atmospheric conditions from current climate, $C_{0,}$ to a new climate, C_1, on tropical cyclone damages can be calculated by:

$$CC = E[D(Z_1, X(C_1))] - E[D(Z_{1,} X(C_0))] \tag{9.3}$$

which is the difference between the expected damages of each climate holding all other factors constant, including socioeconomic conditions at their future level.

9.3 Methodology

We start with the insights about tropical cyclone damage and fatality functions gained from global data (Bakkensen and Mendelsohn 2016). We conduct a few additional analyses using ordinary least squares regressions of historical global hurricane and socioeconomic panel data. These new damage and fatality functions capture the heterogeneity of outcomes across levels of development. We estimate separate coefficients in the damage function for the United States, for the other wealthy countries of the Organization of Economic Cooperation and Development (OECD), and for Non-OECD countries (Bakkensen and Mendelsohn 2016).[2] The damage function has a log-log functional form to account for the count-data nature of the dependent variables. This functional form is easy to interpret and easy to incorporate into the integrated assessment model. The damage function of tropical cyclones is:

$$D_{ij} = \beta_0 + \beta_1 X_{ij} + \beta_2 Z_{ij} + \varepsilon_{ij} \tag{9.4}$$

where D_{ij} is the tropical cyclone damage from storm j in country i. X_{ij} represents the tropical cyclone intensity (either the minimum sea level barometric pressure (MSLP) or the maximum sustained wind speed upon landfall) as well as distance of closest approach of the cyclone (Mendelsohn et al. 2012; Bakkensen and Mendelsohn 2016).[3] Z_{ij} represents a vector of socioeconomic variables describing the conditions in location i where the cyclone j landed, and includes the average country-level population density and per capita income. We estimate this equation for a sample of all countries and for a sample of just the United States, all other rich countries

[2]In our dataset, the following is the fraction of OECD country landfalls by member state: Australia (11.7%), Canada (2.26%), Japan (26.8%), South Korea (10.6%), New Zealand (1.13%) and the United States (45.7%). France, Germany, Ireland, and the United Kingdom together receive 1.9% of OECD cyclone landfalls.

[3]If a tropical cyclone does not make landfall in a country and damages were observed in the historical evidence, characteristics were used from the storm when it was at its closest point to the given country.

(members of the Organization for Economic Cooperation and Development (OECD) excluding the United States), and a sample of other countries (Non-OECD).

Following Bakkensen and Mendelsohn (2016), we estimate the following log-log tropical cyclone fatality function:

$$F_{ij} = \alpha_0 + \alpha_1 X_{ij} + \alpha_2 Z_{ij} + u_{ij} \tag{9.5}$$

where F_{ij} is a record of tropical cyclone fatalities from storm j in country i. Similar to the damage function, we include cyclone intensity characteristics (MSLP or wind speed) and distance of closest approach of the cyclone, as well as socioeconomic characteristics (population density and per capita income). We estimate this regression on all countries. We also estimate the regression for all OECD countries (including the US) and for Non-OECD countries. We combine the United States and other OECD countries in the fatality regression because there is no difference in fatality regression for the United States and other OECD countries. A fatality function using a negative binomial estimator was found to have qualitatively similar results as the log-log functional form employed here (Bakkensen and Mendelsohn 2016).

The underlying emission scenario in all model runs is the IPCC AR4 A1B emissions scenario (IPCC 2007) stabilizing carbon dioxide equivalent atmospheric concentrations at 720 ppm by the year 2100 (Emanuel et al. 2008).[4] The emissions scenario is then translated to changes in global climate through four general circulation models: CNRM (Gueremy et al. 2005), ECHAM (Cubasch et al. 1997), GFDL (Manabe et al. 1991), and MIROC (Hasumi and Emori 2004).[5] By exploring alternative climate models, the TCIAM provides the reader with a sense of the uncertainty coming from the climate forecasts.

Simulated storms are randomly seeded across the globe and then allowed to develop and move by the cyclone simulator. Each track contains the simulated cyclone location and characteristics at 6-h intervals for the lifetime of the storm. A total of 5000 tracks are simulated for the Atlantic basin and 3000 for each of the Western and Eastern Pacific, Indian Ocean, and Southern Hemisphere basins, for each of four climate models, for both current (1980–2000) and future (2080–2100)

[4]This emission scenario is similar to RCP 6.0 in IPCC (2013).

[5]The baseline simulated tracks reflect climate from 1980 to 2000. Using a more severe climate change assumption (IPCC AR5 RCP8.5), Emanuel (2013) finds only minor increases in cyclone power from 1995 to 2015, thus these tracks are still arguably a relevant baseline for the climate from 2000 to 2020. Climate signals can take up to a few decades to impact cyclones given the complex responses across ocean and atmosphere dynamics. In addition, by employing these simulation tracks, we can directly compare across the Mendelsohn et al. (2012) earlier results and the present results. All differences between these two papers are driven by assumptions of the damage caused by each simulation track since the tracks have not changed.

climate, resulting in a total of 136,000 storms. The TCIAM then calculates when a simulated cyclone track intersects with land. The intensity of the storm and the location of landfall is then recorded for that storm. Socioeconomic characteristics of that location are matched with the storm.

Cyclone outcomes in each basin are predicted for both the current climate and future climates for all storms. Note that many storms do not make landfall and therefore cause no damage. The predictions of cyclones in the current climate are similar to observed outcomes in all but the GFDL climate model (Emanuel et al. 2008).

We then calculate the consequence of socioeconomic change (population and income) on future baseline cyclone damage and fatality, holding climate constant at its current level. We then examine how changes in cyclones caused by climate change alter future cyclone damage and fatalities. That is, we compare the future outcome with the current climate with the future outcome with the new climate, all at the future baseline income and population. The impact of climate change is the difference between the expected outcome from the future climate and the current climate, given future baseline socioeconomic projections.

9.3.1 Data

The analysis utilizes data from multiple sources. The first part of the analysis relies on country-level historical tropical cyclone damage and fatality data, as well as affiliated historical country population and income data. Data on tropical cyclone damages and fatalities are from Bakkensen and Mendelsohn (2016) and the sources, processing, and considerations of measurement error are more fully explained and explored in the previous paper. Altogether, more than 1400 landfalls are included from 1960 to 2010 and account for approximately $0.75 trillion in damages and 400,000 fatalities. Note that this represents the full history of storms for which damage or fatalities are publicly recorded and can be linked with cyclone and local socioeconomic data. Damage and fatality reports are obtained from EM-DAT, the International Disaster Database managed by the Center for Research on the Epidemiology of Disasters, as well as Nordhaus (2010) for the United States. The EM-DAT database includes information on over 17,000 natural and technological disasters, and is sponsored in part by the United Nations and United States Agency for International Development. Data on historical country population and income data are gathered from the Penn World Table v7.1, the USDA ERS International Macroeconomic Data, the CIA World Factbook, and Columbia University's CIESIN's Gridded Population of the World v3. Further, we collect local data at the county-level for six large countries across the globe, including Australia, China, India, Japan, Philippines, and United States. In addition, we collect data at the state

level for Mexico. Future Gross Domestic Product (GDP) by country are projected from current (real observed) levels assuming a 2% constant growth rate for highly developed countries, 2.7% for transitioning countries, and 3.3% for developing countries (Mendelsohn et al. 2012). Projections of population are compiled by the United Nations (2018). GDP per capita are estimated by the ratio of future GDP to future population. We assume land area is constant over time to estimate population density.

Historical tropical cyclone data are collected from several sources including the National Oceanic and Atmospheric Administration's International Best Track Archive for Climate Stewardship (IBTrACS; Knapp et al. 2010), the U.S. Navy's Joint Typhoon Warning Center's Tropical Cyclone Reports, and Nordhaus (2010). These sources include variables such as location, wind speed, and minimum barometric pressure at 6-h intervals for each hurricane since the mid-1800s (NOAA 2010). Affiliated tropical cyclone characteristics from these sources were matched by hand with the country level damages data and affiliated socioeconomic data to complete the historical data set (Bakkensen and Mendelsohn 2016). Simulated storm tracks are detailed in Sect. 9.3.

9.4 Results

9.4.1 Historical Global Damage and Fatality Functions

In this section, we present and discuss our historical damage and fatality functions. Note that these regressions mirror the work of Bakkensen and Mendelsohn (2016) in their Sect. 3.5 (including Table 7) for damages and their Appendix Section F (including Table 16) for fatalities. However, in this analysis, we present all three specifications (all countries, OECD versus Non-OECD, and USA versus Non-USA OECD versus Non-OECD) in this section and in the Appendix.

Table 9.1 presents our historical global damage functions partitioned between United States, OECD, and Non-OECD countries for both minimum sea level pressure in columns 1 through 3, respectively, and maximum wind speed in columns 4 through 6, respectively. Appendix Table 9.7 presents the results for all countries and the OECD versus Non-OECD specifications for both minimum pressure and wind speed. Due to the log-log functional form, the estimated coefficients are elasticities (the percent change in damage or fatalities for a percent change in the explanatory variable). Looking first at the socioeconomic coefficients, we find the United States to be significantly different than the rest of the world. Specifically, we find the estimated income coefficient of 1.15 in the pressure specification and 1.64 in the wind specification, indicating that damages scale at least proportionately with economic growth. The Non-OECD countries have a lower income elasticity of

Table 9.1 Historical damage functions

	(1)	(2)	(3)	(4)	(5)	(6)
	Ln damages	Ln damages	Ln damages	Ln damages	Ln damages	Ln damages
	MSLP	MSLP	MSLP	Wind	Wind	Wind
	USA	OECD (non-USA)	Non-OECD	USA	OECD (non-USA)	Non-OECD
Ln income per capita	1.148**	−0.624	0.285***	1.636***	−0.459	0.229**
	(0.577)	(0.472)	(0.0976)	(0.607)	(0.579)	(0.0991)
Ln population density	−0.300*	0.298***	0.0980	−0.342**	0.309**	0.0677
	(0.162)	(0.0821)	(0.0783)	(0.169)	(0.137)	(0.0776)
Ln MSLP	−84.75***	−34.35***	−23.70***			
	(9.254)	(12.45)	(3.631)			
Ln wind				5.069***	2.005**	1.425***
				(0.616)	(1.005)	(0.235)
Ln distance	−0.135	−0.690***	−0.351***	−0.0339	−0.680***	−0.322***
	(0.271)	(0.123)	(0.0406)	(0.247)	(0.132)	(0.0406)
Constant	592.1***	260.0***	177.9***	−17.07**	13.88**	9.737***
	(63.37)	(86.73)	(25.03)	(7.245)	(6.806)	(1.227)
Observations	108	95	653	110	81	652
R-squared	0.498	0.334	0.171	0.446	0.315	0.155

Standard errors in parentheses. ***p < 0.01, **p < 0.05, *p < 0.1. Note that these regression results are identical to the specification in estimation Eq. 9.4 but are formatted as separate regressions here for ease of presentation and comparison

between 0.23 and 0.29. The income elasticity for the other OECD countries is less than one, but not significantly different from zero, implying that damage does not increase as their incomes rise. This is a striking difference compared to the United States. It is also important to note that damages do not scale proportionately with population density, meaning damages are not much larger, and in some cases lower, in highly urban areas.[6] This could be reflective of better building codes, or higher resilience in cities relative to more sparsely populated rural regions.

Turning to the cyclone characteristic coefficients, we again find the United States to be a large outlier in terms of damage, with damage scaling to the –84th power of pressure and the 5th power of wind speed. This is much larger than the intensity coefficients for other OECD and Non-OECD countries. For example, damage increases with the square of wind speed in other OECD countries and 1.4 times

[6]This finding is empirically tested and discussed in Bakkensen and Mendelsohn (2016). In their analysis, they estimate damage and fatality functions using country-level data and, in a separate regression, county-level data for six large countries (plus Mexico at the state level). The results are qualitatively similar across the two geographic scales yet have important nuance to the interpretation. The country-level analysis examines the differences driven by more densely populated versus less densely populated countries. The county-level analysis explores the differences between urban and rural locations hit by storms.

Table 9.2 Historical fatality functions

	(1)	(2)	(3)	(4)
	Ln fatalities	Ln fatalities	Ln fatalities	Ln fatalities
	MSLP	MSLP	Wind	Wind
	OECD	Non-OECD	OECD	Non-OECD
Ln income per capita	−1.223***	−0.758***	−1.257***	−0.743***
	(0.184)	(0.0564)	(0.191)	(0.0580)
Ln population density	0.247***	0.159***	0.246***	0.107**
	(0.0465)	(0.0418)	(0.0546)	(0.0427)
Ln MSLP	−9.356**	−9.047***		
	(4.599)	(2.235)		
Ln wind			0.628**	0.511***
			(0.312)	(0.136)
Ln distance	−0.155***	−0.187***	−0.156***	−0.187***
	(0.0454)	(0.0240)	(0.0455)	(0.0248)
	78.15**	70.90***	11.59***	6.746***
	(31.87)	(15.40)	(2.393)	(0.730)
	172	848	166	842
	0.327	0.247	0.333	0.232

Standard errors in parentheses. ***p < 0.01, **p < 0.05, *p < 0.1. Note that these regression results are identical to the specification in estimation Eq. 9.5 but are formatted as separate regressions here for ease of presentation and comparison

wind speed in Non-OECD countries. Most of the literature assumes damage increases with the cube of wind speed. Finally, as expected, we find that the closer a cyclone comes to land, the larger the damages, all else equal. Using an F-Test comparing the joint equivalency of all estimated coefficients across the models, we can reject that the USA is the same as OECD and Non-OECD countries at the 0.001% level. We find the OECD to be different from Non-OECD countries at the 2.5% level. Thus, we find systematic differences in cross-country determinants of cyclones damage.

Table 9.2 presents the results from our global fatality functions partitioned by OECD and Non-OECD countries, with minimum sea level pressure in columns 1 and 2, and maximum wind speed in columns 3 and 4. We find the United States and the OECD fatality coefficients are not statistically different, so we combine the two samples in the fatality function (Bakkensen and Mendelsohn 2016). The socio-economic coefficients of fatalities resemble the previous literature (e.g., Kahn 2005; Bakkensen and Mendelsohn 2016). Higher income lowers fatalities especially in more developed countries. Wealthier countries place a high value on human life and do a lot to reduce fatalities (Fankhauser and McDermott 2014).[7] While we find fatalities to increase with population density, fatalities do not scale proportionately with increases in population density. Cities are able to protect human life more

[7]We leave empirical exploration of the efficiency versus demand hypothesis for future work.

Table 9.3 Current and future cyclone damage from socioeconomic change by 2100 ($ billions)

		3 regions model		All countries model	
	Current	Future baseline damages	% increase	Future baseline damages	% increase
USA	15.3	46.2	201.7%	30.4	99.0%
(Non-USA) OECD	3.6	0.8	−78.8%	10.0	176.4%
Non-OECD	6.7	12.9	92.2%	18.2	171.4%
Total	**25.6**	**59.8**	**133.6%**	**58.6**	**128.8%**

Column 1 presents summary statistics for current average annual damages (in $ Billions) across the three (USA, Non-USA OECD, and Non-OECD) regions. The second column presents the future baseline damage assuming current climate and future projections of socioeconomic factors. Column 3 states the percent increase between columns 1 and 2. This is our preferred specification. Columns 4 and 5 mirror the results of columns 2 and 3 except using the all countries regression model to value the simulated cyclone landfalls

effectively than rural areas (Bakkensen and Mendelsohn 2016).[8] Turning to cyclone characteristics, we find fatalities increase with the –9th power of pressure and the 0.5th or 0.6th power of wind speed. We do not find statistically significant differences in the coefficient of intensity across OECD and Non-OECD countries. However, there is a significant difference in the coefficients of the socioeconomic coefficients between the OECD and Non-OECD regressions at the 0.001% level.

9.4.2 Socioeconomic Change Impact on Tropical Cyclone Damages and Fatalities

Tropical cyclones currently lead to about $26 billion in damages, on average, across the globe each year (Mendelsohn et al. 2012). However, the damage varies a great deal across space with the United States, accounting for approximately 60% of global annual damages despite only receiving an average of two landfalls per year (NHC 2010). The other OECD countries suffer 14% of damage and the 86 Non-OECD countries and territories account for $6.7 billion (26%) of global damage.

We first assess the impact of future socioeconomic change on projected cyclone damage and fatalities, assuming that the world's climate remains unchanged. The future will be a much richer and more populated world. In Table 9.3, we calculate how much tropical cyclone damage would change simply because of these future socioeconomic changes given the minimum pressure damage model in Tables 9.1 and 9.2. We compare the results using a single damage function for the whole globe and a separate damage function for the United States, Non-US OECD countries, and

[8] Bakkensen and Mendelsohn (2016) find evidence in heterogeneity of damages across urban versus rural locations. We leave exploration of the specific relationship for future work.

Non-OECD countries. The results of the two models lead to a very similar aggregate prediction of global damage in 2100 of almost $60 billion per year. However, the distribution of damage changes a lot. The single damage function for the world projects the future damage in the United States would increase by almost 100%, and the damage in the rest of the world would rise by 175%. With the three-region model, the United States future damage rises 200% to $46 billion/year. The other OECD country damage falls to 20% of its former level while Non-OECD damage doubles. China, India, and the Philippines' future losses will be approximately 125% more than today.

This analysis does not account for the cost of adaptive measures that many countries might take to reduce storm damage and is not meant to be a welfare analysis. Nonetheless, the results highlight the potential for countries to significantly decrease their losses as they develop. One interesting question for Non-OECD countries is whether to follow the no adaptation path of the United States or the adaptation path of other OECD countries as they develop.

Sensitivity analysis is critical in validating climate-economy models (Burke et al. 2015; Milner and McDermott 2016). Thus, we re-run our model using different valuation assumptions. Using wind instead of minimum sea level pressure, the story is qualitatively similar, with damages increasing in the "all countries model" by approximately 80% for the United States and between 140% and 150% for the rest of the world. Turning to the all countries model, the wind model estimates similar results for OECD and Non-OECD countries when compared with the pressure results, with losses decreasing for the former by approximately 70% and increasing for the latter by the same magnitude. However, given the larger income elasticity for the United States in the wind model relative to the pressure model, the wind model estimates future damage due to socioeconomic change alone of more than $153 billion/year, a 900% increase from the current levels. All these estimates assume that damage will be truncated at complete destruction of the capital stock, which we operationalize as $1 trillion for a single landfall.[9] Relaxing this truncation assumption only impacts estimates for the United States. In the three countries pressure model, losses would increase by about 400%, instead of the estimated 200% in Table 9.3. We also compare these results with the sensitivity analysis originally performed by Mendelsohn et al. (2012). In their analysis, they find future damage is most sensitive to assumptions of the estimated income elasticity, and less so to the population density elasticity. We find this in our results as well for the all countries versus three regions model, the latter of which leads to the largest spread in future damage projections. The model sensitivity is larger than the sensitivity to projections of future income and population. Additional sensitivity results are presented below for climate change.

[9]The truncation assumption is an estimate of the maximum damage a single future cyclone could destroy. We calculate it as six time the losses of the most damaging cyclone to date (Hurricane Katrina at approximately $165 billion in losses, NCEI 2018).

Table 9.4 Current and future cyclone fatalities under socioeconomic change

		2 regions model		All countries model	
	Current	Future baseline fatalities	% increase	Future baseline fatalities	% increase
OECD	155	11	−92.83%	46	−70.37%
Non-OECD	8033	2116	−73.66%	2583	−67.85%
Total	**8187**	**2127**	**−74.02%**	**2628**	**−67.90%**

Column 1 presents summary statistics for current average annual fatalities across the three (USA, Non-USA OECD, and Non-OECD) regions. The second column presents the future baseline fatalities assuming current climate and future projections of socioeconomic factors. Column 3 states the percent increase between columns 1 and 2. This is our preferred specification. Columns 4 and 5 mirror the results of columns 2 and 3 except using the all countries regression model to value the simulated cyclone landfalls

Table 9.4 presents the results for the impact of socioeconomic change on future cyclone fatalities. Here, our preferred model combines the United States and other OECD countries. We compare this model with a model that combines all countries. The "all countries model" projects a 68% decrease in overall fatalities and not much difference between regions. The two regions model predicts a larger effect with OECD fatalities falling from 155 to approximately 11 per year, and Non-OECD countries fatalities falling from 8000 to 2000 per year.[10, 11] The qualitative fatality results are similar whether one uses wind or minimum pressure.

9.4.3 Climate Change Impact on Global Tropical Cyclone Damages and Fatalities

We now evaluate the effect of climate change given these future baseline impacts from population and economic development. We again compare the "all countries model" with the more spatially explicit damage and fatality functions. Changes in losses are now due solely to changes in cyclone characteristics, including the frequency of hits and especially intensity. The cyclone intensity coefficient coupled with changes in cyclone intensity estimates from the four general circulation models are the key determinants in these projections.

[10]Note that we include Bangladesh and Myanmar, two high fatality outlier countries, in the current annual fatality statistic.

[11]We note that we use the same underlying income and population projections across both the damage and fatality estimates. Thus, the difference is driven by the estimated income and population density elasticities across the damage versus fatality functions across the outcomes. For the United States, damages increase sharply because they scale proportionately with GDP growth whereas fatalities decrease with development.

Table 9.5 Future cyclone damage with climate change (USD billions/year)

	Future baseline	CNRM	ECHAM	GFDL	MIROC	Average
All countries model						
USA	30.4	37.5	34.3	52.6	28.7	38.3
(Non-USA) OECD	10.0	10.7	11.3	8.8	9.3	10.0
Non-OECD	18.2	19.6	18.4	22.2	18.6	19.7
Total	**58.6**	**67.7**	**64.1**	**83.6**	**56.6**	**68.0**
3 regions model						
USA	46.2	79.3	86.4	97.5	41.6	76.2
(Non-USA) OECD	0.8	0.8	0.9	0.8	0.7	0.8
Non-OECD	12.9	13.3	12.9	14.2	13.2	13.4
Total	**59.8**	**93.3**	**100.2**	**112.5**	**55.5**	**90.4**

Column 1 presents summary statistics for the future average annual baseline damages – assuming future socioeconomic conditions but current climate conditions – across the three (USA, Non-USA OECD, and Non-OECD) regions. The next four columns present average annual future damages assuming future socioeconomic and climate conditions. The final column presents the average across the four models. All values are in real 2008 Billions of USD

The hurricane model across the four climate scenarios predicts that cyclone intensity increases in three models in the North Atlantic Ocean and across all four models in the Northeast Pacific Ocean (Mendelsohn et al. 2012). Changes in the other basins were less systematic. A comprehensive analysis of the impact of climate change on cyclone behavior is provided by Emanuel (2013).

Table 9.5 presents the tropical cyclone damage estimates from climate change. In the all countries model, climate change increases damage by about 25% in the United States. Climate change causes no consistent impact on other OECD countries and only an 8% increase in damage in Non-OECD countries. The three region model suggests that United States tropical cyclone damage would increase by 67% to $76 billion/year. The rest of the world would see an average increase of between 2% and 4%. Damage in Australia would increase by about 6% and damage in Japan would fall by about 13%. China, India, and the Philippines are estimated to see a reduction in damage of between 10% and 15% from the future baseline level. The results suggest it is the United States who is the most vulnerable to tropical cyclones and the most vulnerable to changes in tropical cyclones from climate change. In our sensitivity analysis, the wind model predicts future United States damages could increase by $50 billion/year due to climate change, topping more than $205 billion/year, compared to just $1.1 and $11.5 billion/year in other OECD and Non-OECD countries, respectively.

Lastly, we consider future fatalities under climate change in Table 9.6. Due to a weak intensification signal coupled with smaller (closer to zero) intensity elasticities, we find that climate change will have a very small effect on future fatalities. Specifically, future fatalities will only increase by about 3% for OECD countries

Table 9.6 Future cyclone fatalities under climate change

	Future baseline	CNRM	ECHAM	GFDL	MIROC	Average
All countries model						
OECD	46	47	47	50	46	47
NonOECD	2583	2633	2816	2904	2903	2814
Total	**2628**	**2681**	**2863**	**2954**	**2948**	**2862**
2 regions model						
OECD	11	11	11	12	11	11
NonOECD	2116	2158	2377	2534	2451	2380
Total	**2127**	**2169**	**2388**	**2546**	**2462**	**2391**

Column 1 presents summary statistics for the future average annual baseline fatalities – assuming future socioeconomic conditions but current climate conditions – across the three (USA, Non-USA OECD, and Non-OECD) regions. The next four columns present average annual future damages assuming future socioeconomic and climate conditions. The final column presents the average across the four models

and 12.5% for Non-OECD countries. The all countries model predicts climate change will cause the same percentage changes in fatalities as the two regions model. The absolute numbers differ because the baseline fatalities are different. The fatality estimates are similar across the wind model as well.

9.5 Conclusion

We provide updated estimates of the costs of climate and socioeconomic change on tropical cyclone losses, utilizing the methodology of Mendelsohn et al. (2012) and new insights surrounding cyclone damage and fatality functions (Bakkensen and Mendelsohn 2016). Future development is predicted to reduce overall fatalities from 8000 to 2100 per year. Climate change is predicted to increase these future deaths on average by 260 per year, entirely in Non-OECD countries.

Climate change will have a larger impact on damage. Allowing the damage function to vary across the United States, other OECD countries, and non-OECD countries, overall damage will increase from a future baseline of $60 billion/year to $90 billion/year, an increase of 50%. The striking result in both current tropical cyclone damage and future damage is the outsized role of damage in the United States. The United States is currently responsible for 60% of global damage, and that percentage could increase to 84% by 2100. The data suggests that the United States is doing very little to adapt to tropical cyclones compared to other countries in the world. If these trends continue, future tropical cyclone damage will reach $76 billion/year in the United States alone.

We note some important limitations of this analysis. Similar to previous work, we do not include rainfall or storm surge in our analysis, although both are likely to be important (Bakkensen et al. 2017; Seo and Bakkensen 2016). There are important uncertainties in these projections. We do not model alternative paths of economic growth. Faster growth will lead to more emissions but also higher income. The future level of mitigation is uncertain. The analysis examines a modest mitigation path, but the world may do no mitigation at all or engage in more rigorous efforts. By comparing the results of four climate models, the paper reveals there is uncertainty in climate projections. The paper utilized only a single model of tropical cyclones. This is also an important source of uncertainty. The damage and fatality functions are uncertain, as is evident from the uncertainty surrounding the coefficients. Finally, adaptation may change over time. To the extent that countries may adapt differently in the future, future losses could be quite different. Of particular policy relevance for developing countries, the three regions model highlights that their development trajectory will have critical implications for future losses. If developing countries follow the model of the United States, tropical cyclone damage will accelerate rapidly with development. However, if developing countries follow the model of the rest of the OECD, they will see only modest increases in tropical cyclone damage. Perhaps most urgent is that the United States revisit their own strategy for adapting to tropical cyclones and invest in a more rigorous coastal protection program.

Appendix

Additional Historical Damage and Fatality Functions

In this section, we present additional historical damage and fatality functions. Namely, in Table 9.7, we present the all countries functions as well as damage functions partitioned based on OECD (including the United States) versus Non-OECD countries. While the estimated coefficients are qualitatively similar (in terms of coefficient sign) across the regressions, important differences are present, especially with respect to the magnitude of the cyclone elasticity coefficients. However, given Table 9.1, combining US and Non-US OECD countries hides the underlying heterogeneity in coefficient magnitudes. Thus, Table 9.1 is a preferred partitioning. Also see Bakkensen and Mendelsohn (2016) for a much more detailed analysis of damage and fatality functions.

Lastly, Table 9.8 presents additional historical fatality functions, namely the all countries model and partitioning between US, Non-US OECD, and Non-OECD countries. We find the estimated coefficient on US income and pressure to be imprecisely estimated, perhaps partly due to the small sample size. Thus, we prefer the partitioning in Table 9.2 in the main paper.

Table 9.7 Additional historical damage functions

	(1)	(2)	(3)	(4)	(5)	(6)
	Ln damages	Ln damages	Ln damages	Ln damages	Ln damages	Ln damages
	MSLP	Wind	MSLP	MSLP	Wind	Wind
	All	All	OECD	Non- OECD	OECD	Non-OECD
Ln income per capita	0.447***	0.394***	0.249	0.285***	0.279	0.229**
	(0.0737)	(0.0760)	(0.372)	(0.0976)	(0.417)	(0.0991)
Ln population density	0.0688	0.0112	0.187**	0.0980	0.0613	0.0677
	(0.0539)	(0.0627)	(0.0791)	(0.0783)	(0.110)	(0.0776)
Ln MSLP	−29.48***		−59.94***	−23.70***		
	(3.318)		(7.689)	(3.631)		
Ln wind		1.808***			4.148***	1.425***
		(0.219)			(0.553)	(0.235)
Ln distance	−0.396***	−0.363***	−0.569***	−0.351***	−0.466***	−0.322***
	(0.0373)	(0.0377)	(0.116)	(0.0406)	(0.117)	(0.0406)
Constant	216.7***	7.198***	428.0***	177.9***	−1.247	9.737***
	(22.83)	(1.136)	(52.91)	(25.03)	(5.141)	(1.227)
Observations	856	843	203	653	191	652
R-squared	0.223	0.206	0.295	0.171	0.292	0.155

Standard errors in parentheses. ***p < 0.01, **p < 0.05, *p < 0.1

Table 9.8 Additional historical fatality functions

	(1)	(2)	(3)	(4)	(5)	(6)	(7)	(8)
	Ln fatalities	Ln fatalities	Ln fatalities	Ln fatalities	Ln fatalities	Ln fatalities	Ln fatalities	Ln fatalities
	MSLP	Wind	MSLP	MSLP	MSLP	Wind	Wind	Wind
	All	All	USA	OECD (Non-USA)	Non-OECD	USA	OECD (Non-USA)	Non-OECD
Ln income per capita	−0.616***	−0.615***	−0.538	−1.701***	−0.758***	−0.609	−1.715***	−0.743***
	(0.0439)	(0.0454)	(0.456)	(0.215)	(0.0564)	(0.466)	(0.212)	(0.0580)
Ln population density	0.165***	0.134***	0.242*	0.273***	0.159***	0.285**	0.273***	0.107**
	(0.0336)	(0.0359)	(0.129)	(0.0469)	(0.0418)	(0.133)	(0.0576)	(0.0427)
Ln MSLP	−9.707***		−23.28***	−3.003	−9.047***			
	(2.050)		(7.146)	(5.719)	(2.235)			
Ln wind		0.562***				1.574***	−0.0774	0.511***
		(0.127)				(0.532)	(0.358)	(0.136)
Ln distance	−0.189***	−0.186***	−0.246**	−0.142***	−0.187***	−0.235**	−0.144***	−0.187***
	(0.0216)	(0.0223)	(0.105)	(0.0465)	(0.0240)	(0.103)	(0.0458)	(0.0248)
Constant	74.34***	5.446***	167.2***	38.91	70.90***	1.007	18.75***	6.746***
	(14.14)	(0.642)	(48.89)	(39.91)	(15.40)	(5.672)	(2.569)	(0.730)
Observations	1020	1008	56	116	848	58	108	842
R-squared	0.229	0.216	0.320	0.466	0.247	0.317	0.485	0.232

Standard errors in parentheses. ***p < 0.01, **p < 0.05, *p < 0.1

References

Bakkensen L, Mendelsohn R (2016) Risk and adaptation: evidence from global hurricane damages and fatalities. J Assoc Environ Res Econ 3:555–587

Bakkensen L, Park S, Sarkar R (2017) Climate costs of tropical cyclone losses depend also on rain. Working paper

Bakkensen LA, Shi X, Zurita BD (2018) The impact of disaster data on estimating damage determinants and climate costs. Econ Disaster Clim Chang 2:1–23

Burke M, Dykema J, Lobell D, Miguel E, Satyanath S (2015) Incorporating climate uncertainty into estimates of climate change impacts. Rev Econ Stat 97:461–471

Cavallo E, Noy I (2011) Natural disasters and the economy—a survey. Int Rev Environ Res Econ 5:63–102

Cubasch U, Voss R, Hegerl G, Waskiewitz J, Crowley T (1997) Simulation of the influence of solar radiation variations on the global climate with an ocean-atmosphere general circulation model. Clim Dyn 13:757–767

Dinan T (2017) Projected increases in hurricane damage in the United States: the role of climate change and coastal development. Ecol Econ 138:186–198

Emanuel K (2005) Divine wind. Oxford University Press, New York

Emanuel KA (2013) Downscaling CMIP5 climate models shows increased tropical cyclone activity over the 21st century. Proc Natl Acad Sci 110:12219–12224

Emanuel K, Sundararajan R, Williams J (2008) Hurricanes and global warming: results from downscaling IPCC AR4 simulations. Bull Am Meteorol Soc 89:347–367

Fankhauser S, McDermott T (2014) Understanding the adaptation deficit: why are poor countries more vulnerable to climate events than rich countries? Glob Environ Chang 27:9–18

Gueremy JF, Deque M, Braun A, Evre JP (2005) Actual and potential skill of seasonal predictions using the CNRM contribution to DEMETER: coupled versus uncoupled model. Tellus 57:308–319

Hallegatte S (2007) The use of synthetic hurricane tracks in risk analysis and climate change damage assessment. J Appl Meteorol Climatol 46:1956–1966

Hasumi H, Emori S (2004) K-1 coupled GCM (MIROC) description. Center for Climate System Research, University of Tokyo, Tokyo

IPCC (Intergovernmental Panel on Climate Change) (2007) State of the science, Working Group I Report to the 4th Assessment. Cambridge University Press, Cambridge

IPCC (Intergovernmental Panel on Climate Change) (2012) Managing the risks of extreme events and disasters to advance climate change adaptation, A special report of Working Groups I and II of the Intergovernmental Panel on Climate Change. Cambridge University Press, Cambridge

IPCC (Intergovernmental Panel on Climate Change) (2013) State of the science, Working Group I Report to the 5th Assessment. Cambridge University Press, Cambridge, UK

Kahn ME (2005) The death toll from natural disasters: the role of income, geography, and institutions. Rev Econ Stat 87:271–284

Knapp KR, Kruk MC, Levinson DH, Diamond HJ, Neumann CJ (2010) The international best track archive for climate stewardship (IBTrACS) unifying tropical cyclone data. Bull Am Meteorol Soc 91:363–376

Kousky C (2014) Informing climate adaptation: a review of the economic costs of natural disasters. Energy Econ 46:576–592

Manabe S, Stouffer J, Spelman MJ, Bryan K (1991) Transient responses of a coupled ocean-atmosphere model to gradual changes of atmospheric CO2. Part I: mean annual response. J Clim 4:785–818

Mendelsohn R, Emanuel K, Chonabayashi S, Bakkensen L (2012) The impact of climate change on global tropical cyclone damage. Nat Clim Chang 2:205–209

Millner A, McDermott T (2016) Model confirmation in climate economics. Proc Natl Acad Sci 113:8675–8680

Narita D, Tol RS, Anthoff D (2009) Damage costs of climate change through intensification of tropical cyclone activities: an application of FUND. Clim Res 39:87–97

National Centers for Environmental Information (NCEI) (2018) Billion-dollar weather and climate disasters: table of events. https://www.ncdc.noaa.gov/billions/events/US/1980-2018. Accessed 20 Apr 2018

National Hurricane Center (NHC) (2010) Hurricane research division: frequently asked questions. Retrieved Dec 2010 from: http://www.aoml.noaa.gov/hrd/tcfaq/A1.html

National Oceanic and Atmospheric Administration (NOAA) (2010) Hurricane research division: re-analysis project. Retrieved Dec 2010 from: http://www.aoml.noaa.gov/hrd/hurdat/

Nordhaus WD (2010) The economics of hurricanes and implications of global warming. Clim Chang Econ 1:1–20

Pearce D (2003) The social cost of carbon and its policy implications. Oxf Rev Econ Pol 19:362–384

Pielke RA (2007) Future economic damage from tropical cyclones: sensitivities to societal and climate changes. Phil Trans Roy Soc Lond A Math Phys Eng Sci 365:2717–2729

Ranson M, Kousky C, Ruth M, Jantarasami L, Crimmins A, Tarquinio L (2014) Tropical and extratropical cyclone damages under climate change. Clim Chang 127:227–241

Seo SN, Bakkensen LA (2016) Did adaptation strategies work? High fatalities from tropical cyclones in the North Indian Ocean and future vulnerability under global warming. Nat Haz 82:1341–1355

Shultz JM, Russell J, Espinel Z (2005) Epidemiology of tropical cyclones: the dynamics of disaster, disease, and development. Epidemiol Rev 27:21–35

Stern N (2007) The economics of climate change: the Stern review. Cambridge University Press, Cambridge, UK

Tol RS (2008) The social cost of carbon. In: The Oxford handbook of the macroeconomics of global warming

United Nations (UN) (2018) World population prospects 2017. Retrieved Apr 2018 from: https://esa.un.org/unpd/wpp/

Walsh KJE, McBride JL, Klotzbach PJ et al (2016) Tropical cyclones and climate change. WIRES Clim Chang 7:65–89. https://doi.org/10.1002/wcc.371

World Bank (2010) Natural hazards, unnatural disasters: the economics of effective prevention. World Bank Publications, Washington, DC

Chapter 10
Poleward Migration of Tropical Cyclone Activity in the Southern Hemisphere: Perspectives and Challenges for the Built Environment in Australia

Richard J. Krupar III and Daniel J. Smith

Abstract With statistically significant trends suggesting that tropical cyclones are migrating poleward in the Southern Hemisphere, specifically in the South Pacific Ocean basin, it is important to review the current state of knowledge on poleward migrating tropical cyclone activity. Furthermore, given the potential impacts they may have on regions traditionally unaffected by tropical cyclones, review of current residential building practice in Australia is warranted. This chapter highlights the significance of the long-term poleward trends in the Southern Hemisphere and potential mechanisms that are driving the geographical shift. Residential building practice in cyclonic and non-cyclonic regions in Australia is discussed to address existing vulnerabilities and how they can lead to catastrophic impacts. Methods and tools to evaluate tropical cyclone risk as well as future research needs are then discussed in the context of adapting to and mitigating for tropical cyclone activity that may migrate poleward. Finally, the chapter concludes with a summary and some finishing thoughts about the advantages of forming multidisciplinary teams to address the grand challenge of disaster resilience in the built environment in Australia.

Keywords Tropical cyclones · Poleward migration · Disaster resilience · Damage assessment · Mitigation · Vulnerability

R. J. Krupar III (✉)
Berkshire Hathaway Specialty Insurance, San Ramon, CA, USA
e-mail: Richard.Krupar@bhspecialty.com

D. J. Smith
Cyclone Testing Station, James Cook University, Townsville, QLD, Australia

J. M. Collins, K. Walsh (eds.), *Hurricane Risk*, Hurricane Risk 1,
https://doi.org/10.1007/978-3-030-02402-4_10

10.1 Introduction

Tropical cyclones cause significant damage to the built environment globally through the concomitant hazards of wind, rainfall and storm surge. Recent tropical cyclone events like Hurricane Sandy (2012) in the U.S., Severe Tropical Cyclone Marcia (2015) in Australia, and others that have impacted areas outside the "traditional" tropical latitudes have motivated atmospheric and climate scientists to determine what physical mechanism(s) within a changing climate system are driving the poleward migration of tropical cyclones (Kossin et al. 2014; Moon et al. 2015). This motivation is largely driven by the potential impacts that a poleward shift in tropical cyclone activity would have on regions historically unaffected by tropical cyclones (Ramsay 2014). Regions that are historically unaffected by tropical cyclones design for lower wind speed requirements than those employed for tropical cyclone-prone regions. These requirements put infrastructure systems at a significantly higher risk of structural damage compared with identical storms impacting infrastructure systems designed for regions that experience landfalling tropical cyclones more frequently.

Given recent observations of tropical cyclone activity migrating away from the "traditional" tropical latitudes, it is important to review existing research on this subject and how building codes and standards are employed in regions traditionally affected and unaffected by this type of activity. The scope of this manuscript is to provide a qualitative assessment of the potential issues with poleward migration of tropical cyclones to motivate future quantitative impact studies. This chapter begins with a summary of the meteorological perspective on the poleward migration of tropical cyclones in the Southern Hemisphere; specifically, what metrics are used to assess it and what are the key drivers. Then, we provide a brief discussion on the Australian building codes and standards and its application in cyclonic and non-cyclonic regions. Next, a discussion on what actions and methods non-cyclonic regions in Australia can take to prepare for future tropical cyclone activity and improve infrastructure resilience is discussed. Finally, the chapter concludes with a summary and some finishing thoughts on what future research needs to address within the context of future impacts of tropical cyclones that may continue migrating poleward.

10.2 Poleward Migration of Tropical Cyclones

Recently, atmospheric and climate scientists have begun to examine long-term poleward shifts in tropical cyclone activity, especially at their peak storm intensity. Work conducted by Kossin et al. (2014) sheds light on this topic by examining at what latitude tropical cyclones reach their peak storm intensity. This latitude is referred to as the lifetime-maximum intensity (LMI) in their study. Key findings from their research suggest that there are statistically significant mean poleward

trends in the latitude of LMI in both the Northern and Southern Hemispheres. The largest poleward trend is observed in the Southern Hemisphere, where the observed shift in distance from the equator is 62 km per decade based on a 31-year period between 1982 and 2012 (Fig. 10.1). Within each respective hemisphere, there exists year-to-year and basin-to-basin variability that suggests poleward migration of tropical cyclone activity is not occurring in every ocean basin. Nonetheless, the authors imply that increased wind shear in the deep tropics, decreased wind shear at higher latitudes, and greater potential intensity due to expansion and anthropogenic warming is conceivably linked to the poleward migration of LMI during the period considered.

Moon et al. (2015) questioned the statistical significance of the global and hemispheric mean poleward trends in annual-mean latitude of LMI that were noted by Kossin et al. (2014) and used a quantitative method to examine the contributions to the observed trends. The method determines the annual global-mean latitude of LMI ($\overline{LLMI}_{global}$) by summing the product of the annual-mean LMI latitude for each ocean basin ($\overline{LLMI}_{basin}$) by the ratio of the annual tropical cyclone frequency for each ocean basin (N_{basin}) to the total global tropical cyclone frequency in all ocean basins (N_{global}):

$$LLMI_{global} = \sum_{basin} \left(LLMI_{basin} + \frac{N_{basin}}{N_{global}} \right). \tag{10.1}$$

The contributions of global poleward migration trends can be further separated into two components: the frequency and pure migration contributions. The frequency contribution represents changes in relative annual tropical cyclone frequency within each ocean basin. The pure migration contribution solely constitutes the poleward migration of LMI within each ocean basin. An analysis of the trends in annual-mean latitudes of LMI shows that the frequency contribution strongly influences the trend in the Northern Hemisphere, while the pure migration contribution primarily controls the trend in the Southern Hemisphere (Fig. 10.2). This result implies that the environmental influences proposed by Kossin et al. (2014) are not necessarily linked to poleward migration trends in both hemispheres.

The results from Kossin et al. (2014) and Moon et al. (2015) explicitly suggest that cities in the Southern Hemisphere mid-latitudes may realize a growing threat to landfalling tropical cyclones if current poleward trends continue. This is a significant problem because current building codes and standards enforced in non-cyclonic regions in Australia do not currently require the building construction industry to design at the same level of strength as required in cyclonic regions. While the causes of the observed poleward trends have yet to be proven (Walsh et al. 2016), it is still important that communities in the mid-latitudes of the Southern Hemisphere begin thinking about adaptation strategies for buildings and critical infrastructure. The next section describes the current building design practice in Australia in non-cyclonic and cyclonic regions and what challenges exist for retrofitting from economic and social perspectives.

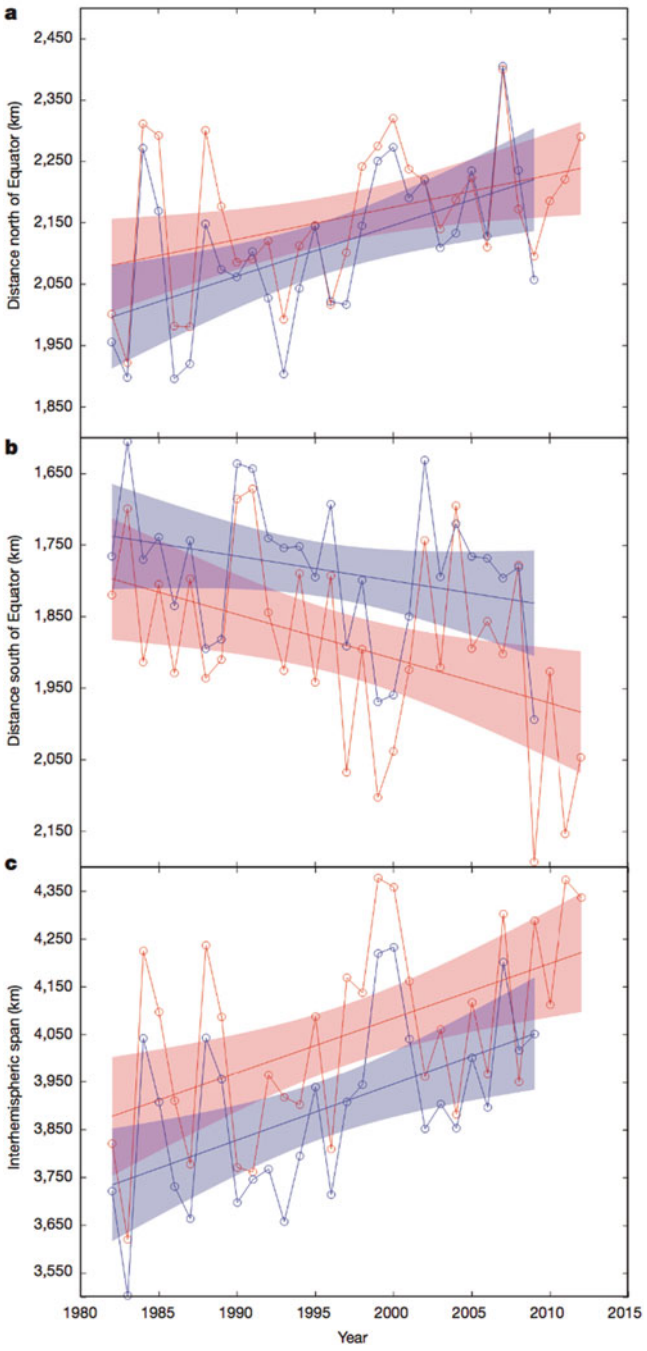

Fig. 10.1 Time series of annual-mean distance (km) north (**a**) and south (**b**) of the equator and interhemispheric span (km) across the Northern and Southern Hemispheres (**c**) calculated from best-track historical data (red) and ADT-HURSAT reanalysis (blue). Linear trend lines in each plot are shown with shaded 95% two-sided confidence intervals (see Kossin et al. 2014, Fig.1)

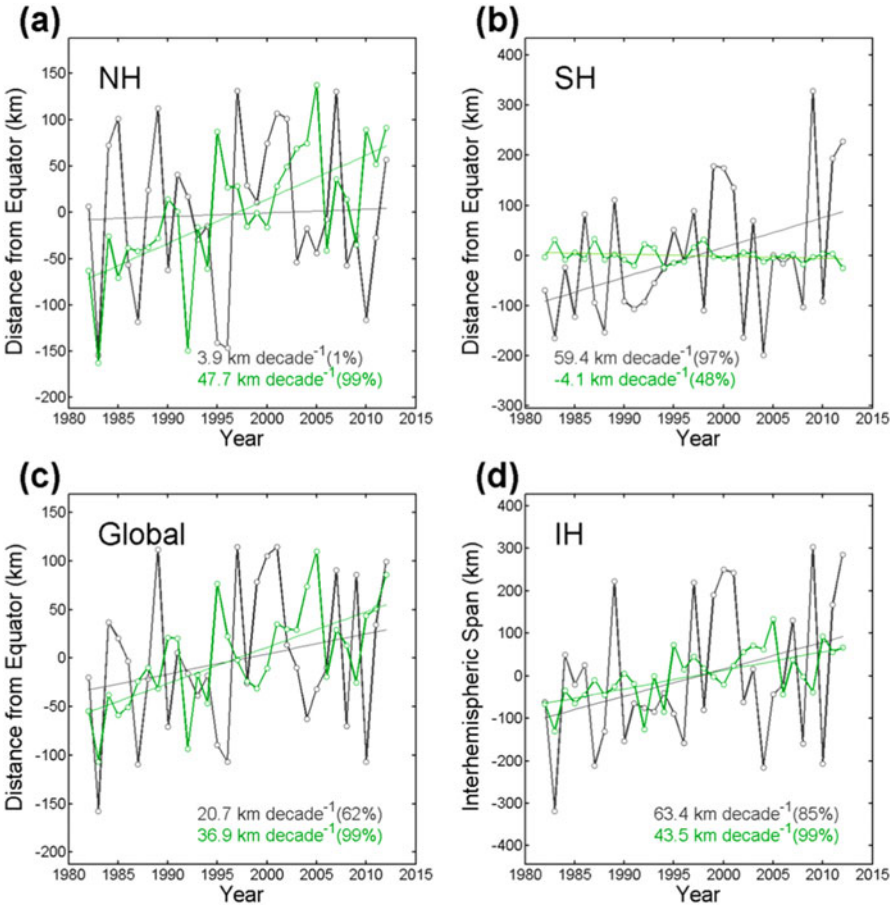

Fig. 10.2 Time series of annual-mean distance from the equator (km) in the Northern Hemisphere (**a**), Southern Hemisphere (**b**), and globally (**c**) considering frequency contribution (green open circles and solid line) and pure migration contribution (black open circles and solid line) with effects of ENSO reduced. Interhemispheric span (km) across the Northern and Southern Hemispheres (**d**) considering frequency contribution and pure migration contribution with reduced effects of ENSO is also displayed. Straight linear trends for the frequency (thin green line) and pure migration (thin black line) contributions in each plot are shown with their significance levels in the legends (see Moon et al. 2015, Fig. 3)

10.3 Engineering for Tropical Cyclones in Australia

Building design in Australia is governed by the National Construction Code (NCC; ABCB 2016). The NCC's structural performance requirements specify that a building or structure, to the degree necessary, must resist the wind actions to which it may reasonably be subjected and should also:

Table 10.1 Importance levels and design events for safety for wind design from Tables B1.2a and B1.2b of NCC 2016 Building Code of Australia

Level	Building type	Annual prob. of exceedance	
		Non-cyclonic	Cyclonic
1	Buildings or structures representing a low degree of hazard to life and other property in the case of failure	1:100	1:200
2	Buildings or structures not included in Importance levels 1, 3 and 4	1:500	1:500
3	Buildings or structures that are designed to contain a large number of people	1:1000	1:1000
4	Buildings or structures that are essential to post disaster recovery or associated with hazardous facilities	1:2000	1:2000

- Remain stable and not collapse.
- Prevent progressive collapse.
- Minimise local damage and loss of amenity.
- Avoid causing damage to other properties.

The NCC sets the societal risk for the ultimate limit state strength of a structure. The level of risk is evaluated as an annual probability of exceedance value depending on the location and importance of a structure, as shown in Table 10.1. Housing is deemed Level 2 importance, which has a minimum annual probability of exceedance of 1:500. Other structure types assume different risk levels. For example, a hospital has a higher level of importance (Level 4) and therefore a greater exceedance value, than an isolated farm shed (Level 1).

The building standards for wind design, AS/NZS 1170.2 (Standards Australia 2011) and AS 4055 (Standards Australia 2012), establish the design wind speed (i.e. wind pressure load criteria) associated with a given exceedance value. Although the exceedance value may be the same for a given importance level, the design wind speed varies significantly across geographical regions because the likelihood of high wind events occurring varies significantly (e.g. currently much higher in lower latitudes versus higher latitudes). These variations are accounted for in AS/NZS 1170.2 by dividing Australia into the four wind regions A, B, C and D, as shown in Fig. 10.3. Regions A and B are deemed "non-cyclonic" while C and D are "cyclonic".

For a building in cyclonic Region C, the regional 10 m height 3-s gust wind speed for a 1:500 exceedance level is 69 m/s (mid-range Category 4 cyclone per Australian Bureau of Meteorology tropical cyclone storm intensity scale). This wind speed has a nominal probability of occurring on the order of 10% in 50 years. In contrast, the same building in non-cyclonic Region B has a design wind speed of 57 m/s. The design pressure varies with the square of the wind speed. The difference in loading criteria means that a home in Region B is designed for wind loads that are 69% of those for the same home in Region C.

If cyclones exhibit a poleward shift to higher latitudes (i.e. between 25°S and 30°S and perhaps south of 30°S) that have not experienced tropical cyclones

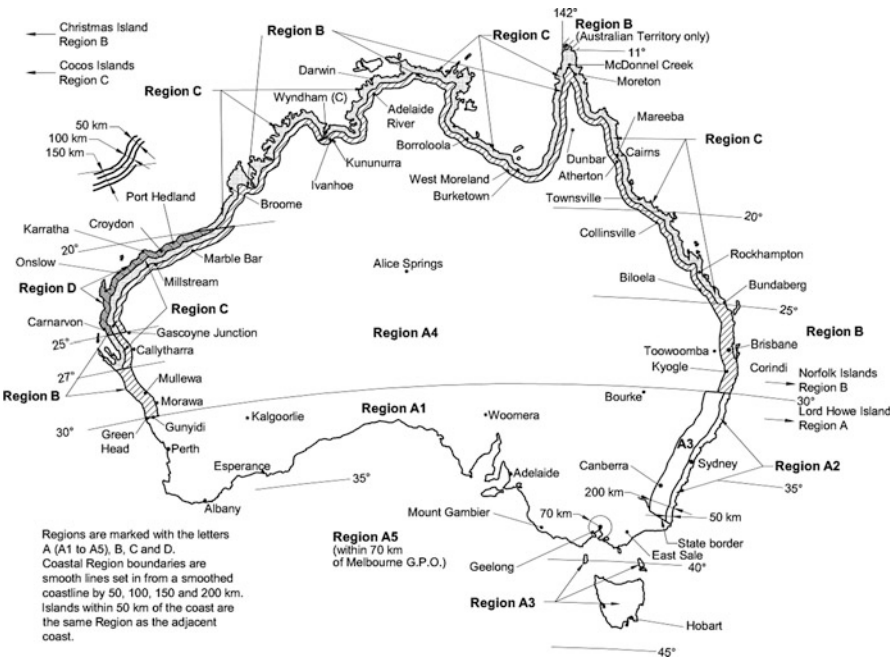

Fig. 10.3 Wind regions for building design from AS/NZS 1170.2 (2011)

historically, the risk implications for existing buildings and critical infrastructure as well as design challenges in non-cyclonic regions would be significant. However, before discussing the potential impacts in non-cyclonic regions, a closer look should be taken at the issues and solutions present in lower latitudes, where the cyclone threat is already relatively high and therefore a significant aspect of community planning.

10.3.1 Buildings in Cyclonic Regions

In Australia, communities along the northeastern coastline of Queensland experience tropical cyclones frequently. Over the last 40 years, the Cyclone Testing Station (CTS) has conducted post-event damage assessments in this region. These post-storm analyses provide useful information about the performance of infrastructure in a variety of tropical cyclone landfall events and common failure modes amongst similar infrastructure systems.

One of the key proxies for predicting tropical cyclone-induced damage intensity is age of construction. There is a stark contrast in performance for homes constructed before and after the mid-1980s. This contrast is a result of Tropical Cyclone Tracy, which caused widespread severe damage to housing in December 1974, especially in

the Northern suburbs of Darwin (Walker 1975). Changes to design and building standards of houses were implemented during the reconstruction. The Queensland Home Building Code (HBC) was introduced as legislation in 1982, with provisions that stemmed from the lessons learned from Tracy. By 1984 it is reasonable to presume that houses in the cyclonic region of Queensland were being fully designed and built to its requirements.

Damage investigations carried out by the CTS following severe windstorms over the last 15 years have typically shown that Australian unstrengthened houses built prior to the mid-1980s offer a lower level of structural performance and life safety protection during windstorms compared with houses constructed to contemporary building standards. The NCC (ABCB 2016) is continually reviewed to ensure that it supports acceptable performance of new housing. However, only a small fraction of our housing stock is replaced per annum, therefore most Australians will spend most of their lives in houses that are already built. Given that these older houses will represent the bulk of the housing stock for many decades, practical structural upgrading solutions based on the latest research can make a significant improvement to housing performance and to the economic and social well-being of communities. Structural retrofitting details exist for some forms of older housing, but the use of these details for mitigation upgrades is limited (Smith et al. 2016). There is also evidence of retrofitting details not being included into houses, requiring major repairs following severe storm events, thus missing the ideal opportunity to improve resilience of the house and community at the time when doing so is most economical. Hence, the issues of retrofitting legacy housing, including feasibility and hindrances on take-up, etc., are difficult, and largely unsolved challenges that coastal communities in cyclonic regions are faced with.

It is important to note that CTS damage investigations also report failures of contemporary construction at wind speeds below design requirements, for water-ingress related issues (e.g. Boughton et al. 2017). The poor performance of these structures commonly results from design and construction failings, poor connections (i.e. batten/rafter, rafter/top plate) (Figs. 10.4 and 10.5), or from degradation of construction elements (i.e. corroded screws, nails and straps, and decayed or insect-attacked timber). A damage survey after Cyclone Yasi, which hit the north Queensland coast in 2011, showed substantial corrosion of roof elements in houses less than 10 years old (Boughton et al. 2011), emphasizing that ongoing maintenance is an important part of improving community resilience for all ages of housing. The analysis highlights that development of retrofit solutions is a key area of ongoing research for cyclonic areas and critical to the performance and longevity of both legacy and contemporary housing.

10.3.2 Buildings in Current Non-cyclonic Regions

The age dependence of housing performance in severe wind events and issues related to poor construction practices in renovation, degradation of materials (lack

Fig. 10.4 Wind-induced failure of a new (<1 year) metal cladding roof on an old house at the rafter to top-plate connection during Cyclone Marcia (2015) in Yeppoon, Australia – there appeared to be no retrofitting of the weaker connections

Fig. 10.5 Wind-induced failure of a metal cladding roof (left) at the batten to rafter connection (right) during Cyclone Marcia (2015) in Yeppoon, Australia

of maintenance), etc. are not constrained to only the cyclonic regions of northern Australia. Damage investigations of severe thunderstorms in Brisbane, Dubbo, and Perth (e.g. Parackal et al. 2015) revealed similar issues. If the frequency of storms at higher latitudes increases, residential buildings and critical infrastructure systems south of 25°S will face the same issues cyclonic regions face today. In addition, lower design wind speed requirements and construction practices in these regions (compared to cyclonic regions) will result in a significantly higher risk of structural damage compared with a similar storm making landfall in a cyclonic design region.

During a cyclone, dynamic fluctuating winds subject the building envelope and structure to a multitude of spatially and temporally varying loads. Generally, the

structural design of housing uses peak gust wind speeds for determining the positive and negative pressure loads the structure must resist. The storm duration and temporally varying forces are important for assessing elements of the envelope and frame (i.e. roofing, battens, connections, etc.) that may be subject to low cycle fatigue. Testing and approval of building products in cyclonic regions requires load cases that include cyclic (i.e. repeated) loading over a period of several hours to mimic the conditions occurring during cyclone passage. Building components in non-cyclonic areas are not subject to this requirement and therefore may be more inclined to fail when subjected to the longer duration of loading from cyclones.

Internal pressure effects are also handled very differently in cyclonic versus non-cyclonic design. Maintaining a sealed building envelope is critical to the wind resistance of buildings. If there is a breach on the windward face (i.e. from broken window or failed door), the internal pressure of the house can be dramatically increased. The internal loads act in concert with external pressures, thereby increasing the load on cladding elements and the structure. Depending on the geometry of the building, the increase in internal pressure caused by this opening can double the load in certain areas, increasing the risk of failure, especially if the building has not been designed for such an opening. Residential structures in cyclonic regions designed in accordance with contemporary design standard AS 4055 are required to incorporate load cases for internal pressure increases created by envelope breaches. Houses in non-cyclonic regions designed to AS 4055 are not required to account for this load case, resulting in a higher probability of significant structural failure if such an opening were to occur.

10.3.3 Damage Mitigation

Two of the key issues related to mitigation and poleward migrating cyclones are (a) mitigation against wind damage in older housing (pre-1980s) in all wind regions – even for existing levels of wind (this addresses known problems of structural adequacy in those houses) and (b) mitigation against damage from more intense cyclones for both old and new houses in mid-latitudes – Region B south of 25°S and Region A south of 30°S (this addresses the poleward shift of cyclone activity). Regardless of whether a residential building is in what is currently classified as a cyclonic or non-cyclonic design region, from an engineering perspective, the adaptive strengthening solutions are largely the same (e.g. opening protection, improved vertical load path from roof to foundation, proper maintenance). Although these solutions are proven effective at reducing severe damage and loss, post-event analysis and observations regularly note their lack of implementation (Smith et al. 2015). This aspect of the mitigation problem has not been part of traditional engineering rhetoric; however, Smith et al. (2016) stresses the importance of multidisciplinary thinking and consideration of behavioral and socio-economic factors to improve overall community engagement with structural mitigation programs in cyclone-prone areas.

There have been several retrofit incentive programs in the U.S. (e.g. My Safe Florida Home, etc.). These programs focus on perceived financial benefit (Poussin et al. 2014), an obvious driver of preparedness action. Although financial incentives are an important motivator (Boon et al. 2012), they do not ensure mitigation action. A public opinion survey during the 'My Safe Florida Home' program found that only 40% of respondents indicated that reduced insurance premiums were a key motivator in undertaking improvements to their home (Sink 2008). Financial incentives of this nature are more likely to be effective if used in concert with other behavioral drivers.

Missing from the existing approaches is a holistic perspective on what drives individuals to take mitigation actions. Each of the programs reviewed hinge on financial incentive and fail to encompass other motivators. Identifying other incentives can be difficult as they can be situationally and contextually specific to the individual. Factors affecting the success of mitigation activities therefore differ by region, event type, and citizen-behavior patterns. Four key factors were identified in the literature that show factors beyond financial incentive, including prior event experience, mitigation capacity, social connectedness, and freedom of choice.

10.4 Discussion

Given the current state of knowledge on poleward migrating tropical cyclones and building practice in both cyclonic and non-cyclonic regions in Australia, it is appropriate to discuss what methods and tools are available to communities in these regions and how they can be used in non-cyclonic regions to evaluate tropical cyclone risk. Furthermore, it is also of interest to discuss how communities can develop better adaptation and mitigation strategies in preparation for potential tropical cyclone activity in the future.

10.4.1 Tropical Cyclone Impact Assessment

Impact assessments for tropical cyclones often begin with an evaluation of the hazard (e.g. wind, rainfall, and storm surge) using either probabilistic or scenario-based analysis methods. Both methods leverage a historical catalog that contains storm intensity and position data. Given the statistical distribution of key storm parameters (e.g. minimum central pressure, radius of maximum wind, translation speed, etc.), probabilistic methods use a Monte Carlo approach to randomly sample the storm parameters. In contrast, scenario-based methods use event-specific or synthetic storm parameters.

Storm parameters from either the probabilistic or scenario-based methods are used as input in a mathematical tropical cyclone wind field model to produce a specific scenario or set of possible scenarios. Once wind fields are generated by the

tropical cyclone wind hazard model, simulated or adjusted wind fields (i.e. accounting for exposure and averaging time) are used as input to drive rainfall (i.e. inland flood) and storm surge hazard models. Existing rainfall models use either statistical or analytical models to estimate rainfall rates. The simulated rainfall rates can then be ingested by inland flood models to evaluate flood risk. Storm surge hazard models ingest simulated wind fields from the wind hazard model to drive hydrodynamic numerical models. Simulations without wind give an estimate of the tidal height, and when wind is included, an estimate of the tidal height plus storm surge is produced (i.e. storm tide).

Once hazard metrics are generated by each peril model, they are ingested by a hazard-specific vulnerability model to estimate the degree of damage to a specific type of infrastructure system (e.g. buildings, electrical distribution networks, etc.). Wind vulnerability models for buildings (e.g. commercial, industrial, and residential) in Australia are created using past loss data, past loss data enhanced with expert judgement, heuristic methods, component-based methods, and simulation-based methods to determine the damage index (DI) for a specific building type (Mason and Parackal 2015). The DI is defined as the ratio of the repair cost to the total replacement cost of a specific building. Once a DI is computed for a specific design wind speed (i.e. 3-s gust at 10 m above ground level in open exposure terrain conditions), mean damage functions for different building construction can be produced. Mason and Parackal (2015) reviewed vulnerability of buildings and civil infrastructure to tropical cyclones worldwide and found that wind vulnerability models for Australia are the most refined compared with inland flood and storm surge vulnerability models for residential buildings. Limited data has been compiled and little research has been done to develop wind, flood, and storm surge vulnerability models for commercial and industrial buildings in Australia. Flood and storm surge models are also extremely limited or non-existent for residential buildings in Australia.

Community-based projects that leverage tropical cyclone risk models for different scenarios are very useful tools for assessing future tropical cyclone hazards and impacts. Recently, Krupar and Mason (2017) developed a multi-hazard (i.e. wind, rainfall, and storm surge) tropical cyclone disaster impact scenario model for Queensland. The model framework consists of both public and private hazard models as well as wind and flood vulnerability models consisting of heuristic damage functions for a variety of different types of infrastructure. A modified Severe Tropical Cyclone Marcia (2015) scenario was developed to examine what the potential impacts on Yeppoon, Queensland could have been if the cyclone had made landfall further south. This case study was selected for examination because Marcia is the southernmost Category 5 cyclone on the Australian tropical cyclone intensity scale to make landfall in Queensland and is an example that supports the recent poleward migration trend of tropical cyclones noted in the Southern Hemisphere by Kossin et al. (2014) and Moon et al. (2015). Results from the case study suggest that Livingstone Shire Council would have experienced greater wind and storm surge damage across all building construction types had Marcia made landfall further south of the observed landfall location. For instance, 43% of the synthetic

residential building exposure (primarily in Byfield and Yeppoon) would require major structural repairs for the 10% probability of exceedance scenarios. Also, low-lying residential buildings in Yeppoon would be subject to 3.12–5.83 m storm surge that could cause significant building contents damage and lead to severe business interruption.

For a non-cyclonic region located south of, say, 25°S, the methods used for conducting tropical cyclone impact assessments described above could easily be leveraged to evaluate potential tropical cyclone risk, with some slight modifications. For example, one modification would involve updating wind vulnerability curves for residential buildings in Region B to account for the lack of wind resistance, as pointed out in Sect. 10.3. With this modification, local emergency managers and community planners can run pre-incident training exercises based on realistic tropical cyclone scenarios for the region of interest. During the pre-incident training exercise, emergency services personnel would respond to the landfall event as if it were occurring with available personnel and resources. Response activities would be documented to learn how to improve inefficiencies and identify what additional resources may be needed to adequately respond to the disaster.

10.4.2 Challenges in Adapting to and Mitigating for Future Tropical Cyclone Impacts

While scenario case studies can provide unique insight to potential future impacts that may arise from landfalling tropical cyclones, these case studies, alone, cannot drive adaptation and mitigation planning. As alluded to in Sect. 10.3.3, only a relatively small proportion of citizens (based on U.S. statistics) suggest they would make improvements to their houses if reduced insurance premiums were made available. Other behavioral drivers need further exploration to better understand complex behavior in human decision making. A better understanding of this behavior could potentially inform building codes and standards we use today as well as the insurance industry to create incentive programs that meet the needs of communities. To acquire this behavioral information, multidisciplinary teams made up of actuaries, atmospheric scientists, economists, engineers, geographers, psychologists, social scientists, and underwriters need to be formed to address how humans respond to changes in built environments. This can provide the missing perspective on what drives individuals to take adaptation actions.

In concert with acquiring a better understanding of what drives individuals to take adaptation actions, we also need to focus our attention on the performance of the built environment and predicting future disaster outcomes. Currently, we lack quantitative information about the built environment we dwell in and heavily utilize. In a post-event scenario, we rely on post-event failure analysis assessments to infer performance. Using a combination of existing information generated from both aerial (e.g. satellite imagery) and ground-based damage assessments

(e.g. insurance claims, rapid damage assessments), data-driven approaches to assessing built environment performance need to be developed to inform mitigation strategies that improve overall disaster resilience. This approach introduces sensor technology to fill in data gaps about our built environment and combines existing information about not only the built environment, but also the natural (i.e. atmosphere and human) environment to improve our understanding of complex system behavior and response to "shocks." Davies (2015) defines a "shock" as a change in system conditions that has a deleterious impact on the system. These changes may be sudden (e.g. explosions, tornadoes, etc.) or more gradual over time (e.g. roof aging). In some instances, the gradual change may be unacknowledged by the system members and an irreversible damage trajectory gets established (Davies 2015).

Once a better understanding of the physical characteristics of these shocks is achieved and how they introduce vulnerabilities in our built environments, we can then start discussing what drives individuals to adapt and take mitigation actions. Also, we can consider what changes can be made to our existing building codes and standards. Changes to building codes take a long time to implement, so the process of ratifying and updating the building codes and standards would inevitably need to become more dynamic to remain as current as possible. Moreover, with the introduction of smart technologies (i.e. sensors, deep learning algorithms, etc.), there is tremendous potential to begin developing better predictive tools to evaluate infrastructure system performance of our built environment and implement new design and manufacturing strategies that allow our communities to build back better from disasters and recover quicker.

10.5 Summary and Conclusions

The primary aim of this chapter was to qualitatively summarize the current state of knowledge on poleward migrating tropical cyclone activity in the Southern Hemisphere and current building practice in Australia to better understand how poleward migration of tropical cyclones could impact communities in Australia in traditionally non-cyclonic regions. The chapter begins with a summary of research activities on poleward migrating tropical cyclones and highlights the statistical significance of the poleward shifts in the Southern Hemisphere. Potential drivers of the geographical shift were discussed. It is still unclear what mechanisms are driving the poleward shift in tropical cyclone activity and research in this area is becoming more critical as we become accustomed to experiencing stronger tropical cyclone activity as the "traditional" tropical latitudes continue to expand.

Following the discussion on poleward migration of tropical cyclone activity, a summary of current building practice in cyclonic and non-cyclonic regions of Australia is presented. While building codes and practice has evolved over time to a point where our residences are performing better in extreme events, we still lack (i) appropriate means of assessing quantitative building performance in cyclonic and

non-cyclonic regions; (ii) information on human responses to shocks in our built and natural complex systems; and (iii) robust programs to incentivize adaptation and mitigation measures. This lack of knowledge and tools is due in large part to the influence of cultural norms that sway human decision making. To improve disaster resilience in Australia and globally, more research needs to be conducted using cross-disciplinary approaches that observe built and natural complex system behavior to improve our understanding of shocks and their impacts on human decision making.

References

Australia Building Codes Board (2016). National construction code series: building code of Australia. Class 2 to class 9 buildings, vol 1

Boon H, Cottrell A, King D, Stevenson R, Millar J (2012) Bronfenbrenner's bioecological theory for modelling community resilience to natural disasters. Nat Hazards 60:381–408

Boughton G, Henderson D, Ginger J, Holmes J, Walker G, Leitch C, Somerville L, Frye U, Jayasinghe N, Kim P (2011). Tropical Cyclone Yasi: structural damage to buildings. Cyclone Testing Station, James Cook University, Report TR57. http://www.jcu.edu.au/cts/research_reports/index.htm

Boughton GN, Falck DJ, Henderson DJ, Smith DJ, Parackal K, Kloetzke T, Mason M, Krupar RJ, Humphreys MT, Navaratnam S, Bodhinayake G, Ingham S, Ginger JD, Krupar RJ (2017) Technical report No. 63: tropical cyclone Debbie damage to buildings in the Whitsunday Region. Cyclone Testing Station, James Cook University Townsville, Australia

Davies T (2015) Developing resilience to naturally triggered disasters. Env Syst Decis 35:237–251

Kossin J, Emanuel K, Vecchi GA (2014) The poleward migration of the location of tropical cyclone maximum intensity. Nature 509:349–352

Krupar RJ III, Mason MS (2017) A modified Severe Tropical Cyclone Marcia (2015) scenario: wind and storm tide hazards and impacts. Bushfire and Natural Hazards Cooperative Research Centre, Melbourne

Mason MS, Parackal KI (2015) Vulnerability of buildings and civil infrastructure to tropical cyclones: a preliminary review of modelling approaches and literature. Bushire and Natural Hazards CRC, Melbourne

Moon IL-J, Kim S-H, Klotzbach P, Chan JCL (2015) Roles of interbasin frequency changes in the poleward shifts of the maximum intensity location of tropical cyclones. Env Res Lett 10:1–9

Parackal K, Mason M, Henderson D, Stark G, Ginger J, Somerville LR, Harper B, Smith DJ, Humphreys MT (2015) Investigation of damage: Brisbane QLD, 27 November 2014 severe storm event. Cyclone Testing Station, James Cook University

Poussin JK, Botzen WJW, Aerts JCJH (2014) Factors of influence on flood damage mitigation behaviour by households. Environ Sci Pol 40:69–77

Ramsay H (2014) Shifting storms. Nature 509:290–291

Sink A (2008) My Safe Florida Home program. In: Proceedings of the Hurricane risk mitigation forum

Smith DJ, Henderson DJ, Ginger JD (2015) Insurance loss drivers and mitigation for Australian housing in severe wind events. 14th International Conference on Wind Engineering, Porto Alegre, Brazil, June 21–26

Smith DJ, McShane C, Swinbourne A, Henderson DJ (2016) Toward effective mitigation strategies for severe wind events. Aust J Emerg Manag 31:33–39

Standards Australia (2011) AS/NZS 1170.2 structural design actions, part 2 wind actions. Sydney

Standards Australia (2012) AS 4055 wind loads for housing. Sydney

Walker G (1975). Report on Cyclone Tracy – effect on buildings – Dec 1974. Australian Department of Housing and Construction

Walsh K, Mcbride J, Klotzbach P, Balachandran S, Camargo S, Holland G, Knutson T, Kossin J, Lee T, Sobel A, Sugi M (2016) Tropical cyclones and climate change. Wiley Interdiscip Rev Clim Chang 7:65–89

Chapter 11
Metocean Conditions in Future Hurricane Environments

James M. Done, Cindy L. Bruyère, and Ming Ge

Abstract The offshore energy industry in the Gulf of Mexico is exposed to substantial hurricane risk. The plausible scenario of the hurricane climate changing in response to climate change could severely impact the industry, yet understanding changes in hurricanes on regional scales is challenging due to the small number of events and high variability. For impacts, loading on facilities is a complex function of wind, waves and ocean currents. To understand future loading scenarios, it therefore becomes necessary to account for these multiple load drivers. An approach is developed to assess future changes to metocean (Metocean is an offshore engineering term used to describe combined meteorological and oceanographic conditions) conditions in hurricane environments using physical modeling that captures relationships between wind, waves, and current. For a set of nine historical Gulf of Mexico hurricanes, the effects of the hurricane wind fields on ocean waves and currents are simulated using analysis winds to drive a wave model and a regional ocean model. The generalized extreme value distribution describes wind, wave height, wave period, and surface ocean current well. In addition, significant wave height is significantly correlated with wave period and wind speed in hurricane environments. The effects of the hurricane wind fields are simulated again with modified hurricane wind fields consistent with future climate scenarios, while keeping the current climate ocean forcing fixed. Under the future scenario of 10% increase in wind speed and 10% reduction in storm size, the distributions shift to

J. M. Done (✉)
National Center for Atmospheric Research, Boulder, CO, USA

Willis Research Network, London, UK
e-mail: done@ucar.edu

C. L. Bruyère
National Center for Atmospheric Research, Boulder, CO, USA

Environmental Sciences and Management, North-West University, Potchefstroom, South Africa
e-mail: bruyerec@ucar.edu

M. Ge
National Center for Atmospheric Research, Boulder, CO, USA
e-mail: mingge@ucar.edu

J. M. Collins, K. Walsh (eds.), *Hurricane Risk*, Hurricane Risk 1,
https://doi.org/10.1007/978-3-030-02402-4_11

higher significant wave heights and longer peak wave periods with the largest proportional increases at the highest percentiles. The higher percentiles show future increases of up to 16% across the metocean variables with significant wave heights seeing the largest proportional increases. Integrating these results with engineering design protocols is anticipated to lead to better planning guidelines that will enable improved design of structures and operating procedures, and minimize environmental and safety risks.

Keywords Future hurricanes · Metocean conditions · Significant wave height

11.1 Introduction

Hurricane Katrina resulted in major losses to the offshore energy industry, including damage to numerous offshore facilities and severe damage to Royal Dutch Shell's Mars platform that was built to withstand 140 mph winds and simultaneous 70 ft waves (Hays 2007). Average loss per storm is in the billions of US dollars in lost production, evacuation costs, and damage to rigs, pipelines, ships, and onshore facilities (Somerville 2010). Any change in hurricane activity will therefore substantially impact the offshore energy industry.

The North Atlantic basin has experienced decadal variability and longer-term trends in hurricane activity (Holland and Bruyère 2014; Holland and Webster 2007; Bell and Chelliah 2006), bringing dramatic swings in metocean conditions. Changes in extreme metocean conditions arise mainly from variations in hurricane frequency, intensity, size, and forward speed that drive damaging waves and currents. Major hurricanes have become more frequent in recent decades (Holland and Bruyère 2014) and, according to recent assessments, average and maximum hurricane intensity is projected to increase in the future (Walsh et al. 2016; Knutson et al. 2013; Done et al. 2015; Tye et al. 2014). Such changes will have far reaching effects on offshore energy safety and production. However, little can be said with confidence about future hurricane activity on small regional scales such as the Gulf of Mexico due to large interannual and internal variability (e.g., Done et al. 2014). This lack of clarity presents potential safety, environmental, and production risks of an uncertain magnitude. Offshore facilities may be under-designed, and older facilities may need hardening in order to maintain presently accepted risk levels.

Accurate estimates of loading are critical to avoid damage in the case of underestimation and unwarranted costs in the case of overestimation. Accepted annual failure rates typically span 1/100–1/1000 year for non-life risk and up to 1/10,000 year for life risk. Steel jackets, for example, are normally designed for the 1/100 year storm because they have reserve strength after impact (Forristall and Cooper 2016). Loading on facilities is a complex function of characteristics of the wind field and characteristics of the wave field and ocean currents. For example, the pitch of a vessel is a combined function of wave period and wave height, and loading on some structures can depend critically on directional criteria. Adding to this complexity are correlations among wind, waves, and currents (WWC) under hurricane conditions (Forristall and Cooper 2016). Simple empirical relationships

between WWC therefore miss some of the essential physics under hurricane conditions, and this asymptotic dependence therefore needs to be accounted for in risk assessments. For example, hurricanes alter the surface temperature of the ocean over which they pass through wind-driven ocean mixing across the thermocline and the excitation of inertial oscillations in the wake of the storm that can lead to substantial additional mixing and cooling of the upper ocean (Price 1981). The cooler sea surface temperatures can, in turn, feed back to the atmosphere and weaken the storm. These physical processes therefore need to be incorporated to account for the non-linear processes that result in extreme loading events.

Future hurricane activity has been assessed using free running global climate models (Wehner et al. 2017) or regional climate models (Bruyère et al. 2017; Knutson et al. 2013); However, these approaches suffer from a low sample size and struggle to identify a climate change signal on the scale of basin sub-regions such as the Gulf of Mexico (Cobb and Done 2017). An alternative approach downscales the large-scale environment from the global climate model using a fast hurricane model to generate a large number of events (e.g., Emanuel et al. 2006, 2008). Meza-Padilla et al. (2015) used this approach to drive wave and surge models to assess extreme wave and water heights in the Gulf of Mexico. Appendini et al. (2017) extended this approach to quantify future change in wave heights in the Gulf of Mexico. Results were dependent on the specific global climate model projection. The more controlled approach of Pseudo Global Warming (PGW) adds a climate change 'delta' to historical environmental conditions (Gutmann et al. 2018; Parker et al. 2018; Lackmann 2015). Here, we design a novel controlled simulation approach to assess metocean conditions for historical hurricanes. Historical events have been used previously to characterize extreme wave heights in the Gulf of Mexico (Panchang et al. 2013). We extend this approach to study future changes. We borrow the concept of PGW, but rather than modifying the historical environment, the hurricane winds themselves are modified according to scientific consensus climate change effects. Future changes in metocean conditions are quantified by combining the physical modeling results with statistical distribution fitting, described in the next section.

The physical and statistical modeling approaches are described in the next section. Results are presented in Sect. 11.3 and a discussion and conclusions are presented in Sect. 11.4.

11.2 Methods

A controlled modeling approach to assess future changes in extreme metocean conditions in hurricane environments is described in the following subsections. First, for nine historical Gulf of Mexico hurricanes, the effects of the hurricane wind field on ocean currents and waves is simulated using numerical modeling. Historical hurricane wind fields are reconstructed using available analysis data and used to drive regional ocean and wave models. Second, a statistical description of

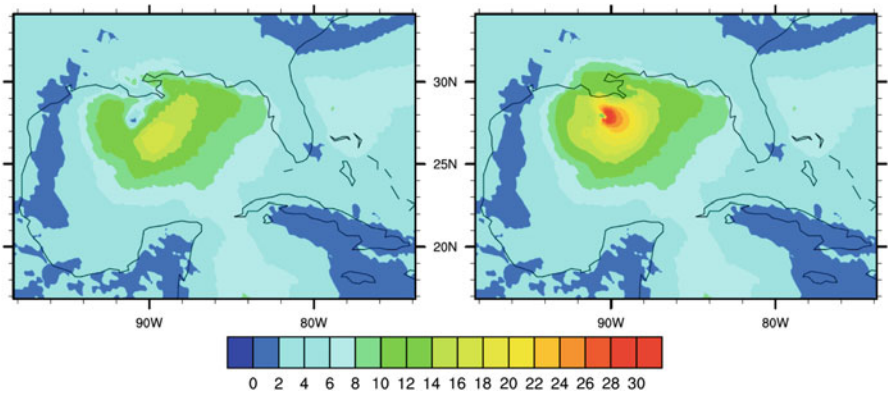

Fig. 11.1 Wind speed (ms^{-1}) for Hurricane Lili (2002) just prior to landfall shown in (left) NARR, and (right) H*WIND combined with NARR

metocean variables from the nine simulations is developed and used to assess WWC probabilities in the current climate. Finally, the hurricane wind fields are modified according to scientific consensus on likely climate change effects on hurricane winds and used to rerun the ocean and wave models. Statistical modeling is again used to assess potential future changes in WWC probabilities.

11.2.1 Historical Hurricane Wind Field Reconstruction

Historical hurricane wind fields are taken from the National Oceanic and Atmospheric Administration (NOAA) Hurricane Research Division (HRD) Real-time Hurricane Wind Analysis System (H*WIND) project (http://www.hwind.co/legacy_data/, Powell et al. 1998). H*Wind is an approximation of the actual wind field based on available surface, aircraft, and remote sensing data and is a readily accessible, publicly available surface wind analysis for historical hurricanes. H*WIND only covers a small geographic region, therefore the less detailed North American Regional Reanalysis (NARR, Mesinger et al. 2006) is used to fill in the wind field in the surrounding environment. Figure 11.1 shows the impact of merging H*WIND with NARR for the case of Hurricane Lili (2002). Lili approached offshore structures in the Gulf of Mexico as a category 4 hurricane, resulting in half a billion (2002) US dollars in losses to the offshore energy industry (Willis Energy Loss Database, unpublished data, 2009). H*WIND captures smaller scale hurricane structure, a tighter hurricane core, and higher peak wind speeds of 40 ms^{-1} compared to the 18 ms^{-1} produced by NARR (Fig. 11.1). Peak winds are still less than the observed 64 ms^{-1} (IBTrACS, Knapp et al. 2010) largely because the 12-km grid used to construct the regional wind field is too coarse to retain fine scale wind maxima. This improved wind field characterization leads to much-improved simulated peak significant wave heights, as described in the next subsection.

11.2.2 Simulating Historical Waves and Currents

The reconstructed hurricane wind fields are used to drive the Regional Ocean Modeling System (ROMS, Shchepetkin and McWilliams 2005), and the Shallow Waves Nearshore (SWAN: Booij et al. 1999) model. ROMS and SWAN are two-way coupled to capture the two-way wave-current interactions and operate within the coupling framework of the Coupled-Ocean-Atmosphere-Wave-Sediment Transport Modeling System (COAWST: Warner et al. 2010). Prior work has shown COAWST can produce a reasonable simulation of waves and ocean currents in hurricane environments (e.g., Zambon et al. 2014; Olabarrieta et al. 2012).

11.2.2.1 Ocean Model

ROMS is a free-surface, hydrostatic, primitive equation ocean model. For this study, ROMS is employed with a 12 km grid spacing on a 159×159 grid and a terrain following coordinate with 16 vertical levels. The model domain and bathymetry are shown in Fig. 11.2. Bathymetry has a minimum depth of 5 m. Model initialization and lateral boundary conditions along the eastern and southern portions of the domain for the variables of free surface, three-dimensional momentum, potential temperature and salinity are specified, with values from the 1/25° Hybrid Coordinate Ocean Model (HYCOM) with Naval Research Lab Coupled Ocean Data Assimilation (NCODA, Cummings 2005) Southeast United States analysis (2003–2010), or the HYCOM + NCODA Global 1/12° Reanalysis for earlier storms. Lateral boundaries use a 0.5-day relaxation for inflow and 10-day relaxation for outflow conditions. ROMS receives surface heat fluxes from HYCOM at the surface. The model uses a 30-s baroclinic timestep with model-splitting ratio of 30. The Generic Length-Scale turbulence closure is used for vertical mixing and to specify the quadratic drag formulation for the bottom friction (Warner et al. 2005).

11.2.2.2 Wave Model

SWAN is a spectral wave model that includes wave generation, propagation, defraction, non-linear wave interactions, and dissipation. It computes random, short-crested, wind-generated waves and uses the same grid as ROMS (Fig. 11.2). SWAN is spun up from a state of rest after initial time, and boundary data are provided by 3-hourly output from the 10 arc minute North Atlantic regional wave spectral model WAVEWATCH III. We use 36 directional bins and 24 frequency bins of 1 s width between 1 and 25 s. Nonlinear quadruplet wave interactions are activated, wave bottom friction is parameterized using the Jonswap formulation, and the depth-induced breaking constant is set to 0.73. Whitecapping is activated and wind-wave growth is generated using the Komen formulation. The drag coefficient

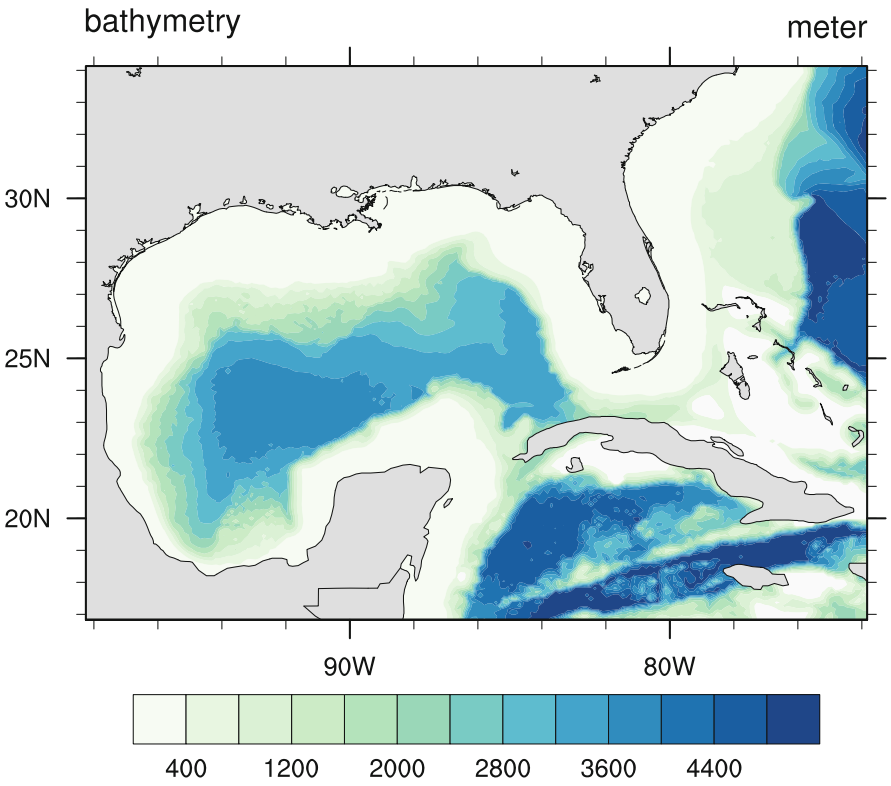

Fig. 11.2 ROMS and SWAN model domains with bathymetry contoured (m)

is capped at 0.0022, based on measurements showing the coefficient saturates at hurricane wind speeds (Powell et al. 2003).

11.2.2.3 Model Coupling

Although full coupling brings a more physically realistic air-sea interaction (e.g., Mooney et al. 2016), we choose not to use a fully coupled atmosphere-ocean simulation system in order to retain control of the wind fields and explore the ocean response to specified changes in the wind fields. This approach follows that of Wang and Oey (2008) who were able to control the wind speed of Hurricane Katrina using prescribed winds to drive the ocean. Our model components, input data, and flow of information between model components are summarized in Fig. 11.3. Data are exchanged between ROMS and SWAN every 10 min using the Modeling Coupling Toolkit (MCT, Warner et al. 2008). Hydrodynamic information such as surface elevations and currents are provided to SWAN by ROMS. Currents modify the effective wind forcing and the propagation velocity of wave energy.

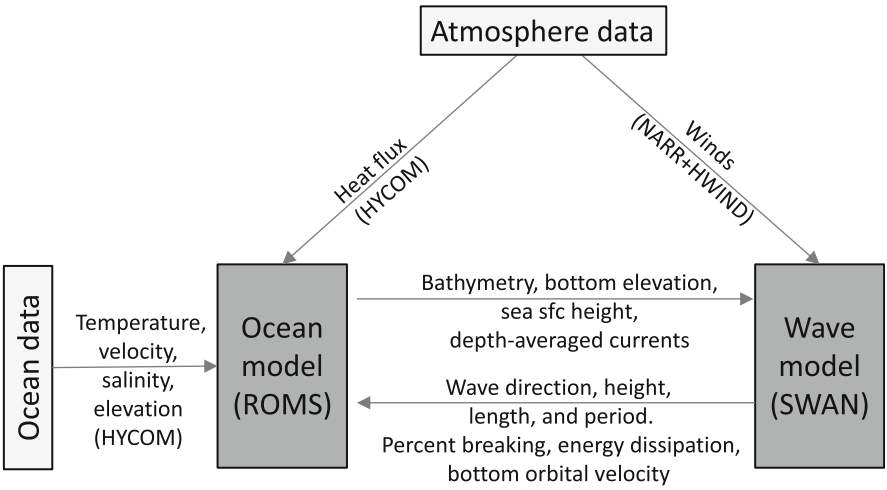

Fig. 11.3 Flow diagram of the numerical modeling approach, indicating input data sources and flow of information between model components

Currents can also cause wave refraction and wave modification due to bottom drag. In return, SWAN sends wave information including wave height, direction, period, length, and energy dissipation to ROMS to modify the bottom shear stress and calculate wave mixing to resolve the wave-current interaction, as summarized in Rong et al. (2014). The full list of variables exchanged are shown in the flow diagram in Fig. 11.3.

11.2.3 Case Studies

Our emphasis on case study scenarios rather than free-running climate simulations has the advantage of assessing historical hurricanes under different scenarios, rather than looking at simulated events in a free-running regional climate simulation. While free-running climate simulations are physically possible, they do not have one-to-one correspondence with historical hurricanes. The set of nine historical Gulf of Mexico hurricanes are shown in Fig. 11.4, including Lili (2002), Ivan (2004), Dennis (2005), Katrina (2005), Rita (2005), Gustav (2008), Ike (2008), Ida (2009) and Isaac (2012). These nine hurricanes were chosen because of their track over the region of spatially dense offshore energy facilities (Fig. 11.4). Katrina was included specifically because of its strong interaction with the Loop Current in the Gulf. These nine cases are simulated using the modeling system described in Sect. 11.2.2 and used to build a statistical characterization of relationships between metocean variables in hurricane environments.

For a coupled simulation of Hurricane Ike, Winterbottom et al. (2012) used a 5-day spin-up period before the analysis period to allow the ocean mixed layer to

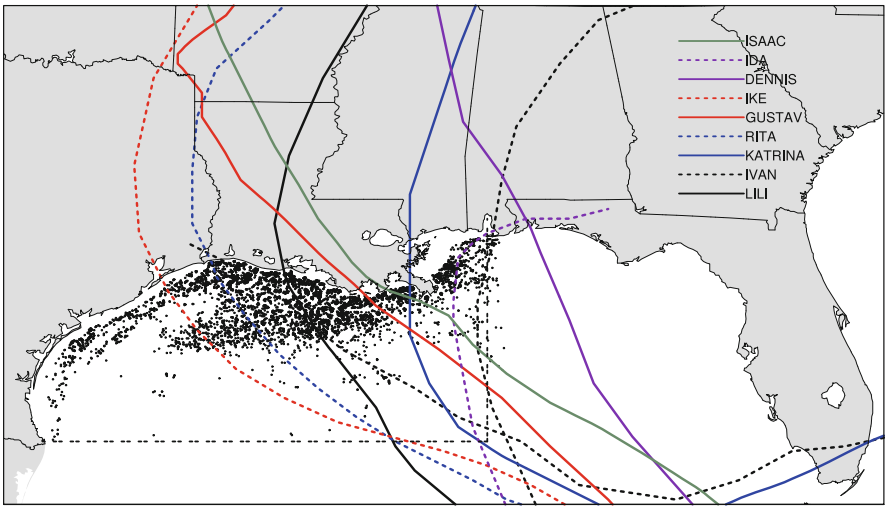

Fig. 11.4 Tracks of the nine historical Gulf of Mexico hurricanes used in this study: Lili (2002), Ivan (2004), Dennis (2005), Katrina (2005), Rita (2005), Gustav (2008), Ike (2008), Ida (2009) and Isaac (2012). Platform locations in the Gulf of Mexico as of 02/03/15 (black dots) mostly lie within the region bounded by (26°N, 88°W, black dashed lines). (Data sources: Bureau of Ocean Energy Management, IBTrACS)

Table 11.1 Simulation start times, times of peak wind speed in the northern Gulf of Mexico (taken from IBTrACS, Knapp et al. 2010), and simulation length for the nine hurricanes

Hurricane	Simulation start time	Time of peak wind speed	Simulation length (hours)
Lili	2002-10-01 00Z	2002-10-03 00Z	60
Ivan	2004-09-13 00Z	2004-09-14 00Z	84
Dennis	2005-07-08 00Z	2005-07-10 12Z	72
Katrina	2005-08-27 00Z	2005-08-28 18Z	72
Rita	2005-09-20 12Z	2005-09-22 06Z	96
Gustav	2008-08-30 00Z	2008-09-01 12Z	72
Ike	2008-09-09 00Z	2008-09-13 00Z	108
Ida	2009-11-08 00Z	2009-11-09 18Z	60
Isaac	2012-08-26 12Z	2012-08-29 00Z	84

spin up with the atmospheric forcing. They showed substantial variability in the ocean mixed layer kinetic energy in the first 24–36 h of spin-up as the ocean state adjusted to the atmosphere. Our simulation lengths vary between 2.5 and 4.5 days depending on the hurricane track and we do not explicitly allow for a period of spin up. However, most of the simulations begin when the hurricanes are outside the Gulf of Mexico and all begin well before the peak hurricane intensity in the northern Gulf (Table 11.1). Therefore, the extreme values of WWC should be reasonably spun up.

The extent to which this modeling approach can capture observed significant wave height (defined as the average of the highest one-third of waves, measured

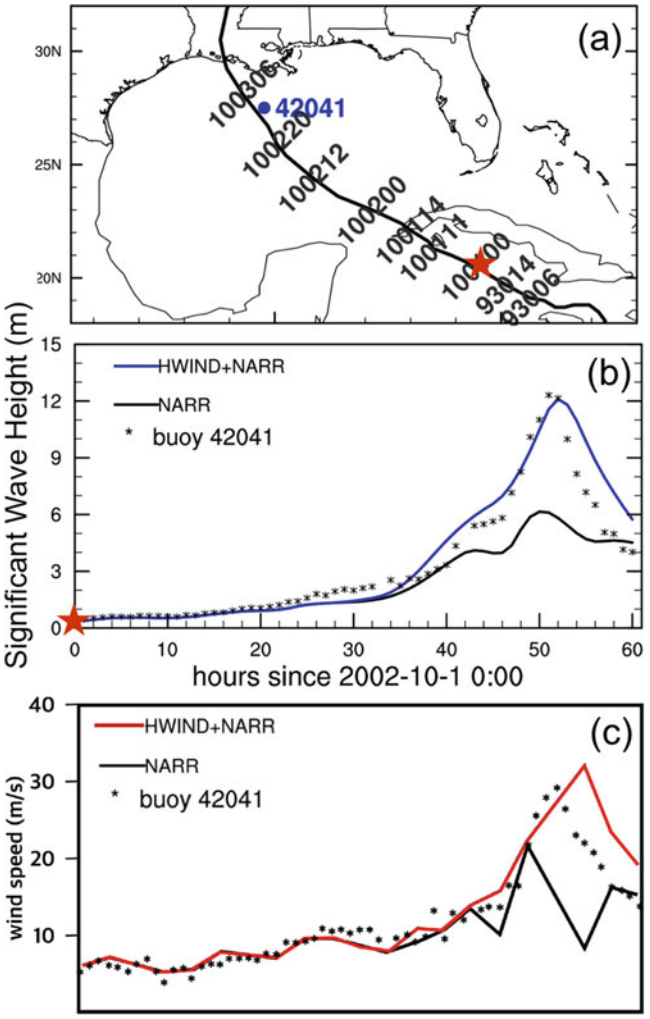

Fig. 11.5 (**a**) Track of Hurricane Lili (2002) and the location of buoy 42041. The red star indicates the location of the hurricane at the start of the simulation. (**b**) Timeseries of significant wave height (m) at the location of buoy 42041. (**c**) Timeseries of wind speed (ms^{-1}) at the location of buoy 42041. Shown in (**b**) and (**c**) are observations (black stars), simulation driven by NARR winds (black lines), and the simulation driven by combined NARR and H*WIND winds (colored lines). Observations are provided by the NOAA National Data Buoy Center

from trough to crest) is illustrated for the case of Hurricane Lili (2002) using data at the location of NOAA buoy 42041. The location of buoy 42041 and the track of Lili are shown in Fig. 11.5a. Figure 11.5b shows that the use of the combined NARR and H*WIND analyses doubles the storm maximum significant wave height from 6 to 12 m due to the substantial increase in wind speeds (Fig. 11.5c). The simulation is

also able to reasonably reproduce the observed time-series and storm maximum significant wave height of 12 m at the location of buoy 42041.

11.2.4 Statistical Assessments of the Extremes

In the absence of readily available response functions for specific structures, we explore relationships among metocean variables and future changes more generally for the region of the Gulf of Mexico. Using a fixed location in time would be more appropriate for a point assessment for a given offshore facility, but here we develop a more regional assessment over the Gulf of Mexico. This regional approach also increases our sample size of extreme conditions compared to a fixed location.

The simulations produce spatial snapshots of wind, wave, and current fields every hour, giving approximately 699 data times (the sum of the simulation lengths shown in Table 11.1). To minimize the effects of spatial dependency between data points, we take a single data value for each variable at each time. Given that the significant wave height is a common variable in a response function (Forristall and Cooper 2016), all variables are taken at the location of the maximum significant wave height every hour. This approach does not remove any temporal dependence in the data, but we consider this secondary to the high spatial dependence.

Assessing extremes requires extrapolation beyond the sample of nine storms. Fitting theoretical generalized extreme value (GEV) distributions to the simulated distributions allows us to assess the extremes. In Panchang et al. (2013), the Gumbel, Weibull, and the GEV distributions are applied to significant wave height data with 100-year values ranging from 19.1 to 26.7 m. They note the high uncertainty introduced by few observations in the tail but conclude that GEV is preferential for applications sensitive to the extremes. The use of GEV was also justified in Meza-Padilla et al. (2015) since it combines many families of distributions and is adaptive to the data. While the GEV can produced higher values in the tail than, say, the Weibull, they suggest GEV is more reliable since the Weibull rarely goes above the maximum observed values. We therefore apply GEV and take the simple approach of block maxima, taking 1 value per hour.

11.2.5 Idealized Future Climate Scenarios

A simple and controlled simulation approach is designed to assess future changes in metocean conditions in hurricane environments. This approach modifies the set of historical hurricane wind fields according to scientific consensus about the effects of climate change on hurricane wind fields. We choose to only change the hurricane wind fields and not also change the ocean state. However, climate change is likely to impact Gulf of Mexico temperatures (e.g., Biasutti et al. 2012), stratification, and ocean currents, and this may change the ocean response to the hurricane wind field.

While our approach includes the hurricane response to this enhanced oceanic energy source through the controlled increase in wind speed, possible differences in the ocean current and wave response due to the changed ocean state are excluded. This intentionally isolates the effects of future hurricane wind conditions on a given ocean state.

Three idealized future climate scenarios are chosen to sample physically plausible future changes to hurricane wind fields; a uniform 10% increase in hurricane wind speed, a 10% reduction in hurricane size (as defined by the radius of 64-knot winds), and both a 10% increase in hurricane wind speeds and a 10% reduction in hurricane size. The 10% increase in hurricane wind speeds is at the upper end of scientific consensus in the change in hurricane intensity over the twenty-first century (Walsh et al. 2016; Knutson et al. 2010). There is no scientific consensus on future changes to hurricane size, so our chosen size changes should be interpreted as a sensitivity study within physically plausible bounds. However, a reduction of hurricane size was projected in a regional climate change experiment by Done et al. (2015) and represents a physically plausible future scenario.

The three idealized scenarios only sample a small range of possible future scenarios. For example, larger hurricanes in the future are not considered nor is the potential for faster or slower moving hurricanes. However, constrained by computational resources, the three scenarios explored here provide an indication of the potential magnitude of future changes and provide a foundation to explore the broader range of future scenarios. Perhaps more important is that this approach does not allow for potential future changes in hurricane frequency. Given that there is no consensus indication from the community of significant change in hurricane frequency, particularly on small regional scales such as the Gulf of Mexico, our approach of no change in hurricane frequency is appropriate. There is even a lack of consensus for North Atlantic hurricane frequency change, with the average over many studies pointing to no change in frequency of all TCs or a slight decrease (Walsh et al. 2016).

11.3 Results

11.3.1 Current Climate

The probability distributions of peak wave period, significant wave height, maximum wind speed, and surface ocean current for the nine hurricanes under current climate conditions are shown in Fig. 11.6. These distributions use data at the locations of maximum significant wave height every hour. GEV fits to the data describe the distributions well (Fig. 11.6). The fitted distribution parameters and estimates of the 1% annual exceedance values are given in Table 11.2. The shape parameter is negative for wind speed and significant wave height, indicative of a reverse Weibull-type distribution that has a bounded upper tail. This is not to be confused with the ordinary Weibull distribution that has a positive-definite shape

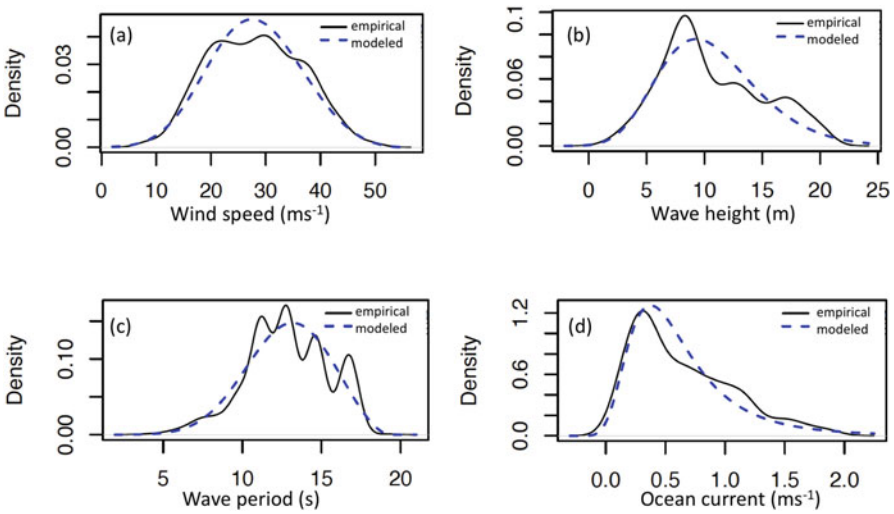

Fig. 11.6 Probability distributions of wind speed (**a**), wave height (**b**), wave period (**c**) and upper ocean current (**d**) for the nine historical hurricanes under current climate conditions. Data are at the location of the maximum significant wave height every hour through the simulations. Blue dashed lines indicate the fitted generalized extreme value distribution

Table 11.2 Attributes of the GEV distributions fitted to wind speed, wave period, significant wave height and ocean current for current climate

	Significant wave height (m)	Wave period (s)	Surface Ocean current (ms^{-1})	Wind speed (ms^{-1})
Location	8.8 (0.17)	12.0 (0.11)	0.42 (0.01)	25.1 (0.35)
Scale	3.9 (0.12)	2.7 (0.08)	0.29 (0.01)	8.3 (0.25)
Shape	−0.11 (0.03)	−0.37 (0.01)	0.17 (0.04)	−0.26 (0.03)
1% annual probability	22.6 ± 1.6	18.0 ± 0.2	2.45 ± 0.4	47.1 ± 1.5

Standard errors are given in parentheses. Ninety percent confidence bounds are given for the 1% annual probabilities

parameter and a bounded lower tail. The reverse Weibull has been used to describe hurricane wind speeds (Heckert et al. 1998) and is consistent with physical constraints on storm intensity dictated by maximum potential intensity theory (Holland 1997; Emanuel 1988). It also seems physically plausible for an upper bound to exist for wave height (as indicated here by the negative shape parameter) given the geographic constraints of water depth and fetch limitations, and physical constraints on the hurricane wind field.

The 1% annual exceedance wind probability of 47.1 ms^{-1} (high category 2 wind speeds) is lower than expected because the 12 km analysis grid does not retain small-scale wind maxima. Also, wind data are taken at the locations of maximum significant wave height and so the maximum values in the wind field may be missed. The 1% annual exceedance significant wave height of 22.6 m falls in the middle of the range found by Panchang et al. (2013), but is higher than the maximum values observed during recent major hurricanes. For example, 16.9 m was observed by National Buoy Data Center's buoy number 42040 during Hurricane Katrina. This apparent high value could be due to a combination of model bias and the fact that the 1% exceedance value is for anywhere in the Gulf of Mexico rather than for a single location. Peak surface current of almost 2.5 ms^{-1} were observed during Hurricane Katrina at the Telemark platform (Frolov 2010) and is similar to the 1% annual exceedance value estimated here.

11.3.2 Relationships Among Metocean Variables

While univariate analyses characterize extremes of metocean variables, structural response functions are often combinations of metocean variables. Without a specific structure to guide the analysis of joint extremes, dependence among metocean variables is explored briefly here through an analysis of relationships among key pairs of variables. Given that the significant wave height is a common variable in a response function (Forristall and Cooper 2016) we explore significant wave height paired with other metocean variables. Significant wave height is positively correlated with peak wave period and maximum wind speed. The bulk distributions of significant wave height and peak wave period are correlated at $r^2 = 0.85$, and significant wave height and maximum wind speed are correlated at $r^2 = 0.77$. The implications of such strongly correlated load drivers is discussed in Sect. 11.4.

11.3.3 Future Climate

The impact of the three idealized future climate scenarios on significant wave height for the case of Hurricane Lili is conveyed in Fig. 11.7. The results of future changes are in agreement with expectations, with the 10% increase in wind speed increasing the significant wave heights and the 10% decrease in hurricanes size decreasing the significant wave heights. The combination of 10% increase in wind speed and 10% decrease in hurricane size also led to a decrease in significant wave heights.

Increased wind speeds increase the wind stress on the ocean surface. For neutral stability conditions within the hurricane boundary layer, the wind stress is proportional to the square of the wind speed. This means a 10% increase in wind speed increases the wind stress by 21%; however, the drag coefficient also increases with wind speed, thus further increasing the wind stress. Here, the drag coefficient is

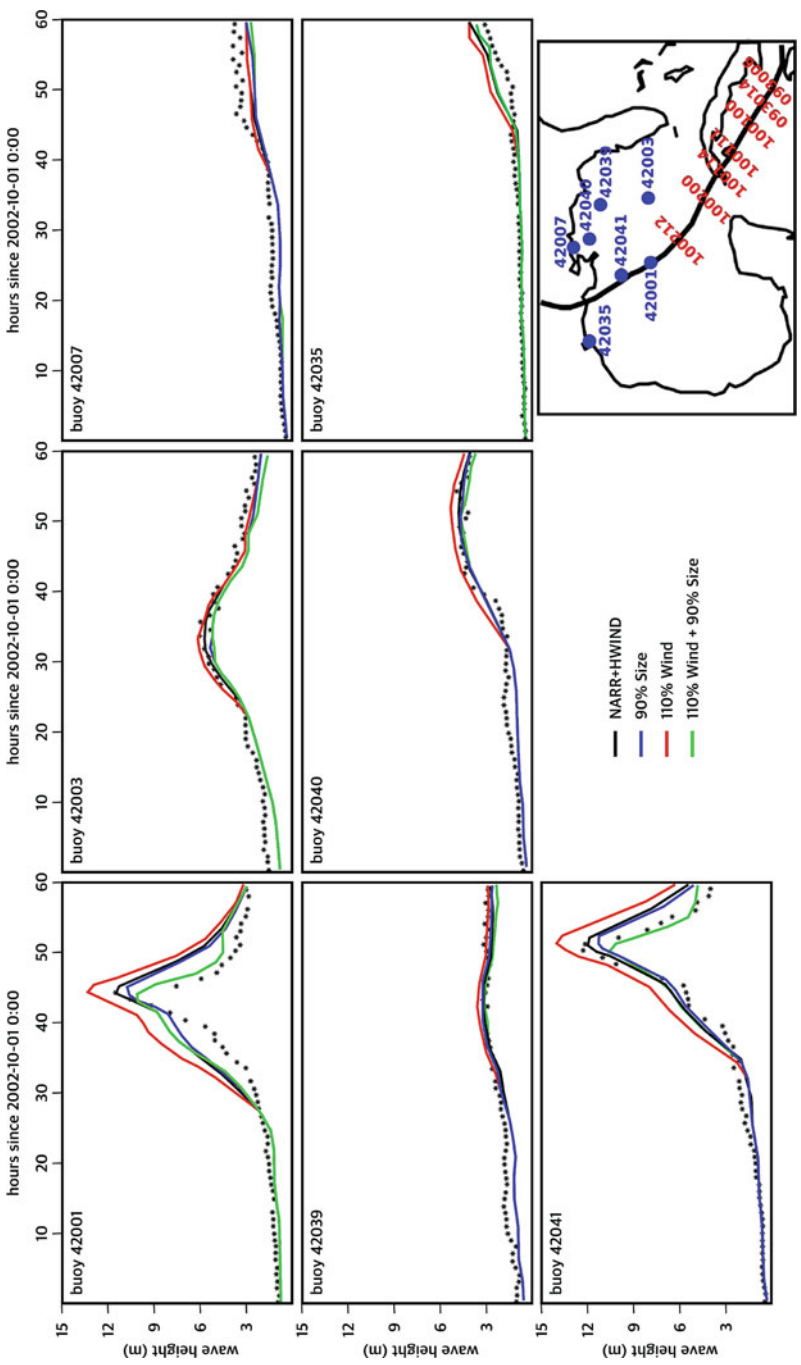

Fig. 11.7 Time series of significant wave height (m) during Hurricane Lili (2002) at seven buoys for (black stars) buoy observations, (black line) using H*WIND+NARR winds, and three future climate scenarios: (red line) 10% increase in wind speed, (blue line) 10% decrease in size, and (green) 10% increase in wind speed and 10% decrease in size. The locations of the buoys are indicated in the bottom right panel

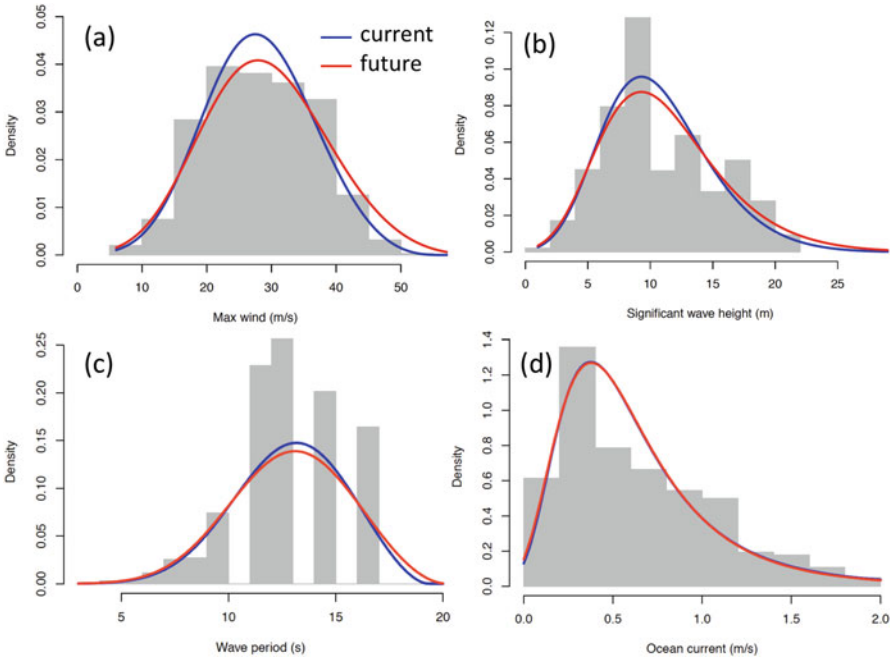

Fig. 11.8 Probability distributions of wind speed (**a**), wave height (**b**), wave period (**c**) and upper ocean current (**d**) for the nine historical hurricanes. Grey bars are the empirical distributions for current climate. Data are at the location of the maximum significant wave height every hour through the simulations. The lines indicate the generalized extreme value distribution fitted to current climate data (blue) and future climate data (red)

capped at 0.0022 based on measurements showing the coefficient saturates at hurricane wind speeds (Powell et al. 2003). This enhanced wind stress increases the momentum exchanged from the winds to the waves.

The decrease in storm size reduced the area of strongest winds and decreased the peak winds experienced at the location of the buoys in Fig. 11.7 (not shown). This reduction in momentum transferred from the winds to the waves resulted in a reduction in the wave heights. The net effect of increased wind speed and decreased storm size was a reduction in wave height at buoy locations. This suggests that the area of strong winds is more important than the magnitude of the peak wind speeds for simulating wave heights at specific buoy locations. This arises from large changes in wind speed at buoy locations within regions of strong wind gradients. However, the wave heights shown in Fig. 11.7 are constrained to specific buoy locations. As shown next, analyzing the peak wave height anywhere within the storm allows us to explore changes to the highest wave heights.

Considering all storms and all times, a comparison of the modeled distributions of wind speed, significant wave height, wave period, and ocean current at the locations of peak wave height for the current climate and for the future scenario of +10% wind speed and −10% hurricane size is included in Fig. 11.8. The enhanced wind stress in

Table 11.3 Percent future changes in the 90th, 99th and 99.9th percentile values of metocean variables under the idealized future scenario of 10% increase in wind speed and a 10% decrease in hurricane size

	90th	99th	99.9th
Wind speed	7	10	12
Significant wave height	7	12	16
Wave period	2	3	3
Ocean current	−2	−5	−9

the future climate, albeit over a smaller area, results in increased density of the highest values of wave height, wave period, and wind speed. This is reflected in higher scale and location parameters, and reduced magnitude shape parameters of the fitted distributions (not shown). The majority of these highest values occur for the large and intense Hurricanes Ivan and Katrina. For upper ocean current, however, there is no apparent change.

Given that offshore structures are impacted primarily by the extremes, it is instructive to quantify the changes in the most extreme values. The future change in the high percentile values of metocean variables under the future scenario of +10% wind speed and −10% hurricane size is given in Table 11.3. This emphasis on proportional change sidesteps model bias, particularly the low wind speed bias on the 12 km grid. The high percentiles show future increases of up to 16% across the metocean variables, with significant wave heights seeing the largest proportional increases. In contrast, surface ocean currents are reduced under this scenario, seemingly at odds with the enhanced wind stress increasing the momentum exchanged from the winds to the ocean currents. We hypothesize that the smaller storms reduce the resonance effect (Forristall and Cooper 2016) between the Coriolis-driven current rotation and wind stress turning associated with the passage of the storms.

11.4 Conclusions

Reconstructions of historical hurricane wind fields were used to drive physical ocean wave and ocean current models for a set of nine historical Gulf of Mexico hurricanes. The historical events were simulated under historical and future climate conditions to assess potential future changes to metocean variables. The GEV distribution describes the model-simulated metocean variables well, with regional estimates of the 1% annual exceedance values agreeing with previous work. The plausible future scenario of a 10% increase in wind speed and a 10% decrease in size led to future increases in the extremes of all metocean variables, except for surface ocean current

where a decrease was indicated. The biggest proportional increase was in the significant wave height. The future changes are a similar order of magnitude as the change in the 100 year return value when adding a single intense storm to the historical record (Cooper et al. 2005), and highlights the level of uncertainty in assessing extreme values.

Significant relationships are found among metocean variables in hurricane environments, suggesting the need for a more formal multivariate analysis of the extremes. A more simple analysis that reflects the high correlation of metocean variables in hurricane environments would be to combine the n-year wave with 0.95*n-year wind speed and 0.75*n-year current speed. Alternatively, a more comprehensive view mapping the full space could be obtained through environmental contours, in recognition that the maximum structural response may not be at the maxima of the variables. Ultimately, the future changes should be presented in terms of design criteria for specific structures.

These estimations were based on a small sample of nine hurricanes. It is likely that this sample misses portions of the full range of hurricane behavior, such as slow moving or stalled intense hurricanes or very small, intense, and fast-moving storms. While our sample of storms was limited by the availability of high-resolution wind analyses through H*WIND, a more comprehensive study is needed to better characterize the full range of climate change effects. We also assume the same hurricane frequency in current and future climates based on the lack of consensus in the scientific community on future change in hurricane frequency, particularly for small geographical regions such as the Gulf of Mexico. The future wind scenarios considered here are just a few of many possible scenarios, so this study provides an indication of the potential magnitude of future changes. Other limitations include the 12 km grid spacing and the lack of full coupling between the atmosphere, ocean, and waves. This constrained approach misses small-scale coupled processes that are potentially important for assessing future changes to WWC, such as the effect of changes in sea surface roughness on the hurricane wind field. Given that we chose to only change the hurricane wind fields and not also change the ocean state, this study is limited to the effects of future hurricane wind conditions. The effects of a changed future ocean state, such as changed momentum transfer through altered ocean stratification, may be incorporated into future work to understand a broader range of future WWC scenarios.

Integrating these results with engineering design protocols is anticipated to lead to better planning guidelines. For example, the sensitivity of the pitch of a vessel or loading on a structure to climate change may be assessed by modifying the input metocean data by the climate change perturbation found in this study. These improved guidelines will support design of structures and operating procedures, and minimize environmental and safety risks in a changing climate.

Acknowledgements NCAR is funded by the National Science Foundation and this work was partially supported by the Research Partnership to Secure Energy for America (RPSEA), the CASE-EJIP JIP, and the Willis Research Network. We would like to acknowledge high-performance

computing support from Yellowstone (ark:/85065/d7wd3xhc) provided by NCAR's Computational and Information Systems Laboratory's NCAR Strategic Capability allocation.

References

Appendini CM, Pedrozo-Acuña A, Meza-Padilla R, Torres-Freyermuth A, Cerezo-Mota R, López-González J, Ruiz-Salcines P (2017) On the role of climate change on wind waves generated by tropical cyclones in the Gulf of Mexico. Coast Eng J 59:1740001. https://doi.org/10.1142/S0578563417400010

Bell GD, Chelliah M (2006) Leading tropical modes associated with interannual and multidecadal fluctuations in North Atlantic hurricane activity. J Clim 19:590–612. https://doi.org/10.1175/JCLI3659.1

Biasutti M, Sobel AH, Camargo SJ, Creyts TT (2012) Projected changes in the physical climate of the Gulf Coast and Caribbean. Clim Chang 112(3–4):819–845. https://doi.org/10.1007/s10584-011-0254-y

Booij N, Ris RC, Holthuijsen LH (1999) A third-generation wave model for coastal regions, 1. Model description and validation. J Geophys Res 104:7649–7666

Bruyère CL, Coauthors (2017) Impact of climate change on Gulf of Mexico hurricanes. NCAR technical note NCAR/TN-535+STR. https://doi.org/10.5065/D6RN36J3

Cobb A, Done JM (2017) The use of global climate models for tropical cyclone risk assessment. In: Walsh K, Collins J (eds) Hurricanes and climate change. Springer, Cham, pp 167–186

Cooper C, Stear J, Heideman, J, Santala, M Forristall G, Driver D, Fourchy P (2005) Implications of hurricane Ivan on deepwater Gulf of Mexico metocean design criteria. In: Proceedings of the offshore technology conference, Houston Texas, 2–5 May. https://doi.org/10.4043/17740-MS

Cummings JA (2005) Operational multivariate ocean data assimilation. Q J R Meteorol Soc 131:3583–3604. https://doi.org/10.1256/qj.05.105

Done JM, Bruyère CL, Ge M, Jaye A (2014) Internal variability of North Atlantic tropical cyclones. J Geophys Res Atmos 119:6506–6519. https://doi.org/10.1002/2014JD021542

Done JM, Holland GJ, Bruyère CL, Leung LR, Suzuki-Parker A (2015) Modeling high-impact weather and climate: lessons from a tropical cyclone perspective. Clim Chang 129 (3–4):381–395. https://doi.org/10.1007/s10584-013-0954-6

Emanuel KA (1988) The maximum intensity of hurricanes. J Atmos Sci 45:1143–1155

Emanuel K, Ravela S, Vivant E, Risi C (2006) A statistical-deterministic approach to hurricane risk assessment. Bull Am Meteorol Soc 87:299–314

Emanuel K, Sundararajan R, Williams J (2008) Hurricanes and global warming: results from downscaling IPCC AR4 simulations. Bull Am Meteorol Soc 89:347–367

Forristall GZ, Cooper CK (2016) Metocean extreme and operating conditions. In: Dhanak MR, Xiros NI (eds) Springer handbook of ocean engineering. Springer, Cham. https://doi.org/10.1007/978-3-319-16649-0_3

Frolov S (2010) Ocean response to hurricanes in presence of the loop current. In: Proceedings of the offshore technology conference, Houston Texas, 3–6 May. https://doi.org/10.4043/20968-MS

Gutmann ED, Rasmussen RM, Liu C, Ikeda K, Bruyère CL, Done JM, Garrè L, Friis-Hansen P, Veldore V (2018) Changes in hurricanes from a 13 year convection permitting pseudo-global warming simulation. J Clim 31:3643–3657 In Press

Hays K (2007) A survivor in the Gulf: platform producing more oil than it was when Katrina hit. Houston Chronicle. http://royaldutchshellgroup.com/2007/01/21/houston-chronicle-a-survivor-in-the-gulf-shells-mars-platform-producing-more-oil-than-it-was-when-katrina-hit/. Accessed 1 July 2017

Heckert NA, Simiu E, Whalen T (1998) Estimates of hurricane wind speeds by peaks over threshold method. J Struct Eng 124:445–449

Holland GJ (1997) The maximum potential intensity of tropical cyclones. J Atmos Sci 54:2519–2541

Holland G, Bruyère CL (2014) Recent intense hurricane response to global climate change. Clim Dyn 42(3–4):617–627. https://doi.org/10.1007/s00382-013-1713

Holland G, Webster PJ (2007) Heightened tropical cyclone activity in the North Atlantic: natural variability or climate trend? Phil Trans R Soc A 365:2695–2716

Knapp KR, Kruk MC, Levinson DH, Diamond HJ, Neumann CJ (2010) The international best track archive for climate stewardship (IBTrACS): unifying tropical cyclone best track data. Bull Am Meteorol Soc 91:363–376

Knutson TR, McBride J, Chan J, Emanuel KA, Holland GJ, Landsea C, Held IM, Kossin J, Srivastava AK, Sugi M (2010) Tropical cyclones and climate change. Nat Geosci 3:157–163. https://doi.org/10.1038/ngeo779

Knutson TR, Sirutis JJ, Vecchi GA, Garner S, Zhao M, Kim H, Bender M, Tuleya RE, Held IM, Villarini G (2013) Dynamical downscaling projections of 21st century Atlantic hurricane activity: CMIP3 and CMIP5 model-based scenario. J Clim 26:6591–6617

Lackmann GM (2015) Hurricane Sandy before 1900 and after 2100. Bull Am Meteorol Soc 96:547–560. https://doi.org/10.1175/BAMS-D-14-00123.1

Mesinger F, DiMego G, Kalnay E, Mitchell K, Shafran PC, Ebisuzaki W, Jović D, Woollen J, Rogers E, Berbery EH, Ek MB, Fan Y, Grumbine R, Higgins W, Li H, Lin Y, Manikin G, Parrish D, Shi W (2006) North American regional reanalysis. Bull Am Meteorol Soc 87 (3):343–360

Meza-Padilla R, Appendini C, Pedrozo-Acuña A (2015) Hurricane induced waves and storm surge modeling for the Mexican coast. Ocean Dyn 65(8):1199–1211. https://doi.org/10.1007/s10236-015-0861-7

Mooney PA, Gill DO, Mulligan FJ, Bruyère CL (2016) Hurricane simulation using different representations of atmosphere–ocean interaction: the case of Irene (2011). Atmos Sci Lett 17:415–421. https://doi.org/10.1002/asl.673

Olabarieta M, Warner JC, Armstrong B, He R, Zambon JB (2012) Ocean–atmosphere dynamics during Hurricane Ida and Nor'Ida: an application of the coupled ocean–atmosphere–wave–sediment transport (COAWST) modeling system. Ocean Model 43–44:112–137. https://doi.org/10.1029/2011JC007387

Panchang V, Jeong CK, Demirbilek Z (2013) Analyses of extreme wave heights in the Gulf of Mexico for offshore engineering applications. J Offshore Mech Arct Eng 135:031104. https://doi.org/10.1115/1.4023205

Parker CL, Bruyère CL, Mooney PA, Lynch AH (2018) The response of tropical cyclone characteristics to projected climate change in Northeast Australia. Clim Dyn. https://doi.org/10.1007/s00382-018-4091-9

Powell MD, Houston SH, Amat LR, Morisseau-Leroy N (1998) The HRD real-time hurricane wind analysis system. J Wind Eng Ind Aerodyn 77:53–64

Powell MD, Vickery PJ, Reinhold TA (2003) Reduced drag coefficient for high wind speeds in tropical cyclones. Nature 422:279–283

Price JF (1981) Upper ocean response to a hurricane. J Phys Oceanogr 11:153–175

Rong Z, Hetland RD, Zhang W, Zhang X (2014) Current-wave interaction in the Mississippi-Atchafalaya river plume on the Texas-Louisiana shelf. Ocean Model 84:67–83

Shchepetkin AF, McWilliams JC (2005) The regional ocean modeling system (ROMS): a split-explicit, free-surface, topography-following-coordinates ocean model. Ocean Model 9:347–404

Somerville R (2010) Willis energy market review. Willis Limited. http://www.willis.com/Documents/Publications/Industries/Energy/Energy_Market_Review_March_2010.pdf. Accessed 1 Mar 2016

Tye MR, Stephenson DB, Holland GJ, Katz RW (2014) A weibull approach for improving climate model projections of tropical cyclone wind-speed distributions. J Clim 27:6119–6133. https://doi.org/10.1175/JCLI-D-14-00121.1

Walsh KJE, McBride JL, Klotzbach PJ, Balachandran S, Camargo SJ, Holland GJ, Knutson TR, Kossin JP, Lee T-C, Sobel A, Sugi M (2016) Tropical cyclones and climate change. WIREs Clim Chang 7:65–89. https://doi.org/10.1002/wcc371

Wang D-P, Oey L-Y (2008) Hindcast of waves and currents in Hurricane Katrina. Bull Am Meteorol Soc 89:487–495

Warner JC, Sherwood CR, Arango HG, Signell RP (2005) Performance of four turbulence closure methods implemented using a generic length scale method. Ocean Model 8:81–113

Warner JC, Perlin N, Skyllingstad E (2008) Using the model coupling toolkit to couple earth system models. Environ Model Softw 23:1240–1249

Warner JC, Armstrong B, He R, Zambon JB (2010) Development of a coupled ocean-atmosphere-wave-sediment transport (COAWST) modeling system. Ocean Model 35(3):230–244

Wehner MF, Reed KA, Zarzycki CM (2017) High-resolution multi-decadal simulation of tropical cyclones. In: Collins J, Walsh K (eds) Hurricanes and climate change. Springer, Cham, pp 187–211

Winterbottom HR, Uhlhorn EW, Chassignet EP (2012) A design and an application of a regional coupled atmosphere-ocean model for tropical cyclone prediction. J Adv Model Earth Syst 4: M10002. https://doi.org/10.1029/2012MS000172

Zambon JB, He R, Warner JC (2014) Investigation of hurricane Ivan using the coupled ocean–atmosphere–wave–sediment transport (COAWST) model. Ocean Dyn 64(11):1535–1554. https://doi.org/10.1007/s10236-014-0777-7

Chapter 12
Estimating the Human Influence on Tropical Cyclone Intensity as the Climate Changes

Michael F. Wehner, Colin Zarzycki, and Christina Patricola

Abstract Quantifying the human influence on individual extreme weather events is a new and rapidly developing science. Understanding the influence of climate change on tropical cyclones poses special challenges due to their intensities and scales. We present a method designed to overcome these challenges using high-resolution hindcasts of individual tropical cyclones under their actual large-scale meteorological conditions, counterfactual conditions without human influences on the climate system, and scenarios of increased climate change. Two practical case studies are presented along with a discussion of the conditions and limitations of attribution statements that can be made with this hindcast attribution method.

Keywords Tropical cyclone · Climate change · Attribution · Modeling

12.1 Introduction to Extreme Event Attribution

The quantification of the human influence on specific extreme weather events due to climate change began with the pioneering study of the 2003 European heat wave by Stott et al. (2004). The large spatial extent and lengthy duration of that heat wave allowed them to use the output of a standard climate model of that era to analyze the frequency and magnitude of the heat wave in simulations of both the actual world and a counterfactual world without the influence of human changes to the composition of the atmosphere. Since that first study, the human influence on many different individual extreme weather events has been studied. A series of reports published as supplements to the Annual State of the Climate Report in the Bulletin of the American Meteorological Society (BAMS) (Peterson et al. 2012, 2013; Herring

M. F. Wehner (✉) · C. Patricola
Lawrence Berkeley National Laboratory, Berkeley, CA, USA
e-mail: mfwehner@lbl.gov

C. Zarzycki
National Center for Atmospheric Research, Boulder, CO, USA

J. M. Collins, K. Walsh (eds.), *Hurricane Risk*, Hurricane Risk 1,
https://doi.org/10.1007/978-3-030-02402-4_12

et al. 2014, 2015, 2016) describe extreme events of all types using a wide variety of methods of varying sophistication. Reviews of the statistically rigorous class of analyses referred to as "Probabilistic Extreme Event Attribution" include Pall et al. (2014), Easterling et al. (2016), and Stott et al. (2016), among others. Furthermore, attribution of the human influences on individual extreme events was reviewed by the National Academies of Sciences, Engineering, and Medicine (2016).

Probabilistic Extreme Event Attribution analysis expresses the human influence on a specific weather event in two ways. The first is to quantify the anthropogenic change in the probability of the event's occurrence at its observed magnitude. The second is to quantify the anthropogenic change in the event's magnitude when fixing its occurrence probability at an estimate appropriate to that in the actual world. These quantities both can be estimated by comparing climate model simulations with and without the human forcing changes to the climate system. Stott et al. (2004) used simulations of the UK MetOffice's fully coupled climate model HadCM3. Simulations with only the natural external forcings of volcanoes and solar variations served as the counterfactual world and were compared to simulations of the actual world that were forced with both these natural agents and the anthropogenic forcings of well-mixed greenhouse gases, ozone, and sulfate aerosols. Since the HadCM3 well represents European temperatures, they could then estimate the change in the event's frequency as well as uncertainty estimates on this change. It is important to note that while these two types of attribution statements are equivalent ways of stating the same information, interpretation of the magnitude of the human influence may appear quite different (Otto et al. 2012; Easterling et al. 2016). For instance, relatively small changes in the magnitude of an event may imply large ratios of factual to counterfactual probabilities (Wehner et al. 2018a). However, the lower bound on this probability ratio is often quite insensitive to uncertainty in estimates of the actual observed event magnitude and its probability (Jeon et al. 2016; Pall et al. 2017; Risser and Wehner 2017).

Pall et al. (2011) extended this technique in an analysis of the Autumn 2000 floods in England and Wales. As the unusual seasonal precipitation was found to be highly dependent on the state of the ocean, free running fully coupled models would not produce enough, if any, simulations that were comparable to the observed precipitation totals. Hence, they performed a very large ensemble of atmospheric models with prescribed sea surface temperatures (SSTs) representative of the year 2000 to quantify the statistics of the "world that was". An ensemble simulation of the "world that might have been" had humans not influenced the climate system required the construction of counterfactual SSTs and sea ice concentrations. This was done by using simulations from the Coupled Model Intercomparison Project (CMIP) database to quantify the attributable change in SST and sea ice concentrations and subtracting them from the observed SST and sea ice concentrations used in the factual "world that was" simulations. This method of extreme event attribution is applicable to a wide variety of seasonal extremes including heat waves, droughts, and floods. Because of these opportunities, a great deal of effort has been put into constructing general purpose ensembles of paired factual and counterfactual simulations. The weather@home group at the University of Oxford has utilized the

publics' personal computers to generate very large ensembles, often containing several thousand realizations (https://www.climateprediction.net/weatherathome/). The Detection and Attribution subproject of CLIVAR's Climate of the 20th Century project (C20C+) has constructed a multi-model database of factual and counterfactual global atmospheric model simulations (Stone et al. 2018) and provided the data to the scientific community (http://portal.nersc.gov/c20c). Because the C20C+ database spans many years (1959–2016), this methodology permits some separation of the anthropogenic and natural contributions to the risk of extreme events (Risser et al. 2017). For instance, certain extreme events are more likely in El Niño years than in La Niña years, or vice versa. This technique then permits isolating the attribution statement to years where the ocean is in a state conducive to the extreme event of interest. While these databases are constructed to attribute extreme events that have already occurred, it is possible to operationally forecast the risk of near future seasonal extremes by utilizing seasonally forecasted SSTs and sea ice concentrations (Haustein et al. 2016).

This revision of event attribution methodology imposes further conditions on the resulting attribution statements. In the original 2003 European heat wave study using fully coupled models (Stott et al. 2004), the attribution statement that it is "*very likely* that human influence has at least doubled the risk of a heat wave exceeding this (observed) threshold magnitude" is conditional on only the changes in the anthropogenic forcing agents of well-mixed greenhouse gases, ozone, and sulfate aerosols and the sensitivity of HadCM3. In the attribution statement about the UK 2000 floods (Pall et al. 2011), "that twentieth-century anthropogenic greenhouse gas emissions increased the risk of floods ... by more than 90%," additional conditions must be added. The first is that the ocean state was as observed. The second is that the attributable change in SST and sea ice concentration is as calculated from the coupled climate models. This latter condition also introduces another uncertainty, as there are many ways to estimate this attributable change. In fact, Pall et al. (2011) examined this uncertainty by considering SST and sea ice concentration changes from four different coupled climate models. Conditionality on the ocean state implies that attribution statements may exhibit interannual variations (Risser et al. 2017; Stone et al. 2017).

Angelil et al. (2017) considered 63 extreme events already analyzed in the BAMS Supplements and cautioned that credible attribution statements can only be made using models that are "fit for purpose". By this they meant that the factual simulations must be able to produce reasonable simulated statistics of the observed event. If the climate model, under these conditions, cannot produce events of the observed magnitude, quantile bias correction techniques (Jeon et al. 2016) can sometimes be used to modify the output of both the factual and counterfactual simulations to make a confident attribution statement. However, if the model does not represent the fundamental processes, bias correction will not lead to such confidence. The Pall et al. (2011) method of targeted factual and counterfactual ensembles of prescribed ocean climate model simulations is widely applicable to seasonal extremes of temperature and precipitation (Angelil et al. 2017). It is also suitable, with an appropriate modeling framework and caveats, to construct attribution statements

about extremely active or inactive storm seasons, including tropical cyclone seasons. However, it is not well suited for constructing attribution statements about individual shorter duration extreme weather events, particularly intense storms such as tropical cyclones. The principal reason for this is that the technique is unlikely to produce storms in the right place and time to compare with the actual observed event in question, even with very large ensemble sizes.

Tropical cyclones are a case in point. The resolutions of the models used in the C20C+, neither the weather@home nor the CMIP5 database are refined to the point where realistic tropical cyclones are simulated. No amount of bias correction can fix that and these models are not fit for purpose to directly attribute the human influence on this class of extreme storms. To remedy this deficiency, Pall et al. (2017) further modified extreme event attribution methodology to analyze the September 2013 flood in Colorado by using hindcast technologies. Similar to a forecast, a hindcast is a simulation of a specific period of weather initialized a few days prior, but with the difference being that the period is already observed. In this method, a "hindcast that was" is compared to a "hindcast that might have been", constructed with estimates of changes not only to the boundary conditions as before but also to the initial conditions. Hence, in their attribution statement about the Colorado flood "that anthropogenic drivers increased the magnitude . . . by 30%", the additional condition is that the large-scale meteorological patterns (LSMP) were as observed and the anthropogenic changes to the LSMP were as estimated. While this technique as an attribution method was originally applied to a non-cyclonic extreme storm, it is equally applicable to tropical cyclones. In fact, the original notion of perturbing individual storms was first proposed by Schär et al. (1996) to gain insight into how future climate change will affect extreme weather. This pseudo-global warming approach to extreme event attribution has been termed a "storyline" by Shepherd (2016). He correctly points out that this attribution method only describes a portion of the relevant anthropogenic mechanisms that may influence a particular extreme event. No statements about the LSMP can be made in this method as it is prescribed as discussed below. For instance, in the attribution of the human influence on a tropical cyclone, no statement is made in this method on the chances of cyclogenesis or landfall. However, unlike Shepherd (2016), we prefer to describe the unattributable aspects of changes in extreme storms by the hindcast methodology as "nonlocal" rather than "dynamical", and the attributable portion as "local" rather than "thermodynamic". This is motivated by the findings discussed below that dynamical storm properties (winds and pressures) in addition to thermodynamic properties (temperature and precipitation) can be significantly influenced by climate change.

As discussed in the subsequent sections of this chapter, there are many sources of uncertainties in extreme event attribution statements, especially for tropical cyclones. Principal among these is that no definitive trends in observed tropical cyclone statistics have been detected nor attributed to human influences due to both the short record and its large variability. Hence, tropical cyclone attribution statements are made "without detection" (Knutson 2017). Nonetheless, some confidence

can be ascribed to these statements drawn both from physical understanding of the relevant processes and other numerical modeling experiments. Maximum potential intensity (MPI) theory (Bister and Emanuel 1998) suggests an increase in tropical cyclone destructiveness in a warmer world (Emanuel 1987). Tropical cyclone permitting experiments with both regional and global models all suggest an increase in both the frequency of intense tropical cyclones and in the wind speeds of the most intense storms despite decreases or little change in the total number of tropical storms (Knutson et al. 2015; Walsh et al. 2015; Kossin et al. 2017; Wehner et al. 2018b). These results about the climatology of intense tropical cyclones set an expectation that the human influence on individual storms might be to make them stronger. However, the hindcast methodology presented here reveals that the human influence on any individual tropical cyclone may be far more nuanced.

For ease of discussion in the rest of this chapter, we refer to the original technique of Stott et al. (2004) as the "CMIP" attribution method, although any coupled climate model simulations could be used. Furthermore, we will refer to the revised technique of Pall et al. (2011) as the "C20C+" attribution method, although again any set of atmospheric models could be used. Finally, we will refer to the storyline technique of Pall et al. (2017) as the "hindcast" attribution method, which is the central focus of this chapter. Details of the implementation of this hindcast attribution method and the application to tropical cyclones are discussed in the next section.

12.2 The Hindcast Attribution Method Applied to Tropical Cyclones

The complex meteorology that led to the September 2013 flood in Colorado was excessively rare to occur at that place and time of year making its representation in free-running climate models difficult to quantify. Nonetheless, with appropriate initial and boundary conditions, it was well simulated in the "hindcast that was" with a high-resolution (12 km) version of the Weather Research and Forecast (WRF) model (Skamarock et al. 2008) by Pall et al. (2017). Tropical cyclones are no different in this regard as they are well forecasted routinely with this and many other numerical weather prediction models (e.g., Davis et al. 2008). In this section, we discuss implementation details of the hindcast attribution method using as examples both WRF as a regional model and the variable-resolution version of the Community Atmospheric Model (VR-CAM5), as a global model. However, the method could be used with any model in either of these classes.

As in the other paired ensemble event attribution methods described in the previous section, it is critical to demonstrate that the hindcast model is "fit for purpose" to analyze the event in question. For individual storms, standard forecast diagnostics are useful to determine the quality of the "hindcast that was" ensemble. For tropical cyclones, these could include comparison to observations of the simulated storm

track, peak wind speed, and central pressure minima histories, precipitation totals or other well-measured quantities. High horizontal resolution, often finer than 25 km, is generally required to reproduce these observations, as is a high quality set of initial and boundary conditions. Furthermore, the event itself must be able to be well predicted, as it will undergo a sizable perturbation when simulated again in the counterfactual hindcast.

The generation of a sample of plausible hindcasts of the actual storm can be constructed by standard techniques to perturb the simulation. As simple perturbations to the initial conditions will not permit differences between a limited number of realizations to grow fast enough for the sample to adequately represent the full distribution of plausible hindcasts, forecasters typically employ strategies to produce larger perturbations. Comparison of the resulting hindcast under actual conditions to the observations is necessary to determine whether it is "fit for purpose". However, the predictability of tropical cyclones, especially their tracks, varies. While some intense tropical cyclones, such as Super Typhoon Haiyan, take relatively straight paths from cyclogenesis to landfall; others such as Hurricane Sandy may be dramatically steered by the large-scale environmental conditions. As a result, the time of initialization can determine whether the simulations are "fit for purpose". For storms like Sandy, if initialized too early, the hindcasted tracks may veer into the open ocean rather than make landfall at the New York and New Jersey coastlines as actually occurred (Magnusson et al. 2014; Bassill 2014).

The construction of a counterfactual ensemble of hindcast simulations is straightforward, but the details depend on whether a global or regional model is employed. For either class of model, the composition of the counterfactual atmosphere is prescribed to be representative of a preindustrial state as would be in the CMIP or C20C+ attribution methods. Also, the counterfactual SST and sea ice concentration patterns and magnitude are altered in a similar manner as in a C20C+ attribution method. For the hindcast attribution method, counterfactual initial conditions also must be prescribed by perturbing the actual initial conditions. If a regional model is used, lateral boundary conditions are additionally perturbed.

Actual initial and lateral boundary conditions can be obtained from reanalyses. However, if "rapid" attribution (Haustein et al. 2016) is required, reanalyses may not be available as there is usually a lag time of a month or more before they are released. In such cases, initial and boundary conditions used in forecasts are an option if they are available, and in some cases may be preferable to reanalysis products if they are available on higher-resolution grids. As the tropical cyclone case studies below will reveal, careful construction of attribution statements for this class of storm can be considerably more difficult than for other classes of extreme events. Rapid attribution statements about tropical cyclones might then be contradicted by later analyses with more accurate initial and boundary conditions. Communicating these uncertainties is thus a critical part of the process.

As the perturbation to the actual conditions that define the counterfactual conditions represent an anthropogenic climate change to the environment that the extreme

weather event occurred in, it is generally obtained from other climate model simulations. The fields that must be perturbed, in addition to SST and sea ice concentration, would include at least the surface pressure, wind vector components, humidity, temperature, and geopotential height (or similar fields). Other than surface pressure, these other perturbations need to be calculated at the vertical levels of the hindcast model using the appropriate vertical coordinate system. As the lower boundary conditions of SST and sea ice concentration are already perturbed following a C20C+ attribution methodology, one way to provide initial and lateral boundary condition perturbations would be to use estimates of the anthropogenic influence on these additional fields from the same source. For instance, if the SST is estimated from the anthropogenic change of an ensemble of CMIP5 models, differences between the "historical" (all forcings) and "historicalNat" (natural-only forcings) at an appropriate point in time could be a reasonable perturbation. However, a more nuanced perturbation can be obtained from the databases constructed for C20C+ attribution methods. In these databases, differences between the ensembles of simulations of all forcing and natural forcing alone for these additional fields can be calculated at the same time as the extreme weather event of interest. These differences represent the anthropogenic change to the large-scale environment conditional on the state of the ocean at the time of the event. As the goal of the hindcast attribution method is to characterize the extreme weather event and its counterfactual equivalent, accounting for dependence of the anthropogenic change on the ocean state is more self-consistent than not doing so. However, interannual variability in the anthropogenic change to the climate system is certainly smaller than the change itself, and if a suitable C20C+ class ensemble is not available, other model output, such as CMIP5, must suffice. Indeed, this would be the case for rapid attribution, as the generation of C20C+ class ensembles requires observed SST and sea ice concentrations that are only available with a several week delay. As a practical matter, it is convenient to calculate the perturbations using the monthly averages drawn from the month and year that the event of interest occurred in rather than over the event's actual duration. Such a practice has an additional advantage of further damping any residual natural variability in the ensemble average.

The case studies presented below will reveal that, while applying this methodology may be straightforward, interpretation and construction of attribution statements for individual tropical cyclones may not be. Many factors can complicate attribution including changes in initial storm structure or resultant track difference. Furthermore, different hindcast models may respond differently due to differences in model formulation or resolution. Even results from a single model could depend on resolution. Consistency across multiple methods leads to greater confidence in any attribution statement, but expert judgment is also a part of that confidence. The hindcast attribution method indeed may require yet more expert judgment than other methods given both its highly constrained design and the increased possibility of conflicting or unfit for purpose results. In particular, expert judgment must be exercised for the suitability of the factual and counterfactual tracks and the spread of the ensembles as well as the simulated factual intensities.

12.3 Tropical Cyclone Attribution Case Studies

12.3.1 Case Study 1: Global Atmospheric Model Analysis of Super Typhoon Haiyan

Super Typhoon Haiyan was a devastating Category 5 storm that made landfall near Manila (the Philippines) in November 2013. Over 6000 fatalities and 4 million displaced persons stressed humanitarian efforts to their limits (Lum and Margesson 2014). Its storm track was not unusual and was well-forecast (Xiang et al. 2015) making it a good candidate for the hindcast attribution method. For this case study, we used the variable resolution version of the Community Atmospheric Model (VR-CAM5, Zarzycki et al. 2014b). This global atmospheric model, based on a spectral element dynamical core (Dennis et al. 2011), enables the refinement of the computational grid to accelerate simulation throughput (Zarzycki et al. 2014a). While an atmosphere-only model such as VR-CAM5 does not include atmosphere-ocean interactions, we note that the ocean boundary layer was particularly deep during Haiyan, partially allaying concerns about important missing processes. To simulate Haiyan, we began with a global mesh of approximately 69 km on a side, then progressively refined to 34 km, 17 km, and 8 km. Given these resolution constraints, the effects of deep cumulus convection are parameterized in VR-CAM5 (Neale et al. 2012). SSTs are obtained from the 0.25° National Oceanic and Atmospheric Administration Optimum Interpolation (NOAA-OI) dataset (Reynolds et al. 2007) and are not varied throughout the hindcast. Figure 12.1

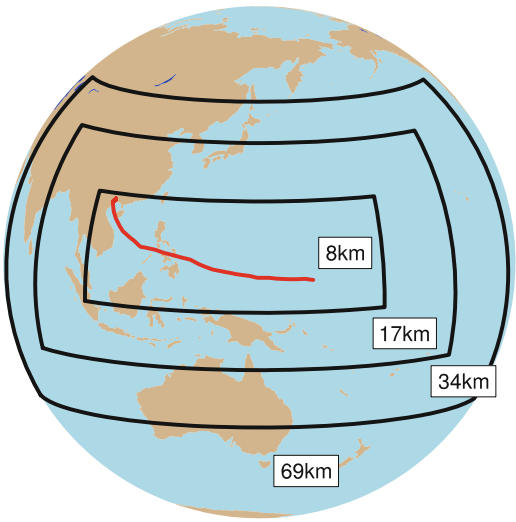

Fig. 12.1 The refinement regions of VR-CAM5 used in the global model attribution case study of Typhoon Haiyan

shows the refinement regions, with the track of Haiyan completely contained within the finest grid spacing within the domain.

Hindcasts using VR-CAM5 are initialized and integrated as described in Zarzycki and Jablonowski (2015) and readers are referred to that manuscript for technical details regarding the configuration used here. VR-CAM5 simulations replicate observed structural characteristics of the actual storm well. Figure 12.2 shows a comparison of brightness counts from the Japanese MTSAT satellite at 21UTC on November 21, 2013 and simulated outgoing longwave radiation (OLR) from CAM hindcasts at the same time. Here we analyze these images qualitatively, although the colormaps have been designed to make the observations and model panels comparable. The middle panel shows that the simulated cloud field from VR-CAM5 (initialized 3 days prior) refined to 8 km compares favorably with the satellite image shown in the top panel. We note that the size and shape (including an "eye") of the storm are remarkably well-simulated. We conclude from figures like this that the model itself is "fit for purpose" to simulate the actual storm. Comparing other analyzed fields such as peak wind speeds, storm track, etc. can reinforce this claim. In contrast, the lower panel shows the same simulation except showing the solution with resolution of approximately 111 km (no grid refinement). While the size of the storm is surprisingly realistic, simulated wind speeds and central pressures are too weak compared to observational estimates and significant structural deficiencies (e.g., lack of an eye and spiral rainbands) are obvious. We conclude that this low-resolution version of the model is not fit for purpose to confidently attribute the human influence on Haiyan, principally because it cannot reproduce the observed storm intensity. In general, CMIP5 class models, with resolutions between 100 and 200 km, would not be judged fit for purpose for intense tropical cyclone attribution for this reason.

Even if a model is found to be fit for purpose to simulate the actual tropical cyclone, the hindcast methodology as a whole must be judged to be fit for purpose or not. The perturbations that define the counterfactual hindcast can be significant and the resulting counterfactual tropical cyclone may bear little resemblance to the actual storm. While the predictability of the actual tropical cyclone, reflected somewhat by the stability of the actual hindcast, is a good indicator of the applicability of the hindcast attribution method to a particular storm, only subjective expert judgment is available to make a final decision on the fit for purpose question. Figure 12.3 shows the observed and simulated tracks for Haiyan. VR-CAM5 was initialized at 12UTC November 4, 2013 in all of these simulations. Each VR-CAM5 ensemble consisted of ten individual realizations, which were generated using small-scale perturbations within the initial conditions as well as perturbations to subgrid parameterizations. The ensemble generated from actual conditions, shown in red, is a reasonable hindcast of the observed track from IBTrACS (Knapp et al. 2010), shown in black. The anthropogenic influences were estimated by selecting the November 2013 monthly averages contributed by the CAM5 model (Angelil et al. 2017) to

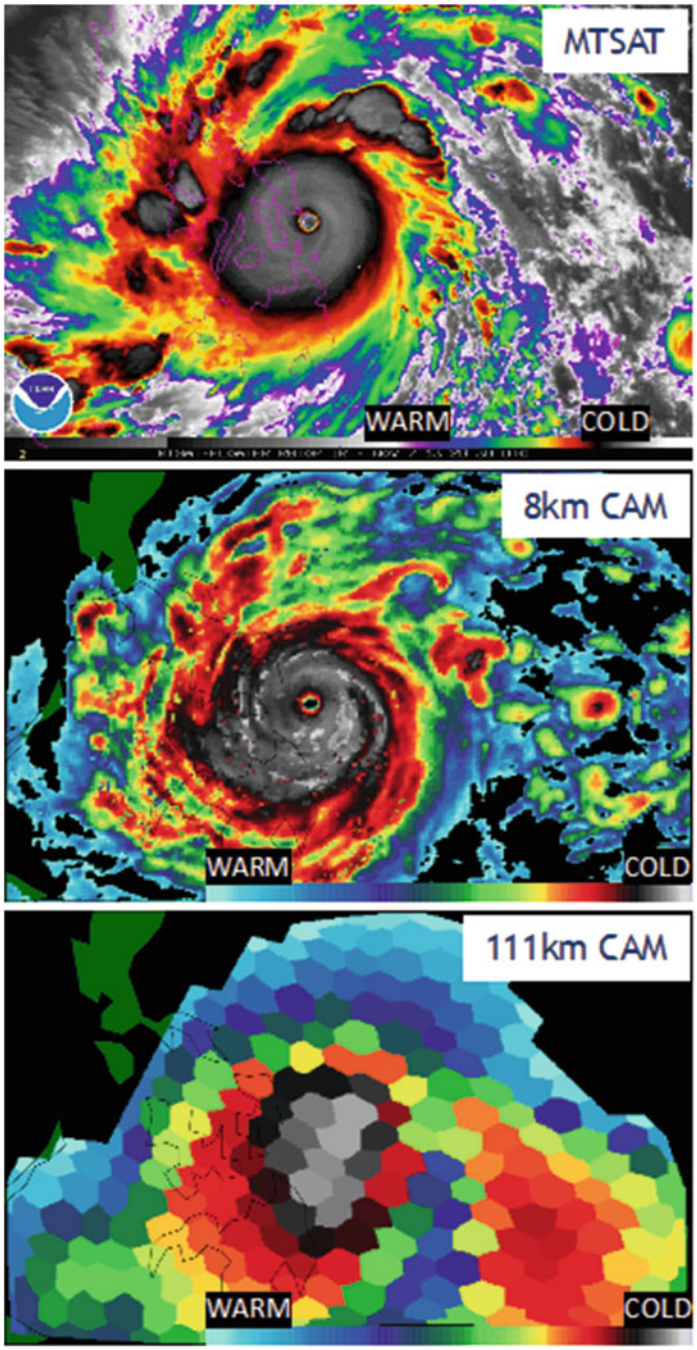

Fig. 12.2 Observed (brightness count) and simulated (outgoing longwave radiation) cloud structure of Typhoon Haiyan at 21UCT on November 7, 2013. Top panel: MTSAT satellite (NOAA image). Middle panel: VR-CAM5 at 8 km. Bottom panel: CAM5 at 111 km without refinement. Both warmer and colder cloud tops are noted on relative locations of each panel's colorscale

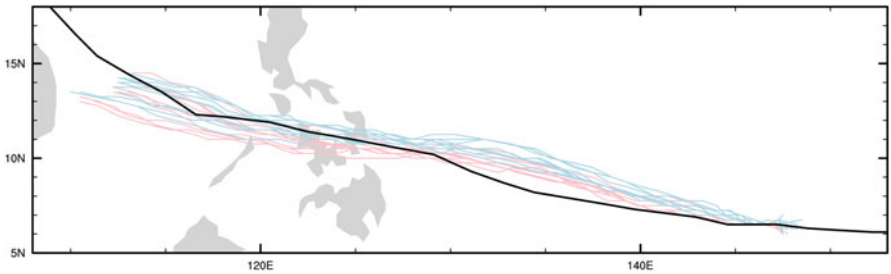

Fig. 12.3 Observed and simulated tracks of Super Typhoon Haiyan. Black: Observed (IBTrACS). Red: Ensemble of actual conditions as simulated by 8 km VR-CAM5. Blue: Ensemble of counterfactual conditions as simulated by 8 km VR-CAM5

the C20C+ experiment.[1] This results in a "delta" (or "difference") in the mean synoptic state with and without a human-induced signal. The counterfactual ensemble is then generated by applying these "deltas" to the initial conditions from the actual ensemble to simulate the same weather pattern but with the anthropogenic signal stripped from the background state. Expert judgment in the evaluation of these tracks should include not only the assessment of the track location, but also timing of storm centers.

While tracks from the counterfactual ensemble, shown in blue, may be shifted equatorward a bit from the factual ensemble, this shift is not large. This both implies that the anthropogenic influences do not significantly modify storm speed and direction, and that we can credibly assess differences in storm intensity between the runs. Therefore, we judge that the simulations and hence the hindcast attribution methodology is indeed fit for purpose for attributing the human influence on Super Typhoon Haiyan. Clearly, this need not be the case. While models that can simulate observed tropical cyclone intensity may be available, if the storm tracks are sensitive to the large-scale environment and the perturbations significantly alter that environment, counterfactual storms may take paths that cause them to be so unlike the actual storm that comparison is imprudent. Superstorm Sandy, as mentioned previously, is a good example as even in the factual ensemble, simulated tracks may diverge just due to the perturbations applied to create the ensemble spread (Lackmann 2015). In general, tropical cyclones embedded within weak steering flow conditions will be less amenable to the hindcast attribution method than those determined by a strong steering flow that is resilient to perturbations, like Haiyan. By moving the initialization time closer to landfall, this problem of diverging tracks may be ameliorated. However, the simulated storms must be given enough time to develop on their own from the initial conditions to give a credible spread in the hindcasts. Experience is limited in this regard and again expert judgment must be relied upon.

[1]The CAM5 contribution to the C20C+ experiment consisted of 100 simulations in both the factual and counterfactual scenarios. We also repeated this attribution analysis with the MIROC5 contribution finding the same behavior as detailed here.

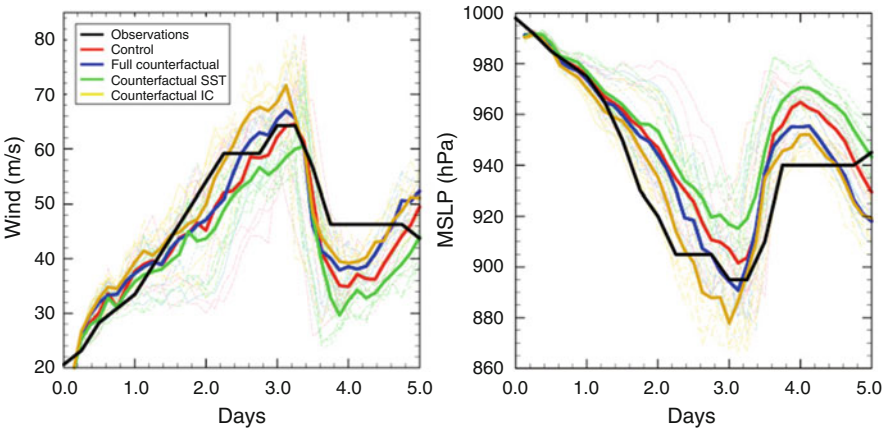

Fig. 12.4 Observed and simulated (8 km VR-CAM5) instantaneous peak wind speeds (left) and central pressure minima (right) as a function of days since model initialization. Black: Observations. Red: Actual conditions. Blue: Counterfactual conditions as simulated by. Green: Counterfactual SST only. Yellow: Counterfactual initial conditions only. Heavy lines are the ensemble averages. Thin lines are individual realizations. Storm landfall occurs just after Day 3

The response of Super Typhoon Haiyan to anthropogenic perturbations in VR-CAM5 is complex and not completely as expected. Figure 12.4 shows the observed and simulated instantaneous peak wind speeds (left) and central pressure minima (right). This figure shows that ensemble averaged simulated peak wind speeds under the actual conditions (red) are close to observed (black) at landfall (just past Day 3) but that the model's central pressure minima is slightly too weak. Under counterfactual conditions (blue), a small increase in simulated peak wind speeds and a substantial decrease in central pressure minimum of the ensemble averages are found. One might expect that Haiyan would be weaker under the cooler counterfactual conditions, however this is not the case, at least as simulated by this configuration of VR-CAM5.

The hindcast attribution method permits further exploration about the effect of anthropogenic forcing changes on tropical cyclone intensity. By recomputing the counterfactual hindcast with subsets of the perturbed conditions, some of these effects can be further isolated. The green curves in Fig. 12.4 show the peak wind speed and central pressure minima obtained when only SST is perturbed. In these simulations, the initial vertical structure of the storm is set to the actual conditions. Because Haiyan is so stable to perturbations, the storm can adjust to this unbalanced initial state and the simulated storms weaken in both wind speeds and pressure minima in response to the cooler counterfactual ocean (and, correspondingly, reduced enthalpy fluxes). Conversely, the yellow curves in Fig. 12.4 show these fields when the SST is maintained at the actual values and the initial conditions are set to the counterfactual case. Here, the effect of only changing the vertical structure of the storm is to intensify the wind speeds and pressure minima. Although not shown, further numerical experimentation reveals that this effect is primarily due to

the perturbation of the vertical temperature profile. The vertical tropospheric temperature profile is more strongly heated aloft than at the surface when anthropogenic influences are configured (Santer et al. 2005). Therefore, even though the counterfactual profile is cooler, there are larger amounts of convective instability. Analysis using maximum potential intensity (MPI) theory (Bister and Emanuel 1998) shows that a sounding from the cooler counterfactual atmosphere as simulated by VR-CAM5 can support a storm 10–20 hPa deeper (stronger) than the control case because of this effect.

We learn from this that the effects of climate change on an individual storm is at least twofold. Increases in SST cause tropical cyclones to be more intense, while the anthropogenic change in the vertical temperature profile causes them to be less intense. The net effect is, of course, a combination of these two counteracting effects. In the present example, these two effects combined for a slightly weaker storm due to anthropogenic climate change. However, their relative magnitude will vary by the specifics of individual storms, as well as choice of hindcast model and the details of the anthropogenic perturbations. In fact, a similar analysis by Takayabu et al. (2015) and in Sect. 12.3.2 using different models comes to an opposite conclusion, i.e. that anthropogenic climate change slightly increased Haiyan's intensity. Methods to quantify this sort of structural uncertainty are currently under development (private communication, Richard Smith, University of North arolina-Chapel Hill, 2017) and it is worth noting that there is likely significant regional and temporal variability that may also influence these results.

12.3.2 Case Study 2: Regional Atmospheric Model Analysis of Super Typhoon Haiyan

While most of the experimental design for hindcast attribution with regional atmospheric models is the same as outlined in Case Study 1 using global atmospheric models, there is an important difference. Regional models require the imposition of lateral boundary conditions in addition to the surface boundary and initial conditions and greenhouse gas concentrations. Fortunately, all the information necessary to construct counterfactual initial conditions can be used to construct counterfactual lateral boundary conditions. Consistency mandates that the lateral boundary conditions come from the same source as the initial conditions. Hence, if a reanalysis is used, then the only additional task is to apply the perturbations to each time step that reads the lateral boundary conditions.

There are significant advantages to using regional models over global models. For the same resolution, they offer a computational advantage. But perhaps more importantly, many regional models, such as WRF (Skamarock et al. 2008) are often non-hydrostatic, and can be configured at high enough resolutions that cloud systems are simulated directly, eliminating the need for deep cumulus convection parameterizations. This is a significant point, as most cumulus convection

parameterizations are not developed with extreme precipitation in mind but are tuned to replicate average precipitation. This can lead to significant errors in convectively active storms such as tropical cyclones (Wehner et al. 2014).

Models specifically developed for forecasting, such as WRF, are usually enabled to produce ensemble forecasts. As mentioned above, the microscopic perturbations typically used to generate independent realizations of multi-decadal climate simulations are not large enough to produce the significant spread of ensemble members necessary to quantify forecast uncertainty. WRF is equipped with the Stochastic Kinetic Energy Backscatter Scheme (SKEBS) (Shutts 2005), which represents the uncertainty from interactions with unresolved scales by introducing temporally and spatially correlated perturbations to the rotational wind components and potential temperature.

Another potential advantage of using regional over global models is that the constraints provided by the lateral boundary conditions may control the path the hindcasted storm takes. Because the prescribed lateral boundary conditions in a hindcast incorporate the actual LSMP as observed (and as represented by the reanalysis), simulated tropical cyclone tracks are more likely to resemble the actual storm track than in a hindcast with a global model unconstrained in this manner. Similarly, we would expect that a forecast would not be as accurate as a hindcast initialized at the same time, as the LSMP would also be subject to forecast errors.

Simulated anthropogenic tropical cyclone intensity response tends to be dominated by changes in the thermodynamic variables (humidity, temperature, geopotential height) applied to the initial and boundary conditions, rather than the dynamical variables (wind vectors), which are more likely to alter the simulated storm track. Hence, construction of counterfactual hindcasts may be made more likely to succeed in difficult cases in being "fit for purpose" by altering only the thermodynamic variables in the initial and boundary conditions.

Patricola and Wehner (2018) have undertaken a hindcast attribution study using WRF of 15 different tropical cyclones focusing on the effect of future climate changes on counterfactual equivalent storms. The response of Super Typhoon Haiyan to warming is quite different in WRF than in VR-CAM5, as discussed above, and illustrates the need to understand the structural uncertainty in attribution statements due to model differences. In the WRF study, horizontal resolution was set to 4.5 km and initial and boundary conditions were obtained from the National Centers for Environmental Prediction Climate Forecast System Reanalysis (NCEP-CFSR) (Saha et al. 2010). Similar to the VR-CAM5 case study, the SSTs are obtained from the NOAA-OI dataset (Reynolds et al. 2007) except that they vary daily throughout the hindcast. In this WRF case study, the perturbations are chosen from future simulations using the Community Earth System Model's (CESM) contribution to CMIP5. This variation on the hindcast method is in the spirit of the original pseudo-global warming ideas of Schär et al. (1996) and may be useful in interpreting projections of future extreme weather. For instance, by applying perturbations characteristic of a warmer climate to storms that had a known impact, decision makers can more readily construct adaptation plans specific to their needs and past experience (private communication, Anna Roche, San Francisco Public

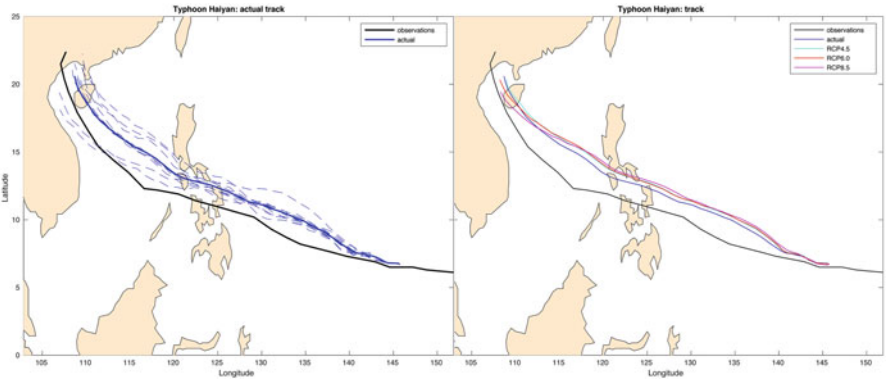

Fig. 12.5 Observed (black) and WRF simulated Super Typhoon Haiyan storm tracks. Left panel: Individual (blue dash) and ensemble mean (blue solid) under actual November 2013 conditions. Right panel: Observed track (black) and ten-member ensemble mean under actual conditions (blue) and RCP4.5 (cyan), RCP6.0 (red), and RCP8.5 (magenta) future (2080–2100) conditions

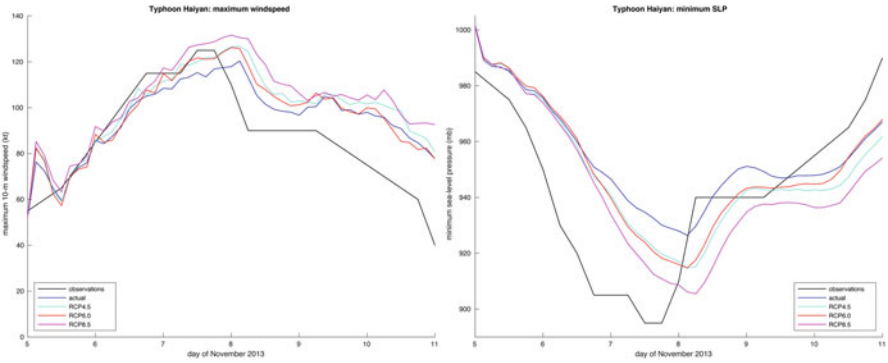

Fig. 12.6 The observed (black) and ten-member ensemble mean of WRF simulated intensities of Super Typhoon Haiyan under actual (blue) and RCP4.5 (cyan), RCP6.0 (red), and RCP8.5 (magenta) future (2080–2100) conditions. Left panel. Instantaneous maximum wind speed (knots). Right panel. Instantaneous minimum central pressure (mb)

Utilities Commission, 2017). The left panel of Fig. 12.5 shows Super Typhoon Haiyan's observed track, together with a ten-member ensemble of storm tracks under the actual conditions at the time of Haiyan, while the right panel shows the ensemble mean tracks under the actual conditions and three different end of twenty-first century warming scenarios. Observations of Haiyan are from IBTrACS (Knapp et al. 2010). There is a slight difference between the actual and future tracks, but the three sets of future ensemble mean storm tracks are remarkably similar.

Figure 12.6 shows Super Typhoon Haiyan's instantaneous maximum wind speeds (left panel) and central pressure minima (right panel) as simulated by WRF under actual and warmer conditions. Unlike the simulations from VR-CAM5, WRF

produces more intense hindcasts of Haiyan in warmer climates. Such a striking difference between model behaviors, including the sign of the change in storm intensity, illustrates that model structural uncertainty in attributing the human influence on intense tropical cyclones can be large. Possible explanations could be in differences in the response of the tropical tropopause height. Due to the warming of the lower and middle troposphere mentioned above, thermal expansion raises the height of the tropical tropopause resulting in a cooling at this now elevated boundary (Santer et al. 2003). Our WRF configuration features higher vertical resolution in this region than does VR-CAM5. Tropical tropopause height variations are known to modulate maximum potential winds (Wing et al. 2015) and global models may not replicate observed trends in the associated temperatures (Emanuel et al. 2013). While further discussion of this particular issue is outside the scope of this chapter, these differences highlight the necessity of performing hindcast attribution with many different models to construct confident attribution statements.

These first two case studies illustrate that different models can lead to different attribution statements, clearly illustrating the important role of expert judgment. While it is entirely possible that certain models might always respond to warming by intensifying tropical cyclones (or the opposite), experience with one of these models (WRF) suggests that the model response can be storm dependent. Both the Japanese group and ourselves using similar approaches with the WRF model have found a mix of both increases and decreases in tropical cyclone intensity across a variety of storms (Ito et al. 2016; Takemi et al. 2016; Patricola and Wehner 2018). Given any clear reason at this time to reject either analysis of Super Typhoon Haiyan in these two case studies, our expert judgment is that it is unclear whether climate change had any effect on its intensity.

12.3.3 Case Study 3: Failure Modes

There are multiple ways for the hindcast methodology to fail to provide simulations that can be useful in making confident attribution statements, even if the hindcast model can be expected to produce hurricane-force winds. For instance, some storms such as Hurricane Irma in 2017 exhibit rapid intensification, a storm behavior that is notoriously difficult to reproduce (Rappaport et al. 2009; Kaplan et al. 2010). Other storms exhibit complex track behavior, such as Hurricane Harvey, also in 2017, which stalled just after landfall. In such cases, initialization may have to be moved up closer to the time of interest. The risk in doing so is that the simulated storm may not properly adjust to the model configuration, contaminating the result. Another, somewhat typical failure mode is that, while the simulation of the tropical cyclone under actual conditions may be acceptable, the perturbation from an altered climate

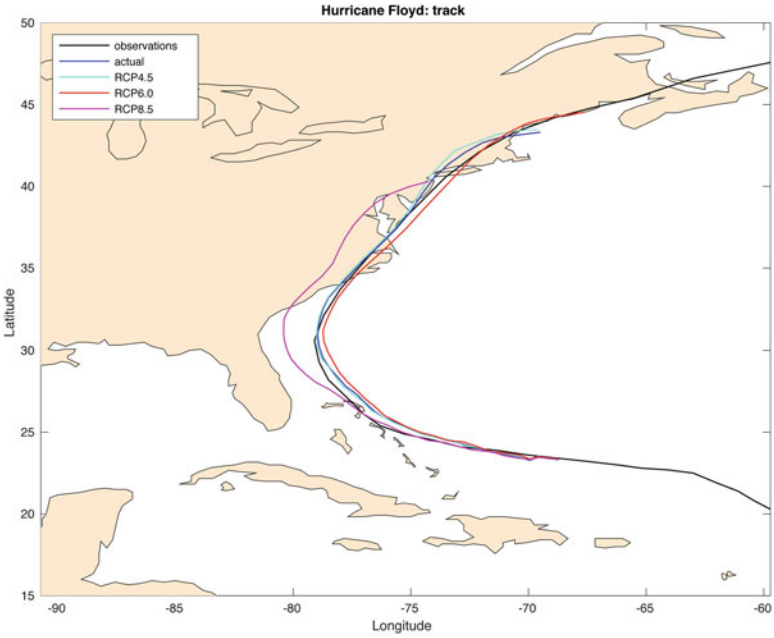

Fig. 12.7 The observed (black) and ten-member ensemble mean of WRF simulated Hurricane Floyd storm tracks under actual (blue) and RCP4.5 (cyan), RCP6.0 (red), and RCP8.5 (magenta) future (2080–2100) conditions. Observations are from the Revised Hurricane Database (HURDAT2, Landsea et al. 2004; Landsea and Franklin 2013)

may be large enough to cause the counterfactual storms to be too dissimilar to the actual storm for a legitimate comparison. For instance, the Cape Verde-type Hurricane Floyd made landfall in September 1999, at the southeastern part of North Carolina, and is simulated by WRF reasonably well as seen in Fig. 12.7. Perturbations from the modest warmings of end of century RCP4.5 and RCP6.0 conditions result in counterfactual storms that similarly skim the coastline and retain a substantial fraction of the storms' areas over the coastal Atlantic. However, perturbations from the warmer climate of the end of century RCP8.5 cause a significant track shift, with landfall occurring substantially farther south in WRF simulations as shown by the pink track in Fig. 12.6. Furthermore, rather than tracking inland, this counterfactual version of Floyd penetrates much further inland. As this counterfactual storm is substantially different than the actual simulated storm, these simulations are judged to not be fit for purpose, at least for this magnitude of warming. It is important to stress that in all usage of the hindcast attribution method, whether for assessing the influence of both past or future climate change on a tropical cyclone, that expert judgment is an important part of the process and that the appropriate rationale for accepting simulations be part of the caveats in the attribution statements.

12.4 Discussion

We present a hierarchy of event attribution methodologies that are designed for different purposes. The seminal study of Stott et al. (2004) used fully coupled models to analyze heat waves, phenomena that occur frequently enough to enable the usage of existing databases such as the Coupled Model Intercomparison Project (CMIP5). Pall et al. (2011) extended the methodology to encompass events that were strongly driven by the state of the ocean by utilizing atmosphere-only models where the ocean is prescribed rather than prognostic. Customized multi-year ensembles of such simulations also enable some separation of anthropogenic and natural influences on individual extreme events. However, to attribute the human influence on individual tropical cyclones, if any, requires another revision: the use of sufficient model resolution to represent TC structure and intensity and the imposition of appropriate large-scale environmental conditions necessary to initiate and propagate cyclogenesis.

The hindcast attribution method may or may not be "fit for purpose" to attribute the human influence on a specific aspect of an individual tropical cyclone. A necessary but not sufficient condition is that the model used must be high-resolution enough to be able to simulate the storm at a credible intensity. Furthermore, the storm track must be robust to perturbations, both the small ones used to generate a credible spread in each ensemble and the large one that defines the counterfactual "world that might have been" had humans not impacted the climate system. In the case studies presented here, the fit for purpose decision was based only on expert judgment of the simulated track locations and timings compared to observations. Additional criteria may also be used, including the quality of simulated wind speeds and pressure minima or precipitation amounts. These could pose very stringent criteria in some cases, particularly those that involve rapid intensification. Despite the limitations on this hindcast or pseudo- global warming approach, other authors, in addition to ourselves, are proceeding to apply it to gain insight into tropical cyclone attributions and projections (Takayabu et al. 2015; Ito et al. 2016; Takemi et al. 2016). We fully expect the method to become a part of the standard analysis of the effects climate change on tropical cyclones.

Any attribution statement made using this "hindcast" attribution method comes with a number of conditions. Besides the conditionality on atmospheric composition changes and the state of the ocean, such statements are also conditional on the prescribed large-scale circulation. This then limits the interpretation of causality. No statement about the change in probability due to changes in characteristics and frequency of coupled atmosphere-ocean climate modes (e.g., Patricola et al. 2014, 2016, 2017) and large-scale circulation can be made with the hindcast attribution method. However, we make note that this is only a further restriction on previous work, as Pall's 2011 revised methodology makes no attribution statement about the change in the ocean state either. Arguably, the conditional aspects of attribution statements made with this method could be quantified. For the conditions are principally on the LSMPs responsible for cyclogenesis and/or intensification

which is further influenced by the pattern and magnitude of changes in the ocean state. Vautard et al. (2016) present a methodology to separate non-local dynamical and local thermodynamic anthropogenic changes to extreme events which could likely be extended to the hindcast attribution method for tropical cyclones presented here.

We note that atmosphere-ocean interactions are a critical process missing from the models described here. For the strongest tropical cyclones, especially those with a cold wake trailing behind them, atmosphere-only models would tend to simulate storms of stronger intensity than they should. This could be important in constructing attribution statements if changes in intensity due to anthropogenic warming affect this heat exchange process. Any effect would vary greatly according to the depth of the ocean mixed layer during the passage of the tropical cyclone at its highest intensities. Hence, it would be valuable to further develop this hindcast methodology to include the atmosphere-ocean interactions known to influence tropical cyclone intensity (Huang et al. 2015; Zarzycki 2016). In particular, replacing the infinite heat capacity ocean implied by prescribed SST conditions with a mixed layer ocean model offers a promising, computationally tractable compromise (private communication, John Chiang, UC-Berkeley, 2018).

Causality is a complex philosophical topic. Attribution statements using the hindcast methodology make no statement about possible changes in cyclogenesis rates. High-resolution multidecadal climate model simulations (Oouchi et al. 2006; Zhao et al. 2009; Sugi et al. 2009; Murakami and Sugi 2010; Held and Zhao 2011; Murakami et al. 2012; Zhao et al. 2013; Wehner et al. 2015, 2018b; Walsh et al. 2015, Bacmeister et al. 2018) often project an increase in intense tropical cyclone frequency and magnitude but a decrease in weaker tropical storm frequency as the climate system warms. Folding such information into a more comprehensive attribution statement has not yet been done, partly due to a lack of consensus on the magnitude of these changes. Nonetheless, attribution statements from the hindcast methodology, subject to the conditions described, can be interpreted in a strict Pearl causality sense (Pearl 2000; Hannart et al. 2016). Pearl causality involves an intervention in an experiment to isolate a single causal element. For instance, in a clinical trial, one test group might receive an experimental treatment while the other would receive a placebo. Similarly, we isolate the causal influence of anthropogenic climate change on a tropical cyclone by comparing simulations of the actual world with the counterfactual world without human changes to the composition of the atmosphere. In the clinical trial, both the treated and untreated groups would typically have been screened for some risk factor for an ailment. Similarly, in the hindcast attribution method presented in this chapter, both ensembles of simulations are subject to similar LSMPs and cyclogenesis conditions.

Formal extreme event attribution statements generally fall into two distinct but related categories (Pall et al. 2014; Easterling et al. 2016; Stott et al. 2016). A "probabilistic" interpretation quantifies the change in probability of an extreme weather event occurring above a fixed magnitude, usually determined by an observation. A "mechanistic" interpretation quantifies the change in magnitude of an extreme weather event at a fixed probability, also estimated from a long

observational record. The probabilistic interpretation of tropical cyclone attribution is only modified by the additional conditions imposed by the construction of the hindcast. However, the mechanistic interpretation requires a subtle modification in the hindcast attribution method. In the two less conditional attribution methods, large samples of events, many of which are not extreme, are generated. Hence, using a fixed probability threshold to subsample only the extreme events permits a mechanistic attribution statement relevant to the actual observed event. However, by design, all the events simulated in the hindcast attribution method are extreme, at least compared to a climatological sample at the same time and place. In other words, the hindcast samples are constructed to be representative of the observed event, and comparing mean magnitudes of the factual and counterfactual ensembles form the relevant mechanistic attribution statement.

For tropical cyclones, attributable quantities of interest include peak wind speeds, precipitation totals or rates, Accumulated Cyclonic Energy, storm surge, and other measures important to impacts. Some fields, most notably inland precipitation, have long observational records, and a different class of attribution statements without the use of climate models may be feasible. For instance, Risser and Wehner (2017) and Van Oldenbourgh et al. (2017) both analyzed lengthy time series from Texas rain gauges in the region flooded by Hurricane Harvey. By applying non-stationary extreme value statistical methods, both groups could estimate the trend in extreme precipitation and made attribution statements that anthropogenic climate change increased the observed rainfall accumulated over several days in the Houston area. However, unlike the hindcast attribution method that uses dynamical models, this class of analysis has no direct intervention as described above. Hence, attribution statements based only on the observational record are causality statements interpretable in the Granger sense (Granger 1969; Ebert-Uphoff and Deng 2012). This type of causality can explicitly rule out a cause but not directly confirm a particular cause, as there may be other hidden causes not included in the covariates used to develop the non-stationary statistical model. However, it does have the advantage of being readily calculable from available observations and is ideally suited for real-time attribution, albeit producing weaker statements by construction. In the case of Hurricane Harvey, a subsequent hindcast attribution, similar to that presented above, found human induced precipitation changes consistent with these two solely observational analyses (Wang et al. 2018). Readers interested in Granger attribution are referred to Hannart et al. (2016) and Ebert-Uphoff and Deng (2012) for further details on causal theory and attribution of human induced climate change.

Another alternative method to construct attribution statements about tropical cyclone precipitation has been put forth by Emanuel (2017). This strategy uses a specialized tropical cyclone model that "seeds" the output of coarser global climate models. It has the advantage of being computationally inexpensive and can more easily explore climate model structural uncertainty such as exhibited by the CMIP ensembles. In the case of Hurricane Harvey precipitation, it provided another independent assessment of the human influence on the storm's precipitation, enhancing confidence in the results of Van Oldenborgh et al. (2017) and Risser and Wehner (2017).

Any attribution statement is incomplete without a quantification of its uncertainty. Attribution statements about intense storms such as tropical cyclones are likely to contain more sources of uncertainty than for other types of extreme weather. In particular, the dependence of the attribution statement on the selection of hindcast models should be made clear. Results from multiple hindcast models can increase or decrease attribution statement confidence depending on the consistency of the results. Also, in some cases, the additional usage of statistical techniques based purely on observations can increase confidence in attribution statements developed from the hindcast technique.

We conclude by stating that, while the hindcast attribution method presented here cannot provide a complete description of the human influence on individual tropical cyclones, it does provide a conditional description that can provide valuable insight into how climate change affects those aspects of tropical cyclones that cause damages.

Acknowledgement This work was supported by the Department of Energy Office of Science under contract number DE-AC02-05CH11231. This document was prepared as an account of work sponsored by the United States Government. While this document is believed to contain correct information, neither the United States Government nor any agency thereof, nor the Regents of the University of California, nor any of their employees, makes any warranty, express or implied, or assumes any legal responsibility for the accuracy, completeness, or usefulness of any information, apparatus, product, or process disclosed, or represents that its use would not infringe privately owned rights. Reference herein to any specific commercial product, process, or service by its trade name, trademark, manufacturer, or otherwise, does not necessarily constitute or imply its endorsement, recommendation, or favoring by the United States Government or any agency thereof, or the Regents of the University of California. The views and opinions of authors expressed herein do not necessarily state or reflect those of the United States Government or any agency thereof or the Regents of the University of California.

The National Center for Atmospheric Research is sponsored by the National Science Foundation. CMZ was partially supported under NSF's Advanced Study Program (ASP).

This research used resources of the National Energy Research Scientific Computing Center (NERSC), also supported by the Office of Science of the U.S. Department of Energy, under Contract No. DE-AC02-05CH11231.

References

Angelil O, Stone D, Wehner M, Paciorek CJ, Krishnan H, Collins W (2017) An independent assessment of anthropogenic attribution statements for recent extreme weather events. J Clim 30:5–16. https://doi.org/10.1175/JCLI-D-16-0077.1

Bacmeister JT, Reed KA, Hannay C, Lawrence PJ, Bates SC, Truesdale JE, Rosenbloom NA, Levy MN (2018) Projected changes in tropical cyclone activity under future warming scenarios using a high-resolution climate model. Clim Chang 146:547–560. https://doi.org/10.1007/s10584-016-1750-x

Bassill NP (2014) Accuracy of early GFS and ECMWF Sandy (2012) track forecasts: evidence for a dependence on cumulus parameterization. Geophys Res Lett 41:3274–3281. https://doi.org/10.1002/2014GL059839

Bister M, Emanuel K (1998) Dissipative heating and hurricane intensity. Meteorol Atmos Phys 65:223–240

Davis C, Wang W, Chen SS, Chen Y, Corbosiero K, DeMaria M, Dudhia J, Holland G, Klemp J, Michalakes J, Reeves H, Rotunno R, Snyder C, Xiao Q (2008) Prediction of landfalling hurricanes with the advanced hurricane WRF model. Mon Weather Rev 136:1990–2005

Dennis JM, Edwards J, Evans KJ, Guba O, Lauritzen PH, Mirin AA, St-Cyr A, Taylor MA, Worley PH (2011) CAMSE: a scalable spectral element dynamical core for the community atmosphere model. Int J High Perform Comput Appl 26(1):74–89. https://doi.org/10.1177/1094342011428142

Easterling DR, Kunkel KE, Wehner MF, Sun L (2016) Detection and attribution of climate extremes in the observed record. Weather Clim Extremes 11:17–27. https://doi.org/10.1016/j.wace.2016.01.001

Ebert-Uphoff I, Deng Y (2012) Causal discovery for climate research using graphical models. J Clim 25(17):5648–5665

Emanuel KA (1987) The dependence of hurricane intensity on climate. Nature 326:483–485

Emanuel K (2017) Assessing the present and future probability of hurricane Harveys rainfall. Proc Natl Acad Sci 114(48):12681–12684. https://doi.org/10.1073/pnas.1716222114

Emanuel KA, Solomon S, Folini D, Davis S, Cagnazzo C (2013) Influence of tropical tropopause layer cooling on Atlantic hurricane activity. J Clim 26:2288–2301. https://doi.org/10.1175/JCLI-D-12-00242.1

Granger CW (1969) Investigating causal relations by econometric models and cross spectral methods. Econometrica 37(3):424–438. https://doi.org/10.2307/1912791

Hannart A, Pearl J, Otto FE, Naveau P, Ghil M (2016) Causal counterfactual theory for the attribution of weather and climate-related events. Bull Am Meteor Soc 97:99–110. https://doi.org/10.1175/BAMS-D-14-00034.1

Haustein K, Otto FEL, Uhe P, Schaller N, Allen MR, Hermanson L, Christidis M, McLean P, Cullen H (2016) Real-time extreme weather event attribution with forecast seasonal SSTs. Environ Rev Lett 11:064006. https://doi.org/10.1088/1748-9326/11/6/064006

Held IM, Zhao M (2011) The response of tropical cyclone statistics to an increase in CO2 with fixed sea surface temperatures. J Clim 24:5353–5364. https://doi.org/10.1175/JCLI-D-11-00050.1

Herring SC, Hoerling MP, Peterson TC, Stott PA (eds) (2014) Explaining extreme events of 2013 from a climate perspective. Bull Am Meteorol Soc 95(9):S1–S96

Herring SC, Hoerling MP, Kossin JP, Peterson TC, Stott PA (eds) (2015) Explaining extreme events of 2014 from a climate perspective. Bull Am Meteorol Soc 96(12):S1–S172

Herring SC, Hoell A, Hoerling MP, Kossin JP, Schreck CJ, Stott PA (2016) Explaining extreme events of 2015 from a climate perspective. Bull Am Meteorol Soc 97:S1–S145

Huang P, Lin II, Chou C, Huang RH (2015) Change in ocean subsurface environment to suppress tropical cyclone intensification under global warming. Nat Commun 6:7188. https://doi.org/10.1038/ncomms8188

Ito R, Takemi T, Arakawa O (2016) A possible reduction in the severity of typhoon wind in the northern part of Japan under global warming: a case study. Sci Online Let Atmos 12:100–105. https://doi.org/10.2151/sola.2016-023

Jeon S, Paciorek CJ, Wehner MF (2016) Quantile-based bias correction and uncertainty quantification of extreme event attribution statements. Weather Clim Extremes 12:24–32. https://doi.org/10.1016/j.wace.2016.02.001

Kaplan J, DeMaria M, Knaff JA (2010) A revised tropical cyclone rapid intensification index for the Atlantic and eastern North Pacific basins. Weather Forecast 25:220–241

Knapp KR, Kruk MC, Levinson DH, Diamond HJ, Neumann CJ (2010) The international best track archive for climate stewardship (IBTrACS). Bull Am Meteorol Soc 91(3):363–376. https://doi.org/10.1175/2009BAMS2755.1

Knutson T (2017) Detection and attribution methodologies overview. In: Wuebbles DJ, Fahey DW, Hibbard KA, Dokken DJ, Stewart BC, Maycock TK (eds) Climate science special report: fourth

national climate assessment, volume I. U.S. Global Change Research Program, Washington, DC, pp 443–451. https://doi.org/10.7930/J0319T2J

Knutson TR, Sirutis JJ, Zhao M, Tuleya RE, Bender M, Vecchi GA, Villarini G, Chavas D (2015) Global projections of intense tropical cyclone activity for the late twenty-first century from dynamical downscaling of CMIP5/RCP4.5 scenarios. J Clim 28:7203–7224. https://doi.org/10.1175/JCLI-D-15-0129.1

Kossin JP, Hall T, Knutson T, Kunkel KE, Trapp RJ, Waliser DE, Wehner MF (2017) Extreme storms. In: Wuebbles DJ, Fahey DW, Hibbard KA, Dokken DJ, Stewart BC, Maycock TK (eds) Climate science special report: fourth national climate assessment, volume I. U.S. Global Change Research Program, Washington, DC, pp 257–276. https://doi.org/10.7930/J07S7KXX

Lackmann GM (2015) Hurricane Sandy before 1900 and after 2100. Bull Am Meteorol Soc 96:547–559

Landsea CW, Franklin JL (2013) Atlantic hurricane database uncertainty and presentation of a new database format. Mon Weather Rev 141:3576–3592

Landsea CW et al (2004) The Atlantic Hurricane Database Re-analysis Project: documentation for the 1851–1910 alterations and additions to the HURDAT database. In: Murnane RJ, Liu K-B (eds) Hurricanes and typhoons: past, present and future. Columbia University Press, New York, pp 177–221

Lum T, Margesson R (2014) Typhoon Haiyan (Yolanda): U.S. and international response to Philippines disaster. Curr Polit Econ South 23:209–246

Magnusson L, Bidlot J-R, Lang STK, Thorpe A, Wedi N, Yamaguchi M (2014) Evaluation of medium-range forecasts for Hurricane Sandy. Mon Weather Rev 142:1962–1981. https://doi.org/10.1175/MWR-D-13-00228.1

Murakami H, Sugi M (2010) Effect of model resolution on tropical cyclone climate projections. Sci Online Lett Atmos 6:73–76. https://doi.org/10.2151/sola.2010-019

Murakami H, Wang Y, Yoshimura H, Mizuta R, Sugi M, Shindo E, Adachi Y, Yukimoto S, Hosaka M, Kusunoki S, Ose T, Kitoh A (2012) Future changes in tropical cyclone activity projected by the new high-resolution MRI-AGCM. J Clim 25:3237–3260. https://doi.org/10.1175/JCLI-D-11-00415.1

National Academies of Sciences, Engineering, and Medicine (2016) Attribution of extreme weather events in the context of climate change. The National Academies Press, Washington, DC. https://doi.org/10.17226/21852

Neale RB et al (2012) Description of the NCAR Community Atmosphere Model (CAM 5.0). NCAR Tech. Note NCAR/TN-4861STR, National Center for Atmospheric Research. http://www.cesm.ucar.edu/models/cesm1.0/cam/docs/description/cam5_desc.pdf

Oouchi K, Yoshimura J, Yoshimura H, Mizuta R, Kusunoki S, Noda S (2006) Tropical cyclone climatology in a global-warming climate as simulated in a 20 km mesh global atmospheric model: frequency and wind intensity analyses. J Meteor Soc Jpn 84(2):259–276

Otto FEL, Massey N, van Oldenborgh GJ, Jones RG, Allen MR (2012) Reconciling two approaches to attribution of the 2010 Russian heat wave. Geophys Res Lett 39:L04702

Pall P, Aina T, Stone DA, Stott PA, Nozawa T, Hilberts AGJ, Lohmann D, Allen MR (2011) Anthropogenic greenhouse gas contribution to UK autumn flood risk. Nature 470:382–385

Pall P, Wehner M, Stone D (2014) Probabilistic extreme event attribution. In: Grojahn R, Li J, Swinbank R, Volkert H (eds) Dynamics and predictability of large-scale, high-impact weather and climate events. Cambridge University Press, Cambridge, pp 37–46 ISBN 978-1-107-07142-1

Pall P, Patricola CM, Wehner MF, Stone DA, Paciorek C, Collins WD (2017) Diagnosing anthropogenic contributions to heavy Colorado rainfall in September 2013. Weather Clim Extremes 17:1–6. https://doi.org/10.1016/j.wace.2017.03.004

Patricola CM, Wehner MF (2018) Anthropogenic Influences on Major Tropical Cyclone Events. To appear Nature.

Patricola CM, Saravanan R, Chang P (2014) The impact of the El Niño-Southern oscillation and Atlantic meridional mode on seasonal Atlantic tropical cyclone activity. J Clim 27:5311–5328

Patricola CM, Chang P, Saravanan R (2016) Degree of simulated suppression of Atlantic tropical cyclones modulated by flavour of El Niño. Nat Geosci 9:155–160

Patricola CM, Saravanan R, Chang P (2017) A teleconnection between Atlantic sea surface temperature and eastern and central North Pacific tropical cyclones. Geophys Res Lett 44:1167–1174

Pearl J (2000) Causality: models, reasoning, and inference. Cambridge University Press, New York

Peterson TC, Stott PA, Herring S (eds) (2012) Explaining extreme events of 2011 from a climate perspective. Bull Am Meteor Soc 93:1041–1067

Peterson TC, Hoerling MP, Stott PA, Herring S (eds) (2013) Explaining extreme events of 2012 from a climate perspective. Bull Am Meteorol Soc 94:S1–S74

Rappaport EN et al (2009) Advances and challenges at the National Hurricane Center. Weather Forecast 24:395–419. https://doi.org/10.1175/2008WAF2222128.1

Reynolds RW, Smith TM, Liu C, Chelton DB, Casey KS, Schlax MG (2007) Daily high-resolution-blended analyses for sea surface temperature. J Clim 20:5473–5496

Risser MD, Wehner MF (2017) Attributable human-induced changes in the likelihood and magnitude of the observed extreme precipitation in the Houston, Texas region during hurricane Harvey. Geophys Rev Lett 44:12457–12464. https://doi.org/10.1002/2017GL075888

Risser MD, Stone DA, Paciorek CJ, Wehner MF, Angelil O (2017) Quantifying the effect of interannual ocean variability on the attribution of extreme climate events to human influence. Clim Dyn 49:3051–3073. https://doi.org/10.1007/s00382-016-3492-x

Saha S et al (2010) The NCEP climate forecast system reanalysis. Bull Am Meteorol Soc 91:1015–1057

Santer BD, Wehner MF, Wigley TML, Sausen R, Meehl GA, Ammann C, Arblaster J, Washington WM, Boyle JS, Brueggemann W (2003) Contributions of anthropogenic and natural forcing to recent tropopause height changes. Science 301:479–483

Santer BD, Wigley TML, Mears C, Wentz FJ, Klein SA, Seidel DJ, Taylor KE, Thorne PW, Wehner MF, Gleckler PJ, Boyle JS, Collins W, Dixon KW, Doutriaux C, Free M, Fu Q, Hansen JE, Jones GS, Ruedy R, Karl TR, Lanzante JR, Meehl GA, Ramaswamy V, Russell G, Schmidt GA (2005) Amplification of surface temperature trends and variability in the tropical atmosphere. Science 309:1551–1556

Schär C, Frei C, Lüthi D, Davies HC (1996) Surrogate climate-change scenarios for regional climate models. Geophys Res Lett 23:669–672

Shepherd TG (2016) A common framework for approaches to extreme event attribution. Curr Clim Chang Rep 2:28–38

Shutts G (2005) A kinetic energy backscatter algorithm for use in ensemble prediction systems. Q J Roy Meteor Soc 131:3079–3102

Skamarock WC et al (2008) A description of the advanced research WRF version 3, NCAR Tech Note, NCAR/TN–475+STR. National Center for Atmospheric Research, Boulder

Stone DA, Risser MD, Ang'elil OM, Wehner MF, Cholia S, Keen N, Krishnan H, O'Brien TA, Paciorek CJ, Collins WD (2017) A basis set for exploration of sensitivity to prescribed ocean conditions for estimating human contributions to extreme weather in CAM5.1-1degree. Weather Clim Extremes 19:10–19. https://doi.org/10.1016/j.wace.2017.12.003

Stone DA, Christidis N, Folland C, Perkins-Kirkpatrick S, Perlwitz J, Shiogama H, Wehner MF, Wolski P, Cholia S, Krishnan H, Murray D, Ang'elil O, Beyerle U, Ciavarella A, Dittus A, Quan X-W (2018) Experiment design of the International CLIVAR C20C+ Detection and Attribution Project. Weather Clim Extremes. in preparation

Stott PA, Stone DA, Allen MR (2004) Human contribution to the European heatwave of 2003. Nature 432:610–614

Stott PA, Christidis N, Otto FEL, Sun Y, Vanderlinden J-P, van Oldenborgh GJ, Vautard R, von Storch H, Walton P, Yiou P, Zwiers FW (2016) Attribution of extreme weather and climate-related events. WIREs Clim Chang 7:23–41. https://doi.org/10.1002/wcc.380

Sugi M, Murakami H, Yoshimura J (2009) A reduction in global tropical cyclone frequency due to global warming. Sci Online Lett Atmos 5:164–167. https://doi.org/10.2151/sola.2009-042

Takayabu I, Hibino K, Sasaki H, Shiogama H, Mori N, Shibutani Y, Takemi T (2015) Climate change effects on the worst-case storm surge: a case study of Typhoon Haiyan. Environ Res Lett 10:089502. https://doi.org/10.1088/1748-9326/10/8/089502

Takemi T, Ito R, Arakawa O (2016) Robustness and uncertainty of projected changes in the impacts of Typhoon Vera (1959) under global warming. Hydrol Res Lett 10(3):88–94. https://doi.org/10.3178/hrl.10.88

van Oldenborgh GJ, van der Wiel K, Sebastian A, Singh R, Arrighi J, Otto F, Haustein K, Li S, Vecchi G, Cullen H (2017) Attribution of extreme rainfall from Hurricane Harvey, August 2017. Environ Res Lett 12:124009

Vautard R, Yiou P, Otto F, Stott P, Christidis N, van Oldenborgh GJ, Schaller N (2016) Attribution of human-induced dynamical and thermodynamical contributions in extreme weather events. Environ Res Lett 11:114009. https://doi.org/10.1088/1748-9326/11/11/114009

Walsh KJE, Camargo S, Vecchi G, Daloz AS, Elsner J, Emanuel K, Horn M, Lim Y-K, Roberts M, Patricola C, Scoccimarro E, Sobel A, Strazzo S, Villarini G, Wehner M, Zhao M, Kossin J, LaRow T, Oouchi K, Schubert S, Wang H, Bacmeister J, Chang P, Chauvin F, Jablonowski C, Kumar A, Murakami H, Ose T, Reed K, Saravanan R, Yamada Y, Zarzycki C, Vidale P-L, Jonas J, Henderson N (2015) Hurricanes and climate: the U.S. CLIVAR working group on hurricanes. Bull Am Meteorol Soc 96:997–1017. https://doi.org/10.1175/BAMS-D-13-00242.1

Wang S-YS, Zhao L, Yoon J-H, Klotzbach P, Gillies RR (2018) Quantitative attribution of climate effects on Hurricane Harvey's extreme rainfall in Texas. Environ Res Lett 13(5):054014. https://doi.org/10.1088/1748-9326/aabb85

Wehner MF, Reed K, Li F, Prabhat, Bacmeister J, Chen C-T, Paciorek C, Gleckler P, Sperber K, Collins WD, Gettelman A, Jablonowski C (2014) The effect of horizontal resolution on simulation quality in the Community Atmospheric Model, CAM5.1. J Model Earth Syst 6:980–997. https://doi.org/10.1002/2013MS000276

Wehner MF, Prabhat, Reed K, Stone D, Collins WD, Bacmeister J (2015) Resolution dependence of future tropical cyclone projections of CAM5.1 in the US CLIVAR Hurricane Working Group idealized configurations. J Clim 28:3905–3925. https://doi.org/10.1175/JCLI-D-14-00311.1

Wehner M, Stone D, Mitchell D, Shiogama H, Fischer E, Graff LS, Kharin VV, Sanderson B, Krishnan H (2018a) Changes in extremely hot days under stabilized 1.5°C and 2.0°C global warming scenarios as simulated by the HAPPI multi-model ensemble. Earth Syst Dyn 9:299–311 https://www.earth-syst-dynam.net/9/299/2018/esd-9-299-2018.html

Wehner MF, Reed KA, Loring B, Stone D, Krishnan H (2018b) Changes in tropical cyclones under stabilized 1.5°C and 2.0°C global warming scenarios as simulated by the Community Atmospheric Model under the HAPPI protocols. Earth Syst Dyn 9:187–195. https://doi.org/10.5194/esd-9-187-2018

Wing AA, Emanuel K, Solomon S (2015) On the factors affecting trends and variability in tropical cyclone potential intensity. Geophys Res Lett 42:8669–8677. https://doi.org/10.1002/2015GL066145

Xiang B, Lin S-J, Zhao M, Zhang S, Vecchi G, Li T, Jiang X, Harris L, Chen J-H (2015) Beyond weather time scale prediction for Hurricane Sandy and Super Typhoon Haiyan in a global climate model. Mon Weather Rev 143:524–535. https://doi.org/10.1175/MWR-D-14-00227.1

Zarzycki CM (2016) Tropical cyclone intensity errors associated with lack of two-way ocean coupling in high-resolution global simulations. J Clim 29:8589–8610

Zarzycki CM, Jablonowski C (2015) Experimental tropical cyclone forecasts using a variable-resolution global model. Mon Weather Rev 143:4012–4037. https://doi.org/10.1175/MWR-D-15-0159.1

Zarzycki CM et al (2014a) Using variable resolution meshes to model tropical cyclones in the Community Atmosphere Model. Mon Weather Rev 142:1221–1239. https://doi.org/10.1175/MWR-D-13-00179.1

Zarzycki CM et al (2014b) Aquaplanet experiments using CAM's variable-resolution dynamical core. J Clim 27:5481–5503. https://doi.org/10.1175/JCLI-D-14-00004.1

Zhao M, Held IM, Lin SJ, Vecchi GA (2009) Simulations of global hurricane climatology, interannual variability, and response to global warming using a 50-km resolution GCM. J Clim 22:6653–6678

Zhao M, Held IM, Vecchi GA, Scoccimarro E, Wang H, Wehner M, Lim Y-K, LaRow T, Camargo SJ, Walsh K, Gualdi S, Kumar A, Schubert S, Reed KA (2013) Robust direct effect of increasing atmospheric CO2 concentration on global tropical cyclone frequency – a multi-model inter-comparison. US CLIVAR Var Fall 2013 11(3):17–23

Correction to: Hurricane Risk

Jennifer M. Collins and Kevin Walsh

Correction to:
J. M. Collins, K. Walsh (eds.), *Hurricane Risk*, Hurricane Risk 1, https://doi.org/10.1007/978-3-030-02402-4

This book was inadvertently published with the incorrect ISSN numbers for both print and electronic versions. This has now been amended in the copyright page of the book to the correct ISSN numbers as ISSN 2662-3064 (print) ISSN 2662-3072 (electronic).

The updated original online version for this chapter can be found at https://doi.org/10.1007/978-3-030-02402-4

J. M. Collins, K. Walsh (eds.), *Hurricane Risk*, Hurricane Risk 1,
https://doi.org/10.1007/978-3-030-02402-4_13